On diffusion in zeolites : a simulation study

Beerdsen, E.

Publication date
2007
Document Version
Final published version

On Diffusion in Zeolites

A Simulation Study

On Diffusion in Zeolites

A Simulation Study

ACADEMISCH PROEFSCHRIFT

ter verkrijging van de graad van doctor
aan de Universiteit van Amsterdam,
op gezag van de Rector Magnificus
prof. dr. J. W. Zwemmer
ten overstaan van een door het college voor promoties ingestelde
commissie, in het openbaar te verdedigen in de Aula der Universiteit

op woensdag 27 juni 2007, te 12.00 uur

door

Edith Beerdsen
geboren te Alkmaar

Promotiecommissie

Promotor:

- prof. dr. ir. B. Smit

Overige leden:

- prof. dr. P. G. Bolhuis
- prof. dr. S. Calero
- prof. dr. D. Frenkel
- prof. dr. dr. h.c. F. J. Keil
- dr. T. L. M. Maesen
- prof. dr. J. N. H. Reek
- prof. dr. R. A. van Santen

Faculteit der Natuurwetenschappen, Wiskunde en Informatica

The research reported in this thesis was carried out at the Van 't Hoff Institute for Molecular Sciences, Faculty of Science, University of Amsterdam (Nieuwe Achtergracht 166, 1018 WV, Amsterdam, The Netherlands), and at the Centre Européen de Calcul Atomique et Moléculaire (CECAM; Ecole Normale Supérieure, 46 Allée d'Italie, 69007 Lyon, France), with financial support from the Deutsche Forschungsgemeinschaft (DFG, priority program SPP 1155) and computational resources received from NWO/NCF.

Contents

1 Introduction

1.1 Zeolites

In 1756, Swedish mineralogist Axel Fredrick Cronstedt discovered a naturally occurring mineral that, when heated, would start to "froth": water would start to come out and evaporate. He published about his discovery in the Transactions of the Academy of Sciences at Stockholm, coining the name "zeolit", in Swedish, for this new class of materials, meaning "boiling stones" and deriving from the Greek words $\zeta\epsilon\hat{\iota}\nu$ (to boil) and $\lambda\acute{\iota}\theta o\varsigma$ (stone). The English name became "zeolite" [1].

In the twentieth century, zeolites gained widespread application. Today, they are used for a variety of tasks. The largest volume of zeolite is used in detergents, where the material acts as an ion exchanger, to absorb the calcium and magnesium found in tap water. The petrochemical industry uses large quantities of zeolites for separation, cracking, and shape-selective catalysis of hydrocarbons. One can find zeolites as adsorbents in kitty litter, and as desiccants in shoe boxes and camera cases. Other uses include the removal of atmospheric pollutants from the air and radioactive ions from waste solutions.

Zeolites are porous crystalline structures with very regular, well-defined shapes. In their most simple form, zeolites consist of silicon (Si) and oxygen (O) in a proportion SiO_2. Silicon atoms bind four oxygen atoms each, in a tetrahedral arrangement, and, on a higher level of ordering, form rings of varying sizes to connect with other tetrahedrally coordinated silicon atoms. Thus, a large variety of structures can be formed. Currently, there are 193

known structures that have been synthesised [2], each designated by a three-letter code, but many more hypothetical structures could potentially be made [3].

In some zeolitic materials, some of the silicon atoms have been replaced by other metals, such as aluminium or any of a variety of transition metals. The charge created in the framework by such framework substitutions is compensated by the presence of counter-ions in the zeolite's pores.

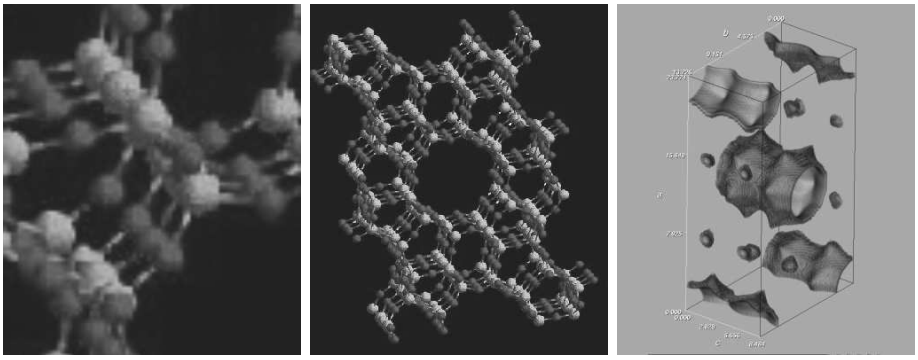

Figure 1.1: *Left: zeolites consist of silicon atoms and oxygen atoms. Middle: Every silicon atom is bound to four oxygen atoms, every oxygen atom to two silicon atoms. Right: by forming rings of various sizes, a structure arises with channels and cavities.*

The widespread use of zeolitic materials is based on three properties: adsorption, diffusion and catalysis. Since the pore diameters are in the order of the size of a molecule, molecules can differ from one another in how easily they adsorb, how fast they diffuse, and how likely they are to react to form new molecules.

Much research has been directed to the topics of adsorption and catalysis, and by now these two topics are quite well understood. In diffusion, however, there are many open questions, and a uniform picture is lacking.

1.2 Diffusion

1.2.1 Experiments

One of the problems one encounters when studying diffusion, is that it can be expressed in a variety of ways. In macroscopic experiments, such as gravimetric measurements of the uptake and permeation rate, the diffusion measured is the

transport diffusion coefficient D_T. This coefficient is defined by Fick's law:

$$J = -D(c)_t \nabla c \tag{1.1}$$

where J is the sorbate flux when a concentration gradient ∇c is applied.

In (microscopic) NMR experiments a different quantity is measured, called the self-diffusion. It is the diffusion of a single particle moving in a sea of other particles. (See figure 1.2).

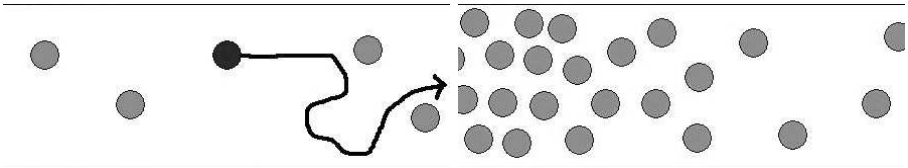

Figure 1.2: *The self-diffusion (left) is the diffusion of a single particle surrounded by other particles. The transport diffusion (right) is the collective diffusion of particles under the influence of a concentration gradient.*

The self-diffusion is related to the average motion of the particles:

$$D_S = \lim_{t\to\infty} \frac{1}{6Nt} \sum_{i=1}^{N} \Delta r_i(t)^2 \tag{1.2}$$

where Δr_i is the displacement of particle i at time t with respect to time 0 and N is the number of particles.

1.2.2 Simulations

When using simulations rather than experiments to calculate diffusivities, it is also possible to compute two different types of diffusion coefficients: D_S, the self-diffusion, which is equivalent to the self-diffusion as obtained from NMR experiments, and a different quantity, known as the collective diffusion coefficient D_C.

The collective diffusivity is the collective diffusion behaviour of all adsorbate particles, including interparticle correlations, and can be interpreted as the movement of the centre of mass of all particles together:

$$D_C = \lim_{t\to\infty} \frac{1}{6Nt} \sum_{i=1}^{N} \sum_{j=1}^{N} r_i(0) r_j(t) = \lim_{t\to\infty} \frac{1}{6Nt} \Big(\sum_{i=1}^{N} \Delta r_i(t) \Big)^2 \tag{1.3}$$

In general, the collective diffusion is higher than the self-diffusion, because the collective diffusion contains interparticle correlations, which have a positive contribution. Viewed differently, the self-diffusion is lowered by single-particle back-correlations, the increased probability of a particle jumping back to its previous position because this position has a higher probability of being empty.

1.2.3 Comparing Simulation and Experiment

To relate the collective diffusivity, obtained from simulation, to the transport diffusion, from experiment, D_T is often converted to the corrected diffusion D_C. This is also known as the Maxwell-Stefan or Darken diffusion coefficient, and is considered to be more loading independent than D_T. It can be compared directly with the collective diffusion coefficient D_C from simulation. It can be obtained from:

$$D_T(\theta) = D_C \frac{\partial \ln f}{\partial \ln \theta} = D_C \times \gamma(\theta) \tag{1.4}$$

where θ is the fractional occupancy in the sorbent, and f the fugacity [29]. $\gamma(\theta)$ can be obtained from – measured or calculated – adsorption isotherms. It is the derivative of the (log plot) adsorption isotherm when the axes are reversed.

As an example of how $D_T(c)$ can be converted into $D_C(c)$, see figure 1.3. Figure 1.3 (left) shows the adsorption isotherm, (middle) the correction factor $\gamma(\theta)$, and (right) D_T as a function of loading, along with D_C obtained from the combination of D_T and $\gamma(\theta)$.

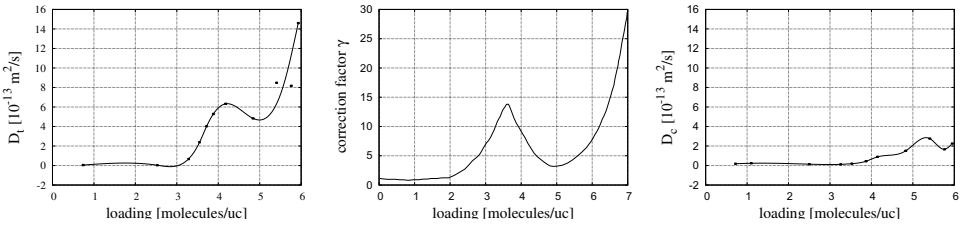

Figure 1.3: *D_T (left) and D_C (right) for benzene in silicalite, from Shah et al. [30]. D_C was calculated from D_T by computing γ (middle) and using equation 1.4, and is now ready to compare with D_C values from simulation.*

1.2.4 The Darken Approximation

At the infinite dilution limit D_S, D_C, and D_T are strictly equivalent. This observation has often been used to approximate eq. 1.4 by replacing D_C with

D_S. This is called the Darken approximation and eq. 1.4, under these conditions, the Darken equation [31]. The corrected diffusivity has been assumed to be relatively insensitive to changes in concentration, thus making it possible to use the Darken equation at arbitrary loading. In the cases where this is true, this is a very convenient way to relate microscopic and macroscopic diffusion processes. Methane in MFI-type zeolite is such a case: support for the concentration independence was found almost up to maximum loading [4, 32].

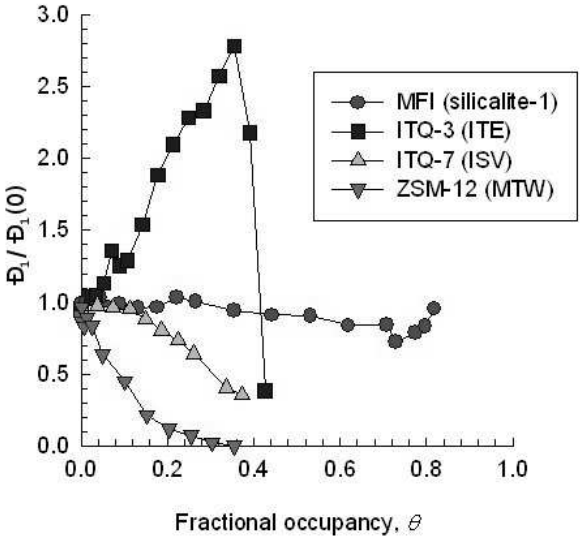

Figure 1.4: *Normalised diffusion as a function of loading for methane in four different zeolites, as calculated by Skoulidas and Sholl [4].*

One motivation for the work in this thesis was an article published by Skoulidas and Sholl in 2003 [4]. They calculated the diffusion of methane as a function of loading and found very interesting behaviour: for some zeolites the diffusion increased as a function of loading, for others it decreased, and for some it remained constant. (See figure 1.4.) What caused these differences was anyone's guess. We set out to solve this problem with a combination of different simulation techniques.

1.3 Simulations

Molecular simulations are a particularly useful tool to study diffusion in these systems. Zeolites are very regularly shaped, and therefore easily represented

by atomic models. Adsorption studies have shown that forcefields can be developed that reproduce and predict adsorption experiments very accurately [5]. But above all, simulations enable us to look inside the structures and see what is happening: where the molecules go, and how they move.

1.3.1 Molecular Dynamics

Intuitively, Molecular Dynamics (MD) simulations are the simplest type of simulation: particles move around in a system, following paths determined by Newton's laws. In an iterative scheme, the forces they exert on one another are calculated from their positions; based on these forces, the velocities are updated; and these velocities, kept fixed for one time step, yield the new positions one time step away.

Various implementations of this scheme are possible. The algorithm used in this thesis was the velocity-Verlet algorithm:

$$\mathbf{r}(t+\Delta t) = \mathbf{r}(t) + \mathbf{v}(t)\Delta t + \frac{\mathbf{f}(t)}{2m}\Delta^2 t \tag{1.5}$$

$$\mathbf{v}(t+\Delta t) = \mathbf{v}(t) + \frac{\mathbf{f}(t)+\mathbf{f}(t+\Delta t)}{2m}\Delta t \tag{1.6}$$

where $\mathbf{r}(t)$, $\mathbf{v}(t)$, and $\mathbf{f}(t)$ are the position, velocity, and force at time t, respectively, Δt is the time step used, and m is the mass of the particle.

From the particles' motion in the system it is possible to calculate diffusion coefficients. For the self-diffusion in one direction, we can use:

$$D_S^\alpha = \frac{1}{2N}\lim_{t\to\infty}\frac{d}{d\,t}\left\langle \sum_{i=1}^{N}\left(r_i^\alpha(t) - r_i^\alpha(0)\right)^2 \right\rangle \tag{1.7}$$

where N is the number of molecules, t the time, and r_i^α the α-component of the position of molecule i, with $\alpha = x, y, z$.

The collective diffusion coefficients D_C^α are given by

$$D_C^\alpha = \frac{1}{2N}\lim_{t\to\infty}\frac{d}{d\,t}\left\langle \left(\sum_{i=1}^{N}\left(r_i^\alpha(t) - r_i^\alpha(0)\right)\right)^2 \right\rangle \tag{1.8}$$

The directionally averaged diffusion coefficient can then be obtained by calculating

$$D = \frac{D_x + D_y + D_z}{3} \tag{1.9}$$

Before starting to acquire diffusion date from Molecular-Dynamics simulations, we prepare the system at the desired temperature in the following way:

1. The desired number of molecules are inserted at random positions in the system, making sure that inaccessible parts of the zeolite are excluded, and no overlap occurs with either the zeolite framework or other particles.

2. We perform a short initialisation run, using a Monte Carlo scheme in the NVT ensemble.

3. A second initialisation phase is used to equilibrate the system. Random velocities, from a Maxwell-Boltzmann distribution at the desired average temperature, are assigned to the particles, and the system is left to equilibrate in an NVT MD simulation. The temperature is controlled using the Nosé-Hoover Chain (NHC) thermostat [33].

After this initialisation procedure, the sample run commences, in either the NVT ensemble (using the NHC thermostat) or the NVE ensemble.

1.3.2 Transition-State Theory

One problem with studying diffusion in zeolites using molecular-dynamics simulations is that the diffusion of many zeolite-adsorbent combinations is very slow, making this traditional approach very impractical. An alternative method that has often been used to study (very) slow diffusion is Transition-State Theory. Transition-State Theory is based on the assumption that diffusive behaviour can be described as a hopping process on a lattice, where particles hop randomly from lattice point to lattice point. This assumption works under the condition that the lattice points are separated by sufficiently high free-energy barriers for the diffusion that a hop is a rare event, and two subsequent hops can be considered uncorrelated.

Once the hopping rate from point to point is known, the self-diffusion can be calculated, using

$$D_S = \frac{1}{2d} k \lambda^2 = k_{A \to B} \lambda^2 \tag{1.10}$$

where D_S is the self-diffusion coefficient, d the dimensionality of the system, k the hopping rate from a lattice site to any adjacent lattice site, λ the distance between two lattice points, and $k_{A \to B}$ the hopping rate from a given lattice point A to a specific lattice point B.

This equation is exact, and shifts the difficulty to the calculation of the hopping rate $k_{A \to B}$. For traditional Transition-State Theory, without dynamical correction, $k_{A \to B}$, the hopping rate from cage A to cage B, is given by

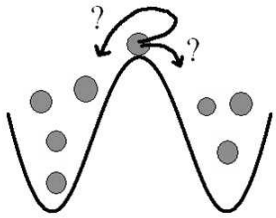

Figure 1.5: *A particle hopping over a free-energy barrier. Transition-State Theory assumes that every particle crossing the barrier coming from the left will equilibrate to the right of it. Dynamically corrected Transition-State Theory takes the possibility into account of particles crossing the barrier but failing to equilibrate on the right-hand side of the barrier, turning back over the barrier and equilibrating on the left instead.*

$$k_{A\to B} = \sqrt{\frac{k_B T}{2\pi m}} \times \frac{e^{-\beta F(q^*)}}{\int\limits_{\text{cage A}} e^{-\beta F(q)}\,\mathrm{d}q} \tag{1.11}$$

where where $\beta = 1/\left(k_B T\right)$, k_B is the Boltzmann constant, T the temperature, m the mass involved in the reaction coordinate, $F(q)$ the free energy as a function of reaction coordinate q, and q^* the value of the reaction coordinate at the barrier position. In this equation $\sqrt{k_B T/2\pi m}$ represents the typical velocity of a particle on top of the barrier, following a Maxwell-Boltzmann distribution. The rest of the right-hand side is the probability density of a particle being on top of the barrier (the numerator), given that it is located somewhere in cage A (the denominator).

If all particles arriving at the barrier from cage A and heading in the direction of cage B do in fact end up in B, eq. 1.11 gives an accurate result for the hopping rate. However, if some of the particles cross the barrier in the direction of cage B, but fail to equilibrate in B – instead turning around and going back to A – a correction factor κ is needed to account for the 'missing' hops. This is the so-called dynamical correction. Examples of cases where it is necessary to include a calculation of κ include systems with asymmetric barriers, and systems that include other particles, having the ability to 'kick' back the crossing particle to its departure point.

When the dynamical correction factor is included, the diffusion coefficient is given by

$$D_S = \kappa k_{A\to B} \lambda^2 \tag{1.12}$$

The details and intricacies of the dynamically corrected Transition-State Theory method are discussed in chapters 2 and 3, where the method is extended and tested for a system at nonzero loading.

1.3.3 Free-Energy Profiles

An additional advantage of calculating diffusion using Transition-State Theory is that the calculation involves the computation of free-energy profiles, which can then not only be used to obtain a diffusion coefficient, but also to get a better understanding of diffusion phenomena. This is discussed in chapter 8.

Free-energy profiles can be obtained from simulations in one of the following two ways:

1. Widom Sampling. In Widom Sampling a "ghost particle" is used to probe the energy of the system. During the course of a Monte-Carlo simulation, the probe particle is inserted at random positions, and the energy U at that position is calculated. This energy is mapped onto the reaction coordinate q, using $\beta F(q) = -\ln \left\langle e^{-\beta \Delta U} \right\rangle_q$, to produce a free-energy profile, where $F(q)$ is the free energy as a function of the reaction coordinate q and $\left\langle e^{-\beta \Delta U} \right\rangle_q$ the average Boltzmann factor over all positions corresponding to a certain value of the reaction coordinate.

2. Histogram Sampling. The system is advanced using either Monte-Carlo or Molecular Dynamics, and during the simulation, a histogram is made of the particle positions. This histogram can then be converted into a free-energy profile using $\beta F(q) = -\ln (P(q))$, where $P(q)$ is the probability for a particle to be at position q according to the histogram.

1.4 Scope of This Thesis

The first part of this thesis, chapters 2 and 3, describes the development of a new method to calculate diffusion in regularly shaped systems of slow diffusion. It is an extension to dynamically corrected Transition-State Theory, that enabled us to study slow diffusion at nonzero loading.

The remainder is devoted to the study of diffusion in zeolites, using this method. In chapters 4 and 5, the method is applied to a large number of different zeolites in order to come to a better understanding of diffusion behaviour as a function of loading, and, ultimately, a classification of zeolite structures based on their diffusion properties for methane.

Chapters 6 and 7 discuss a surprising phenomenon we found along the way: molecular path control, where the preferred direction of diffusion is dependent

on the loading in the system. It was possible to use free-energy calculations and transition-state theory to get a precise understanding of what was happening.

Another surprise was the fact that free-energy profiles were able to shed light on the complex diffusion patterns as a function of loading in zeolite MFI, which are discussed in detail in chapter 8.

Chapter 9, finally, aims to clear up for the specific, but widely studied, case of methane in MFI, why diffusion measurements, gathered by either experiment or simulation, often differ from one another by as much as several orders of magnitude.

Bibliography

[1] Oxford English Dictionary, 2nd ed., J. Simpson and E. Weiner (Ed.), Clarendon Press, Oxford, 1989

[2] http://www.iza-structure.org/databases/.

[3] D. J. Earl and M. W. Deem, Ind. and Eng. Chem. Res. **45**, 5449 (2006).

[4] A. Skoulidas and D. S. Sholl, J. Phys. Chem. A. **107**, 10132 (2003).

[5] D. Dubbeldam, S. Calero, T. Vlugt, R. Krishna, T. Maesen, E. Beerdsen, and B. Smit, Phys. Rev. Lett. **93**, 088302 (2004).

[6] S. Fritzsche, M. Gaub, R. Haberlandt, and G. Hofmann, J. Mol. Model **2**, 286 (1996).

[7] S. Fritzche, M. Wolfsberg, R. Haberlandt, P. Demontis, G. B. Suffritti, and A. Tilocca, Chem. Phys. Lett. **296**, 253 (1998).

[8] C. Saravanan, F. Jousse, and S. M. Auerbach, Phys. Rev. Lett. **80**, 5754 (1998).

[9] S. J. Goodbody, J. K. Watanabe, D. M. Gowan, J. P. R. B. Walton, and N. Quirke, J. Chem. Soc. Farad. Trans. **87**, 1951 (1991).

[10] C. R. A. Catlow, C. M. Freeman, B. Vessal, S. M. Tomlinson, and M. Leslie, J. Chem. Soc. Farad. Trans. **87**, 1947 (1991).

[11] J. B. Nicholas, F. R. Trouw, J. E. Mertz, L. E. Iton, and A. J. Hopfinger, J. Phys. Chem. **97**, 4149 (1993).

[12] S. Kar and C. Chakravarty, JPCA **105**, 5785 (2001).

[13] R. L. June, A. T. Bell, and D. N. Theodorou, J. Phys. Chem **94**, 8232 (1990).

[14] H. L. Tepper and W. J. Briels, J. Chem. Phys **116**, 9464 (2002).

[15] R. Q. Snurr, A. T. Bell, and D. N. Theodorou, J. Phys. Chem. **98**, 11948 (1994).

[16] A. Schüring, S. M. Auerbach, S. Fritzsche, and R. Haberlandt, J. Chem. Phys **116**, 10890 (2002).

[17] F. Jousse and S. M. Auerbach, J. Chem. Phys. **107**, 9629 (1997).

[18] C. Tunca and D. M. Ford, J. Chem. Phys. **111**, 2751 (1999).

[19] C. Tunca and D. M. Ford, J. Phys. Chem. B **106**, 10982 (2002).

[20] C. Tunca and D. M. Ford, Chem. Eng. Sci. **58**, 3373 (2003).

[21] P. K. Ghorai and S. Yashonath, J. Chem. Phys **120**, 5315 (2004).

[22] W. Heink, J. Kärger, H. Pfeifer, P. Salverda, K. P. Datema, and A. Nowak, J. Chem. Soc. Faraday Trans. **88**, 515 (1992).

[23] R. L. June, A. T. Bell, and D. N. Theodorou, J. Phys. Chem. **95**, 8866 (1991).

[24] D. Dubbeldam, S. Calero, T. L. M. Maesen, and B. Smit, Phys. Rev. Lett. **90**, 245901 (2003).

[25] D. Dubbeldam, S. Calero, T. L. M. Maesen, and B. Smit, Angew. Chem. Int. Ed. **42**, 3624 (2003).

[26] J. Caro, M. Bulow, W. Schirmer, J. Karger, W. Heink, and H. Pfeifer, J. Chem. Soc. Farad. Trans. **81**, 2541 (1985).

[27] H. Jobic, M. Bee, J. Caro, M. Bulow, and J. Karger, J. Chem. Soc. Farad. Trans. **85**, 4201 (1989).

[28] F. Kapteyn, W. J. W. Bakker, G. Zheng, and J. A. Moulijn, Chem. Eng. J. **57**, 145 (1995).

[29] S. M. Auerbach, International reviews in physical chemistry **19**, 155 (2000).

[30] D. B. Shah, C.-J. Guo, and D. T. Hayhurst, J. Chem. Soc. Farad. Trans. **91**, 1143 (1995).

[31] H. Ramanan and S. M. Auerbach, in *NATO-ASI Series C: Fluid Transport in Nanopores*, edited by J. Fraissard and W. Conner (Kluwer Academic Publishers, Dordrecht, The Netherlands, 2004).

[32] E. Beerdsen, D. Dubbeldam, and B. Smit, Phys. Rev. Lett. **95**, 164505 (2005).

[33] Martyna, G. J.; Tuckerman, M.; Tobias, D. J.; Klein, M. L. *Mol. Phys.* **1996**, *87*, 1117-1157.

An extension to Transition-State Theory is presented that is capable of computing quantitatively the diffusivity of adsorbed molecules in confined systems at nonzero loading. This extension to traditional Transition-State Theory yields a diffusivity in excellent agreement with that obtained by conventional Molecular Dynamics simulations. While Molecular Dynamics calculations are limited to relatively fast diffusing molecules or small rigid molecules, our approach extends the range of accessible times scales significantly beyond currently available methods. It is applicable in any system containing free-energy barriers and for any type of guest molecule.

E. Beerdsen, B. Smit, and D. Dubbeldam

2

Molecular Simulation of Loading-Dependent Slow Diffusion in Confined Systems

The adsorption and diffusion of molecules in confined systems is of great importance to many industrial processes such as the separation of linear and branched alkanes. The performance of confinements in separation and catalytic processes depends critically on the match between the confinement and the shape and size of the adsorbate [1]. Because diffusion is the rate limiting factor in many catalytic processes, diffusion in systems like zeolites has been widely studied [2–9]. However, in contrast to adsorption and separation, the diffusion of molecules in tight confinement is not yet well understood.

One of the difficulties encountered when studying diffusion behaviour is that many processes occur outside the timescale accessible to Molecular Dynamics (MD), which is typically limited to diffusion rates in the order of 10^{-12} m^2/s. To overcome this, some studies have used dynamically corrected Transition-State Theory (dcTST) methods [10–13]. Hitherto, studies were limited to the infinite dilution limit, whereas many of the processes of practical importance occur at nonzero loading. Coarse-grained kinetic Monte Carlo (kMC) studies have pointed at the difficulties in taking into account the various correlations induced by particle-particle interactions [10, 14]. In this chapter we resolve this problem by extending dcTST to include diffusion of molecules at nonzero loading. We show that these correlations can be taken into account by a

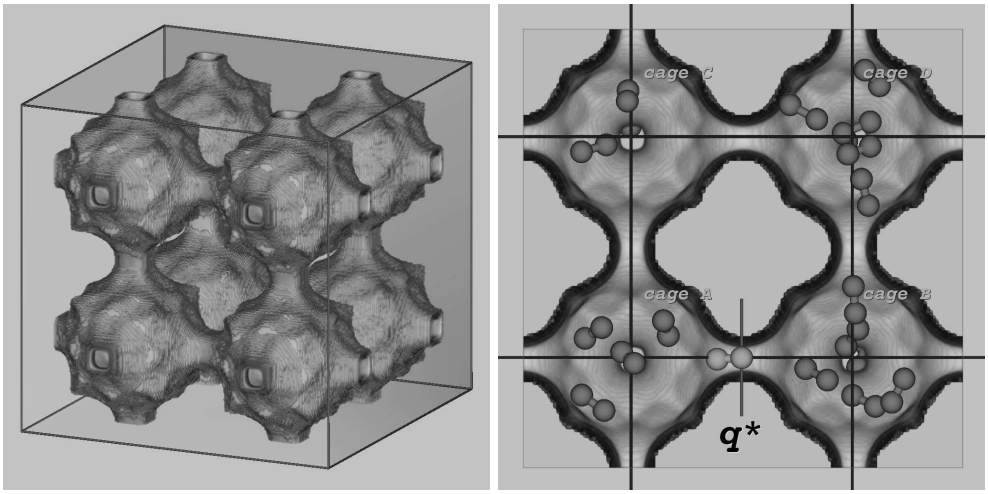

Figure 2.1: *(left) A unit cell of the LTA-type zeolite. The dimensions of the cubic unit cell are 24.555 Å. It contains eight cages connected in a cubic arrangement and each cage is connected to six other cages, by windows of about 5 Å in diameter. (right) Typical snapshot of ethane ($CH_3 - CH_3$) at an average loading of four molecules per cage at 750 K, constraining one tagged molecule at the dividing surface q^*. The hopping events are coarse-grained on a lattice spanned by the cage centers.*

proper definition of an effective hopping rate of a *single* particle. This hopping rate can be computed accurately using rare event simulation techniques at the conditions of interest.

A suitable and well-studied system to study diffusion in confinement is the LTA-type zeolite shown in figure 2.1. The system consists of cubically arranged cages of about 10 Å in size, where each cage has fifteen and twelve distinct adsorption sites for methane and ethane, respectively. The cages are connected by narrow windows that form large free-energy barriers. For small molecules, the positions in the windows regions are favourable adsorption sites, and the windows form *entropic*, not *energetic* barriers. An advantage of this system is that studying diffusion of small molecules with MD is still feasible, and this allows a detailed comparison with our new approach.

In this system, diffusion can be considered an activated process, in which the particle hops from one cage to the next, and the actual crossing time is negligible compared to the time a particle spends inside the cage. One can exploit the large separation in time scales using rare-event simulation techniques. We consider a system which can be in two stable states, A and B with

a dividing free-energy barrier between them. We define a reaction coordinate q, that indicates the progress of the diffusion event from cage A to cage B, as the Cartesian coordinate along the axis parallel to the line connecting the center points of A and B. The location of the dividing barrier is denoted by q^* (see figure 2.1). In the Bennett-Chandler approach [15–17] one computes the hopping rate over the barrier in two steps. First, the relative probability $P(q^*)$ is computed to find a particle on top of the barrier, given that it is in state A, and subsequently the averaged velocity at the top of the barrier $\sqrt{k_B T/2\pi m}$ (assuming that the particle velocities follow a Maxwell-Boltzmann distribution) and the probability κ that the system ends up in state B. The transmission rate $k_{A\to B}$ from cage A to cage B is then given by

$$k_{A\to B} = \kappa \times \sqrt{\frac{k_B T}{2\pi m}} \times P(q^*), \tag{2.1}$$

$$P(q^*) = \frac{e^{-\beta F(q^*)}}{\int\limits_{\text{cage A}} e^{-\beta F(q)}\,\mathrm{d}q}, \tag{2.2}$$

where $\beta = 1/(k_B T)$, k_B is the Boltzmann constant, T the temperature, m the mass involved in the reaction coordinate, and $F(q)$ the free energy as a function of q. In first order approximation, TST assumes that all particles that reach the barrier with a velocity towards B do end up in B, i.e. $\kappa = 1$.

In dcTST, the transmission coefficient κ corrects for recrossing events, i.e. it corrects for trajectories which cross the transition state from A but fail to end up in B. In general, the reaction coordinate q is a function of the configuration of the whole system, i.e. $q = q(\mathbf{r}_1, \ldots, \mathbf{r}_N)$. However, we can choose q as the position of one of the atoms of the diffusing molecules [11]. This choice of order parameter underestimates the free energy of the true transition state, but the dynamical correction κ is the *exact* correction compensating our choice of reaction coordinate [16]. The transmissions and recrossings are fast events and can be computed using MD as the fraction of particles coming from the initial state A that successfully reaches the final state B out of those that cross the dividing surface at $t = 0$. The transmission coefficient reaches a clear plateau value as a function of time, indicating all short-time-scale recrossings have been eliminated.

In the limit of infinite dilution there are no interparticle correlations and the particles perform a random walk on a lattice spanned by the cage centers. The transmission rates are then easily converted to self-diffusion coefficients by:

$$D_S = k_{A\to B}\lambda^2 = \frac{1}{6}k\lambda^2, \tag{2.3}$$

with λ the center-to-center lattice distance of the LTA cages (12.2775 Å). Because we calculate the hopping rate from A to B in one direction only, $k_{A\rightarrow B} = 1/6\ k$.

The extension of dcTST to finite loading is nontrivial. Conventional methods use a hierarchical approach to compute elementary hopping rates for use in a subsequent kMC scheme to obtain self and collective diffusion coefficients [2, 3, 13, 14, 18]. Let us consider the class of window/cage-type systems (e.g. methane in LTA) where the barriers are *entropic* in nature. At nonzero loading a molecule hopping from A to B induces a vacancy. The vacancy induces an increased probability of particles to hop to cage A. These correlated jumps may significantly influence the hopping process and should be included in order to obtain a correct diffusion coefficient. In a kMC simulation, the surrounding particles remain in their fixed positions (no two jumps can occur at the same time) and this constraint suppresses these correlations. We are not aware of a kMC scheme that takes into account these simultaneous jumps.

We take a different view on computing diffusivities in such systems. The correlations can be taken into account by a proper definition of an effective hopping rate of a *single* particle. We compute the self-diffusion coefficient directly. This is done by computing the hopping rate of a molecule over a typical length scale λ given by the smallest repeating zeolite structure (i.e. from the center of cage A to the center of cage B, implicitly integrating over all adsorption sites in the cage, irrespective of whether these are well defined or not). The other particles are regarded as a contribution to the external field exerted on the tagged particle. Since we look at a single tagged particle, the diffusion coefficient can still be computed from the hopping rate using eq. 2.3 at any loading, rendering it unnecessary to perform N-particle kMC simulations. Now, $k_{A\rightarrow B}$ is the *effective* hopping rate, *including* all jump correlations and averaged over all orientations and loading fluctuations. The external field is maintained by an MC NVT simulation (fixed total number of particles, volume, and temperature) in the 'background'. By using an MC approach that includes translational, orientational, and regrow moves, we automatically average over cage distributions, positions, and orientations of neighbouring molecules. To speed up these simulations for longer molecules by several orders of magnitude, these techniques can be combined with configurational bias Monte Carlo (CBMC) [17].

The proposed method relies on the direct inclusion of all interparticle correlations in the *effective* hopping rate of a particle travelling from cage A to cage B. In our calculations, we have observed that to obtain agreement with MD results, one cannot limit the free-energy calculation to the two cages A and B for which the hopping is computed. It is essential to average over fluc-

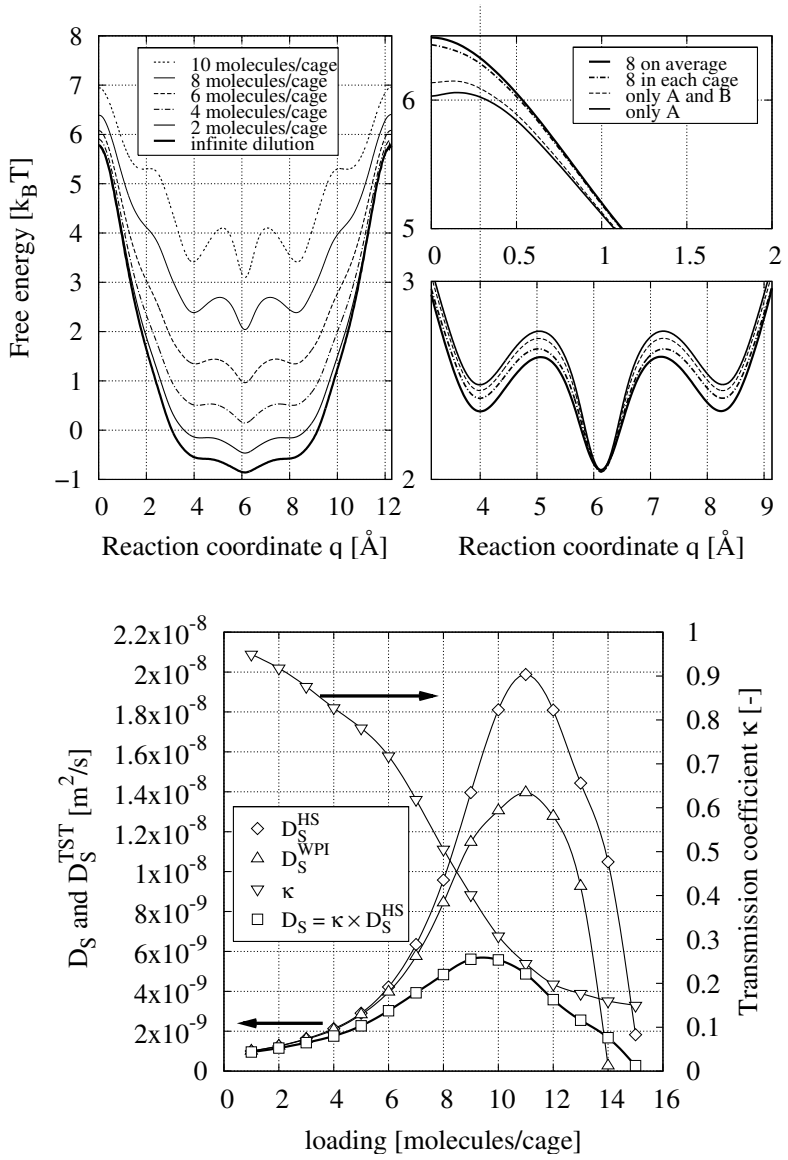

Figure 2.2: *(top left) Free-energy profiles of methane in LTA at 600 K for various loadings, obtained using the HS method, (top right) Details from free-energy profiles for 8 molecules per cage, using different environments (bottom) D_S^{HS}, D_S^{WPI}, and D_S (left axis) and transmission coefficients (right axis) as a function of loading.*

tuations in the number of particles in the neighbouring cages. By 'closing off' cages, the system is intrusively changed. Figure 2.2 (top right) compares the correct free energy (very large simulation box with on average eight molecules per cage), with approximations by simulating a fixed number of eight particles in cage A only, A and B only, and simulations with a fixed number of exactly eight particles in each cage. These small differences in the free-energies result in diffusion coefficients that deviate up to 60%. If we surround cage A with one shell of neighbouring cages, we obtain results that are identical to those obtained in the very large system. Inclusion of a second ring of cages is not necessary, as jump correlations over distances larger than two cages vanish. A similar influence is observed in the calculation of the transmission coefficient. Successful hopping events may induce a chain of hops of other particles, and this can influence the transmission coefficient. Only at low loadings we obtain agreement with MD.

We now discuss the two steps in the computation of the hopping rate using our approach in detail.

The probability $P(q)$ During an NVT-ensemble MC simulation at the required loading we measure the free energy $F(q)$ by using either the Widom Particle Insertion (WPI) method or Histogram Sampling (HS). WPI uses a probe particle that is inserted at random positions, to measure the energy required for or obtained by insertion of the particle in the system. This energy is mapped onto the reaction coordinate q, using $\beta F(q) = -\ln \left\langle e^{-\beta \Delta U} \right\rangle_N$, to produce a free-energy profile, where $\left\langle e^{-\beta \Delta U} \right\rangle_N$ is the average Boltzmann factor over all positions in the slice perpendicular to the reaction coordinate. A "ghost particle" is used as the measuring probe, but the other particles in the system do not feel its presence. In the HS method, a histogram is made of the particle positions, mapped on the reaction coordinate. From the histogram a free-energy profile is computed, by using $\beta F(q) = -\ln \langle P(q) \rangle$. If needed, statistics can be improved by using importance sampling [17]. At higher loadings, WPI is known to give erroneous results [17]. In figure 2.2 (top left) we have plotted the free-energy profiles as obtained from the HS method, for various loadings, and in figure 2.2 (bottom) D_S^{HS} and D_S^{WPI} as a function of loading. At loadings as low as six methane molecules per cage the WPI method starts to deviate.

The transmission coefficient κ We compute the fraction of particles starting on top of the barrier with a velocity towards B that successfully reach cage B. Starting configurations are generated using MC with one particle con-

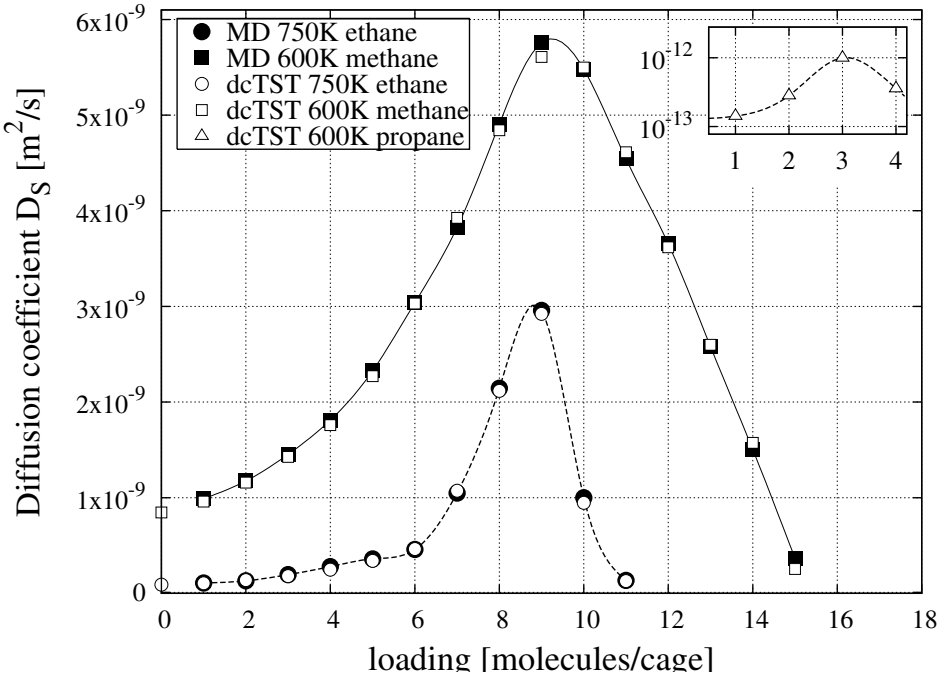

Figure 2.3: *Diffusion of methane, ethane and propane in LTA, as a function of loading, at 600 K, 750 K and 600 K respectively, computed by extended dcTST (HS method) and MD.*

strained to the dividing surface and $N-1$ particles moving around freely (see figure 2.1 (right)). These configurations are then used to compute the ratio in unconstrained NVE-MD simulations, starting with velocities sampled from a Maxwell-Boltzmann distribution at the desired temperature. For this snapshot, cage B contains more molecules than cage A, and the barrier molecule has a high probability of recrossing to cage A. In general, the transmission coefficient is much lower than 1 for chain molecules (*even* at infinite dilution). Note that during the computation none of the windows are blocked and simultaneous jumps (e.g. from cage C to cage A, and cage D to cage B) are allowed.

Figure 2.2 (bottom) shows the individual components of the diffusion process, D_S^{TST} and κ as a function of loading for methane in LTA. Although the transmission coefficient shows a monotonic decrease with density, the diffusion coefficient goes through a maximum. The driving force behind the initial increase in diffusion is a loss of guest-host attraction inside the cages. This in-

teraction is being replaced by less favourable interparticle interaction, causing an increase of the free energy in the cage regions and thus a net decrease of the free-energy barrier (figure 2.2 (bottom)). Eventually, the free-energy barrier increases again, due to packing and free-volume effects, causing a decrease of the diffusion coefficient. While the transmission coefficient only slightly changes the qualitative behaviour of the diffusion as a function of loading, it has a profound quantitative influence (figure 2.2 (bottom)).

To validate our method, we show the diffusion in LTA of methane at 600 K and ethane at 750 K, using both MD and extended dcTST. In addition, we show the diffusion of propane at 600 K, using only dcTST, for which the diffusion is too slow to compute with MD. The LTA-type system used here is a cation-free version of the commonly used LTA 5A zeolite (four Na^+ and four Ca^+ per cage). The system size was a cubic box of 24.555 Å, containing eight cages in total. We used a united-atom model [19], in which we consider CH_x groups as single interaction centers with their own effective Lennard-Jones potentials. We used the position of the CH_4 group, one of the CH_3 groups and the middle CH_2 group as the dcTST reaction coordinate for methane, ethane and propane, respectively [11]. The interactions between the rigid framework and the guest molecules are assumed to be dominated by the oxygen atoms [20]. The potential parameters are optimised to reproduce adsorption properties in pure-silica confinements [21, 22]. In the MD simulations we used a time step of 0.5 fs with the velocity-Verlet integration scheme. The NVT ensemble was imposed using a Nosé-Hoover thermostat. The duration of the computation was such that the error bars are smaller than the symbol size. As is shown in figure 2.3, our extended dcTST method and MD agree quantitatively. The presented methodology provides a general framework for computing diffusivities of molecules in systems where diffusion is sufficiently slow, due to free-energy barriers, irrespective of whether these are energetic or entropic in nature. Longer molecules are efficiently handled, and likewise, diffusion in mixtures can easily be computed; any type of particle can be considered part of the external field. A quantitative comparison with PFG (pulsed field gradient) NMR experimental results requires including the ions in the simulations. An extension exists for the united-atom model with cations [23], and our dcTST method already includes the necessary tools.

In summary, our method applies dcTST at nonzero loadings without introducing assumptions not already present in traditional TST methods. It can be used to explain diffusion behaviour as a function of loading in any system with enough energy dissipation between hops, so that random-walk theory (the assumption of equilibration between two subsequent jumps) and TST are valid,

as we show here for alkanes in LTA. The method gives results in excellent agreement with MD, but is also applicable in the regime of very slow diffusion where MD can not be used. This extends the range of accessible time scales significantly beyond currently available methods. Furthermore, the method enables us to express loading effects in terms of free-energy differences.

Bibliography

[1] J. M. Thomas, Solid acid catalysts. Sci. Am. **266**, 112 (1992).

[2] C. Saravanan, F. Jousse, and S. M. Auerbach, Phys. Rev. Lett. **80**, 5754 (1998).

[3] E. J. Maginn, A. T. Bell, and D. N. Theodorou, J. Phys. Chem. **100**, 7155 (1996).

[4] K. Hahn, J. Karger, and V. Kukla, Phys. Rev. Lett. **76**, 2762 (1996).

[5] H. Jobic, J. Karger, and M. Bee, Phys. Rev. Lett. **82**, 4260 (1999).

[6] L. A. Clark, G. T. Ye, and R. Q. Snurr, Phys. Rev. Lett. **84**, 2893 (2000).

[7] D. S. Sholl and K. A. Fichthorn, Phys. Rev. Lett. **79**, 3569 (1997).

[8] S. Fritzsche, M. Gaub, R. Haberlandt, and G. Hofmann, J. Mol. Model **2**, 286 (1996).

[9] E. B. Webb, G. S. Grest, and M. Mondello, J. Phys. Chem. B. **103**, 4949 (1999).

[10] S. M. Auerbach, International reviews in physical chemistry **19**, 155 (2000).

[11] D. Dubbeldam, S. Calero, T. L. M. Maesen, and B. Smit, Phys. Rev. Lett. **90**, 245901 (2003).

[12] F. Jousse and S. M. Auerbach, J. Chem. Phys. **107**, 9629 (1997).

[13] R. L. June, A. T. Bell, and D. N. Theodorou, J. Phys. Chem. **95**, 8866 (1991).

[14] C. Tunca and D. M. Ford, Chem. Eng. Sci. **58**, 3373 (2003).

[15] C. H. Bennett, in *Diffusion in Solids: Recent Developments*, edited by A. Nowick and J. Burton (Academic Press, New York, 1975), pp. 73–113.

[16] D. Chandler, J. Chem. Phys **68**, 2959 (1978).

[17] D. Frenkel and B. Smit, *Understanding molecular simulation 2nd edition* (Academic Press, London, UK, 2002).

[18] K. F. Czaplewski and R. Q. Snurr, AIChE Journal 2223 (1999).

[19] J. P. Ryckaert and A. Bellemans, Faraday Dicuss. Chem. Soc. **66**, 95 (1978).

[20] A. G. Bezus, A. V. Kiselev, A. A. Lopatkin, and P. Q. J. Du, J. Chem. Soc., Faraday Trans. II **74**, 367 (1978).

[21] D. Dubbeldam, S. Calero, T. Vlugt, R. Krishna, T. Maesen, E. Beerdsen, and B. Smit, Phys. Rev. Lett. **93**, 088302 (2004).

[22] D. Dubbeldam, S. Calero, T. Vlugt, R. Krishna, T. Maesen, and B. Smit, J. Phys. Chem. B. **108**, 12301 (2004).

[23] E. Beerdsen, B. Smit, and S. Calero, J. Phys. Chem. B **106**, 10659 (2002).

A dynamically corrected Transition-State Theory method is presented that is capable of computing quantitatively the self-diffusivity of adsorbed molecules in confined systems at nonzero loading. This extension to traditional Transition-State Theory is free of additional assumptions and yields a diffusivity identical to that obtained by conventional Molecular Dynamics simulations. While Molecular Dynamics calculations are limited to relatively fast-diffusing molecules, our approach extends the range of accessible time scales significantly beyond currently available methods. We show results for methane, ethane, and propane in LTL- and LTA-type zeolites over a wide range of temperatures and loadings, and demonstrate the extensibility of the method to mixtures.

D. Dubbeldam, E. Beerdsen, T. J. H. Vlugt,
and B. Smit

3

Molecular Simulation of Loading-Dependent Diffusion in Nanoporous Materials using Extended Dynamically Corrected Transition-State Theory

3.1 Introduction

Molecular simulation [1,2] has evolved over the years as a powerful tool to study equilibrium and transport properties of molecules adsorbed in nanoporous materials. It provides an understanding of the microscopic dynamics underlying the macroscopic properties of industrial interest such as the separation of mixtures of molecules [3]. The use of zeolites as a means for chemically clean separations can be considered a prime example of how nanomaterials are able to exploit the critical match between the confinement and the shape and size of the adsorbate. One of the difficulties encountered when studying diffusion behaviour in zeolites using simulation is that many processes occur outside the time scale accessible to Molecular Dynamics, which is currently typically limited to diffusion rates in the order of 10^{-12} m^2/s.

New methods have been developed for circumventing this time-scale prob-

lem [4]. Systems characterised by a sequence of rare events can be described by Transition-State Theory (TST) methods such as the Bennett-Chandler approach [5,6], the method of Ruiz-Montero *et al.* [7], path sampling [8], transition interface sampling [9, 10], hyper-dynamics [11], parallel replica dynamics [12], temperature-accelerated dynamics [13], and on-the-fly kinetic Monte Carlo [14]. In principle, all of these methods have the potential to be orders of magnitude more efficient while still retaining full atomistic detail. In TST approximations one computes a rate constant between states A and B by computing the equilibrium particle flux through the dividing surface. The dividing surface should uniquely divide two connected states A and B, and in general the TST rate is an upper bound on the exact rate. The exact rate can be recovered by running short MD trajectories from the dividing surface to compute a dynamical correction (dc).

Many groups have worked on the time-scale problem. The approach of June *et al.* [15] models self-diffusion of xenon and SF_6 in silicalite at infinite dilution as a series of uncorrelated jumps between potential-energy minima (sites). The rate constants for jumping between the sites are converted to diffusivities by generating continuous-time/discrete-space Monte Carlo random walks. The computed diffusivities were reasonably close to the values computed using conventional MD. Snurr *et al.* [16] developed a hierarchical approach for predicting isotherms of benzene in silicalite. The method can be applied to other systems when molecules adsorb at well-defined sites. In a subsequent paper, Snurr *et al.* [17] investigated the dynamical behaviour of benzene using TST. Diffusion paths connecting pairs of potential energy minima are constructed through saddle points (transition states). Given the rate constants, the self-diffusivity was computed with a kinetic Monte-Carlo simulation. Maginn *et al.* [18] presented a hierarchical approach for simulating the diffusion of n-alkanes up to C_{20} in silicalite using modest computational resources. The simulation strategy utilised concepts from Brownian-motion theory and Transition-State-Theory. Jousse and Auerbach [19] used TST to compute exact rate coefficients for benzene jumps in NaY zeolite. Forester and Smith [20] used constrained reaction-coordinate dynamics (Blue-moon ensemble) to characterise the free-energy profile of benzene in silicalite-1 at 300 K along the mean reaction path for diffusion. The free energies, combined with estimates of the transmission coefficient, were used to obtain rate constants for diffusion between the main adsorption sites. Subsequent kinetic Monte Carlo simulations provided the self-diffusion coefficients. Mossel *et al.* [21,22] studied the diffusion of benzene and p-xylene in zeolite NaY by means of constrained reaction-coordinate dynamics. MD simulations were used to determine the

potential of mean force along the coordinate perpendicular to the window connecting two supercages of the zeolite. Diffusion coefficients and activation energies were determined from a hopping model that considers dynamical corrections. Ghorai *et al.* [23] estimated the rate of passage of CCl_4 through the 8-ring window in a model of zeolite A by combining a direct evaluation of the free-energy profile and an adaptation of the rare-events method. The system contains on average one particle per cage, and because particle-particle interactions rarely occur under this condition, the free energy is evaluated from the one-particle partition function. The self-diffusion of ethane in cation-free LTA-type zeolite has been studied by Schüring *et al.* [24] using MD and TST (without dynamical correction) for various temperatures. The bare TST jump rates were similar to the MD jump rates (where the MD results were also not corrected for short-time recrossings). Dubbeldam and co-workers [25, 26] applied dynamically corrected Transition-State Theory (dcTST) to study abnormal diffusion of linear alkane molecules (C_1-C_{20}) in ERI-, CHA-, and LTA-type zeolites at infinite dilution. The exceptionally slow diffusion rates required the combination of rare-event TST techniques with the configurational-bias Monte Carlo (CBMC) algorithm [1, 27]. The diffusivities were evaluated on a lattice spanned by the cage centers.

It is important to note that these works have been performed at infinite dilution, even though many of the processes of industrial importance occur at nonzero loading [28]. Only a limited number of studies deal with nonzero loading. Tunca and Ford [29] used multidimensional TST to obtain the hopping rate of adsorbates from an α-cage in LTA-type zeolite as a function of loading. Various approximations were applied to make the simulations computationally feasible. In a subsequent study [30] the limitations of an empty receiving cage and the use of the Widom insertion method were avoided. Recently, Tunca and Ford presented a new hierarchical approach to the molecular modelling of diffusion and adsorption at nonzero loading in microporous materials [31]. Although adsorption was well represented, the coarse-grained self-diffusivity data under-predicted the diffusivity at low loading, while significantly over-predicting the diffusivities at higher loadings, in comparison to conventional MD.

Coarse-grained kinetic Monte Carlo (FMC) studies have pointed at the difficulties of computing an elementary hopping rate taking into account the various correlations induced by particle-particle interactions [31, 32]. We extended the dcTST Bennett-Chandler approach to include diffusion of molecules at nonzero loading [33]. It was shown that the particle-particle correlations can be taken into account by a proper definition of an effective hopping rate of a

single particle. The self-diffusivity was computed directly by computing the hopping rate of a molecule over a typical length scale given by the smallest repeating zeolite-structure, i.e. from the center of cage A to the center of cage B. The use of kinetic Monte Carlo and its underlying assumptions are therefore avoided. Implicitly one integrates over the whole volume of the cage and hence all adsorption sites in the cage, irrespective of whether these are well defined or not. All other particles are regarded as a contribution to the external field exerted on this tagged particle. The dcTST extension to finite loadings yielded excellent agreement with that obtained by conventional MD simulations and is applicable in any system containing high free-energy barriers and for any type of guest molecule. In this work, we elaborate on the concepts introduced in ref. [33], and show results for methane, ethane, and propane in LTL-, and LTA-type zeolites over a wide range of temperatures and loadings.

The remainder of the chapter is organised as follows. In section 3.2 we explain the used methods and concepts. First the force field is described, and we present in short the canonical MD algorithm focusing on maintaining temperature control and obtaining diffusion coefficients. Next, we discuss some concepts from random-walk theory, e.g. jump rates and memory effects. We show that TST is fully compatible and consistent with random-walk theory and present our dcTST technique for nonzero loading. Section 3.3 starts with the results on the infinite-dilution case. Two different sets of parameters from literature are used and the difference indicates that the physics of adsorption and diffusion in zeolites is often highly parameter dependent. The main emphasis of the chapter lies on the diffusivity results of methane, ethane, and propane in LTL- and LTA-type zeolites using dcTST compared to MD as a function of loading. For LTA-type zeolite we present additional results of a mixture of methane and ethane. We end with a general discussion on lattices, correlations, and dcTST in section 3.4, and conclusions in section 3.5.

3.2 Methodology

3.2.1 Force Field Parameters for Adsorption and Diffusion of Alkanes in Siliceous Nanoporous Materials

Zeolites are confined systems with pore sizes comparable to the molecular size. Adsorption in cation-free zeolite structures usually takes place at specific sites with little or no electric field. For this reason the united-atom model [34] seems the most straightforward choice. We consider the CH_x groups as single, charge-less interaction centers with their own effective potentials. The beads in the chain are connected by harmonic bonding potentials. A harmonic co-

	O	Si	CH_4	CH_3	CH_2
CH_4	115.00 3.47	-	158.50 3.72	130.84 3.74	94.21 3.84
CH_3	93.00 3.48	-	130.84 3.74	108.00 3.76	77.77 3.86
CH_2	60.50 3.58	-	94.21 3.84	77.77 3.86	56.00 3.96
bond	$U^{\text{bond}} = \frac{1}{2}k_1(r - r_0)^2$ $k_1/k_B = 96500$ K/Å^2, $r_0 = 1.54$ Å				
bend	$U^{\text{bend}} = \frac{1}{2}k_2(\cos\theta - \cos\theta_0)^2$ $k_2/k_B = 62500$ K, $\theta_0 = 114^\circ$				

Table 3.1: *Force field of Dubbeldam et al. [39, 40] for guest-host and guest-guest interactions of hydrocarbons in cation-free nanoporous materials. Lennard-Jones parameters, ϵ/k_B [K] in top-left corner of each field, σ [Å] in the bottom-right corner of each field, bond and bend parameters*

sine bending potential models the bond bending between three neighbouring beads. The Lennard-Jones potentials are shifted and cut at 12 Å. Analytical tail-corrections are not applicable in zeolites [35]. A truncated and shifted potential is equally suitable to Monte Carlo and Molecular Dynamics. Flexibility of the framework is not an issue for adsorption of linear and branched alkanes [36]. For methane in LTA-type zeolite it was found that self-diffusion coefficients obtained with flexible and with rigid lattices are also practically equal [37] (in the discussion section we will comment on this further). The interactions between the rigid framework and the guest molecules are assumed to be dominated by the oxygen atoms [38]. The interaction parameters of alkanes listed in Table 3.1 for use in molecular simulations of confined systems have been obtained uniquely and accurately through fitting on experimental isotherms with inflection points [39, 40]. Recently, it was shown that these parameters also give near-quantitative agreement for collective and transport diffusivity for ethane in silicalite compared to neutron-scattering experiments [41]. Details on the simulations can be found in Refs. [39] and [42]. The parameters listed in Table 3.2 are used mainly for comparison with the simulations of Schüring *et al.* [24, 43], and because their very small size parameters enhance the diffusion by two orders of magnitude for ethane in LTA-type zeolite compared to the parameters of Dubbeldam *et al.* Although the parameters of Schüring *et al.* are probably less realistic in our opinion, they are convenient to compare the diffusion of ethane from a simulation-method point of view by

	O	Si	CH_3
CH_3	142 3.17	82 2.12	104 3.78
bond	$U^{\text{bond}} = \frac{1}{2}k_1(r - r_0)^2$ $k_1/k_B = 96500$ K/Å^2, $r_0 = 1.54$ Å		

Table 3.2: *Force field parameters used by Schüring et al. for ethane in LTA-type zeolite [24]. Lennard-Jones parameters, ϵ/k_B [K] in top-left corner of each field, σ [Å] in bottom-right corner of each field, bond and bend parameters*

MD and dcTST in LTA-type zeolite.

3.2.2 Molecular Dynamics (MD)

In MD simulations [1, 2, 44], successive configurations of the system are generated by integrating Newton's laws of motion, which then yields a trajectory that describes the positions, velocities and accelerations of the particles as they vary with time. The self-diffusion coefficients D_S^α in the direction $\alpha = x, y, z$ are computed by taking the slope of the mean squared displacement (MSD) at long times

$$D_S^\alpha = \frac{1}{2N} \lim_{t\to\infty} \frac{d}{d\,t} \left\langle \sum_{i=1}^{N} \left(r_{i\alpha}\left(t\right) - r_{i\alpha}\left(0\right)\right)^2 \right\rangle \tag{3.1}$$

where N is the number of molecules, t the time, and $r_{i\alpha}$ the α component of the center of mass of molecule i. Equivalently, D_α is given by the time integral of the velocity autocorrelation function

$$D_S^\alpha = \frac{1}{N} \int_0^\infty \left\langle \sum_{i=1}^{N} v_{i\alpha}(t) v_{i\alpha}(0) \right\rangle dt \tag{3.2}$$

where $v_{i\alpha}$ is the α component of the center of mass velocity of molecule i. A separation of time scales occurs for interacting particles roughly at the times between particle-particle and particle-zeolite collisions. (See figure 3.1.) The mean squared displacement thus bends over to attain a different slope, and we are interested in the long-time diffusion coefficient. The collective diffusion coefficients D_C^α are given by

$$D_C^\alpha = \frac{1}{2N} \lim_{t\to\infty} \frac{d}{d\,t} \left\langle \left(\sum_{i=1}^{N} \left(r_{i\alpha}\left(t\right) - r_{i\alpha}\left(0\right)\right) \right)^2 \right\rangle \tag{3.3}$$

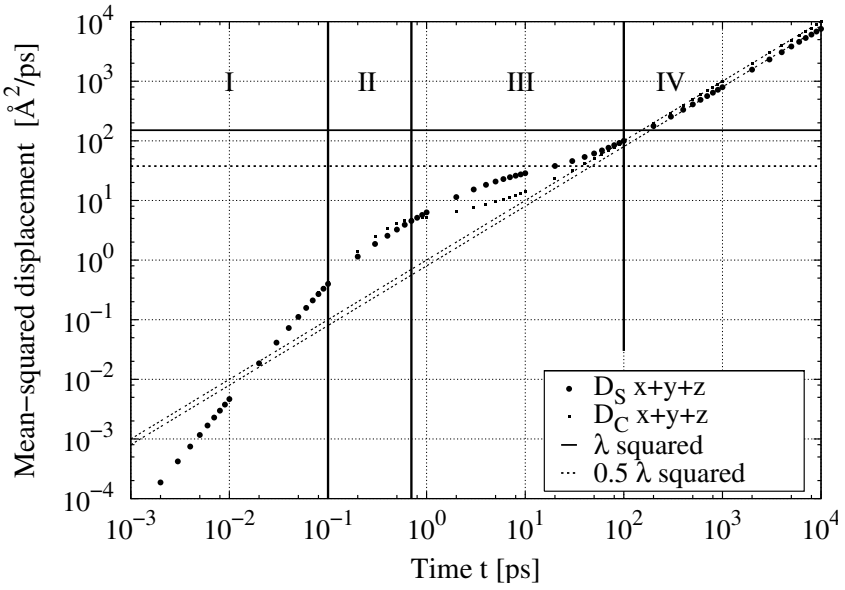

Figure 3.1: *Mean squared displacement of self-diffusivity D_S and collective diffusivity D_C for methane in LTA-type zeolite at 300 K at an average loading of eight molecules per cage. We can identify four distinct regimes (see text). For reference, we show $\left(\frac{1}{2}\lambda\right)^2$ and λ^2, with $\lambda = 12.2775$ Å the cage-center to cage-center lattice distance. The dotted lines are of slope unity and indicate normal diffusive behaviour.*

and

$$D_C^{\alpha} = \frac{1}{N}\int_0^{\infty} \left\langle \left(\sum_{i=1}^{N} v_{i\alpha}(t)\right)\left(\sum_{i=1}^{N} v_{i\alpha}(0)\right)\right\rangle dt \tag{3.4}$$

There are several forms of collective diffusion, the definition given here is in zeolite literature often referred to as *corrected* diffusivity. The inclusion of a thermodynamic factor results in the so-called *transport* diffusivity, which is directly related to the macroscopic Fickian diffusion. The removal of the thermodynamic effect results in a somewhat less loading-dependent quantity. Collective diffusivity measures the transport of mass and the decay of density fluctuations in the system, while self-diffusion measures the diffusive motion of a single particle. The directionally averaged diffusion coefficient is given by

$$D = \frac{D_x + D_y + D_z}{3} \tag{3.5}$$

Note that in simple fluids there is only a time-scale separation for the

self-motion, not for the collective motion. In nanoporous materials, both the displacements of the single particles and the displacements of the center of mass are restricted by the confinement and the time-scale separation is also present in collective diffusion. This is very much related to the diffusion of polymers in melts where similar time-scale separations occur [45]. In figure 3.1 we show the mean squared displacements of the self-and collective motions at 300 K of methane in LTA-type zeolite at an average loading of eight molecules per cage. Several regimes can be identified for this system,

1. At very short time scales both the self and collective motion are ballistic, and the MSD is proportional to t^2.

2. While initially the same, the MSD of self-motion is lowered in comparison to the collective motion due to back-correlation mechanisms that also occur in simple fluids. The onset of regime II is signalling the average mean free time before particles collide.

3. Regime three is dominated by a confinement effect and particles have not yet been able, on average, to hop to the next confinement. The MSD of single particles is restricted to approximately the cage size squared, but results in cancellation for the collective behaviour. The MSD of self-motion is therefore higher than that for collective motion.

4. With increasing times the particles are increasingly able to leave the confinement, and both self-and collective motion increase eventually to a linear diffusive regime IV. Here, particles originating from *different* cages start to collide, and self-motion is again lowered in comparison with collective motion. For collective motion the onset of this hydrodynamic regime is a combined effect of confinement and the time particles start to leave the cage (because here, a change in the collective motion can only be accomplished by cage-to-cage hops of single particles). The onset for self-motion for cage/window-type systems is the cage-size squared, i.e. the average time for a particle to leave a cage.

The calculation of the diffusion coefficients requires much memory and CPU power, especially when fluctuations decay slowly. The order-n algorithm to measure correlations allows us to measure fast and slow dynamics simultaneously at minimal computational cost by using adjustable sampling frequencies [1]. The order-n scheme is equally accurate as the conventional scheme but the savings in memory as well as CPU time are significant for computing the mean squared displacements at long times.

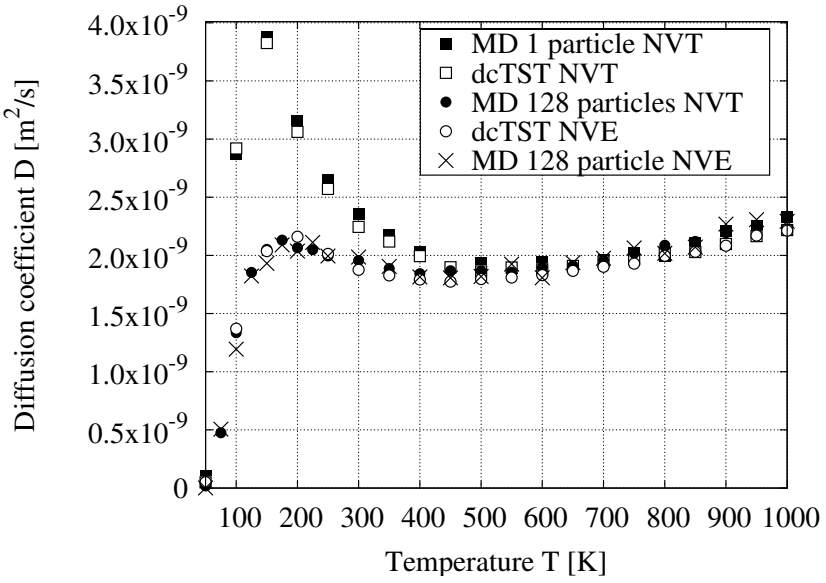

Figure 3.2: *Self-diffusion of ethane at infinite dilution in LTA-type silica using the parameter sets of Schüring et al. The infinite dilution case using MD is simulated by switching the ethane intermolecular forces off, i.e. the particles do not interact (except through the thermostat in NHC-NVT simulations).*

In a conventional NVE Molecular Dynamics simulation, the total energy E, the number of particles N, and the volume V are constant. Hence, MD measures (time) averages in the micro-canonical ensemble, while in a conventional Monte-Carlo simulation the canonical ensemble (NVT ensemble) is probed. The extended Lagrangian approach has become one of the most important tricks for MD in the NVT ensemble and is completely dynamic in origin. The Nosé-Hoover Chain (NHC) formulation extends the Lagrangian with additional coordinates and velocities constraining the system to a constant temperature NVT ensemble. We use the NHC method as implemented by Martyna *et al.* [46] in which the dynamics are still reversible. The instantaneous kinetic temperature fluctuates, but the probability to find the system in a given energy state follows the Maxwell-Boltzmann distribution.

For the instantaneous temperature we measure the total kinetic energy of the system and divide it by the number of degrees of freedom N_f ($3N - 3$ for

a system of N particles with fixed total momentum)

$$k_B T\left(t\right) = \sum_{i=1}^{N} \frac{m_i v_i^2\left(t\right)}{N_f} \tag{3.6}$$

The disadvantage of most methods for working at a constant temperature is that the dynamics are changed in an artificial way. Because in our simulations we do not have photons or electrons, i.e. the system is mechanical, heat is transported at the speed of sound or slower. However, most thermostat methods have a coupling constant, i.e. the masses of the NHC, and the effect of the thermostat on the particles are instantaneous. The NHC masses should therefore be chosen as small possible to alter the dynamics as little as possible. If this is taken care of, the nonphysical effects will be of order $(1/N)$ in general.

Figure 3.2 shows the importance of adequate temperature control. Ideally, a flexible zeolite would provide excellent thermostatting of adsorbed molecules. However, for computational reasons many authors keep the framework rigid, and the thermostatting issue arises. In the NVE ensemble the particles do not exchange energy with the heat bath and thermalization occurs through mutual interactions between the adsorbates. Moreover, rather unphysical ballistic motion may occur, and particles may be stuck in local free-energy minima. The nonphysical effects of the NHC thermostat using a single molecule are clearly present in both MD and dcTST. We note that at high temperatures the thermostat effects are small, but they become significant at very low temperatures. This implies that single-particle diffusion coefficients or correlations *should* be computed in the NVE ensemble, unless a sufficiently large number of particles is used. At infinite dilution this can be accomplished by switching the intermolecular forces off, i.e. the particles do not interact except through the thermostat in NVT NHC simulations. However, even if this is being taken care of, the NHC method is only capable of maintaining adequate temperature control under equilibrium conditions, and therefore breaks down in the limit of high potential-energy barriers [47]. Entropic barriers (e.g. due to constrictions and apertures in zeolite cages and channels) represent no problem.

To prepare the system at the desired temperature in an equilibrium configuration, we initialise the system by the following procedure:

- N molecules are inserted into the framework at random positions in such a way that no overlaps occur with the framework or other particles, and as the positions are accessible from the main cages and channels.
- During the initialisation period we perform an NVT MC simulation to rapidly achieve an equilibrium molecular arrangement.

- After the initialisation steps, we assign all atoms velocities from the Maxwell-Boltzmann distribution at the desired average temperature. The total momentum of the system is set to zero. Next, we equilibrate the system further by performing a NVT MD simulation using the NHC thermostat.

- The equilibration is completed and during the production run we collect statistics using either the NVE or NVT ensemble. Following this equilibration procedure, the average temperature using NVE over the entire production period is usually within a few Kelvins of the desired average temperature, while NVT would give the exact desired average temperature if simulated sufficiently long.

3.2.3 Lattice Random-Walk Theory

Diffusive motion of particles occurs by a series of discrete steps separated by elastic collisions, localised vibrations, and short shuffles. Diffusion is an irreversible macroscopic process, but is actually comprised of reversible microscopic steps, and may be well described by random-walk theory. A random walk is a simple mathematical model for the movement of a particle on a lattice under the influence of some random or stochastic force affecting its direction of motion. It is particularly attractive, because in many instances analytical solutions can be worked out for both static and dynamic properties. From the internal (crystal) structure a lattice can be constructed that determines the lattice topology and the lattice distances. The dynamics of the random walk are uniquely determined once the jumping frequencies k_i for a lattice direction i are specified. The jump frequency is defined as

$$k = \frac{\langle \text{number of successful hops} \rangle}{\text{unit of time}} \tag{3.7}$$

The total jumping frequency k_{tot} is related to the specific jumping frequencies k_i for a given structure by a summation over the lattice connectivity Z:

$$k_{\text{tot}} = \sum_{i=1}^{Z} k_i \tag{3.8}$$

For a jump to be truly random, each of the possible jump directions is chosen with equal probability, the probability that the new lattice site is empty does not enter into any equation (the particles can overlap). The expected value $\langle \mathbf{r}(t) \rangle = 0$, and the chemical-potential driving force $\nabla \mu = 0$ for a simple

regular random walk (necessary for the measurement of the self-diffusivity D_S). However, in real systems, jumps are usually correlated by defined interactions between jumping particles.

Let k_i be the average frequency that a random walker (an atom or molecule) jumps for lattice vector $\boldsymbol{\lambda}_i$, and $\mathbf{r}(t)$ the position of a particular random walker. The position of a particle (relative to the starting position) after a period t (or $n = k\,t$ hops) will be:

$$\mathbf{r}(t) = \sum_{i=1}^{n} \boldsymbol{\lambda}_i \tag{3.9}$$

In primitive cubic crystals there exists one lattice site per unit cell, surrounded by $Z = 6$ neighbours, the lattice vectors are $\boldsymbol{\lambda}_i = \lambda \hat{\boldsymbol{e}}_i$ with

$$\hat{\boldsymbol{e}}_i = \{\{1,0,0\},\{0,1,0\},\{0,0,1\},\{\bar{1},0,0\},\{0,\bar{1},0\},\{0,0,\bar{1}\}\}. \tag{3.10}$$

The distance between two particles should increase with time, which is measured by the spread of the distribution $\langle \mathbf{r}(t) \rangle$

$$\left\langle \mathbf{r}^2(t) \right\rangle = \left\langle \sum_{i=1}^{n} \boldsymbol{\lambda}_i \cdot \boldsymbol{\lambda}_i + 2 \sum_{i=1}^{n-1} \sum_{j=i+1}^{n} \boldsymbol{\lambda}_i \cdot \boldsymbol{\lambda}_j \right\rangle \tag{3.11}$$

written as a sum of diagonal and off-diagonal terms.

For the one-dimensional lattice, the two-dimensional square lattice, and the three-dimensional cubic lattice, all the jumping frequencies k_i and jump vectors are equivalent. Using the relationship

$$\boldsymbol{\lambda}_i \cdot \boldsymbol{\lambda}_j = |\boldsymbol{\lambda}_i|\,|\boldsymbol{\lambda}_j| \cos \Delta\phi_{ij}, \tag{3.12}$$

where $\Delta\phi_{ij}$ is the angle between the i^{th} and j^{th} jump vectors, we find

$$\mathbf{r}^2(t) = n\,\lambda^2 \left(1 + \frac{1}{n} \left\langle \sum_{i=1}^{n} \sum_{j=1}^{n} \cos \Delta\phi_{ij} \right\rangle \right), \tag{3.13}$$

and we can write for $n \to \infty$

$$\left\langle \mathbf{r}(t)^2 \right\rangle = n\,f\lambda^2 = Z k_i\,f\lambda^2 t, \tag{3.14}$$

where f denotes the correlation factor

$$f \equiv 1 + \frac{1}{n} \left\langle \sum_{i=1}^{n} \sum_{j=1}^{n} \cos \Delta\phi_{ij} \right\rangle \tag{3.15}$$

Applying Einstein's equation

$$\left\langle \mathbf{r}\,(t)^2 \right\rangle = n\,2dDt \tag{3.16}$$

yields

$$D = \frac{Z}{2d} f\, k_i \lambda^2 = f\ k_{A\to B} \lambda^2, \tag{3.17}$$

$$= \frac{1}{2d} f\, k_{\mathrm{tot}} \lambda^2. \tag{3.18}$$

This relates the macroscopic self-diffusivity to the jump frequency k, lattice-hop distance λ and correlation factor f. The basic assumption of the random-walk model is the quick loss of memory of the molecules between consecutive jumps, i.e. a molecule will proceed with a probability independent of its history. The correlation factor f contains *all* memory effects, arising from ordering and interparticle interactions.

The regular random walk has no "memory" of the previous step when determining the current one. This feature can be applied to a wide range of physical problems, but there are a number of other interesting problems for which this is not the case. In a persistent walk, the transition (or step) probability depends upon the previous transition, and a particle has a retention to the directional over a certain number of trajectory steps. In order for a simplistic regular lattice model to be valid, the loss of memory is an important condition that has to be satisfied.

3.2.4 Correlations

The collective diffusivity contains all the dynamical correlations. Here, the motion results from the jumps of *different* particles at different times. In contrast, for self-diffusivity the motion results from the jumps of a *tagged* particle at different times. Memory effects [48, 49] have a tendency to decrease D_S with respect to D_C, indicating it is somehow related to the well-known back-correlation mechanism where a diffusing particle has a higher probability to jump backwards than in any other direction, simply because the originating site is guaranteed to be empty. Most of the memory effects arise from ordering and interparticle interactions, the latter giving the leading contribution. Figure 3.3 shows the self- and collective diffusivity of methane in LTA-type zeolite at 300 K as a function of loading. In the low-loading limit both diffusivities converge, because particle-particle interactions vanish. However, at a loading of seven molecules per cage or higher the correlations are clearly visible. Although in principle conventional MD captures all relevant correlations,

the dcTST method of chapter 2 not only captures these correlations correctly but is also suitable for systems with large free-energy barriers [33]. These correlations, originating from particle-particle interactions, are significant at higher loadings as is evidenced by the large difference between collective and self-diffusivities.

Memory effects are stronger on single-particle motion than on the collective motion, where most of the back-correlations cancel out. For a Langmuir gas, where the only interaction is the site exclusion, they cancel out *exactly*. Correlations between successive jumps can be studied by considering *directional* correlations between two jumps separated by m previous jumps by a tagged particle. For a Langmuir gas the factor f reduces in the high-loading limit to [48]

$$f = \frac{1 + \langle \cos \phi \rangle}{1 - \langle \cos \phi \rangle} \tag{3.19}$$

as a correlation factor for vacancy diffusion, where ϕ is the average angle between two consecutive single-particle jumps. This equation assumes that the predominant memory contribution comes from the back-correlation between two consecutive single-particle jumps ($m = 1$). eq. 3.19 is very much related to the end-to-end distance of an isolated, infinitely long, hypothetical model chain comprised of bonds of fixed lengths joined with fixed bend angles [50]. Unlike the freely joined case, the fixing of the angles ϕ imposes correlations.

A particle residing in a lattice point once in a while jumps to a neighbouring site. If thermalization occurs we call it a *single jump*, otherwise we speak of a *long jump* or a *multi-jump*. These kinetic correlations become important at low loadings and in channel-type structures with smooth walls, e.g. carbon nanotubes. However, for entropy-dominated barriers (e.g. methane and ethane in LTA-type zeolites) one can usually neglect kinetic correlations.

3.2.5 Dynamically Corrected Transition-State-Theory (dcTST) at Infinite Dilution

At infinite dilution and sufficient dissipation, the correlation factor $f = 1$ (there are no memory effects), and eq. 3.17 reduces to

$$D = k_i \lambda^2 = k_{AB} \lambda^2 \tag{3.20}$$

The lattice distance λ is fixed and is a property that can be obtained from crystal X-ray scattering experiments. Therefore, eq. 3.20 defines k_i as the hopping rate from lattice point A (in equilibrium) to a neighbouring lattice point B (in equilibrium). Note that an attempt of a hop is always successful,

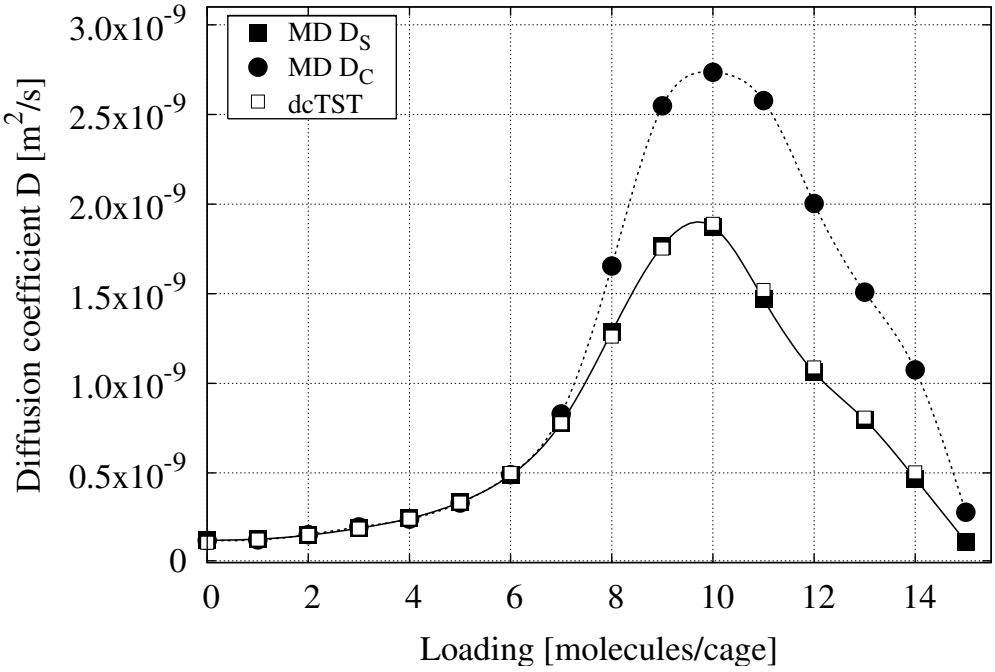

Figure 3.3: *Self-diffusivity D_S and collective diffusivity D_C for methane in LTA-type zeolite at 300 K as a function of loading.*

and that a particle cannot have a position in between the lattice points, i.e. the jump is instantaneous and discrete. In principle, one could use MD simulations to determine this rate, by computing the average residence time of a particle in a cage. However, such a computation using MD proves cumbersome. Firstly, an A-to-B order parameter has to be defined, secondly, a criterion should be used to distinguish unsuccessful hops on a very short time scale from the successful AB-hop on a much longer time scale (the equilibrium one), and thirdly, very few trajectories will involve motion from exactly point A to point B.

Dynamically corrected Transition-State Theory overcomes these problems by computing precisely what we need: the hopping rate from lattice point A (in equilibrium) to a neighbouring lattice point B (in equilibrium). In other words, dcTST is fully compatible and complementary to lattice random-walk theory. We consider a system that can be in two stable states, A and B. The reaction coordinate, a parameter that indicates the progress of the diffusion event from region A to region B, is denoted by q. Here, q is a function of the Cartesian coordinates, $\dot{q}$ denotes its time derivative, q^* is the location of the

dividing surface, and q_A, q_B are the minima in the free energy corresponding to state A and B, respectively. In general, the reaction coordinate q is a function of the configuration of the whole system, i.e. $q = q(\mathbf{r}_1, \ldots, \mathbf{r}_N)$. However, we can choose q as the position of one of the atoms of the diffusing molecules [25]. We introduce two characteristic functions n_A and n_B that measure whether the system is in state A or B. A possible and often-used definition is

$$n_A = \theta\left(q^* - q\right), \tag{3.21}$$

$$n_B = \theta\left(q - q^*\right), \tag{3.22}$$

where θ is the Heaviside function $\theta(x)$, which has a value zero for $x < 0$ and a value of unity for $x \geq 0$. With these definitions the transition rate $k_{A\to B}$ is given by [7]

$$k_{A\to B} = \underbrace{\frac{\langle \delta\left(q^* - q\right)\rangle}{\langle \theta\left(q^* - q\right)\rangle}}_{P_{\in A}(q^*)} \times \underbrace{\frac{\langle \dot{q}(0)\delta\left(q^* - q(0)\right)\theta\left(q\left(t\right) - q^*\right)\rangle}{\langle \delta\left(q^* - q(0)\right)\rangle}}_{R(t)}, \tag{3.23}$$

where δ is the Dirac delta function, $P_{\in A}\left(q^*\right)$ is the equilibrium probability density of finding the system at the top of the barrier divided by the equilibrium probability of finding it at state A, and $R\left(t\right)$ is the averaged particle flux at the top of the barrier multiplied by the probability that the system ends up in state B at time t. From detailed balance follows

$$\frac{k_{A\to B}}{k_{B\to A}} = \frac{\langle n_B\rangle}{\langle n_A\rangle} \tag{3.24}$$

where $\langle n_A\rangle$ is the equilibrium mole fraction of particles in state A,

$$\langle n_A\rangle = \frac{\int_A e^{-\beta F(q)}\, dq}{\int_{A+B} e^{-\beta F(q)}\, dq} \tag{3.25}$$

$$\langle n_B\rangle = \langle 1 - n_A\rangle \tag{3.26}$$

The expression eq. 3.23 is rigorously correct for arbitrary crossings provided that

- the actual crossing time is negligible compared to the time a particle spends inside the cage, i.e. there is a large separation in time scales. This condition is satisfied when the free-energy barrier is much larger than $k_B T$.

- the velocity distribution at the dividing surface is known. (The order parameter q is taken to be the position of a particle, and therefore $\dot{q}$ is simply the velocity of a particle. In TST is it assumed that the top of the barrier is in equilibrium and hence these velocities follow directly from the Maxwell-Boltzmann distribution).

At infinite dilution the molecules perform a random walk on a lattice spanned by the cage centers. The transmission rates are easily converted to diffusion coefficients if the jump distance and the number of equivalent diffusion paths are known.

It turns out that eq. 3.23 can be written a product of a static and a dynamic term.

- the probability $P_{\in A}(q^*)$ of finding the system at the top of the barrier is a *time-independent* equilibrium quantity and can be computed explicitly,

$$P_{\in A}(q^*) = \frac{\langle \delta(q^* - q) \rangle}{\langle \theta(q^* - q) \rangle} = \frac{e^{-\beta F(q^*)}}{\int_{\text{cage A}} e^{-\beta F(q)} \, \mathrm{d}q}, \tag{3.27}$$

  where $F(q)$ is the free energy as a function of the diffusion path q.

- the flux $R(t)$ through the dividing surface is a conditional average, namely the product $\dot{q}(0)\,\theta(q(t) - q^*)$, given that $q(0) = q^*$. Using the assumption that the velocities of the atoms follow the Maxwell-Boltzmann distribution, we can estimate from kinetic theory the long-time value of $R(t)$ by $\left\langle \frac{1}{2}|\dot{q}| \right\rangle = \sqrt{\frac{k_B T}{2\pi m}}$, where m is the mass of the segments of the particle involved in the reaction coordinate (the total mass of the particle if the center of mass is used or the mass of only one segment if the reaction coordinate is a single segment like the middle bead in a molecule). Transition-State Theory predicts a crossing rate $k^{\text{TST}}_{A\to B}$ given by

$$k^{\text{TST}}_{A\to B} = \sqrt{\frac{k_B T}{2\pi m}} \frac{e^{-\beta F(q^*)}}{\int_{\text{cage A}} e^{-\beta F(q)} \, \mathrm{d}q}. \tag{3.28}$$

  Calculating TST rate constants is therefore equivalent to calculating free-energy differences.

  The TST particle-flux estimate $\sqrt{\frac{k_B T}{2\pi m}}$ contains spurious crossings, i.e. some particles that cross the transition state from A in reality would fail to equilibrate in B. The correction $\kappa(t)$ is defined as the ratio between the real rate and the TST expression,

$$\kappa(t) \equiv \frac{k_{A\to B}(t)}{k^{\text{TST}}_{A\to B}} = \frac{\langle \dot{q}(0)\delta(q(0) - q^*)\,\theta(q(t) - q^*) \rangle}{\left\langle \frac{1}{2}|\dot{q}(0)| \right\rangle}. \tag{3.29}$$

It is the probability that a particle that starts with an initial velocity $\dot{q}$ from the dividing surface will in fact cross the barrier, and therefore $\kappa(t)$ corrects for trajectories that cross the transition state from A but fail to equilibrate in B. The numerator in eq. 3.29 counts trajectories with a positive, but also with a negative weight. It can be shown that $\lim_{t\to 0^+} \kappa(t) = 1$ and $\lim_{t\to 0^+} k_{A\to B}(t) = k^{\mathrm{TST}}_{A\to B}$. There is a large separation of time scales. The transmissions are completed in a very short time, and eq. 3.29 will reach a plateau value κ. For classical systems $0 < \kappa \leq 1$ and eq. 3.28 is corrected as

$$k_{A\to B} = \kappa\, k^{\mathrm{TST}}_{A\to B}. \tag{3.30}$$

Standard Molecular Dynamics (MD) yields the transmission coefficients, a separate MC simulation is used to generate the starting configurations. The reaction coordinate is restricted to the dividing surface q^*. The MC moves involved are translations of the reaction bead in the plane of the dividing surface and complete regrowing of the molecule starting from the restricted bead. Subsequently, the transmission coefficient is calculated by standard MD in the NVE ensemble. The beads are given independent velocities, corresponding on average to the desired temperature, by sampling from the Maxwell-Boltzmann distribution.

In the Bennett-Chandler approach it is sufficient to assign the barrier position q^* inside the barrier region. The result of the scheme does not depend on the specific location, although the statistical accuracy does. If the dividing surface is not at the top of the barrier, the probability of finding a particle will be higher than at the optimal q^*, but the fraction of the particles that actually crosses the barrier will be smaller than predicted by Transition-State Theory.

3.2.6 Importance-Sampled MD at Infinite Dilution

The approach of $\kappa(t)$ to its plateau value can be quite slow [7]. Moreover, in the case of diffusive barrier crossings the transmission coefficient is quite small and as a consequence many trajectories have to be generated for an accurate value of κ. The Bennett-Chandler approach becomes inefficient for systems with low transmission coefficients, because the scheme employs the noisy θ function to detect in what state the system is [51]. The scheme can be improved by constructing a more continuous detection function. More importantly, using the free energy we can compensate approximately for the effect of the free-energy barrier. This leads to a more or less uniform tagged-particle density distribution over the entire range of q. However, only trajectories starting in

the barrier region yield relevant information and therefore a weighing function $w(q)$ is applied, restricting the sampling to the barrier region.

A general expression from Transition-State Theory for the rate of hopping from region A to region B over a barrier is [7]:

$$k_{A\to B} = \frac{1}{\langle n_A \rangle_{\text{eq}}} \left\langle \dot{q}\left(0\right) n_A\left(t\right) \frac{\partial \chi\left(q\left(0\right)\right)}{\partial q} \right\rangle, \tag{3.31}$$

where $\chi\left(q\right)$ is a dimensionless function describing the initial distribution function

$$\rho\left(q, t=0\right) = \rho_{\text{eq}}\left(q\right)\chi\left(q\right). \tag{3.32}$$

The initial distribution $\chi\left(q\right)$ can be approximated well by the steady-state distribution determined from the Fokker-Planck equation

$$\chi\left(q\right) = \frac{1}{\langle n_A \rangle}\left[1 - \frac{\int_{q_A}^{q} e^{\beta F(q')}\, dq'}{\int_{q_A}^{q_B} e^{\beta F(q')}\, dq'}\right], \tag{3.33}$$

and varies rapidly with q in the barrier region and slowly elsewhere, so that $\frac{\partial \chi(q)}{\partial q}$ selects initial configurations in the barrier region

$$\frac{\partial \chi\left(q\right)}{\partial q} = -\frac{1}{\langle n_A \rangle} \frac{e^{\beta F(q)}}{\int_{q_A}^{q_B} e^{\beta F(q)}\, dq}. \tag{3.34}$$

We choose

$$n_A\left(q\right) = 1 - \frac{\int_{q_A}^{q} e^{(a-1)\beta F(q')}\, dq'}{\int_{q_A}^{q_B} e^{(a-1)\beta F(q')}\, dq'}, \tag{3.35}$$

$$w(q) = e^{a\beta F(q)}, \tag{3.36}$$

$$\pi\left(q\right) \propto e^{(a-1)\beta F(q)}, \tag{3.37}$$

where $a > 0$ is a biasing parameter, leading to

$$k_{A\to B} = \frac{1}{\langle n_A \rangle} \frac{\left\langle \int_0^\infty \dot{q}\left(t\right)\dot{q}\left(0\right) \frac{w(q(t))}{w(q(0))} \frac{e^{-\beta F(q(t))}}{e^{-\beta F(q(0))}}\, dt \right\rangle_\pi}{\int_{q_A}^{q_B} e^{\beta F(q)}\, dq \int_{q_A}^{q_B} e^{-\beta F(q)}\, dq} \tag{3.38}$$

Although eq. 3.38 can be considered a TST method using a more continuous "detector" function than the noisy θ function, it can also be viewed as an MD method in which starting configurations are sampled in a more convenient ensemble $\pi\left(q\right) \propto w(q)e^{-\beta F(q)}$ and subsequently a weighted velocity autocorrelation is computed. It is important to note that the actual dynamics of the

particles are still generated using MD in the micro-canonical without a biasing potential. Importance-sampled MD is especially applicable to systems with erratic free-energy landscapes, e.g. multiple barriers of possibly different heights. Note that the expression given by Ruiz-Montero *et al* in Ref. [7] reduces to eq. 3.38 with $a = 2$ when the estimated free energy in their expression is the true free energy.

3.2.7 Dynamically Corrected Transition-State Theory at Nonzero Loading

The extension of dcTST to finite loading is nontrivial. Conventional methods use a hierarchical approach to compute elementary hopping rates $k^{\text{iso}}_{A\to B}$ between *isolated* cages A and B for use in a subsequent kMC scheme to obtain diffusion coefficients. However, the fundamental question is whether it is *possible* to compute an elementary hopping rate $k^{\text{iso}}_{A\to B}$, in which the contributions of other cages are separated from the contribution of the cages A and B only. Let us consider the class of window/cage-type systems (e.g. methane in LTA) where the barriers are *entropic* in nature. At nonzero loading a molecule hopping from A to B introduces a vacancy. While in principle a particle originating from any of the surrounding cages could fill the vacancy, hierarchical approaches will allow only a molecule from B to return to A (e.g. by blocking all windows except the window between cages A and B). The fundamental assumption of kMC (no two jumps can occur at the same time) artificially suppresses these correlated jumps, and we are not aware of a scheme that results in effective kMC hopping rates that regain those correlations. Another way of looking at this is that the correlated jumps should be identified as elementary kMC moves.

We proposed a method to compute diffusivity values directly in systems with high free-energy barriers (e.g. cage/window-type zeolites) [33]. Here long-time, large-distance memory effects are negligible, because once a molecule jumps, thermal equilibration takes place and next-nearest cage correlations are rare. It is therefore sufficient to include correlations *during* the jump across the barrier. Hence, we compute

$$D\left(c\right) = \frac{1}{6} k^{\text{eff}}_{A\to B}\left(c\right) \lambda^2 \tag{3.39}$$

$$k^{\text{eff}}_{A\to B}\left(c\right) = f\left(c\right) k_{A\to B}\left(c\right) \tag{3.40}$$

where c denotes the loading in molecules per unit cell, or mol/kg. But rather than attempting to compute $k_{A\to B}\left(c=0\right)$ or $k^{\text{iso}}_{A\to B}$ from a molecular simulation and the correlation factor $f\left(c\right)$ from a coarse-grained kinetic Monte Carlo

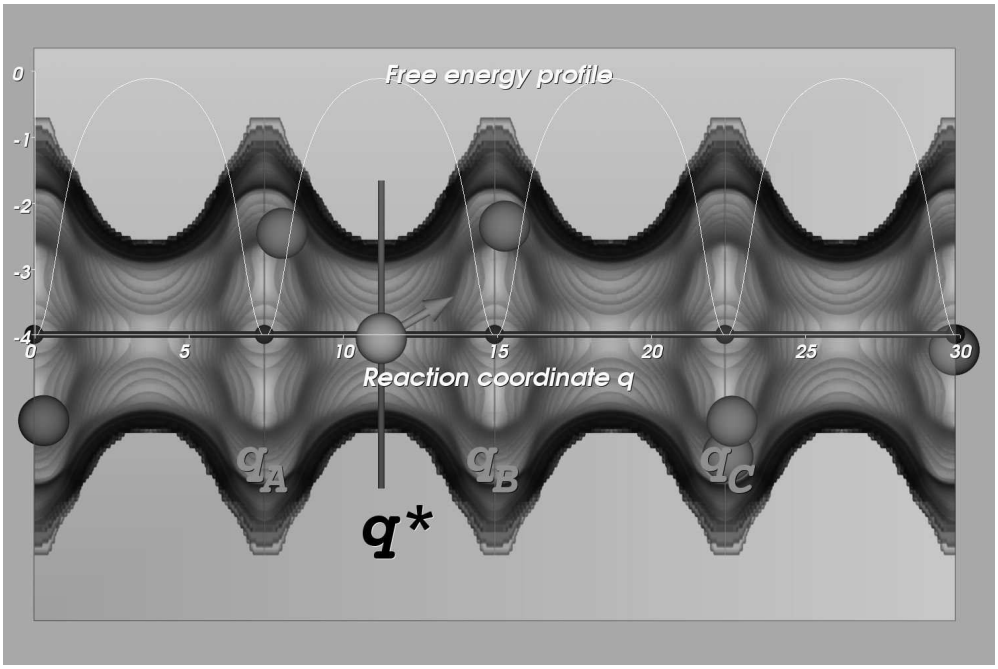

Figure 3.4: *A typical snapshot of a tagged methane particle (with arrow attached) in LTL-type zeolite restrained to the barrier surface q^* at an average loading of three methane molecules per unit cell – there are two parallel channels per unit cell – at 300 K. Four unit cells of 7.474 Å in length are shown. The constrictions are caused by the 12-T-membered rings, which form free-energy barriers impeding diffusion. The free-energy profile in units of $k_B T$ at this average loading is plotted in white, where the reaction coordinate is chosen parallel to the channel direction. If the free-energy barriers are high enough, diffusion can be considered a hopping process from minimum to minimum (q_A, q_B, q_C etc).*

method, we compute $k^{\text{eff}}_{A\to B}(c)$ *directly* from a molecular simulation, where the precise definition of $k^{\text{eff}}_{A\to B}(c)$ is:

> $k^{\text{eff}}_{A\to B}(c)$ is the hopping rate of a single tagged particle at an average loading c from cage A to cage B under the influence of an external field exerted by the molecular sieve *and* the other $N-1$ particles.

By including the nearest neighbouring cages, all relevant short-time correlations are properly captured, including the dominant short-time back-correlation effects due to particle-particle interactions. Correlations at much longer times

than $1/k$ are negligible in cage/window-type systems. The computation once again consists of two parts

- The probability density $P_{\in A}(q^*)$ of finding the system at the top can be computed explicitly by computing free-energy profiles, making use of eq. 3.27. During an separate MC simulation in the NVT ensemble at the desired loading, we measure the free energy $F(q)$, using Histogram Sampling (HS). In the HS method, a histogram is made of the particle positions, mapped on the reaction coordinate. From the histogram a free-energy profile is computed, by using

$$\beta F(q) = -\ln \langle P(q) \rangle \,. \tag{3.41}$$

  At conditions where conventional MC is still feasible, all particles can be considered equivalent and all contributions can be used.

  When displacement of particles is impeded by high free-energy barriers, conventional HS becomes unfeasible. A single tagged particle can be biased to achieve improved statistics by using importance sampling. As a biasing potential, the Widom Particle Insertion (WPI) profile can be used. WPI uses a probe particle that is inserted at random positions, to measure the energy required for, or obtained by, insertion of the particle in the system. This energy is mapped onto the reaction coordinate q, using

$$\beta F(q) = -\ln \left\langle e^{-\beta \Delta U} \right\rangle_N , \tag{3.42}$$

  to produce a free-energy profile, where $\left\langle e^{-\beta \Delta U} \right\rangle_N$ is the average Boltzmann factor over all positions in the slice perpendicular to the reaction coordinate. A "ghost particle" is used as the measuring probe, but the other particles in the system do not feel its presence. At higher loadings, WPI is known to give erroneous results [1, 33] and therefore the WPI method is not used to compute F(q) directly, but rather to estimate the biasing function when needed.

- The particle flux $R(t)$ through the dividing surface can be computed from the fraction of particles starting on top of the barrier that successfully reach cage B. The other particles present in the system influence this fraction. Starting configurations are generated with one particle constrained to the dividing surface and $N-1$ particles moving around (see Figures 3.4 and 3.5). These configurations are then used to compute the particle flux in unconstrained NVE-MD simulations, starting with velocities sampled from a Maxwell-Boltzmann distribution at the desired temperature.

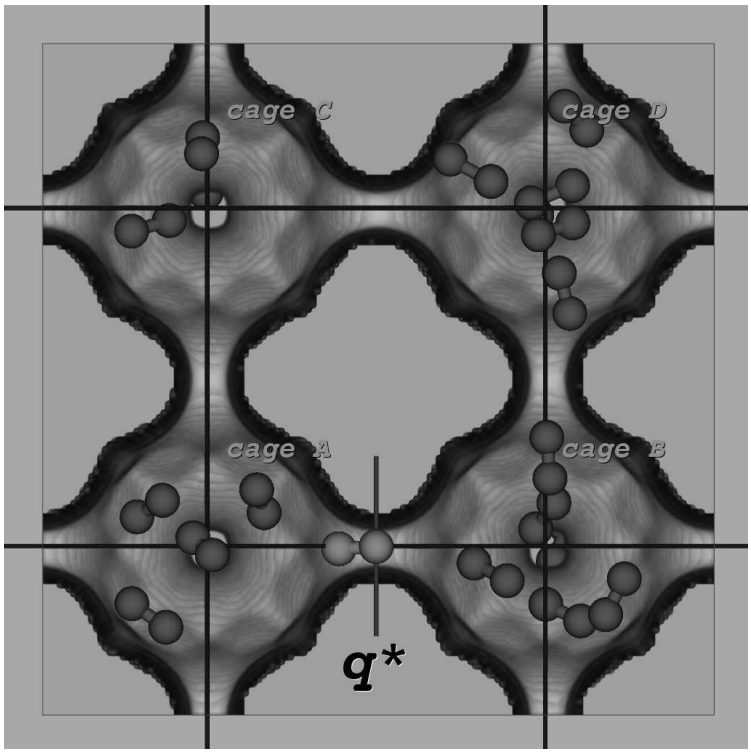

Figure 3.5: *A typical snapshot of ethane ($CH_3 - CH_3$) in LTA-type zeolite at an average loading of four molecules per cage at 750 K, constraining one tagged molecule at the dividing surface q^*. The hopping events are coarse-grained on a lattice spanned by the cage centers.*

In figure 3.4 an instructive snapshot of methane in LTL-type zeolite at a loading of three molecules per unit cell at 300 K is shown. The free energy profile consists of maxima, corresponding to geometric constrictions, and minima, corresponding to the apertures. A natural hopping lattice is formed by the one-dimensional sequences of free-energy minima (q_A, q_B, q_C, etc). As can be inferred from this snapshot, there are strong adsorption sites where the curvature of the zeolite is the highest and commensurate with the shape of the particle. Particles reside in these minima for a long time, before a thermal excitation will eventually give the particles enough mobility to cross the free-energy barrier and proceed to a neighbouring lattice site. The latter process is a *fast* process in comparison to the time a particle spends near the lattice points.

Figure 3.5 shows a snapshot of ethane at an average loading of four molecules

per cage, at 750 K, in LTA-type zeolite. The lattice, formed by the cage centers, is the three-dimensional cubic lattice. For this snapshot, cage B contains more molecules than cage A, and the barrier molecule has a high probability of recrossing to cage A. The time-dependent transmission coefficient will reach a plateau value κ. However, because during a successful hop cage A has donated a particle, while cage B has received an additional particle, there is a slightly higher probability for the particle to return to A on a time scale *larger* than the thermalization time. However, for our systems this effect is negligible. Note that during the computation none of the windows is blocked and simultaneous jumps (e.g. from cage C to cage A, and cage D to cage B) are allowed.

The extension of the importance-sampled MD method of eq. 3.38 to nonzero loading is similar. The method can be summarised as follows.

- The free-energy profiles at the desired average loading are measured as described above.
- The free-energy minima q_A and q_B, and the corresponding hopping lattice are identified.
- A biasing profile $w(q)$ is constructed, ranging from q_A to q_B using eq. 3.36.
- Starting configurations are sampled in the interval q_A to q_B with the biasing potential $w(q)$ operating only on the tagged particle, leaving the other $N-1$ free to move (unbiased).
- These starting configurations of N particles are integrated using MD for short times $t_{\max}$, and eq. 3.38 is evaluated. The time $t_{\max}$ is chosen such that the integral appearing in eq. 3.38 has converged. The trajectories are stopped after $t_{\max}$ time has elapsed or when $q < q_A$ or when $q > q_B$.

As mentioned, in general, the reaction coordinate q is a function of the configuration of the whole system. For dcTST simulations at a certain loading, we choose the reaction coordinate as the position of one of the atoms of the *tagged* molecule [33]. Although it cannot be excluded that better reaction coordinates exists, for physical reasons our choice seems optimal. The diffusion mechanism is divided into two parts. The first is a static term, corresponding to the locations of preferable adsorption sites and estimates of free-energy barriers in between, the latter (or actually the inverse of the transmission coefficient: the recrossing) corresponds to collision frequencies, which generally increase with loading. As such, the dcTST method is able to explain different diffusion regimes over loading, and provides insight into the mechanisms behind an increase or decrease in diffusivity with loading [52].

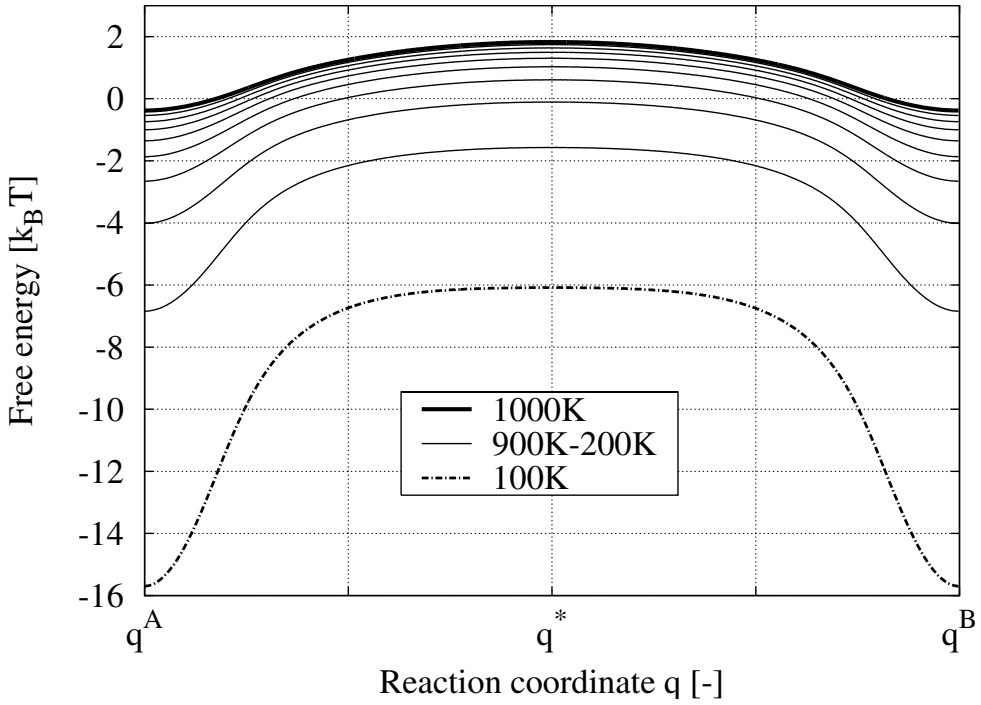

Figure 3.6: *Free-energy profiles $F(q)$ of methane in LTL at various temperatures (100 K to 1000 K in steps of 100 K) at infinite dilution. The reaction coordinate is chosen along the z channel direction (lines from top to bottom in order of the legend).*

3.2.8 Zeolite Descriptions and Simulation Details

To test and explore the limits of our dcTST method, we selected two types of zeolites: the one-dimensional channel LTL-type zeolite structure and the three-dimensional cage/window LTA-type zeolite structure. The LTA-type zeolite is selected because diffusion is slow, but just fast enough for the smallest alkanes to allow for a comparison of dcTST with MD. Here, dcTST is expected to work flawlessly. In LTL-type zeolite the diffusion is relatively fast, the free-energy barriers low, and the system is close to the limits of TST, i.e. in this system it is more difficult to envision a clear separation of time scales. Moreover, the system is one-dimensional and correlations between diffusing particles are even higher.

LTL-type zeolites are used industrially for the aromatisation of alkanes. The structure [53] has space group P_6/mmm with $a = 1.84, b = 1.84, c =$

LTL			LTA		
molec./uc	unit cells	N	molec./cage	unit cells	N
1	1x2x128	256	1	2x2x2	64
2	1x2x64	256	2	2x2x2	128
3	1x2x64	384	3	2x2x2	192
4	1x2x32	256	4	2x2x2	256
5	1x2x32	320	5	2x2x2	320
6	1x2x32	384	6	2x2x2	384
7	1x2x16	224	7	2x2x2	448
8	1x2x16	256	8	1x1x1	64
9	1x2x16	288	9	1x1x1	72
10	1x2x16	320	10	1x1x1	80
11	1x2x16	352	11	1x1x1	88
12	1x2x16	384	12	1x1x1	96
13	1x2x16	416	13	1x1x1	104
14	1x2x16	448	14	1x1x1	112
15	1x2x16	480	15	1x1x1	120
16	1x2x16	512	16	1x1x1	128
Framework density [kg/m^3]					
1626.94			1285.228		
unit-cell sizes [nm]			unit-cell angles [°]		
x	y	z	α	β	γ
3.1984	1.8466	0.7476	2.4555	2.4555	2.4555
90	90	90	90	90	90

Table 3.3: *Simulation details for the LTL- and LTA-type zeolite. Crystallographic positions are taken from Refs. [53, 54].*

0.752 nm, and $\alpha = \beta = 90\circ, \gamma = 120\circ$. For computational efficiency, the unit cell is converted to a rectangular cell. LTL-type zeolite provides a pore system having cancrinite cages (11-hedra) alternating with hexagonal prisms (8-hedra), stacked in columns parallel to the **c** axis. The channels thus formed have nearly planar 12-membered rings with a free diameter of approximately 0.71 nm and expansions of approximately 0.126 nm (see figure 3.4).

The single largest use of zeolites is the use of LTA-type zeolites for laundry detergents. LTA-type zeolite is also used for separations of small molecules from air by exploiting differences in the polarities of molecules, and for bulk separations of linear and branched alkanes. The LTA-type structure [54] has a cubic space group $Fm\bar{3}c$ with $a = b = c = 2.4555$ nm, and $\alpha = \beta = \gamma = 90°$.

The crystallographic unit cell consists of eight large spherical cages (named α cages) of approximately 1.12 nm, interconnected via windows of about 0.41 nm diameter (see figure 3.5).

In addition to the relevant cages and channels, there are also topologically disconnected pockets. A methane molecule does fit at that position, but it is not accessible from the main cages and channels. Both LTA (sodalite cages), and LTL have disconnected pockets. To obtain correct results in MC simulations it is necessary to ensure that molecules will not be inserted into inaccessible pockets for adsorbing molecules.

We have summarised the details of our periodic simulation boxes in Table 3.3. Simulation of one-dimensional channels requires special attention. Here, diffusion results are very much dependent on the length of the channel, and surprisingly long channels are needed to reliably extrapolate to macroscopic diffusion coefficients [55].

3.3 Results

3.3.1 Infinite Dilution

3.3.1.1 Methane, Ethane, and Propane in LTL Zeolite

Figure 3.6 shows the free-energy profiles $F(q)$ of methane along the channel direction. Two free-energy minima are separated by a 12-ring forming the free-energy barrier at q^*. For this system and the chosen reaction coordinate, the transmission coefficient is nearly equal to one, and the dcTST diffusion can be directly computed using Eqs. 3.20 and 3.28. The free-energy barrier ranges from about 10 k_BT at 100 K to less than 3 k_BT at 1000 K. The transmission coefficient can only be assumed equal to one for a single, spherical particle provided the exact barrier is known, and only at infinite dilution. Even for methane in LTL, the barrier is only known approximately, because of the atomic structure of the window, although the value is very close to 1 using the window as the dividing surface. In figure 3.7, the transmission coefficient $\kappa(t)$ for propane using the second/middle-bead as the reaction coordinate is shown as a function of time for various temperatures. The starting configurations are sampled using a Monte-Carlo scheme at the desired temperature, restricting the growing bead to the dividing surface. This distribution of configurations is temperature dependent, as is the transmission coefficient. In general, the transmission coefficient increases with temperature, because a larger fraction of configurations has sufficient kinetic energy to overcome the free-energy part resulting from a nonoptimal reaction coordinate and dividing-surface choice.

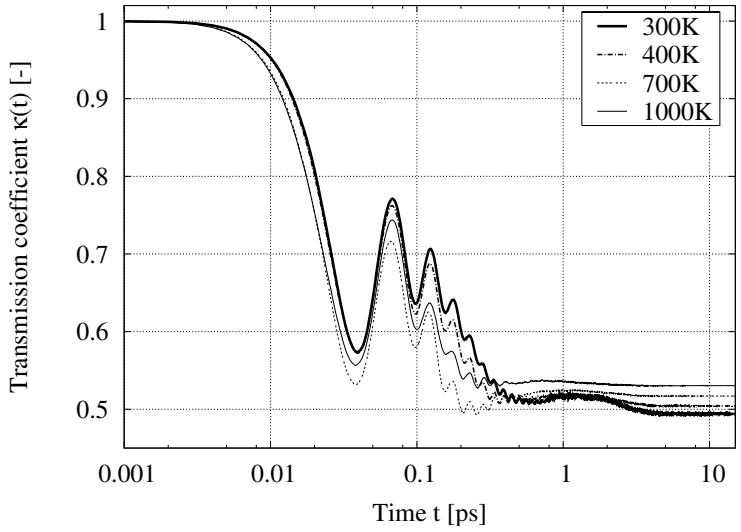

Figure 3.7: *Transmission coefficient $\kappa(t)$ for propane in LTL-type zeolite at infinite dilution using the second/middle-bead as a function of time for various temperatures.*

The transmission coefficient starts at 1 (by definition, because a particle cannot revert its velocity within a single integration step), and slowly converges to a limiting plateau value at about 15 ps. It is this plateau value κ that is of interest, signalling all short-time recrossings have been eliminated. The intermediate oscillatory behaviour is caused by the bond springs within the molecule itself. From the point of view of the reaction coordinate (the position of the second/middle-bead), the other beads connected to the middle-bead with springs are just an external field in addition to the zeolite.

The transmission rates can be computed from the free-energy profiles using eqs. 3.28 and 3.30, and transmission coefficients, and then converted to diffusion coefficients using eq. 3.20. The methane, ethane, and propane diffusivities computed from dcTST are compared to reference MD simulations in Figure 3.8. The MD simulations were performed in the NVE and NVT ensembles (NHC thermostat) with 128 noninteracting particles. For methane, up to 450 K (barriers higher than 3.5 k_BT) dcTST gives results equivalent to MD, but at higher temperatures the methods diverge. For ethane, the methods diverge at 550 K, while for propane both methods overlap. Where the methods diverge, the free-energy barriers become too low for TST to be valid, because there is no longer a clear separation of time scales. The methane molecules do not equilibrate properly, leading to enhanced diffusion due to kinetic correlations,

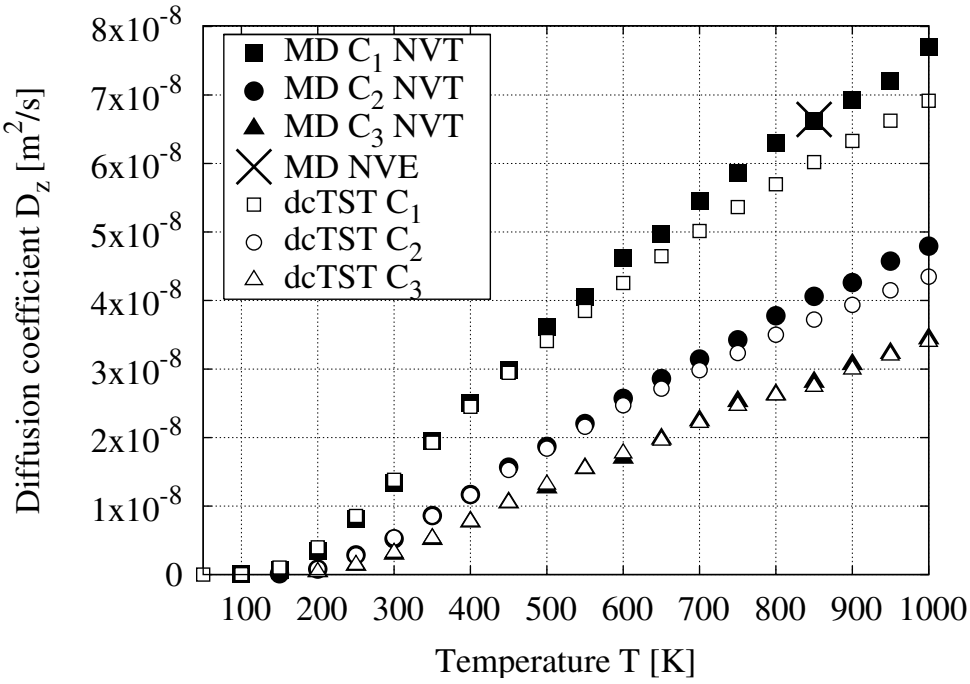

Figure 3.8: *Diffusion of methane, ethane, and propane in LTL-type zeolite at infinite dilution computed by dcTST and MD.*

i.e. the increased probability of particles to continue in their current direction.

There are several ways to include kinetic correlations, amongst them are the dynamical corrections as formulated by Voter and Doll [56], using multistate systems and the recently proposed method of Ruiz-Montero *et al.* (eq. 3.38 with $a = 2$) [7]. The method of Voter and Doll would extend the two-state system A and B, to a multi-state system $A, B, C, D, \ldots$, by computing the hopping rates k_{ij}, dynamical corrections κ_{ij}, and lattice distances λ_{ij} between state i and j. Note that the dynamical correction in this formulation is not restricted to the interval between 0 and 1, but can potentially increase beyond unity when kinetic correlations are abundant. However, at the highest temperatures reported here, the time scales of thermalization and k^{-1} become inseparable, so here we pursue the alternative Ruiz-Montero route. Figure 3.9 shows the method of Ruiz-Montero *et al.* ($a = 2$) at 1000 K for methane in LTL-type zeolite. The eq. 3.38 is reaching a plateau value in time, equal to the MD results. These results differ from the dcTST value, due to the presence of kinetic directional correlations, which are included using (importance-sampled)

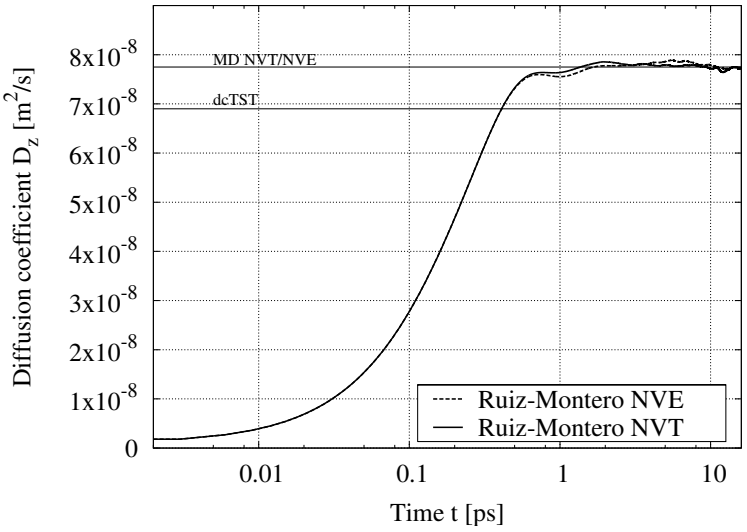

Figure 3.9: *Diffusion of methane at 1000 K in LTL-type zeolite at infinite dilution computed by dcTST and MD compared to the method of Ruiz-Montero et ald.*

MD methods. However, computing eq. 3.38 is very time consuming and the dcTST method is preferable for cage/window-type systems with higher free-energy barriers.

3.3.1.2 Methane in LTA-Type Zeolite

At infinite dilution, the barrier for diffusion of methane in LTA-type zeolite at 300 K is much higher than in LTL-type zeolite. The barrier is approximately 8.5 k_BT and sharply peaked. In figure 3.10, we compare various biasing functions for the importance-sampled MD method. A biasing weighing function of

$$w(q) = \frac{e^{a\beta F(q)}}{\int e^{a\beta F(q)}\, dq} \tag{3.43}$$

using $a = 1$, flattens the free-energy landscape and the initial configurations are sampled uniformly. However, for diffusion only the configurations in the barrier region yield relevant information, and with $a \gg 1$ as a biasing function the configurations are indeed restricted to the barrier regions, and all trajectories contribute significantly to the diffusion coefficient. The results show that for sharply peaked barriers a high biasing function achieves fast convergence. For these barriers the Bennett-Chandler method works well, because diffusive

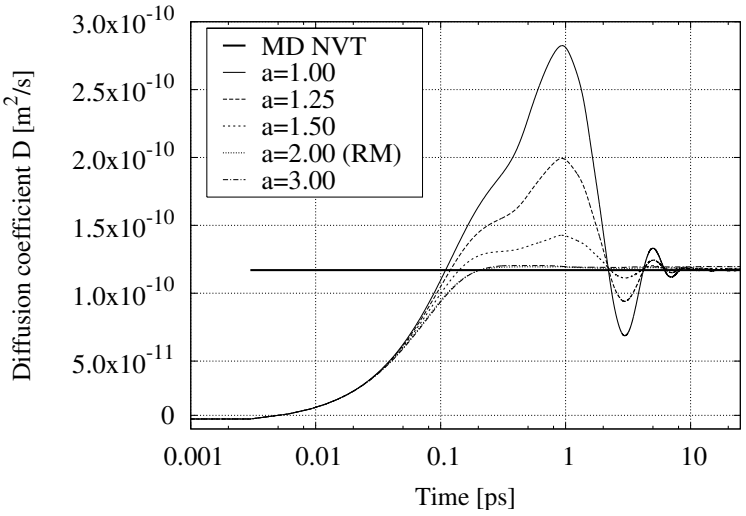

Figure 3.10: *Diffusion of methane over a high free-energy barrier in LTA-type zeolite, at 300 K and infinite dilution, using various biasing functions (eq. 3.43). The method of Ruiz-Montero et al (RM) uses* $a = 2$.

behaviour is negligible and dynamical corrections are easily evaluated. However, the importance-sampled MD method is also applicable in the diffusive regime where $\kappa \ll 1$.

3.3.1.3 Ethane in LTA-Type Zeolite

Ethane molecules in LTA perform jumps on a simple cubic lattice. It was found that self-diffusion *decreases* with increasing temperature at low temperatures [24]. At low temperatures the molecules become less confined in the windows as temperature increases. Heating the system, ethane moves away from the windows, which increases the entropic barrier for cage-to-cage motion. Figure 3.11 shows that the behaviour found by Schüring *et al.* [24] is strongly dependent on the parameter set (Tables 3.1 and 3.2). The parameter set of Dubbeldam *et al.* [39] does not show a decrease with increasing temperature, although for both parameter sets the local activation energy depends on temperature. The size parameter used by Schüring *et al.* is so small that ethane at low temperature is found *in* the window itself, and heating shifts the adsorption sites to just in front of the windows. By contrast, the set of Dubbeldam *et al.* has a larger size parameter for ethane, and also at low temperature the adsorption sites are always in front of window, reducing the behaviour found

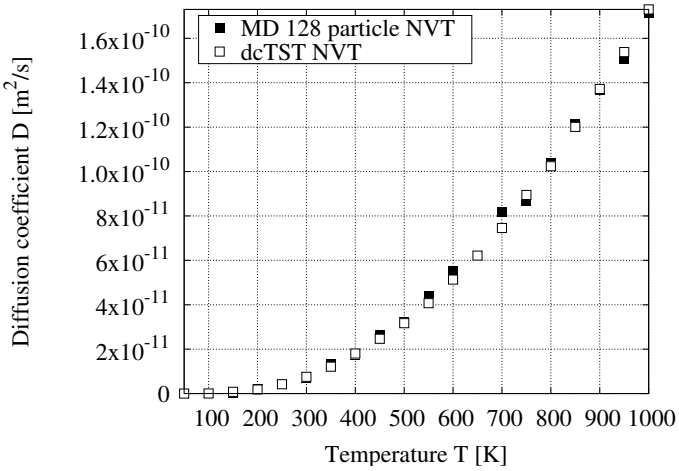

Figure 3.11: *Self-diffusion of ethane at infinite dilution in LTA-type silica using the parameter set of Dubbeldam et al. The infinite dilution case using MD is simulated by switching the intermolecular forces off for ethane, i.e. the particles do not interact (except through the thermostat in NHC-NVT simulations).*

by Schüring *et al.* However, the phenomenon is likely to be generic and present in cage/window-type systems and applicable to small molecules. It shows how much the actual adsorption sites can depend on temperature and simulation parameters.

3.3.2 Nonzero Loading

3.3.2.1 Methane, Ethane, and Propane in LTL-Type Zeolite

The free-energy barriers for various loadings of methane in LTL-type zeolite are plotted in figure 3.12. In comparison to the infinite dilution case, the free energy barrier initially decreases. Adding particles to the system induces an effectively "smoother" channel. For increasing loadings, the top of the barrier flattens and eventually transforms into a barrier region with two local free-energy minima.

Figure 3.13 shows the diffusion behaviour as a function of loading in LTL-type zeolite for methane, ethane, and propane at 300 K. The TST diffusivities based on the free-energy profiles (e.g. for methane shown in figure 3.12) increase, while the dcTST values decrease and are equal to the conventional MD results. Clearly the transmission coefficient corrects the TST results not only

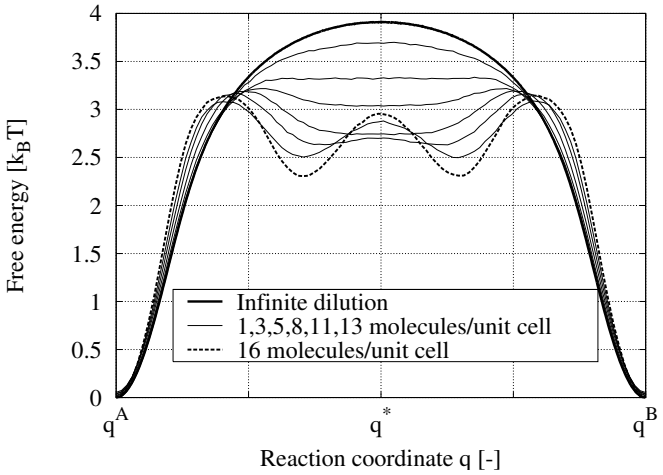

Figure 3.12: *Free-energy profiles $F(q)$ at 300 K of methane in LTL at various loadings (infinite dilution, 1, 3, 5, 8, 11, 13, and 16 molecules per unit cell). The reaction coordinate is chosen along the z channel direction (lines from top to bottom in order of the legend).*

qualitatively, but also quantitatively. The good agreement between dcTST and MD for LTL-type zeolites is encouraging. The diffusion of alkanes in LTL-type zeolite is quite fast, and the fact that our dcTST method also works for such low free-energy barriers as those present in LTL-type zeolite is surprising.

Although this region of diffusion is fully accessible with conventional MD, the dcTST method has a very important advantage: it enables us to explain the qualitative behaviour of diffusion in terms of free-energy difference and transmission coefficients. For example, initially the diffusion of methane in LTL-type zeolite does not change much with loading. The MD results would suggest that the fundamental reason could be that particles hardly notice each other at these lower loadings. However, the picture painted by dcTST is quite different. There are two effects: (1) the free-energy barrier decreases over loading (which means an increase in the diffusion) rendering the channel environment more "uniform", and (2) as the loading increases, the transmission coefficient decreases, due to an increased collision frequency. At low loadings, the two effects almost counterbalance each other, but at higher loadings the rapid increase in the collision frequency wins.

An important observation made in Ref. [52] is that the appearance of the two local minima on top of the free-energy barrier at around 11 molecules per unit cell for methane cause an inflection at the corresponding loading in the

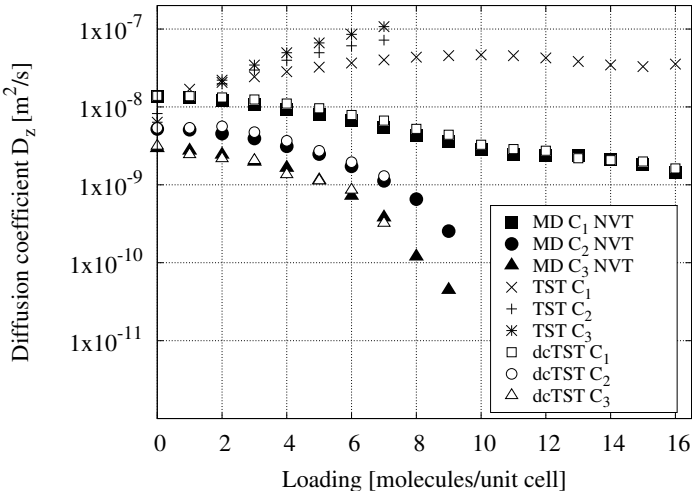

Figure 3.13: *Diffusion of methane, ethane, and propane at 300 K as a function of loading in LTL-type zeolite computed by TST, dcTST and MD.*

diffusion curves. This inflection is similarly found in the adsorption isotherms, and both are related to a change in packing. They show that the dcTST method can generally be used to qualitatively explain the self and collective diffusion behaviour of a molecule/zeolite combination as a function of loading, by carefully analysing the change in free energy (packing effects).

The appearance of extra adsorption sites with loading, and the change of packing, shows that the choice of the random-walk lattice cannot solely be based on a lattice of adsorption sites at low loading. The adsorption-site lattice that is needed to describe diffusion over adsorption sites depends on the zeolite, the guest, the temperature, *and* on the loading of the zeolite. In fact, for every zeolite, guest, temperature, and loading, the lattice should be reconstructed. However, for very slow diffusion in cage/window-type zeolites, the rate determining step is the cage-to-cage motion and all the details of intracage diffusion are present in the free-energy profile. For very fast diffusion using an adsorption-site lattice does not make sense either, as there is too much correlation present between the hops at such a lattice, i.e. the separation of time scales vanishes and the description as "hopping" breaks down. The natural lattice to use would be an effective lattice of cage center to cage center.

For zeolites accessible with conventional MD, the free energy can be obtained using either MC or MD, and we found no differences between both methods. By contrast, the sampling of configurations with a tagged particle restricted to the dividing barrier surface requires more thought. In figure 3.14,

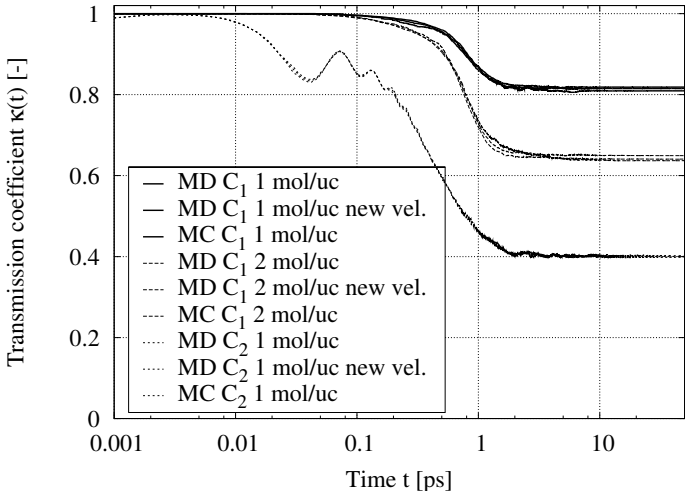

Figure 3.14: *Transmission coefficient $\kappa(t)$ at 300 K for ethane in LTL-type zeolite using the first bead as a function of time for various loadings. The starting configurations are sampled with MC or with MD, where the velocities are either taken from the trajectory or newly resampled from the Maxwell-Boltzmann distribution. The differences are negligible.*

we show results for the transmission coefficients using MC and MD. The MD results are splitted in two types: (1) both the positions and velocities are stored, and (2) only the positions are taken from MD trajectories, the velocities are resampled from a Maxwell-Boltzmann distribution. As can be seen, reinitialising the velocities yields equal results, and one can conclude from the result that the velocities in this system are indeed Maxwell-Boltzmann distributed, even *on top* of the barrier. For systems with higher free-energy barriers configurations are adequately sampled with biased MC, while conventional MD would become impossible.

3.3.2.2 Methane and Ethane in LTA-Type Zeolite

Figure 3.15 shows the free-energy profiles at 600 K for methane in LTA-type zeolite for various loadings. Relative to the infinite dilution case, the addition of particles to the cages leads to an increase of the free energy inside the cage, while the free energy at the barrier remains unchanged up to intermediate loadings. The inner-cage surface of LTA-type zeolite is adsorbophylic (wetting regime), and when the adsorption is increased, favourable adsorbate-adsorbent interactions are being replaced by less favourable interaction with

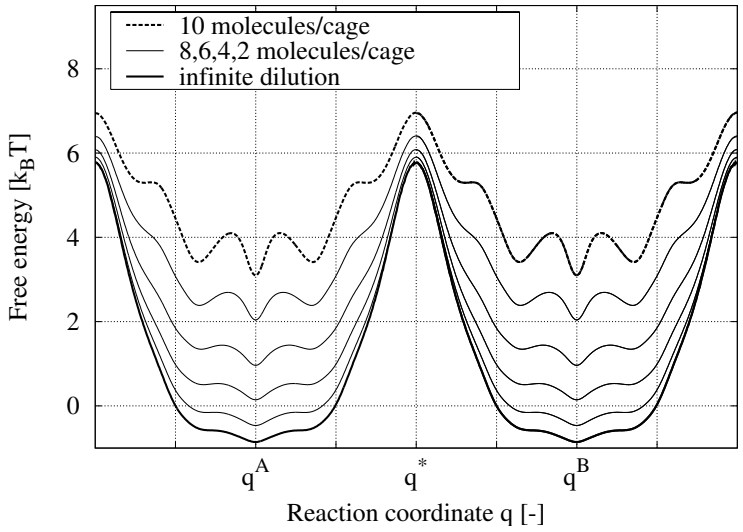

Figure 3.15: *Free-energy profiles of methane in LTA-type zeolite at 600 K for various loadings (10, 8, 6, 4, 2 molecules per cage, and infinite dilution).*

other particles.

Figure 3.16(a) shows the individual components of the diffusion process, D^{TST} and κ, as a function of loading for methane in LTA. Although the transmission coefficient shows a monotonic decrease with density, the diffusion coefficient goes through a maximum. The driving force behind the initial increase in diffusion is a loss of guest-host attraction inside the cages. Eventually, the free-energy barrier increases again, due to packing and free-volume effects, causing a decrease of the diffusion coefficient. While the transmission coefficient only slightly changes the qualitative behaviour of the diffusion as a function of loading, it has a profound quantitative influence. We show the diffusion in LTA of methane at 600 K and ethane at 750 K using both MD and extended dcTST in figure 3.16(b). Our extended dcTST method and MD again agree quantitatively.

3.3.2.3 Methane/Ethane Mixture in LTA-Type Zeolite

In figure 3.17 we plotted the results for a 50%-50% mixture of methane and ethane in LTA-type zeolite, as a function of loading at 300 K. For each of the components the free energy and transmission coefficients are computed. For the computation of κ a single molecule of the component is restricted to the barrier, while the other molecules of the same component, and all molecules

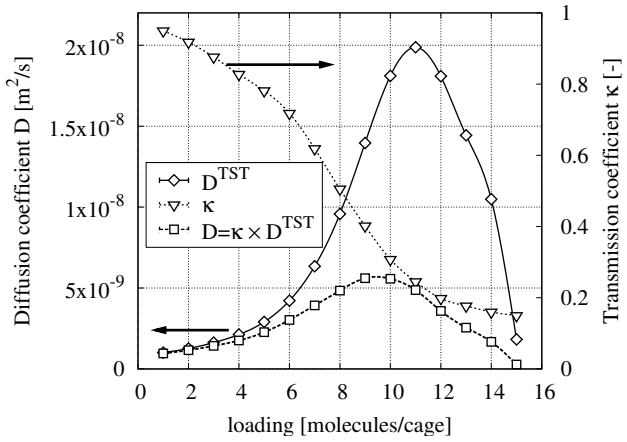

(a)

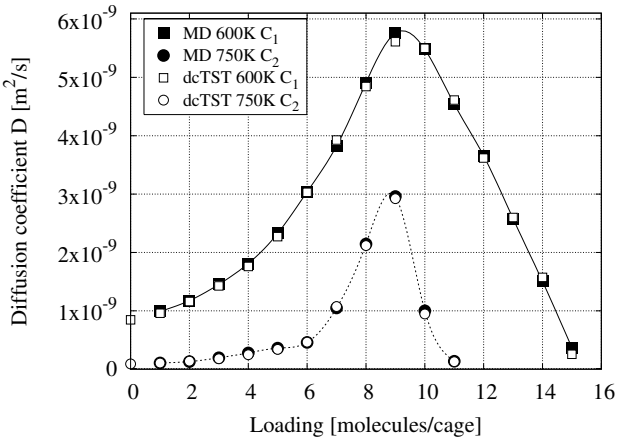

(b)

Figure 3.16: *dcTST and MD in LTA-type zeolite.(a) the TST and dcTST diffusivities for methane at 600 K as a function of loading (left axis), and the tranmission coefficient κ (right axis), (b) diffusion of methane and ethane in LTA-type zeolite, as a function of loading, at 600 K and 750 K, respectively.*

of the other component are free to move. Again, our extended dcTST method and MD agree quantitatively.

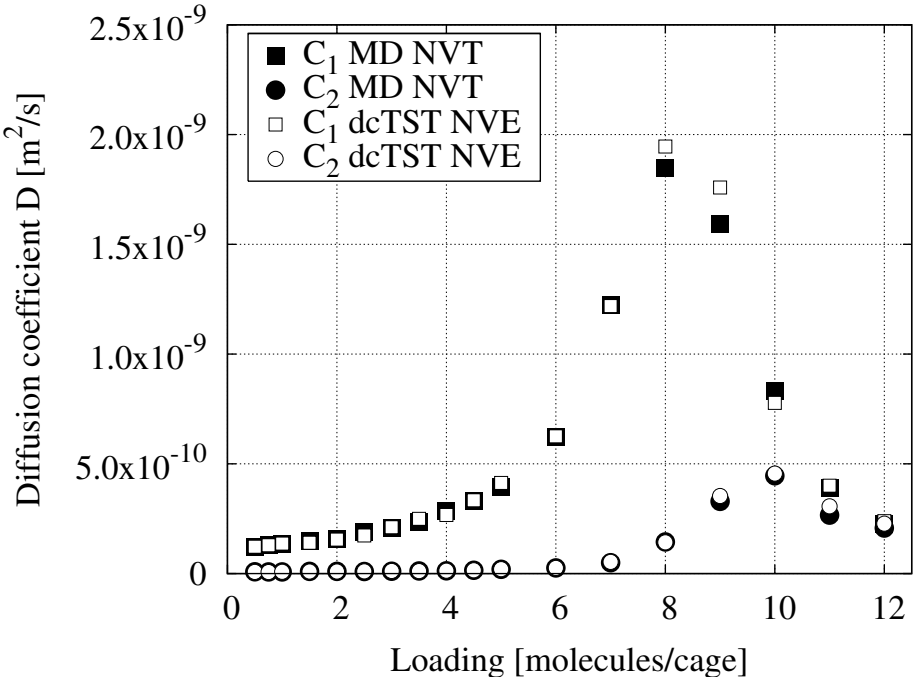

Figure 3.17: *Self-diffusion in a 50%-50% mixture of methane and ethane in LTA-type zeolite, as a function of loading at 300 K.*

3.4 Discussion

We have shown that our method is applicable to simulating self-diffusion in any elementary topology. The extension of eq. 3.17 to more complex structures and lattices is a geometric exercise published in Ref. [57]. The connection between the random walk lattice and the zeolite structure is found by an analysis of the free-energy profiles. The diffusion of a tagged molecule is computed over that typical length scale given by the smallest repeating zeolite structure, i.e. from the center of cage A to the center of cage B. One automatically averages over all adsorption sites in the cage, irrespective of whether the adsorption sites are strong or weak, or even ill defined, i.e. for purely entropic barriers. For most lattices the equivalent of eq. 3.17 has been worked out. Since the lattice is not based on specific adsorption sites, often the same lattice can be used for all temperatures and loadings, although sometimes at high loadings new barriers may be formed.

Tunca and Ford [29–31] computed elementary hopping rates using multi-

dimensional TST for use in a subsequent coarse-grained kinetic Monte Carlo (kMC) scheme. Besides the various approximations necessary to make the computation tractable, this approach relies on the computation of an *elementary* hopping rate. The fundamental question about hierarchical approaches is "Is it possible to compute an elementary hopping rate?". In our calculations, we have observed that to obtain agreement with MD results, one cannot limit the free-energy calculation to the two cages A and B for which the hopping is computed. It is essential to average over fluctuations in the number of particles in the neighbouring cages [33]. By 'closing off' cages, the system is intrusively changed, and we are not aware of any other scheme that can separate the contributions of other cages from the contribution of only the cages A and B. The omitted correlations are not the same as those regained by a kMC simulation later and therefore further corrections are needed to obtain results in exact agreement with MD.

We explicitly avoid the use of kMC and compute the self-diffusion coefficient directly. The diffusion constant we compute is the self-diffusion of a tagged molecule travelling from cage A to cage B considering all other particles as an external field. The external field is maintained by an MC NVT simulation (fixed total number of particles, volume, and temperature) of spectator molecules in the 'background'. By using an MC approach that includes translational, orientational and regrow moves, we average over cage distributions, positions and orientations of neighbouring molecules. This renders it unnecessary to sample the complete phase space by integrating over all particle positions and orientations, weighed with the correct Boltzmann weight. In addition to being computationally much cheaper, it also allows for the use of advanced simulation techniques such as CBMC, which speeds up simulations of longer molecules by orders of magnitude. Longer molecules are efficiently handled and likewise, diffusion in mixtures can easily be computed – all particles are considered part of the external field, irrespective of the type of particle. The LTA-type system used here is a cation-free version of the commonly used LTA 5A zeolite (4 Na^+ and 4 Ca^+ per cage). A quantitative comparison with pulsed field gradient nuclear magnetic resonance (PFG-NMR) experimental results requires including the ions in the simulations. We, in Ref. [58] and Calero *et al.* [59] have extended the united-atom model with cations, and our dcTST method already includes the necessary tools.

The diffusion behaviour of ethane in LTA as a function of temperature has been well studied. In contrast to a previous study of Schüring *et al.* [24, 43], we found that ethane molecules in LTA-type zeolite perform hops on a regular cubic lattice, even when we used the smaller size parameters of Schüring *et*

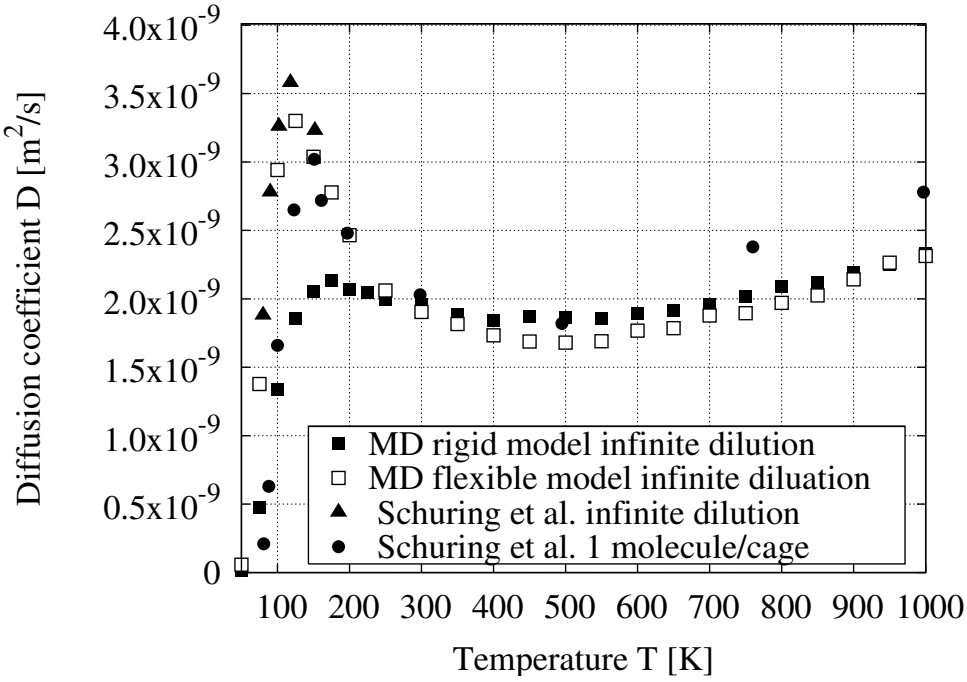

Figure 3.18: *Self-diffusivity of ethane using the LJ parameters of Table 3.2, comparing the results of a rigid zeolite to the flexible model of Demontis et al. [60, 61]. Error bars are smaller or comparable to the symbol size. For comparison we have added the results of Schüring et al. [43] for the infinite dilution case, and for 1 molecule per cage.*

al. However, these authors computed k_{AB} from MD using the number of cage visits divided by the MD time. Such an approach overestimates the actual self-diffusivity by nearly an order of magnitude for ethane in LTA-type zeolite at 100 K. Using the center of mass of ethane as the order parameter, they overestimate the rate, because a molecule coming from A will show diffusive behaviour in the barrier region and change cage many times before equilibrating in A (recrossing) or B (transmission). Only the successful transmissions should be counted and Schüring *et al.* found that the correlation factor f (eq. 3.19), computed using a molecular simulation, approximately corrects for this. Our results show that a proper computation of the effective rate constant *including* the transmission coefficient leads to exact agreement between dcTST and MD. We stress that κ and f are different concepts. The similarity in behaviour for this specific system originates from the fact that κ is dominated by back-

correlations, and for a cubic lattice eq. 3.19 computes the same thing. However, the computation of f using eq. 3.19 is limited to the MD time scale.

We would like to comment on the use of flexible zeolites with regard to our dcTST method. Although for computational reasons we kept the zeolite rigid, our method is fully applicable to flexible zeolites. In Ref. [37] it was found that self-diffusion coefficients for methane in LTA-type zeolite obtained with flexible and with rigid lattices are practically the same. In figure 3.18 we show the self-diffusivity of ethane using the Lennard-Jones parameters of Table 3.2 and compare the results of a rigid zeolite with the flexible model of Demontis *et al.* [60, 61]. Error bars are smaller or comparable to the symbol size. We have added the results of Schüring *et al.* [43] for the infinite dilution case, and for one molecule per cage. The data of Schüring *et al.* compare well and are consistent with our simulations. An important observation is that the differences between flexible and rigid LTA-type zeolites for ethane are significant and temperature dependent. In the low-temperature region, the ethane molecule is tightly confined in the window itself, while at higher temperature the molecule is less tightly confined and located just in front of the window. The method proposed in this chapter would allow a detailed investigation of the effect of framework flexibility on slow-diffusing molecules.

3.5 Conclusions

Our method applies dcTST at nonzero loadings, without introducing assumptions not already present in traditional TST methods. It can be used to explain diffusion behaviour as a function of loading in any system with enough energy dissipation between hops, so that random-walk theory (the assumption of equilibration between two subsequent jumps) and TST are valid, as we showed here for small alkanes in LTL-type and LTA-type zeolites. The method gives results in exact agreement with MD, but is also applicable in the regime of very slow diffusion, where MD can not be used. This extends the range of accessible time scales significantly beyond currently available methods. Furthermore, the method enables us to express loading effects in terms of free-energy differences. It can be used in any lattice and any adsorbate, and also for mixtures.

Bibliography

[1] D. Frenkel and B. Smit, *Understanding molecular simulation 2nd edition* (Academic Press, London, UK, 2002).

[2] M. P. Allen and D. J. Tildesley, *Computer simulation of liquids* (Clarendon Press, Oxford, 1987).

[3] J. M. Thomas, Solid acid catalysts. Sci. Am. **266**, 112 (1992).

[4] A. F. Voter, F. Montalenti, and T. C. Germann, Annu. Rev. Mater. Res. **32**, 321 (2002).

[5] C. H. Bennett, in *Diffusion in Solids: Recent Developments*, edited by A. Nowick and J. Burton (Academic Press, New York, 1975), pp. 73–113.

[6] D. Chandler, J. Chem. Phys **68**, 2959 (1978).

[7] M. J. Ruiz-Montero, D. Frenkel, and J. J. Brey, Mol. Phys. **90**, 925 (1996).

[8] P. G. Bolhuis, C. Dellago, and D. Chandler, Faraday Discuss. **110**, 421 (1998).

[9] T. S. van Erp, D. Moroni, and P. G. Bolhuis, J. Chem. Phys **118**, 7762 (2003).

[10] D. Moroni, P. G. Bolhuis, and T. S. van Erp, J. Chem. Phys **120**, 4055 (2004).

[11] A. F. Voter, Phys. Rev. Lett. **78**, 3908 (1997).

[12] A. F. Voter, Phys. Rev. B **57**, 13985 (1998).

[13] M. R. Sorensen and A. F. Voter, J. Chem. Phys **112**, 9599 (2000).

[14] G. Henkelman and H. Jónsson, J. Chem. Phys **115**, 9657 (2001).

[15] R. L. June, A. T. Bell, and D. N. Theodorou, J. Phys. Chem. **95**, 8866 (1991).

[16] R. Q. Snurr, A. T. Bell, and D. N. Theodorou, J. Phys. Chem. **98**, 5111 (1994).

[17] R. Q. Snurr, A. T. Bell, and D. N. Theodorou, J. Phys. Chem. **98**, 11948 (1994).

[18] E. J. Maginn, A. T. Bell, and D. N. Theodorou, J. Phys. Chem. **100**, 7155 (1996).

[19] F. Jousse and S. M. Auerbach, J. Chem. Phys. **107**, 9629 (1997).

[20] T. R. F. TR and W. Smith, J. Chem. Soc. Faraday Trans. **93**, 3249 (1997).

[21] T. Mosell, G. Schrimpf, and J. Brickmann, J. Phys. Chem. B. **101**, 9476 (1997).

[22] T. Mosell, G. Schrimpf, and J. Brickmann, J. Phys. Chem. B. **101**, 9485 (1997).

[23] P. K. Ghorai, S. Yashonath, and R. M. Lynden-Bell, Mol. Phys. **100**, 641 (2002).

[24] A. Schüring, S. M. Auerbach, S. Fritzsche, and R. Haberlandt, J. Chem. Phys **116**, 10890 (2002).

[25] D. Dubbeldam, S. Calero, T. L. M. Maesen, and B. Smit, Phys. Rev. Lett. **90**, 245901 (2003).

[26] D. Dubbeldam and B. Smit, J. Phys. Chem. B. **107**, 12138 (2003).

[27] B. Smit and J. I. Siepmann, J. Phys. Chem. **98**, 8442 (1994).

[28] Schenk, M.; Calero, S.; Maesen, T. L. M.; Benthem, L. van; Verbeek, M. G.; Smit, B. *Angew. Chem. Int. Ed.* **2002**, *41*, 2500-2502.

[29] C. Tunca and D. M. Ford, J. Chem. Phys. **111**, 2751 (1999).

[30] C. Tunca and D. M. Ford, J. Phys. Chem. B **106**, 10982 (2002).

[31] C. Tunca and D. M. Ford, Chem. Eng. Sci. **58**, 3373 (2003).

[32] S. M. Auerbach, International reviews in physical chemistry **19**, 155 (2000).

[33] E. Beerdsen, B. Smit, and D. Dubbeldam, Phys. Rev. Lett. **93**, 248301 (2004).

[34] J. P. Ryckaert and A. Bellemans, Faraday Dicuss. Chem. Soc. **66**, 95 (1978).

[35] M. D. Macedonia and E. J. Maginn, Mol. Phys. **96**, 1375 (1999).

[36] T. J. H. Vlugt and M. Schenk, J. Phys. Chem. B. **106**, 12757 (2002).

[37] S. Fritzsche, M. Wolfsberg, R. Haberlandt, P. Demontis, G. B. Suffritti, and A. Tilocca, Chem. Phys. Lett. **296**, 253 (1998).

[38] A. G. Bezus, A. V. Kiselev, A. A. Lopatkin, and P. Q. J. Du, J. Chem. Soc., Faraday Trans. II **74**, 367 (1978).

[39] D. Dubbeldam, S. Calero, T. J. H. Vlugt, R. Krishna, T. L. M. Maesen, and B. Smit, J. Phys. Chem. B. **108**, 12301 (2004).

[40] D. Dubbeldam, S. Calero, T. J. H. Vlugt, R. Krishna, T. L. M. Maesen, E. Beerdsen, and B. Smit, Phys. Rev. Lett. **93**, 088302 (2004).

[41] S. S. Chong, H. Jobic, M. Plazanet, and D. S. Sholl, Chem. Phys. Lett. **408**, 157 (2005)

[42] T. J. H. Vlugt, R. Krishna, and B. Smit, J. Phys. Chem. B. **103**, 1102 (1999).

[43] A. Schüring, S. M. Auerbach, S. Fritzsche, and R. Haberlandt, in *Random Walk Treatment of Dumb-Bell molecules in an LTA Zeolite and in Chabazite*, Proceedings of the 14th International Zeolite Conference, edited by E. van Steen, L. Callanan, and M. Claeys (Elsevier, Cape Town, 2004), pp. 2110–2117.

[44] D. C. Rapaport, *The art of molecular dynamics simulation* (Cambridge University Press, Cambridge, 1995).

[45] K. Kremer and G. S. Grest, J. Chem. Phys **92**, 5057 (1990).

[46] G. J. Martyna, M. Tuckerman, D. J. Tobias, and M. L. Klein, Mol. Phys. **87**, 1117 (1996).

[47] Y. Liu and M. E. Tuckerman, J. Chem. Phys **112**, 1685 (2000).

[48] I. Vattulainen, S. C. Ying, T. Ala-Nissila, and J. Merikoski, Phys. Rev. B **59**, 7697 (1999).

[49] T. Ala-Nissila, R. Ferrando, and S. C. Ying, Advances in Physics **51**, 949 (2002).

[50] P. J. Flory, *Statistical Mechanics of Chain Molecules* (Interscience, Wiley, New York, 1969), pp. 16–17.

[51] G. W. N. White, S. Goldman, and C. G. Gray, Mol. Phys. **98**, 1871 (2000).

[52] E. Beerdsen, D. Dubbeldam, and B. Smit, J. Phys. Chem. B **110**, 22754 (2006).

[53] R. M. Barrer and H. Villiger, Z. Kristallogr. **128**, 352 (1969).

[54] J. J. Pluth and J. V. Smith, J. Am. Chem. Soc. **102**, 4707 (1980).

[55] H. L. Tepper and W. J. Briels, J. Chem. Phys **116**, 9464 (2002).

[56] A. F. Voter and J. D. Doll, J. Chem. Phys **82**, 80 (1985).

[57] D. Dubbeldam, E. Beerdsen, S. Calero, and B. Smit, Proc. Natl. Acad. Sci. U.S.A. **102**, 12317 (2005)

[58] E. Beerdsen, B. Smit, and S. Calero, J. Phys. Chem. B **106**, 10659 (2002).

[59] S. Calero, D. Dubbeldam, R. Krishna, B. Smit, T. J. H. Vlugt, J. F. M. Denayer, J. A. Martens, and T. L. M. Maesen, J. Am. Chem. Soc. **126**, 11377 (2004).

[60] P. Demontis, G. B. Suffritti, S. Quartieri, E. S. Fois, and A. Gamba, Zeolites **7**, 522 (1987).

[61] P. Demontis, G. B. Suffritti, S. Quartieri, E. S. Fois, and A. Gamba, J. Phys. Chem. **92**, 867871 (1988).

Can we predict diffusion behaviour of molecules in confinement by looking at the match between the molecule and the structure of the confinement? This question has proven difficult to answer for many decades. As a case study, we use methane and a simple model of ellipsoids to arrive at a molecular picture that allows us to make a classification of pore topologies and to explain their diffusion behaviour as a function of loading. Our model is surprisingly simple: regarding a structure as consisting of interconnected ellipsoids is enough to understand the full loading dependence.

E. Beerdsen, B. Smit, and D. Dubbeldam

4 Understanding Diffusion in Nanoporous Materials

Membranes function because of differences in diffusion coefficients of the molecules that are adsorbed in these materials. Many different materials are used as membranes. Lipid bilayers in cell membranes and molecular sieves such as zeolites in industrial separation are just a few examples. Common to these nanoporous materials is that they contain pores that have sizes similar to the dimensions of the adsorbed molecules, and therefore impose a tight confinement. This makes the diffusion behaviour of adsorbed molecules in these materials very different from diffusion in a bulk fluid [1–10]. Well studied though these systems are, their diffusion properties remain poorly understood. In an elaborate study, comparing the diffusion of four gases in four zeolite topologies, Skoulidas and Sholl found widely varying diffusion trends, showing the potential of tuning diffusion for industrial processes by adjusting the loading [4, 11]. Despite the importance for many applications, conventional methods cannot explain when and why, for a given system, the diffusion will increase, decrease, or remain constant as a function of loading.

In this work, we make use of a very simple model based on ellipsoids, to present a fundamental understanding of the loading dependence, and analyse the molecular factors causing the observed behaviour.

There are many ways of expressing diffusion behaviour in a diffusion co-

efficient. Macroscopic methods, such as the measurements of the uptake rate and permeation rate, typically yield the transport diffusion coefficient D_T. It is given by Fick's law: $J = -D_T \nabla c$, where J is the sorbate flux when a concentration gradient ∇c is applied. To obtain a diffusion coefficient that is presumably less dependent on the loading [1], D_T is often converted to the collective diffusivity $D_C = \frac{\partial \ln c}{\partial ln f}$ (with c the sorbent concentration or loading and f the fugacity). The self- or tracer diffusion coefficient D_S, finally, is a quantity that can be obtained by microscopic methods, such as pulsed field gradient NMR (PFG NMR). It can be interpreted as the diffusion of a single tagged particle making its way through the porous medium and, if present, other particles. At the infinite dilution limit, D_S, D_C and D_T are strictly equivalent. For reasons of convenience, the collective diffusivity has been assumed to be relatively insensitive to changes in concentration. Although historically inaccurate, this is often referred to as the Darken approximation [9, 12] and it has received widespread application [1]. It has been the basis for extrapolations to compare different data sets and relate microscopic and macroscopic diffusion processes. Although many deviations have been found, where the collective diffusivity was concentration dependent, they were seen as exceptions on the general rule [4].

In this work we focus on the influence of the confinement on the various diffusion coefficients. Therefore, we use rigid siliceous molecular-sieve structures, devoid of cations. Owing to their regular crystalline shapes and wide variety of topologies, they are ideal model systems [2–7, 13–16]

We use a combination of conventional MD calculations and our recently proposed dynamically corrected Transition-State Theory (dcTST) method [17–19]. In addition to diffusion coefficients, this method can yield an explanation of the diffusion behaviour in terms of free-energy differences. Free-energy profiles are computed during an NVT-ensemble Monte Carlo or MD simulation, in which we compute the probability to find a particle at a particular value of the reaction coordinate q. Further details about the method can be found in ref. [17].

Zeolites are designated by three-letter codes. D_S and D_C were obtained for methane in 10 different sieve topologies: LTA, CHA, ERI, SAS, AFI, MTW, LTL, MFI, BOG, and BEC. This set represents a wide range of different topologies (see table 4.1). We focused on methane, since even for this simple molecule the diffusion behaviour is not understood. The results are shown in figure 4.1.

We can interpret our results by making use of a very simple concept based on ellipsoids. The molecular sieve's pores or cavities form confinements that can be thought of as interconnected ellipsoids. There are three ways to inter-

	ring size	window diameter [Å]	cage diameter [Å]	R_{ctw}
LTA	8	4.1	10	2.44
ERI	8	$3.6 - 5.1$	11	3.06
CHA	8	3.8	8.5	2.24
SAS	8	4.2	10	2.38
LTL	12	7.1	13	1.83
MTW	12	$5.6 - 6.0$	8	1.42
AFI	12	7.3	10	1.37
BOG	12/10	$7.0/5.5 - 5.8$	$*$	$-$
ISV	12/12	$6.1 - 6.5/5.9 - 6.6$	$*$	$-$
MFI	10/10	$5.1 - 5.5/5.3 - 5.6$	$*$	$-$

Table 4.1: *Structural data for the ten examined structures. For each topology, the table lists the window ring size in number of oxygen atoms per ring, the window diameter, the cage diameter [Å] (perpendicular to the long axis a), and the cage-to-window ratio R_{ctw}. The cage and window data left and right for intersecting-channel topologies are the values for the channels in the different directions. Where the window diameter is given as a range, this signifies that the windows have an oval shape. The values for R_{wtc} in these cases are calculated as the ratio of the smallest diameter of the oval to the diameter of the cage.*

connect these ellipsoids (see figure 4.2 (left)): aligned in a direction perpendicular to the long axis a (top), aligned along a (middle), or aligned alternatingly (bottom). The three base models form confinement types that we refer to as 'cage type', 'channel type', and 'intersecting-channel type', respectively, and each of these types gives rise to a very distinct diffusion behaviour (see figure 4.1). The first and second model differ only in the direction in which the ellipsoids are connected. In fact we can make a transition from a cagelike system (top) to a tubelike structure (middle) by changing the aspect ratio of the ellipsoids. However, the diffusion behaviour is qualitatively different when the ellipsoids are connected along their long axis or along their short axis. Therefore, we see them as different classes. The left-hand side of figure 4.2 shows the way in which the ellipsoids are connected in each of the three models, along with the predicted free-energy profiles. The right-hand side of the figure shows examples of sieve topologies from each class, together with the calculated free-energy profiles, strikingly similar to the schematic predictions.

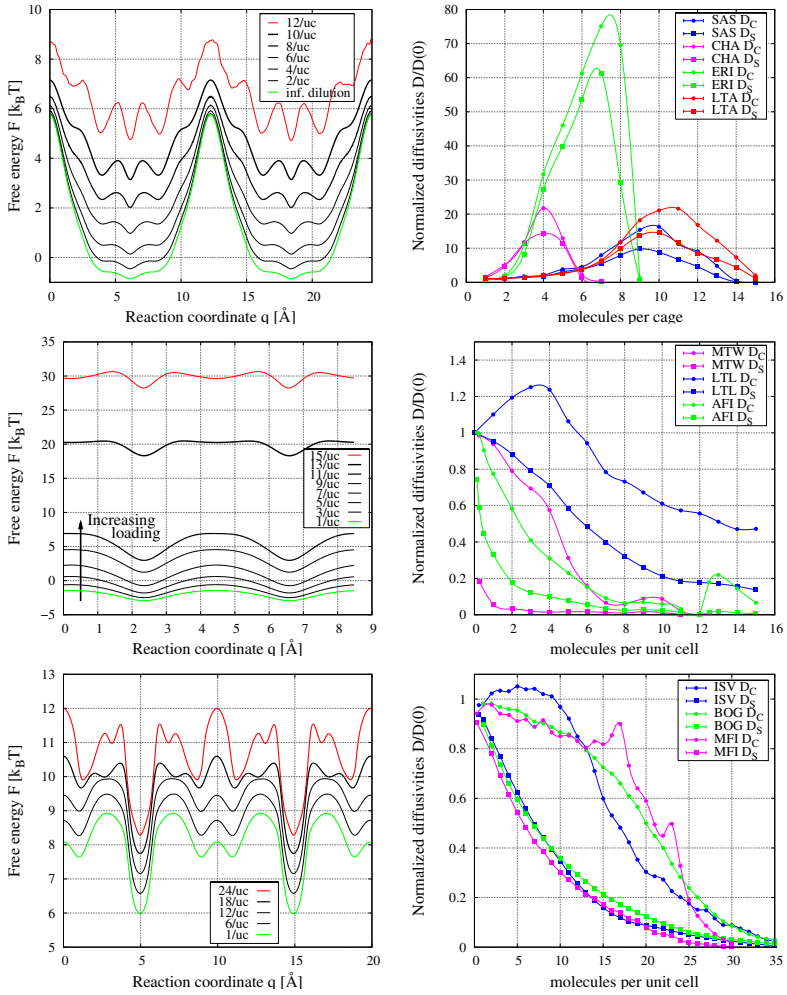

Figure 4.1: *(left) Free-energy profiles as a function of loading for cage-type LTA (top), channel-type AFI (middle), and intersecting channel-type MFI (bottom), at 300 K. For MFI, the free-energy minimum remains approximately constant as a function of loading; for clarity, the profiles have been vertically shifted. (right) Normalised D_S and D_C as a function of loading for cage-type SAS, CHA, ERI, and LTA (top), channel-type MTW, LTL, and AFI (middle), and intersecting channel-type ISV, BOG, and MFI (bottom).*

The cage-type molecular sieves (figure 4.2 (top)) generally consist of large cages, connected by narrow windows forming large free-energy barriers. The molecules' interaction with the sieve wall is favourable. With every molecule

that is added to a cage, more of this interaction is being exchanged for less favourable interaction with other molecules [17], causing an increase of the free energy of the bottom of the well, as shown in figure 4.1 (top) for methane in LTA-type molecular sieve. The influence of particles at the window region is much smaller, so that as the structure is being filled up, the net free-energy barrier decreases, causing an *increase* in both the self- and the transport-diffusion coefficient. At very high density, packing and free-volume effects cause the emergence of new, smaller, free-energy barriers, inside the cages, in addition to those in the windows, causing the diffusion to decrease. In figure 4.1 (top right) we show that LTA, ERI, CHA, and SAS-type systems all conform to this scenario for the diffusion of methane. The increase in both self- and collective diffusion compared to the infinite dilution limit can be a surprising *two orders* of magnitude. As expected, $D_C > D_S$ in all cases, due to positively contributing correlations present in D_C, but not in D_S. Clearly, if we change the size of the cage, the position of the maximum of the diffusion coefficient will change accordingly. This is exactly what we observe for SAS, LTA, ERI and CHA. LTA and SAS have the same type of cages, the largest of the four topologies, while CHA has the smallest (based on the saturation loading).

The second class of confinement consist of channel-type molecular sieves (figure 4.2 (middle)). Upon insertion of new molecules, again the free energy in the interior of the cage rises, but this time the effect on the free energy is even larger at the barriers, mainly due to a reduced entropy with respect to the cage regions (figure 4.1 (middle, left)). As a result, the diffusivity (both D_S and D_C) is a decreasing function of loading (figure 4.1 (middle, right)). The details of the diffusion graph depend on the exact topology of the channels. The smoother the channel (i.e. the wider the windows with respect to the cages, or the smaller the cage-to-window ratio R_{ctw}), the steeper the decreasing function will be. In channel-type structures, the amount of collective behaviour is much higher than in cage-type structures, because the barriers are lower. The difference between D_S and D_C depends on the window size: the smaller the intersection between ellipsoids, the larger the ratio D_C/D_S. MTW has the narrowest windows and has the largest D_C/D_S. LTL, which consists of relatively wide cages interconnected by intermediate windows, can be considered as a transition between the truly cage-type and the smooth channel-type molecular sieves. Note the small peak in D_C for AFI at high loadings. At 12 molecules per unit cell, there is an optimal packing of molecules, which does not allow them to shift around much. Increasing the loading further requires a large increase in pressure (accordingely, there is an inflection in the adsorption isotherm), and forces the molecules to leave their optimum-packing positions (the number of

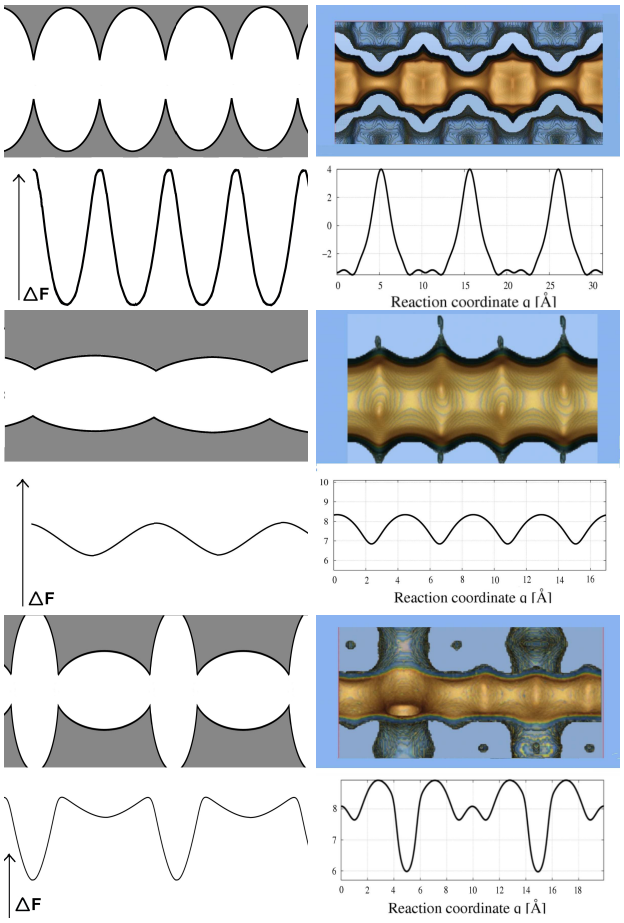

Figure 4.2: *(left) Three ways to connect ellipsoids, (top) aligned in a direction perpendicular to the long axis a, (middle) aligned along a, (bottom) aligned alternatingly. Below each ellipsoidal model on the left, a schematic representation is given of the associated free-energy profile. (right) Examples of molecular sieves that correspond to each of the ellipsoidal models: SAS (top), AFI (middle) and MFI (bottom), each with their calculated free-energy profile (zero loading); the true free-energy profiles are very similar to the schematic ones.*

molecules becomes incommensurate with the lattice). This causes a rise in the diffusion, peaking around 13 molecules per unit cell, upon which the molecules reorder according to a new optimum packing, allowing 15 molecules per unit cell.

The third class of confinement is the class of intersecting channel-type structures (figure 4.2 (bottom)), of which MFI is the most famous example. Any type of structure with channels running in different directions that mutually intersect falls into this category. The barriers are formed by the horizontally aligned ellipsoids, creating entropic traps between consecutive vertical ellipsoids. The influence of loading in these systems is complex as it involves effects such as unsimultaneous freezing in vertical and horizontal ellipsoids/channels, due to differences in ellipsoid diameter and length, causing varying degrees of commensurability of the particles with the structure, as a function of loading and direction. Here, as in the case of channel-type molecular sieves, the self diffusion still sharply decreases when the loading is increased, but the collective diffusivity initially only slightly decreases with density, until packing effects sharply decrease the collective diffusivity to zero, causing a kink in the diffusion curve at intermediate loading (figure 4.1 (bottom, right)). The position of the highest free-energy barrier is not the same for every loading. Importantly, the collective diffusion starts its fast decrease at the exact loading where the barrier that is highest at low loadings is overtaken by a new barrier, at a different position, giving rise to a new diffusion regime.

Note that for all scenarios, both D_S and D_C approach zero at the maximum loading, due to packing effects that halt the diffusion, irrespective of the topology of the confinement, in violation of the Darken approximation. This decrease of diffusion can be delayed to higher loading by free-energy effects: adsorbing molecules that lower the free-energy barrier have a favourable effect on the diffusion. The loading at which the final decrease sets in is determined by the size of the cage and the topology of the confinement. This observation implies that the Darken approximation generally cannot be used outside a very small region near zero loading [19].

We stress that the ordering of molecular sieve structures in classes depends strictly on the combination of adsorbate and adsorbent. The method employed in this study can be used to make a classification of pore structures for any given adsorbate molecule. It turns out that for methane the border between cage-type and channel-type structures lies at an R_{ctw} of around 2. For larger molecules, such as benzene, this border is likely to shift towards lower values of R_{ctw}. When applying this classification to larger molecules, sieve structures can therefore 'switch class', but the general behaviour will be the same: when the cages are large (with respect to the adsorbed molecule) and the windows are narrow, the diffusion as a function of loading will go through a maximum; when the confinement is experienced as a smooth channel, the diffusion is a decreasing function of loading (this has also been observed for small alkanes in

carbon-nanotubes [20]); when the confinement consists of intersecting channels, D_S will be monotonously decreasing as a function of loading, and D_C will show a kink. At high loadings in MFI, the diffusion becomes increasingly dominated by secondary corrugation. A better description of the diffusivity as a function of loading would require a higher-order model, consisting of ellipsoids of different types. In a recent Letter, we have shown that the erratic diffusion graph of MFI can be fully explained by the free-energy profiles [19].

It would be instructive to compare our simulation results with experimental data. A detailed comparison, however, requires experimental transport and self-diffusion coefficients for a large range of loadings. At present, such sets of experimental data are not available. Experimentally, it is difficult to measure diffusion over a large range of loadings. Different methods often result in diffusion coefficients that can differ orders of magnitude from one another [1]. Only recently an experimental technique became available to measure D_S and D_C simultaneously [6]. Chong *et al.* have performed self- and collective diffusion measurements of ethane in MFI, using one single experimental technique over the entire loading range [21]. It is encouraging that for the systems where experimental data have been obtained, namely ethane in MFI, the agreement between simulation and experiment is good. This gives some confidence that the classification gives a correct prediction for the examined all-silica versions of the structures. Our classification methodology may also help the interpretation of those experimental data that are often limited to a narrow (loading) window.

Bibliography

[1] J. Kaerger and D. M. Ruthven, *Diffusion in Zeolites and other microporous solids* (John Wiley & Sons, Inc., New York, 1992).

[2] E. J. Maginn, A. T. Bell, and D. N. Theodorou, J. Phys. Chem. **100**, 7155 (1996).

[3] R. Q. Snurr, A. T. Bell, and D. N. Theodorou, J. Phys. Chem. **98**, 11948 (1994).

[4] A. Skoulidas and D. S. Sholl, J. Phys. Chem. A. **107**, 10132 (2003).

[5] S. M. Auerbach, Int. rev. in phys. chem. **19**, 155 (2000).

[6] H. Jobic, J. Karger, and M. Bee, Phys. Rev. Lett. **82**, 4260 (1999).

[7] S. Fritzsche, M. Gaub, R. Haberlandt, and G. Hofmann, J. Mol. Model **2**, 286 (1996).

[8] R. Krishna, J. M. van Baten, and D. Dubbeldam, J. Phys. Chem. B. **108**, 14820 (2004).

[9] Ramanan, H.; Auerbach, S. M., in *NATO-ASI Series C: Fluid Transport in Nanopores*, edited by Fraissard, J.; Conner, W.C. Kluwer Academic Publishers; Dordrecht, The Netherlands, 2004.

[10] Xiao, J.; Wei, J. *Chem. Eng. Sci.* **1992**, *47*, 1123.

[11] A. I. Skoulidas, D. S. Sholl, and R. Krishna, Langmuir **19**, 7977 (2003).

[12] A. I. Skoulidas and D. S. Sholl, J. Phys. Chem. B. **105**, 3151 (2001).

[13] M. E. Davis, Nature **417**, 813 (2002).

[14] C. Tunca and D. M. Ford, Chem. Eng. Sci. **58**, 3373 (2003).

[15] P. K. Ghorai and S. Yashonath, J. Chem. Phys **120**, 5315 (2004).

[16] R. L. June, A. T. Bell, and D. N. Theodorou, J. Phys. Chem. **95**, 8866 (1991).

[17] E. Beerdsen, B. Smit, and D. Dubbeldam, Phys. Rev. Lett. **93**, 248301 (2004).

[18] D. Dubbeldam, E. Beerdsen, T. J. H. Vlugt, and B. Smit, J. Chem. Phys **122**, 224712 (2005).

[19] E. Beerdsen, D. Dubbeldam, and B. Smit, Phys. Rev. Lett. **95**, 164505 (2005).

[20] A. I. Skoulidas, D. M. Ackerman, J. K. Johnson, and D. S. Sholl, Phys. Rev. Lett. **89**, 185901 (2002).

[21] S. S. Chong, H. Jobic, M. Plazanet, and D. S. Sholl, Chem. Phys. Lett. **408**, 157 (2005).

In this work, we use molecular simulations to study the loading dependence of the self and collective diffusion coefficients of methane in various zeolite structures. To arrive at a microscopic interpretation of the loading dependence, we interpret the diffusion behaviour in terms of hopping rates over a free-energy barrier. These free-energy barriers are computed directly from a molecular simulation. We show that these free-energy profiles are a convenient starting point to explain a particular loading dependence of the diffusion coefficient. On the basis of these observations, we present a classification of zeolite structures for the diffusion of methane as a function of loading; three-dimensional cagelike structures, one-dimensional channels, and intersecting channels. Structures in each of these classes have their loading dependence of the free-energy profiles in common. An important conclusion of this work is that diffusion in nanoporous materials can never be described by one single effect and that we need to distinguish different loading regimes to describe the diffusion over the entire loading range.

E. Beerdsen, D. Dubbeldam, and B. Smit

5

Loading Dependence of the Diffusion Coefficient of Methane in Nanoporous Materials

5.1 Introduction

Membranes function because of differences in diffusion and adsorption of the molecules that are adsorbed in these materials. Many different materials are used as membranes. Lipid bilayers in cell membranes and molecular sieves such as zeolites in industrial separation are just a few examples. Common to these nanoporous materials is that they contain pores that have sizes similar to the dimensions of the adsorbed molecules and therefore impose a tight confinement. This makes the diffusion behaviour of adsorbed molecules in these materials very much different from diffusion in a bulk fluid [1–10].

Although these systems are well studied, their diffusion properties remain poorly understood. An intensive research effort to measure diffusion rates

in nanoporous materials augmented the possibilities of determining diffusion rates in nanoporous materials, such as zeolites, metal-organic frameworks, ion channels, etc. However, while it is often possible to determine the diffusion as a function of adsorbate loading rather accurately, a proper understanding of diffusion behaviour is still lacking. For a given structure, it is usually impossible to predict whether the diffusion will decrease, increase or remain constant when the loading is increased.

Molecular-dynamics simulations have often been used to obtain the diffusion coefficients [1, 2, 11–18]. However, the results of a molecular-dynamics, diffusion coefficients as a function of loading or temperature, are equally difficult to rationalise at the molecular level as the results of experiments, whereas an important part of diffusion research is to relate the observed trends in the diffusion coefficients to the behaviour of the molecules at the molecular level. Some groups have used Transition-State Theory to gain insight in the diffusion properties in zeolites [3, 19–28]. However, these studies were often limited to the infinite dilution limit, whereas most experimental values were obtained at nonzero loading [29–31]. Only recently, a dynamically corrected Transition-State Theory method (dcTST) has been developed that can be applied to study diffusion in confined systems beyond the infinite dilution limit [32]. This method can provide a molecular explanation for diffusion behaviour in terms of free energy [33, 34]. Armed with this method, we can now take a more generalised look on diffusion in confined systems.

In this chapter, we combine molecular-dynamics simulations with calculations using the new dcTST method to gain insight in the diffusion of methane in twelve different types of zeolites. We calculate self- and collective diffusivities as a function of loading and find an explanation by studying the free-energy changes as the loading is increased. Following the work of Skoulidas and Sholl [1], who published MD results for four different zeolite structures, we analyse a representative set of twelve zeolite structures for this study. We can divide the twelve zeolites in four different groups, that each have their own diffusion behaviour. We have chosen methane for this study, because it simplifies the interpretation of free-energy profiles and the explanation of our results. But the method is by no means limited to methane. A similar study could be made for any other molecule.

The remainder of the chapter is organised as follows. We begin in the next section with diffusion theory, the Darken approximation, lattice approaches and the Reed-Ehrlich model. Section 5.3 summarises the methods used, Molecular Dynamics and dynamically corrected Transition-State Theory, section 5.4 introduces the zeolites used for this study. The diffusion results for the four

zeolite groups are presented in section 5.5. In section 5.6 we evaluate the results and compare them to the Reed-Ehrlich method, and section 5.8 contains the conclusions.

5.2 Diffusion Theory

Diffusion can be expressed in a diffusion coefficient in several ways. In practical experiments, such as measurements of the uptake and permeation rate, the diffusion measured is usually the transport diffusion coefficient D_T. This coefficient is defined by Fick's law:

$$J = -D(c)_t \nabla c \tag{5.1}$$

where J is the sorbate flux when a concentration gradient ∇c is applied.

To obtain a diffusion coefficient that is presumably less dependent on loading, D_T is often converted to the collective diffusion D_C. This is also known as the Maxwell-Stefan or Darken diffusion coefficient, and can be obtained from:

$$D_T(\theta) = D_C \frac{\partial \ln f}{\partial \ln q} = D_C \times \gamma(\theta) \tag{5.2}$$

where q is the loading in the sorbent, θ the fractional occupancy, and f the fugacity [4]. The collective diffusivity is the collective diffusion behaviour of all adsorbate particles, including interparticle correlations and can be interpreted as the movement of the centre of mass of all particles together:

$$D_C = \lim_{t\to\infty} \frac{1}{6Nt} \sum_{i=1}^{N} \sum_{j=1}^{N} r_i(0) r_j(t) \tag{5.3}$$

$$= \lim_{t\to\infty} \frac{1}{6Nt} \Big(\sum_{i=1}^{N} \Delta r_i(t) \Big)^2 \tag{5.4}$$

One other common measure of diffusion is the self-diffusion coefficient D_S. It is the diffusion of a single tagged particle moving around in a sea of other particles. It is defined as

$$D_S = \lim_{t\to\infty} \frac{1}{6Nt} \sum_{i=1}^{N} \Delta r_i(t)^2 \tag{5.5}$$

where Δr_i is the displacement of particle i at time t with respect to time 0, and N is the number of particles. This is the diffusion coefficient that can be

obtained by microscopic methods, such as pulsed field gradient NMR (PFG-NMR).

In general, the collective diffusion is higher than the self-diffusion, because the collective diffusion contains interparticle correlations, which have a positive contribution, or, viewed differently, the self-diffusion is lowered by single-particle back-correlations (the increased probability of a particle jumping back to its previous position because this position has a higher probability of being empty).

5.2.1 The Darken Approximation

At the infinite dilution limit, D_S and D_C are strictly equivalent. This observation has often been used to approximate eq. 5.2 by replacing D_C with D_S. This is called the Darken approximation and eq. 5.2, under these conditions, the Darken equation [5]. For reasons of convenience, the collective diffusivity has been assumed to be relatively insensitive to changes in concentration, thus making it possible to use the Darken equation at arbitrary loading. It has for instance been used to relate microscopic and microscopic diffusion processes. Although many deviations have been found, where the collective diffusivity was concentration dependent, they were seen as exceptions to the general rule. For methane in MFI-type zeolite, support for the concentration independence was found almost up to high, but not maximum loading [1, 33].

5.2.2 Lattice Models and Correlations

Diffusion is often studied by considering particles' movements as a hopping process on a lattice. When the hopping rates between the different lattice points are known, the diffusion can be computed by using the formula

$$D_S = \frac{1}{2d} k \lambda^2, \tag{5.6}$$

where D_S is the self-diffusion coefficient, d the dimensionality of the system and k the hopping rate from a lattice site to any of its neighbouring lattice sites. It is often possible to coarse-grain a system for computation on a lattice, but care should be taken when diffusion coefficients are calculated in this way. Particles diffusing in a 'real' system might be inclined to hop onward in the same direction (so-called multijumps) or back in the direction from which they came (vacancy correlations). Particles that jump to a new position can attract other particles to jump after them. To obtain a correct diffusion coefficient, all these effects should be taken into account. For a more elaborate discussion

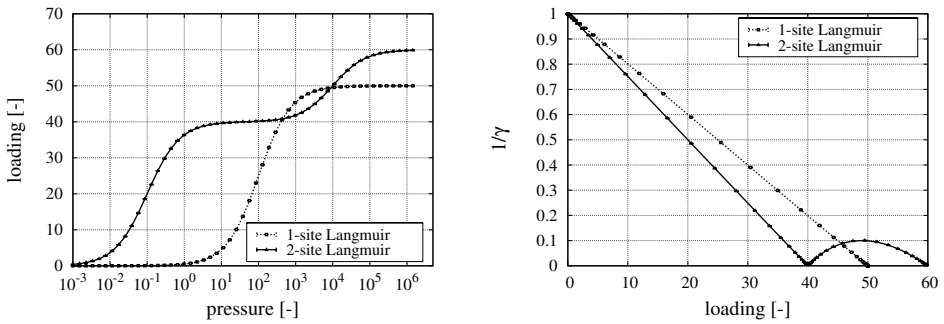

Figure 5.1: *Isotherm and $1/\gamma$ for a single-site Langmuir and a dual-site Langmuir system. Loading and pressures are given in arbitrary units.*

on interparticle and time correlations, we refer to the paper of Ala-Nissila et al. [35].

5.2.3 Diffusion Regimes and the Reed-Ehrlich Model

The starting point for our explanation of diffusion on a molecular scale is the Reed-Ehrlich model, which is often used to describe diffusion phenomena [36]. In this model, diffusion in a nanoporous material is considered as a hopping process on a lattice of adsorption sites, in which all sites have equal adsorption energies. The only restriction is that a particle cannot move to a site that is occupied by another particle. In such a system, the collective diffusion decreases linearly with loading:

$$D_C(q) = D_C(0) \times \frac{(q_{max} - q)}{q_{max}} = D_C(0) \times (1 - \theta) \tag{5.7}$$

where q is the loading, $D_C(0)$ the collective diffusion at infinite dilution, q_{max} the maximum loading and θ the fractional loading or occupancy.

The Reed-Ehrlich method was originally introduced for surface diffusion, but the model has recently been transferred to zeolites by Krishna and coworkers [37] and has been used successfully in several studies [9, 38–40].

The model works well for materials in which all adsorption sites are equal (in other words, diffusional barriers do not change as a function of loading, or $f = 1$ in the Reed-Ehrlich formulation) and for which the adsorption can thus be described by a single Langmuir isotherm.

However, most nanoporous materials have several types of adsorption sites, mutually differing in adsorption energy, and adsorption in such materials is

described by an n-site Langmuir isotherm. For this type of material, eq. 5.7 cannot be used and we have to use eq. 5.8 instead:

$$D_C(q) = D_C(0) \times \frac{\partial \ln q}{\partial \ln f} = D_C(0) \times \frac{1}{\gamma} \tag{5.8}$$

where f is the adsorbate fugacity and $1/\gamma$ gives the fraction of empty sites as a function of loading for an n-site Langmuir isotherm [37, 41–43]. For a single Langmuir isotherm, eq. 5.8 reduces to eq. 5.7. The isotherms and $1/\gamma$ as a function of loading for a single-site and dual-site system are shown in figure 5.1.

Diffusion in systems for which the energy of the different adsorption sites is not influenced by loading (for example, because there are no specific adsorption sites, or the sites are very far apart) can be very well described by equation 5.8. It is in the nature of a Langmuir isotherm that $1/\gamma$ is never constant over loading. This leaves us with two possible diffusion regimes:

A1 As the structure fills up, the diffusion *decreases* with loading. As adsorption sites are being filled up, less space is available for molecules to move around. For single-Langmuir systems, we see a linear decrease of diffusion as a function of loading (see figure 5.1(right)). For multiple-site Langmuir systems, a decrease in the adsorption is only observed in part of the loading range: the parts where the derivative of the adsorption isotherm decreases, or in other words, where the number of available adsorption sites diminishes. This decrease can be linear (as in figure 5.1(right) for a dual site Langmuir isotherm, up to a loading of 40), but it can also have a more complex form. In any nanoporous system, this behaviour is observed at very high loadings. When the available space is almost filled up completely, the molecules move ever more slowly, until their movement comes to a complete halt and the diffusion plunges to zero. The loading at which this happens defines the maximum loading of the material.

A2 At an inflection in the adsorption isotherm, the number of effective adsorption sites increases; the diffusion *increases* with loading. In systems with multiple-Langmuir adsorption behaviour, not all adsorption sites are filled at the same time. At a certain loading, new adsorption sites become available, or a reordering of the adsorbed molecules takes place. This is observed as an inflection in the adsorption isotherm and, correspondingly, an increase in the diffusion.

Most systems' diffusion behaviour cannot be captured completely by the adsorption isotherm. It is not uncommon for the energy of adsorption sites to be dependent on whether or not the neighbouring adsorption sites are occupied. In the Reed-Ehrlich model, this change in the free-energy can be cap-

tured by including a parameter f that is dependent on the loading [37, 39, 40]. This, however, requires a reasonably detailed prior knowledge about the system under study. We can calculate free-energy profiles of periodic nanoporous structures, by plotting the free energy as a function of the position. These profiles can change significantly over loading, following the energy changes of the adsorption sites. This gives rise to two additional diffusion regimes:

B1 Free-energy barriers decrease; the diffusion *increases* with loading. Favourable interaction of particles with the 'wall' of the nanoporous material is replaced by less favourable interactions with neighbouring adsorbed particles. This increases the free energy of adsorption regions and decreases the net free-energy barriers that have to be overcome to move to an adjacent adsorption region. A decrease in the effective free-energy barrier accelerates the diffusion. This is also the underlying cause of the so-called window effect [27, 28, 44–47]

B2 Free-energy barriers increase; the diffusion *decreases* with loading. Likewise, it is possible that the addition of extra molecules causes an increase in the free-energy barriers that molecules have to overcome in order to move around. For example, this could be the case for polar molecules, for which the interaction with other adsorbed molecules is more favourable than the interaction with the wall of the porous material. In such systems, when the loading is increased, the adsorbed molecules will stick more and more to each other and to their preferred positions, causing a decrease in the diffusion. A similar behaviour is observed for any molecule in any nanoporous material, at very high loadings, when the structure is almost completely full. The molecules inside the material are packed tightly, and movement from one position to the next involves crossing increasingly high free-energy barriers.

In real systems, diffusion is a complex interplay of all four effects. To demonstrate this, we will turn our attention to diffusion in zeolites.

5.3 Methods

The zeolites were modelled as rigid frameworks for which the interactions with the alkane molecules are dominated by the oxygen atoms [48]. For the guest molecules, a united atom model was used [49], in which we consider the CH_4 group as single reaction centre with its own effective potential. The potential parameters are optimised to reproduce adsorption properties in pure-silica confinements [50, 51].

5.3.1 Molecular Dynamics

The diffusion was calculated using Molecular Dynamics (MD) calculations. In an MD calculation, Newton's equations are being solved, to study particle positions as a function of time and thus obtain a mean squared displacement as a function of time. This mean squared displacement can easily be converted into a self-diffusion coefficient, by making use of:

$$D_{S,x} = \lim_{t\to\infty} \frac{1}{2Nt} \sum_{i=1}^{N} (\Delta x_i(t))^2 \tag{5.9}$$

and subsequently

$$D_S = \frac{D_{S,x} + D_{S,y} + D_{S,z}}{3} \tag{5.10}$$

In a similar fashion, the collective diffusivity can be obtained by calculating the mean squared displacement of the centre of mass:

$$D_{C,x} = \lim_{t\to\infty} \frac{1}{2Nt} <\Big(\sum_{i=1}^{N} r_{i,x}(t)\Big)^2> \tag{5.11}$$

and subsequently

$$D_C = \frac{D_{C,x} + D_{C,y} + D_{C,z}}{3} \tag{5.12}$$

5.3.2 Dynamically Corrected Transition-State Theory

Alternatively, self-diffusion coefficients can be computed using a dynamically corrected Transition-State Theory method. In addition to diffusion coefficients, such a method can yield an explanation of the diffusion behaviour in terms of free-energy differences. Transition-State Theory regards diffusion as a hopping process on a lattice, where the hopping from some state A to another state B is limited by a free-energy barrier between the two states. When the hopping rates between the different lattice points are known, the self-diffusion coefficient can be obtained using the formula

$$D_S = k_{A\to B}\lambda^2 = \frac{1}{6} k \lambda^2, \tag{5.13}$$

where D_S is the self-diffusion coefficient, $k_{A\to B}$ is the hopping rate from A to B, λ is the lattice distance (i.e. the distance between states A and B), and k the hopping rate from A to any of its neighbouring lattice sites. Eq. 5.13 gives the conversion from hopping rates to diffusion coefficients for a cubic lattice, but a similar equation can be derived for any other lattice topology.

When considering diffusion as a hopping process on a lattice, it is convenient to split the hopping rate k into two parts:

$$k = k^{TST} \times \kappa, \tag{5.14}$$

where k^{TST} is the trial hopping rate, determined from Transition-State Theory, i.e. the frequency with which a particle attempts to jump to a neighbouring lattice site, and κ is the dynamical correction factor, or, in other words, the probability that the particle will be accepted at the next lattice point. In this chapter we will make use of this concept, because it enables us to split the diffusion in a free-energy contribution, arising from the structure of the confinement and the ordering of the adsorbates inside, contained in k^{TST}, and an interparticle-collision contribution κ.

In the Bennett-Chandler approach [52–54] one computes the hopping rate $k_{A\to B}$ over the barrier in two steps. First, the relative probability $P(q^*)$ is computed to find a particle on top of the barrier, given that it is in state A, and subsequently the averaged velocity at the top of the barrier $\sqrt{k_B T/2\pi m}$ (assuming that the particle velocities follow a Maxwell-Boltzmann distribution) and the probability κ that the system ends up in state B. The transmission rate $k_{A\to B}$ from cage A to cage B is then given by

$$k_{A\to B} = \kappa \times \sqrt{\frac{k_B T}{2\pi m}} \times P(q^*), \tag{5.15}$$

$$P(q^*) = \frac{e^{-\beta F(q^*)}}{\int\limits_{\text{cage A}} e^{-\beta F(q)}\,\mathrm{d}q}, \tag{5.16}$$

where $\beta = 1/(k_B T)$, k_B is the Boltzmann constant, T temperature, m the mass involved in the reaction coordinate, and $F(q)$ the free energy as a function of q. In a first order approximation, TST assumes that all particles that reach the barrier with a velocity towards B do eventually end up in B, i.e. $\kappa = 1$. For soft-potential lattice models at nonzero loading, κ will be smaller than 1.

We can choose the reaction coordinate q as the position of one of the atoms of the diffusing molecules [27]. In dynamically corrected TST (dcTST), the transmission coefficient κ corrects for recrossing events, i.e. it corrects for trajectories which cross the transition state from A but fail to end up in B. The return of particles to cage A can be attributed to various causes. If the reaction coordinate is chosen in a nonoptimal way, this choice of order parameter underestimates the free energy of the true transition state, but the dynamical correction κ is the *exact* correction compensating for our choice of reaction coordinate [53]. Furthermore, κ can be smaller than one, due to

	ring size	window diameter [Å]	cage diam. [Å]	R_{ctw}	unit cell dimensions [Å] a	b	c	unit cell type	sim. box
LTA	8	4.1	10	2.44	24.555	24.555	24.555	cubic	$2 \times 2 \times 2$
ERI	8	$3.6 - 5.1$	11	3.06	22.953	13.252	14.810	orthorhombic	$2 \times 3 \times 3$
CHA	8	3.8	8.5	2.24	15.075	23.907	13.803	orthorhombic	$2 \times 2 \times 3$
FAU	12	7.4	9	1.22	25.028	25.028	25.028	cubic	$1 \times 1 \times 1$
SAS	8	4.2	10	2.38	14.322	14.322	10.424	tetragonal	$2 \times 2 \times 3$
LTL	12	7.1	13	1.83	31.984	18.466	7.476	orthorhombic	$1 \times 2 \times 4$
MTW	12	$5.6 - 6.0$	8	1.42	24.863	5.012	24.326	mon. $\beta = 107.722^o$	$1 \times 16 \times 1$
AFI	12	7.3	10	1.37	23.774	13.726	8.484	orthorhombic	$2 \times 2 \times 8$
BOG	12/10	$7.0/5.5 - 5.8$	$*$	–	20.236	23.798	12.798	orthorhombic	$2 \times 2 \times 3$
BEC	12/12	$6.6 - 7.7/5.6$	$*$	–	13.100	13.100	13.800	tetragonal	$3 \times 3 \times 3$
ISV	12/12	$6.1 - 6.5/5.9 - 6.6$	$*$	–	12.853	12.853	25.214	tetragonal	$2 \times 2 \times 1$
MFI	10/10	$5.1 - 5.5/5.3 - 5.6$	$*$	–	20.022	19.899	13.383	orthorhombic	$2 \times 2 \times 4$

Table 5.1: *Data for four cage-type zeolites (LTA, ERI, CHA and FAU), four channel-type zeolites (SAS, LTL, MTW and AFI), and four intersecting channel-type zeolites (BOG, BEC, ISV and MFI). For each zeolite type, the table lists the window ring size in number of oxygen atoms per ring, the window diameter and the cage diameter [Å], the cage-to-window ratio R_{ctw}, the unit cell dimensions in the three directions [Å], the unit cell form, and the size of the simulation box (the number of unit cells in x, y and z direction). The cage and window data (left and right) for intersecting channel-type zeolites are the values for the channels in the different directions. Where the window diameter is given as a range (e.g.* $3.6 - 5.1$ *for ERI-type zeolite), this signifies that the windows have an oval shape. The values for R_{wtc} in these cases are calculated as the ratio of the smallest diameter of the oval, to the diameter of the cage. * For the intersecting channel-type zeolites it is not practical to assign cage widths and window-to-cage ratios, for reasons given in the text.*

interparticle collisions: particles coming off the barrier and colliding with other particles before reaching equilibrium in state B, thereby returning to state A. If one manages to find a 'perfect' reaction coordinate (i.e. $\kappa = 1$ at zero loading), one can regard κ as a correlation and collision-frequency parameter: the lower the value of κ, the higher the number of collisions. In such cases it is possible to consider diffusion as a product of two contributions:

$$D_S = k_{A\to B} \times \lambda^2 = \kappa \times \sqrt{\frac{k_B T}{2\pi m}} \times P(q^*) \times \lambda^2 \tag{5.17}$$

$$= \kappa \times D_S^{TST} \tag{5.18}$$

In this equation, D_S^{TST} is the free-energy contribution to the self-diffusion, the part of the diffusion that is governed by free-energy barriers: effects of the topology of the confinement and the changes in the effective topology as a function of loading. κ is the contribution to the diffusion of interparticle collisions, which in general have a lowering effect on the diffusion. For more details about the dcTST method, we refer the reader to ref. [35].

By calculating diffusion in this way, it is possible to distinguish between topology contributions (included in D_S^{TST}) and particle-collision contributions (included in κ). This leads to a better understanding of diffusion behaviour as a function of loading, as we will show in the results section.

5.3.3 Computational Details

We used the Verlet integration algorithm with a time step of 0.5 fs and, depending on the diffusion speed, a total simulation time of between 1.5 and 1000 ns, such that the error bars were smaller than the symbol size. The NVT ensemble was imposed using a Nosé-Hoover thermostat. Free-energy profiles were obtained from Monte Carlo simulations, using the 'histogram method' described in ref. [32]. The simulation-box sizes for the various simulated systems are given in table 5.1.

5.4 Zeolite Structures

Zeolites are nanoporous solids, very suitable and used frequently as model systems for understanding molecular diffusivity in porous media, owing to their well-defined crystalline structure with highly ordered, periodic confinements [1, 2, 5, 6, 24, 55, 56].

Zeolites exist in a wide variety of structures. Currently, over 130 different topologies are known [57]. These structures are commonly divided in three

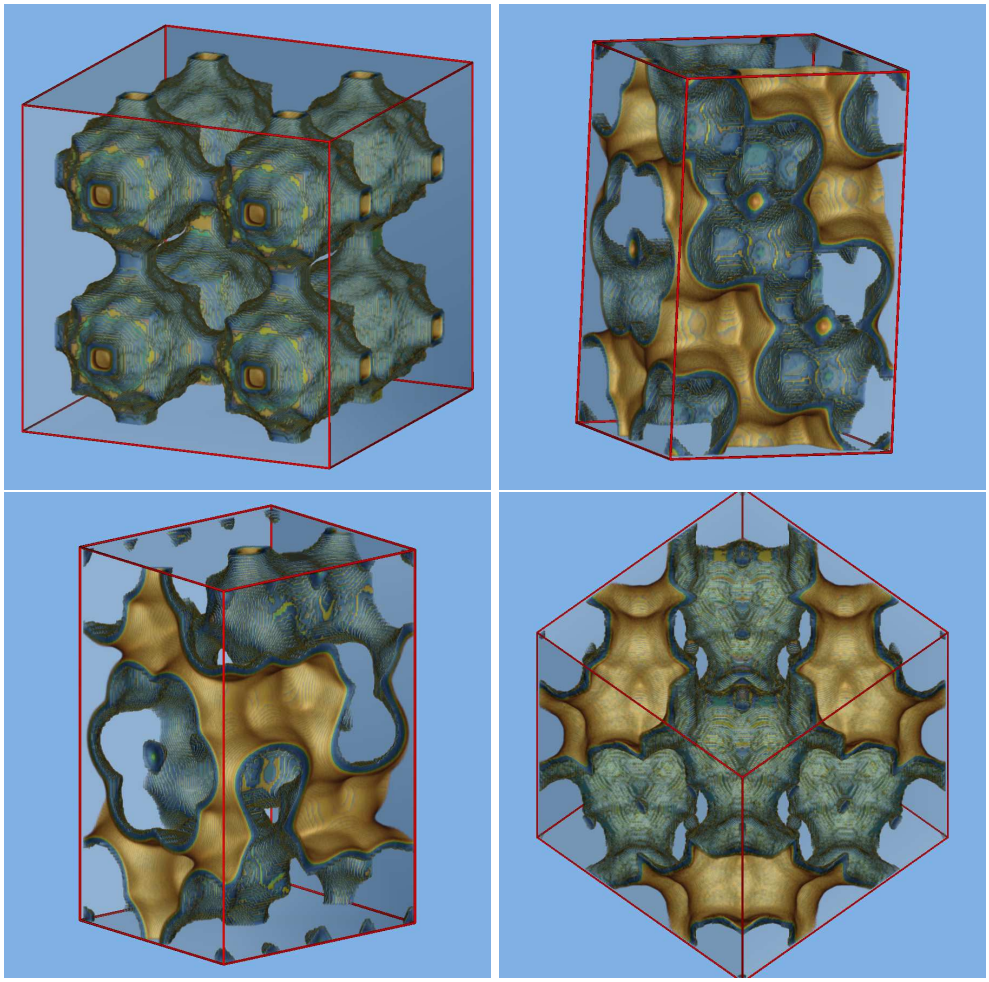

Figure 5.2: *Structure of the unit cells of four cage-type zeolites (LTA, CHA, ERI and FAU)*

types. Channel-type zeolites consist of more or less linear channels that run in one direction only. Therefore, diffusion in such structures occurs in one dimension only. Intersecting channel-type zeolites consist of channels in different directions, that cross each other at so-called intersections. Three dimensional cage-type zeolites consist of cages, connected by narrow windows.

We analyse a representative set of zeolite structures. We have tried to make our set of zeolites as broad as possible, by choosing twelve different, widely varying topologies. We calculated loading-dependent diffusion in four

different cage-type zeolites (LTA, ERI, CHA and FAU), four channel-type zeolites (AFI, MTW, LTL and SAS) and four intersecting channel-type zeolites (MFI, BOG, BEC and ISV). In this section we give a short overview of the different topologies. The structure coordinates for the twelve zeolites were taken from refs. [58–69].

5.4.1 Three-Dimensional Cage-Type Zeolites

Figure 5.2 shows the structures of the cage-type zeolites we used in this study. In table 5.1 we summarise some geometric data on these four structures. For each zeolite, the table lists the window ring size in number of oxygen atoms per ring, the window diameter and the cage diameter, the cage-to-window ratio R_{ctw}, which is defined as $R_{ctw} = cagediameter/windowdiameter$, the unit cell dimensions, the unit cell form, and the size of the simulation box. R_{ctw} can be used as a measure of confinement by the cage-type structure; the larger the value of R_{ctw}, the larger the difference between the cage width and the window diameter and the larger the free-energy barrier at the window is expected to be.

Of the four cage-type zeolites, erionite-type (ERI-type) type zeolite has the largest R_{ctw}. ERI-type zeolites have long cages, elongated in the c direction, that are each connected to six other cages, three on each side of the long cages. The windows connecting these cages are elliptical, their diameter varies from 3.6 Å in the b direction to 5.1 Å in the c direction. In our simulations, we used a rectangular version of the unit cell, where one unit cell of erionite contains four cages.

Zeolite types LTA and CHA have comparable values for R_{ctw}, 2.43 and 2.24 respectively, smaller than ERI-type zeolite. The structure of LTA-type zeolite consists of almost spherical cages of about 10 Å in diameter, connected by narrow windows of about 4 Å in diameter. One unit cell consists of eight cubically arranged cages and the windows form *entropic*, not *energetic* barriers. Zeolite A, Linde Type A (LTA), is a microporous crystalline material widely used in the detergent industry. Its supercage structure is useful in spatiospecific catalysis, typically of n-paraffins and olefins. One use is in paraffin cracking. The small entry pore is selective towards linear paraffins, and cracking can occur on sites within the supercage to produce smaller chain alkanes. [70] Zeolite A is also widely used in in ion-exchange separation [71].

A slightly smaller value for R_{ctw}, we find in chabazite-type (CHA-type) zeolite. It consists of slightly elongated cages, which are each connected to six other cages in a near-cubic fashion: the angles α, β and γ in the trigonal unit cell are all 94^o. For our simulations, a rectangular unit cell was constructed.

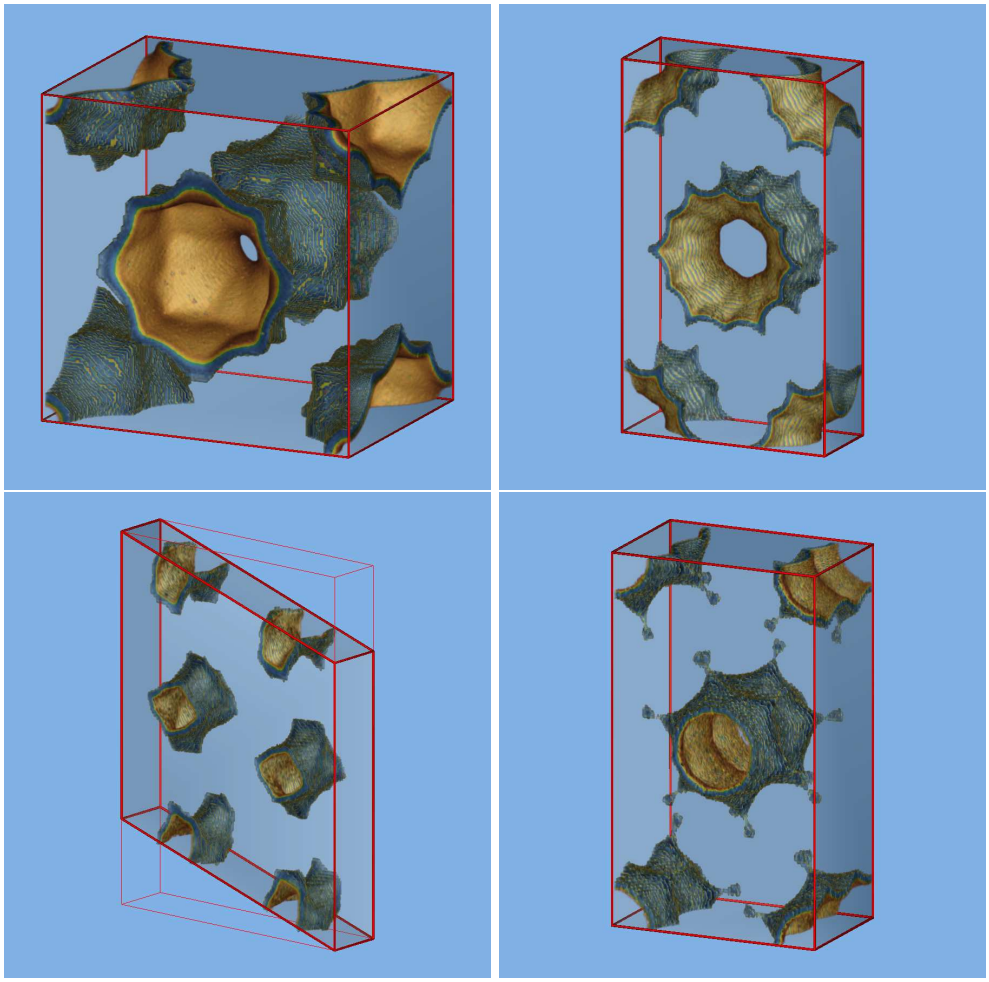

Figure 5.3: *Structure of the unit cells of channel-type structures SAS, LTL, MTW, and AFI*

CHA-type zeolite is industrially used in the formation of light olefins from methanol and in xylene isomerisation.

The smallest value of R_{ctw} we find in faujasite-type (FAU-type) zeolite. This zeolite has both large cages and large windows. One unit cell of FAU-type zeolite contains eight cages with a shape similar to those in LTA-type zeolite, but arranged in a tetrahedral manner. Depending on the atomic composition, FAU-type zeolites include zeolite X and Y. The most important use of zeolite Y is as a cracking catalyst. [72] [71, 73].

5.4.2 Channel-Type Zeolites

The class of channel-type zeolites is very diverse. All zeolites whose diffusion occurs in one direction only, in straight channels that are not interconnected, fall under this category. Thus, channel-type zeolites can consist of one-dimensionally connected cages, but can also consist of very smooth straight tubes, or channels with any degree of smoothness in between. Therefore, we cannot pick a single zeolite to represent the entire class of channel-type zeolites. To gain insight in the diffusion behaviour in this class, we will therefore turn our attention to four different channel-type zeolites: AFI, MTW, LTL and SAS. In this work we only consider channels that are sufficiently big or molecules that are sufficiently small such that two molecules can pass each other. In these one-dimensional channels one can observe an interesting case of geometry correlations if the molecules can not pass each other. In such a system one does not observe diffusive behaviour but single-file diffusion. Single-file diffusion has been extensively investigated in experiments [74–77] and in simulations [78–83].

Figure 5.3 shows the structures of these four zeolites. The accompanying geometric data are given in table 5.1. For channel-type zeolites, the cage-to-window ratio R_{ctw} can be used as a measure of 'cagelikeness': the larger the value of R_{ctw}, the larger the difference in width between the widest parts and the narrowest parts of the channels, and the larger, again, the free-energy barriers are expected to be.

One of the smoothest tubelike zeolites is AFI-type zeolite. It consists of straight channels that are not interconnected. Diffusion occurs in the z direction only. As shown in figure 5.3, a unit cell of AFI contains two channels, and the diameter of the channels varies between about 7.3 Å and 10 Å (a R_{ctw} of 1.37). AFI-type zeolites are used in the so-called Fischer-Tropsch synthesis, for the production of clean fuels and chemical products from natural gas and coal [84,85]. Other applications include the use in a zeolite-dye microlaser [86].

Another relatively smooth channel-type zeolite is MTW-type zeolite. Like AFI, this zeolite consists of straight channels, but in MTW-type zeolite they range between 5.6 and 8 Å in diameter (a R_{ctw} of 1.42) and they run in the y direction. MTW is among the smallest 12-membered ring zeolite structures [87]. A commonly used zeolite with MTW-topology is ZSM-12. It is known for its exceptional time stability and is used in acid-catalyzed reactions [87].

An intermediate channel-type zeolite is LTL-type zeolite. It consists of disklike cavities, whose widths range from about 7.1 Å in the circular 12-membered ring windows to about 13 Å in the broadest regions of the channels ($R_{ctw} = 1.83$). The cavities are connected in the x direction only. Though the

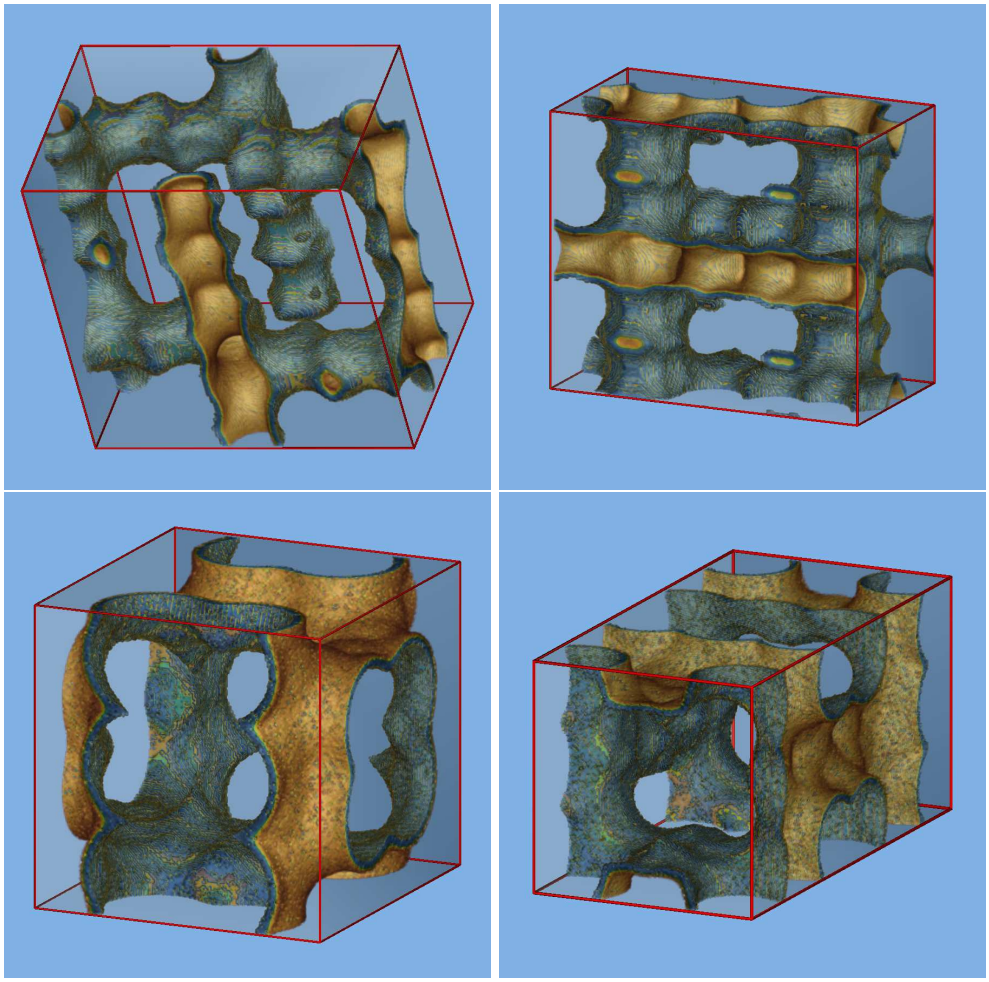

Figure 5.4: *Structure of the unit cells of intersecting channel-type structures MFI, BOG, BEC, and ISV*

windows connecting the cages are similar in size to those in AFI-type zeolite, the difference between the narrow parts and the broad parts of the channels is relatively large and the system can be considered slightly cagelike, where one unit cell contains two LTL "cages". Industrially, LTL-type zeolites are used in aromatisation reactions [88].

On the cagelike side of the channel zeolites, we find SAS-type zeolite. This zeolite is a one-dimensional version of the cage-type zeolite LTA. The cages (of about 10 Å in diameter) are similar to LTA-cages, but they are connected in

one dimension only, by 8-membered-ring windows of about 4.2 Å in diameter, making the window-to-cage diameter ratio $R_{ctw} = 2.38$. One unit cell of SAS-type zeolite contains two SAS cages. As the SAS topology has only recently been discovered, we are not aware of any industrial processes where zeolites of this type have found applications [65].

Simulation of one-dimensional channels requires special attention. Here, diffusion results are very much dependent on the length of the channel, and surprisingly long channels are needed to reliably extrapolate to macroscopic diffusion coefficients [18].

5.4.3 Intersecting Channel-Type Zeolites

The class of intersecting channel-type zeolites is also very diverse. Not only do these structures exist with a wide range of channel widths and window-to-cage ratios, they also differ largely in the way the channels intersect. The channels cannot only intersect at various angles, frequencies and channel numbers (either two or three channels can intersect at one point), but also intersect in different 'amounts'. The intersection can be 'complete', i.e. two (or three) channel axes intersect, or it can be partial, meaning there is a hole large enough for a molecule to pass from one channel to the next, without the two channel axes intersecting exactly.

In this study, we look at four intersecting channel structures: MFI, BOG, BEC, and ISV-type zeolites, the unit-cell structures of which are depicted in figure 5.4. The unit-cell data are summarised in table 5.1. For the intersecting channel-type zeolites it is not practical to talk about 'cage' widths and window-to-cage ratios. Usually the widest parts of the channels are regions where they are intersected by a perpendicular channel.

MFI-type zeolite is perhaps the most famous zeolite of this class. It is widely used industrially (as ZSM-5), because of its ability in promoting hydrocarbon reactions. It consists of straight 10-ring channels, running in the y direction, intersected (in 'complete' intersections) by so-called zigzag channels that run in the x and z directions and also consist of 10-membered ring windows.

Boggsite (BOG topology) is a naturally occurring mineral. Its channels run in x and y direction only, and intersect in 'partial' intersections. The x direction channels consist of 12-membered rings, while those running in y direction contain 10-membered rings.

BEC-type zeolite is one of the zeolite BETA polymorphs. It has 12-membered ring channels in x, y, and z directions. The channels in x and y direction are equivalent, though the z-channels only intersect the channels running in the x direction, in very broad 'complete' intersections.

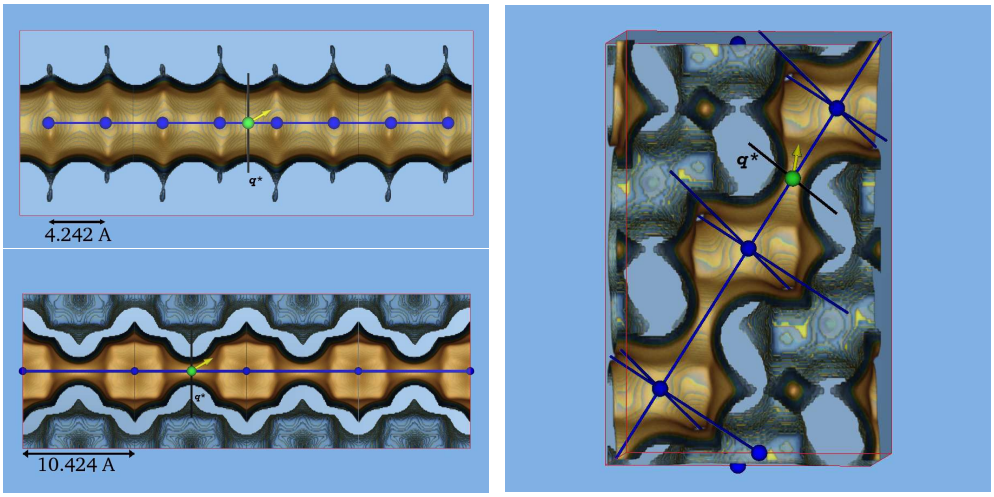

Figure 5.5: *The lattice spanned by the wide parts of the tubes in AFI and SAS type zeolites and the cage centres of CHA-type zeolite. q^* is the position of the barrier, perpendicular to the reaction coordinate. In the computation of κ, the particle starts in this plane.*

Like BEC-type zeolite, ISV consists of straight 12-membered ring channels in x, y, and z directions. Again, the channels in x and y direction are equivalent and the z-channels only intersect the channels running in the x direction, in broad 'complete' intersections. However, in ISV-type zeolite, the channels running in the z direction are merely short cross-links: they only connect two x direction channels, without continuing after the intersection.

5.4.4 Lattice Models in Zeolites

To be able to study diffusion using dcTST, it is necessary to choose a lattice to map on the zeolite structure. As shown in figure 5.5, this is often straightforward, as it follows from the zeolite topology or from the free-energy profiles calculated from it. The lattices shown for AFI and SAS-type zeolites are one-dimensional simple lattices, the lattice shown for CHA-type zeolite is a near-cubic lattice. It can be thought of as a cubic lattice that is slightly sheared in three directions to form angles of 94^o. For all the other studied zeolites, a lattice can be constructed in a similar fashion.

We stress that the used dcTST method is not a coarse-graining method. Knowledge of adsorption-site locations is not necessary to perform the simulation. By calculating free-energy profiles during an MD or MC run, the profiles

are automatically averaged over all possible configurations of the system. Making use of the periodicity of nanoporous materials, we use a lattice point only as the integration region in the dcTST method in order to obtain a diffusion coefficient [32].

5.5 Results and Discussion

We calculated loading-dependent diffusion in cage-type zeolites (LTA, ERI, CHA and FAU), channel-type zeolites (AFI, MTW, LTL and SAS) and intersecting channel-type zeolites (MFI, BOG, BEC and ISV). Free-energy profiles were calculated at different loadings, to help us understand the loading dependence of the diffusion. Free-energy differences play a role in both self and collective diffusion. In this section we discuss the self- and collective diffusion of methane in the three classes of zeolites. We show that while D_S can be computed directly from the free-energy profiles in combination with the recrossing κ, all the details in the behaviour of D_C as a function of loading can be explained very well by looking at these two parameters.

5.5.1 Self-Diffusion

Self-diffusion is a particle property. The self-diffusion as a function of loading reflects the way in which the particles' diffusion is hampered by collisions or enhanced by the presence of other particles in favourable adsorption sites. We show the diffusion behaviour in the three different zeolite classes.

5.5.1.1 Cage-Type Zeolites

We take LTA-type zeolite as a representative example of diffusion in cage-type zeolites and we treat the diffusion of methane in LTA-type zeolite in detail. Although diffusion in this type of zeolite has been studied extensively, the diffusion behaviour as a function of loading remains poorly understood [2, 19, 21–23, 25]. It has been shown to cause a maximum in the diffusion as a function of loading for a number of different molecules.

A density plot of methane in LTA is shown in figure 5.6. For small molecules, the positions in the windows regions constitute six favourable-adsorption sites. Other preferred positions are eight positions inside the cage, near the cage 'wall', in regions with high curvature. Four of these are clearly visible in figure 5.6, the other four are in a parallel plane straight behind, and obscured by, these four positions. These observations are in agreement with Demontis and Suffriti [89]. One more preferred methane position is found exactly in the

middle of the cage, and this makes the total number of preferred adsorption sites fifteen per cage.

Figure 5.7 shows the self and collective diffusion of methane in LTA, as a function of loading. Both exhibit a maximum at a loading of about 9-11 molecules per cage and a minimum at 15 molecules per cage, the loading at which all 15 preferred adsorption sites are occupied. There is a clear difference between D_S and D_C, especially at intermediate loadings $D_C > D_S$, caused by interparticle or back-correlations increasing D_C and diminishing D_S.

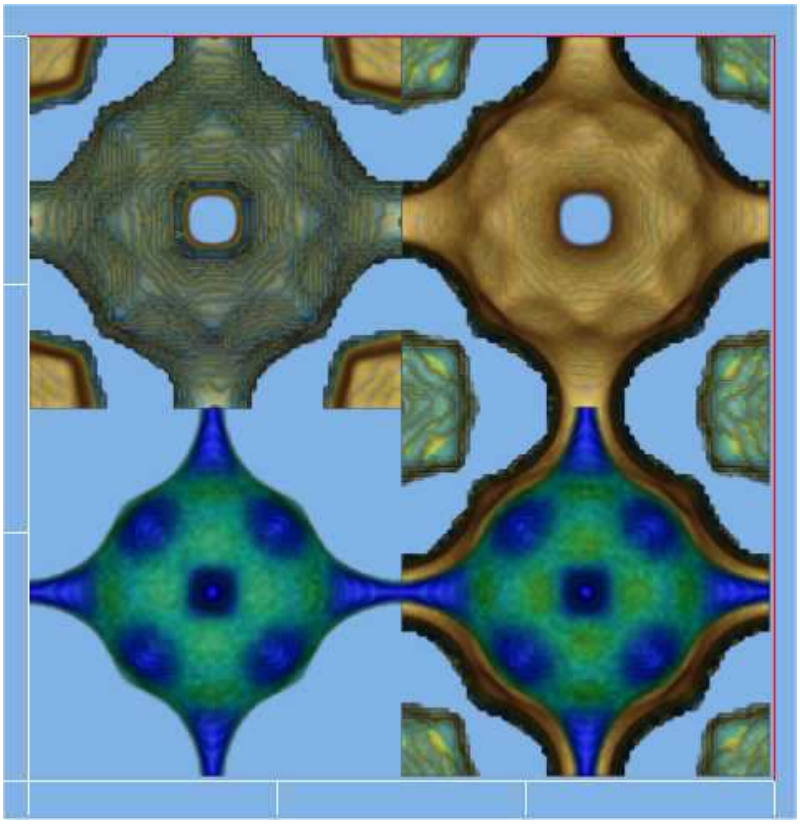

Figure 5.6: *Density plot of the distribution of eight methane molecules per cage in LTA-type zeolite, at 600 K. Blue regions are favourable adsorption sites, green regions have a lower probability of containing a particle.*

To explain this, we look at the free-energy profiles of methane in LTA, calculated at various loadings (see figure 5.8 (left)). Plotted is the free energy as a function of loading across two LTA cages. The lower parts of these profiles correspond to the interior of the cages; the maximum in the free-energy graphs

(around 12.2 Å) is located at the windows connecting two LTA cages. Because a high value of the free energy corresponds to a low probability of occupying this position, one might be tempted to conclude from the profiles in figure 5.8 (left) that the window between two cages is an unfavourable adsorption region. However, because the free energy, calculated in a slice perpendicular to the reaction coordinate (here the x coordinate), is a function of both the potential energy and the entropy, this is not necessarily true. In our example, the slice perpendicular to the window consists of a narrow low-energy window region and a large amount of inaccessible 'zeolite wall'. Figure 5.8 (right) shows the free-energy profile for methane in LTA, at zero loading, together with the potential-energy profile and the entropy (TS) profile. The free energy of the empty zeolite was calculated by performing Widom particle insertion and computing the Boltzmann factors for the separate interactions, in the following way:

$$\beta F(q) = -\ln\left(\left\langle e^{(-\beta U)}\right\rangle_q\right) \tag{5.19}$$

where $F(q)$ is the free energy of the particle-zeolite interaction at position q, and U the particle-zeolite interaction energy.

The potential energy as a function of the reaction coordinate was calculated using:

$$U(q) = \langle U\rangle_q = \frac{\sum_{x,y}\left(U(x,y,q)e^{(-\beta U(x,y,q))}\right)}{\sum_{x,y} e^{(-\beta U(x,y,q))}} \tag{5.20}$$

i.e. $\langle U\rangle_q$ is the average energy at a certain value of the reaction coordinate q, calculated in a plane perpendicular to the reaction coordinate. The entropy, expressed as $TS(q)$, was obtained from $F(q) = U(q) - TS(q)$.

When the minimum in the potential energy is considered, it is clear that the window between the two cages is a favourable adsorption position. However, since this region is so narrow, the window is an entropic barrier, as expressed by a high value of $-TS$ in the barrier region.

As the loading increases, more and more particles enter the cages. The surface of the LTA-cage is adsorbophylic: adding a molecule causes a decrease in the interaction with the walls. This favourable interaction is being replaced by a less favourable interaction with other particles, and hence, in figure 5.8 (left) we observe an increase of the free energy in the bottom of the well. Meanwhile, the free energy in the window region barely changes, so that while the zeolite is being filled up, the net free-energy barrier decreases, causing an increase in the diffusion coefficient.

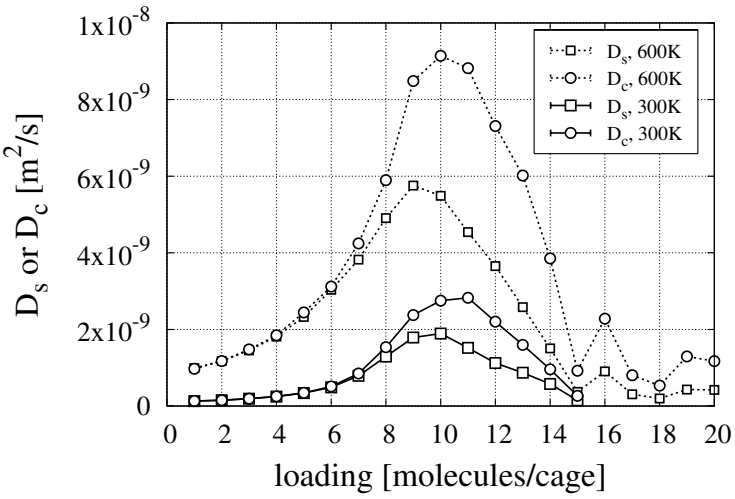

Figure 5.7: *Self and collective Diffusion of methane in cage type (LTA) zeolite, at 300 K and 600 K.*

At about 10 molecules per unit cell, the free-energy barrier starts to decrease again, because of packing effects. As the zeolite fills up, the molecules inside the cages become increasingly ordered. New free-energy barriers appear, and the diffusion slows down. At a loading of 15 molecules per unit cell, the methane molecules follow a highly ordered pattern inside the cages, every preferable position that is indicated in figure 5.6 is now occupied. The addition of another molecule means that this ordered structure has to be disturbed and a new ordering has to be formed. This new ordering changes the shape of the free-energy profile, and the diffusion increases again. Again, the molecule positions in the new ordering fill up, the diffusion increases a bit and afterwards decreases again, causing a second, smaller, maximum in figure 5.7.

We note that the new ordering at high loading and the second maximum in the diffusion graph will be very difficult to observe experimentally, because it would require very high pressures.

As explained in the methods section, Transition-State Theory can be used to calculate a hopping rate k^{TST} for the diffusion from cage to cage from the free-energy profiles. The true hopping rate k is then obtained by multiplying this k^{TST} with a factor κ that contains corrections for a nonideal choice of reaction coordinate, and collisions and correlations with other particles. Since LTA-type cages are highly symmetrical, it is possible to define a 'perfect' re-

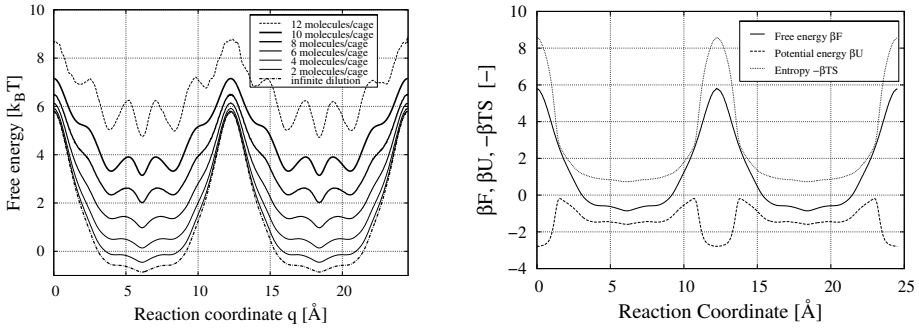

Figure 5.8: *(left) Free-energy profiles as a function of loading, at 600 K, for methane in cage type (LTA) zeolite (right) free-energy profile $\beta F = \beta U - \beta TS$ for methane in the empty zeolite, with potential energy contribution βU and entropy contribution $\beta TS = S/k_B$, as plotted before by Shüring et al. [90]*

action coordinate (i.e. at zero loading κ equals 1). At higher loadings, the deviations in κ are caused solely by interparticle collisions and correlations. It is therefore possible to split the diffusion of methane in LTA-type zeolite in a free-energy part and a collision part. The free-energy part is given by the Transition-State hopping rate from cage to cage, which is calculated directly from the free-energy profiles. The collision part can be obtained by calculation of κ. Figure 5.9 shows the two contributions as a function of loading. As the loading increases the Transition-State hopping rate at first increases to reach a maximum at around 11 molecules per unit cell. It is at this loading that we observe a sharper increase of the free energy at the barrier and the creation of new free-energy barriers inside the cage, caused by an increased ordering of the particles. While the free-energy part of the diffusion thus shows a maximum as a function of loading, the collision term, represented by κ is a continuously decreasing function of the loading, because as the number of particles in the system increases, collisions become ever more frequent events. Figure 5.9 clearly shows that the self-diffusion coefficient follows the trend of k^{TST}. In other words, the qualitative diffusion behaviour is determined by the change in the free-energy profiles. The collision factor κ has a quantitative effect on the diffusion coefficient and shifts the maximum in the diffusion curve slightly towards lower loadings.

Simulations of methane diffusion in different cage/window-type zeolites show that the observed diffusion behaviour is not specific for LTA-type zeolites, but is typical of this class of zeolite structures. Figure 5.10 shows diffusion as

a function of loading in LTA, ERI, CHA, and FAU. The loading at which the maximum in the diffusion coefficient is observed is dependent on the cage size. Clearly, if we increase the size of the cage, the position of the maximum in the diffusion coefficient will change accordingly. This is exactly what we observe for CHA, ERI, and LTA: CHA has the smallest cages of the three, LTA has the largest. We note that this fact is also reflected in the value for the diffusion at zero loading (given in figure 5.10): of these three zeolite types, the highest diffusion in the infinite dilution limit is observed in LTA, followed by ERI and subsequently CHA. The *increase* in self-diffusion compared to the infinite dilution limit can be very large, depending mainly on the size of the window and thus the height of the free-energy barrier. Especially in the case of ERI-type zeolite (whose 3.6 Å windows are the narrowest of the three), we observe an increase in the self-diffusion by a factor of 60. CHA and LTA have slightly wider windows, of 3.8 and 4.1 Å, respectively, and accordingly, the maximum in the normalised self-diffusion is smaller than that in ERI-type zeolite.

The diffusion in FAU-type (figure 5.10 (inset)) is quite different from that in the other three cage-type zeolites. While the initial slope is positive in the case of ERI, CHA and LTA, the self-diffusion of methane in FAU-type zeolites is a continuously decreasing function of loading. The reason for this is the large size of the windows that connect the FAU cages. The diameter of these windows, about 7.1 Å, does not differ much from the diameter of the cages, about 9 Å, and thus the windows hardly form a barrier for the diffusion. Since both the cages and the windows are large, the FAU zeolite structure forms a very weak confinement, the free-energy profiles barely change when the loading is increased, and the diffusion as a function of loading is as expected in a system of particles hopping on a lattice where the lattice does not change with loading. Since the diffusion in FAU-type zeolite is so much different from that in other cage-type zeolites, we will treat it in more detail in section 5.5.3.

5.5.1.2 Channel-Type Zeolites

The diffusion behaviour of methane in these systems is highly dependent on the ratio of the widest parts of the channels to the narrowest parts of the channels, the window-to-cage diameter ratio or R_{wtc}.

The qualitative behaviour is very different compared to that in cage-type zeolites. Whereas in LTA-type zeolite we observe a maximum in the diffusion as a function of loading, in the smooth channels of this class of zeolites, the diffusion slows down when the loading is increased.

An explanation of this behaviour can be found in the free-energy profiles of methane in AFI-type zeolite (figure 5.12). The minimums and maximums

in the profiles correspond to the broader and narrower parts of the AFI tubes, respectively. At zero loading, the height of the effective free-energy barriers is about 1.5 k_BT. Such a low value implies that the diffusion in z direction is barely hampered by the zeolite structure. Unlike in the case of cage-type zeolites, up to a loading of about 12 molecules per unit cell, the free-energy barrier increases rather than decreases when the loading is increased. Apparently, the higher the loading, the larger portion of the particles is located in the wider regions of the AFI channels. At a loading of about 12 molecules per unit cell however, the form of the free-energy profiles changes. This is in agreement with Maris et al. [91] who found a reordering of methane molecules in AFI-type zeolite at higher loadings. In the altered form of the free-energy profile, the free-energy barrier is much lower and this gives rise to an acceleration of the diffusion, as is indeed observed at loadings higher than 12 molecules per unit cell.

When we compare the diffusion of methane in AFI-type zeolite with that in a one-dimensional, channel-type structure with a similar R_{wtc} (e.g. MTW-type zeolite), we observe similar diffusion behaviour (see figure 5.11). Common to these two systems is their preference for a fixed ordering at lower loadings (while this particle arrangement fills up when the loading is increased, the diffusion decreases) and a sudden change of particle positions at higher loadings, which gives rise to a peak in the diffusion as a function of loading. As R_{ctw} in MTW-type zeolite is a bit higher than in AFI-type zeolite, the free-energy barriers in MTW-type zeolite (shown in figure 5.12) are higher and the low-loading behaviour of the diffusion is slightly more cagelike in nature, which is expressed in a slightly convex initial slope of the collective diffusion as a function of loading, as will be discussed in section 5.5.2. However, as the distance between two consecutive free-energy barriers in MTW-type zeolite is much smaller than in AFI-type (5.012 Å vs. 8.484 Å), the back-correlations are much higher, as evidenced by a very low self-diffusion.

In LTL-type zeolite, because the windows are quite broad, the dominant behaviour of methane diffusion in LTL-type zeolite is that of methane in smooth linear tubes such as AFI-type zeolite. However, since the difference in width between the windows and the cage regions is large (i.e. the cages are even broader), at lower loadings we still observe some cagelike behaviour: the self-diffusion of methane is a slightly convex function of loading. The cagelike behaviour becomes more evident in the collective diffusion, in section 5.5.2.

On the cagelike side of the channel zeolites, we find SAS-type zeolite. Considering the topology, which consists of one-dimensionally connected LTA-cages, it is not surprising that the diffusion of methane in SAS-type zeolite

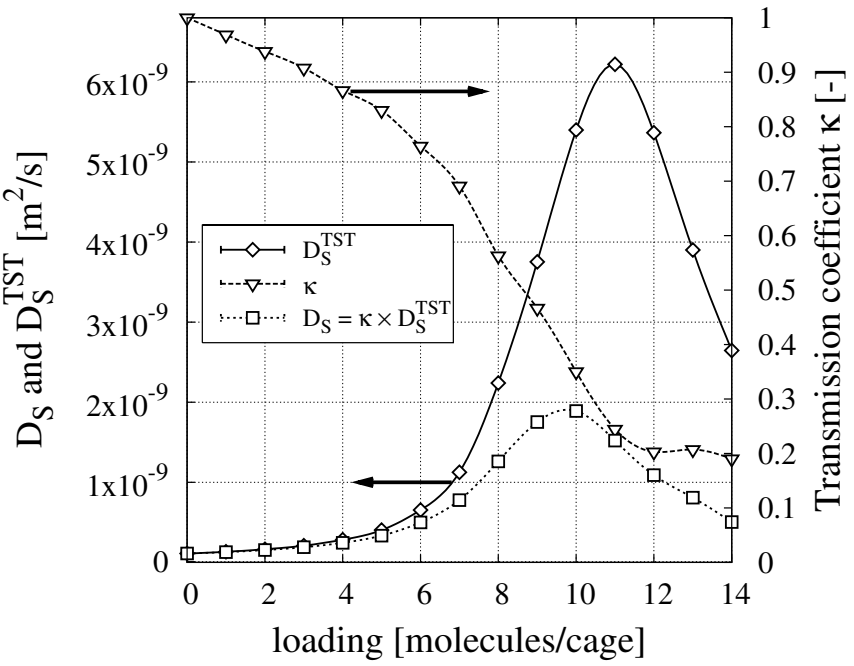

Figure 5.9: *Diffusion of methane in LTA-type zeolite as a function of loading at 300 K (left axis), and the two contributions to this diffusion: the free-energy part, given by the Transition-State self-diffusion coefficient D^{TST} (left axis), and the collision part, given by the transmission coefficient κ (right axis).*

follows a trend similar to that in three-dimensional cage-type zeolites such as LTA, CHA and ERI: an increase rise in the diffusion up to a loading of about half the maximum loading, caused by an increase in the free energy inside the cages (see figure 5.12(bottom,right)), followed by a decrease that approaches zero at the maximum loading. Note that, though the cages of SAS-type zeolite are comparable to those in LTA-type zeolite, the maximum loading is a bit lower than in LTA-type zeolite. The particles are arranged differently, due to the lack of windows in four directions (out of the six available in LTA-type zeolite) and to the fact that the connection between the cages is different from that in LTA-type zeolite.

In summary, the self-diffusion in channel-type zeolites is dependent mainly on R_{wtc}, the height of the free-energy barriers and the distances between them.

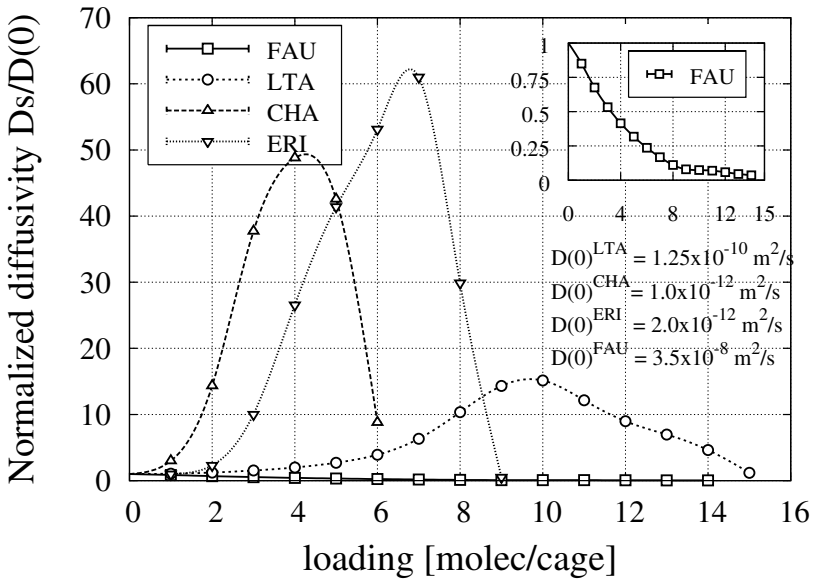

Figure 5.10: *Normalised self-diffusion of methane in cage-type zeolites ERI, LTA, CHA, and FAU, as a function of loading, at 300 K, inset: normalised self-diffusion in FAU*

When we split the diffusion coefficient in two contributions, D_S^{TST} and κ, as shown for AFI-type zeolite in figure 5.13, we see that the diffusion is influenced by both contributions: D_S^{TST} is a steadily decreasing function of loading, but κ also decreases rapidly. As a consequence, the self-diffusion of methane in AFI-type zeolite is a steeply decreasing function of loading, with a small maximum around 12 molecules per unit cell.

Figure 5.14 (top) shows the D_S^{TST} component of the diffusion for AFI, MTW, LTL and SAS-type zeolites. For SAS-type zeolite, we clearly see the same cagelike type of behaviour we saw earlier for LTA-type zeolite. At low loadings, the effective free-energy barrier decreases and the free-energy part of the diffusion is increasing. Also for LTL-type zeolite, D_S^{TST} is an increasing function of loading, although now it is continuously increasing, because of the broad barriers depicted in figure 5.12 (bottom, left). Only for the two 'smooth' channels, AFI and MTW, D_S^{TST} decreases as a function of loading. Figure 5.14 (bottom) shows the κ component of the diffusion. As expected, the value of κ is highest in the high-barrier system of SAS-type zeolite, where interparticle correlations are low, and the lowest in MTW, which has the smallest distance

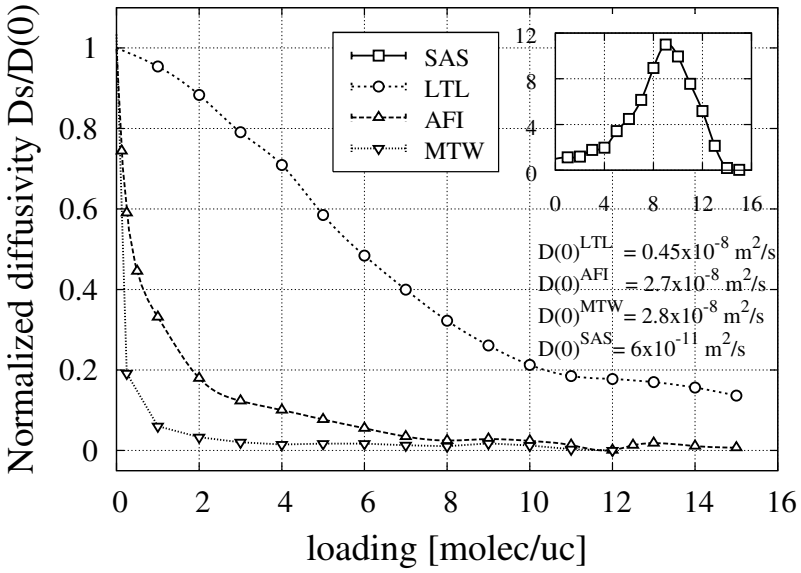

Figure 5.11: *Normalised self-diffusion of methane in channel-type zeolites AFI, MTW, LTL, and SAS (inset), as a function of loading, at 300 K*

between two consecutive barriers and therefore the highest interparticle correlations. LTL and AFI type zeolite have a value of κ in between these two extremes. This leads to the conclusion that from a free-energy point of view SAS and LTL are cage-type zeolites, whereas AFI and MTW are not. From an interparticle-correlations point of view, SAS is a cage-type zeolite, MTW clearly is not, and AFI and LTL are something in between. This results in cage-type diffusion behaviour in SAS-type zeolite, slightly cage-type behaviour in LTL, and smooth channel behaviour in AFI and MTW.

5.5.1.3 Intersecting Channel-Type Zeolites

An important class of zeolites, is the class of intersecting channel-type zeolites, of which MFI is the best known example. These structures consist of three-dimensionally interconnected straight channels. The self-diffusion of methane in four of these structures, MFI, BOG, BEC, and ISV, is shown in figure 5.15. This figure shows the diffusion relative to that in the infinite dilution limit. It is a monotonously decreasing function of loading, similar to that in smooth channel-type zeolites such as AFI and MTW. The self-diffusion behaviour of

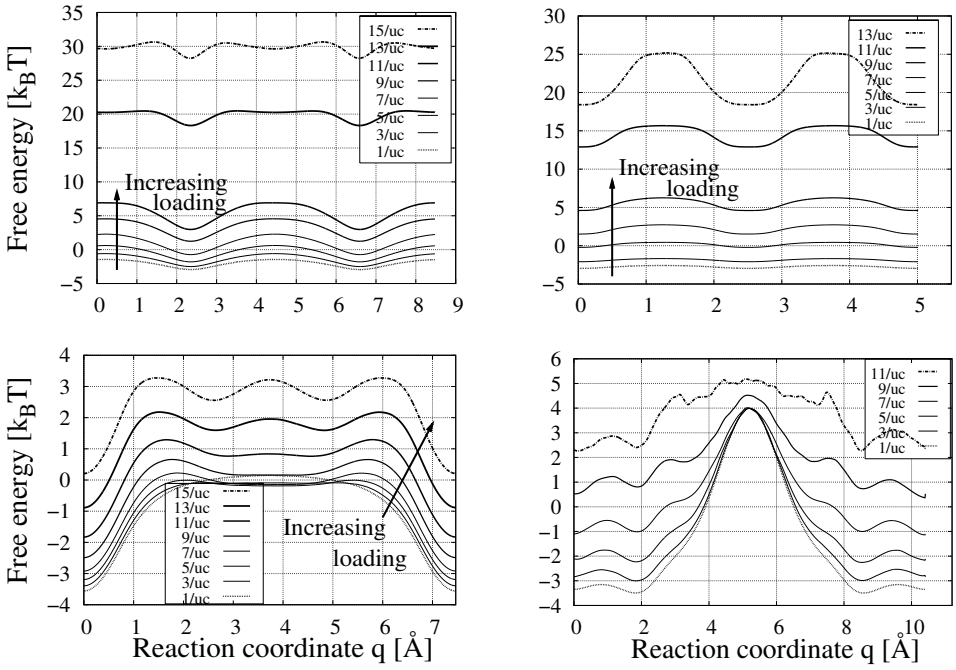

Figure 5.12: *Free-energy profiles at 300 K at different loadings of methane for AFI-type zeolite (top left), MTW-type zeolite (top right), LTL-type zeolite (bottom left) and SAS-type zeolite (bottom right)*

methane in MFI, ISV and BOG-type is almost identical, as the maximum loadings of the three zeolites are similar. The diffusion in BEC-type zeolite is also very similar to the other intersecting channel-type zeolites, although the maximum loading is about half that of MFI, BOG, and ISV, in agreement with the relative size of the unit cell. The unit cell is smaller, and therefore the diffusion behaviour is shifted to lower loadings.

The value of the diffusion coefficients in the infinite dilution limit is dependent mainly on the smallest-ring size of the zeolite channels. $D_0^{BEC} > D_0^{ISV} > D_0^{BOG} > D_0^{MFI}$, while BEC and ISV-type zeolites have a smallest-ring size of 12 in both the straight channels and the perpendicular channels, BOG-type zeolites have 12-membered rings in the x direction and 10-membered rings in the narrower y direction channels, and MFI-type zeolites have 10-membered rings in both the straight and the zigzag channels. However, the exact value of D_0 depends on the exact topology and cannot be determined a priori by the ring size alone.

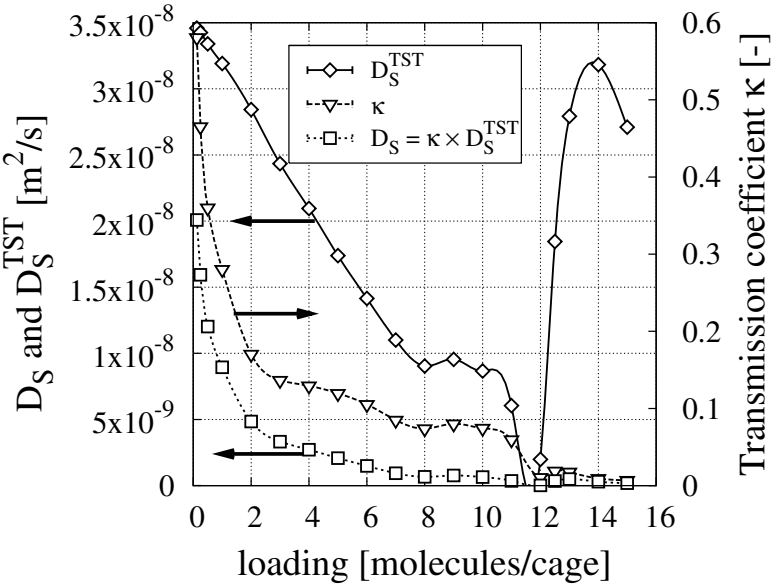

Figure 5.13: *Diffusion of methane in AFI-type zeolite as a function of loading (left axis) at 300 K, and the two contributions to this diffusion: the free-energy part, given by the Transition-State self-diffusion coefficient D^{TST} (left axis), and the collision part, given by the transmission coefficient κ (right axis).*

As an example, we split D_S^{TST} in D^{TST} and κ for diffusion in MFI-type zeolite along the y direction (see figure 5.16). From the behaviour of D_S^{TST} one could expect a cagelike behaviour of the diffusion. However, it is clear that the diffusion is completely dominated by κ, which is a measure of the correlations in the system and the collision frequency. κ decreases more rapidly than D^{TST} decreases, so the net effect is the self-diffusion in MFI-type zeolite is a decreasing function of loading. The cage-type structure suggested by the maximum in D_S^{TST} is more visible in the loading behaviour of the collective diffusion. We note that the figure shows that κ is not equal to 1 at zero loading, which implies that κ also contains some corrections for an nonideal choice of reaction coordinate.

5.5.2 Collective Diffusivity

The collective diffusion behaviour is a system property. It is the collective diffusion of all particles through the zeolite and includes interparticle correlations.

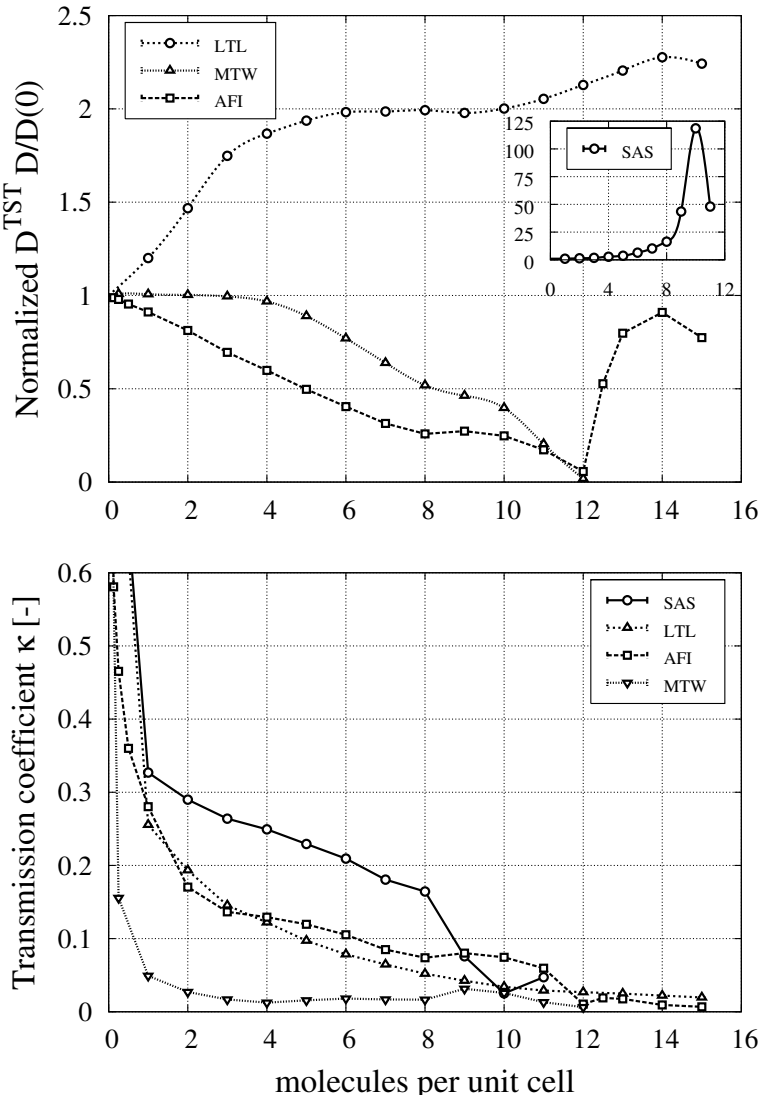

Figure 5.14: *Normalised free-energy contribution D^{TST} for AFI, MTW, LTL, and SAS (inset) type zeolites (top) and Collision contribution κ for the four structures (bottom)*

As it turns out, collective diffusion as a function of loading can be described accurately by looking at the free-energy profiles as a function of loading. Again, each of the three zeolite classes has a very distinct loading-dependent diffusion

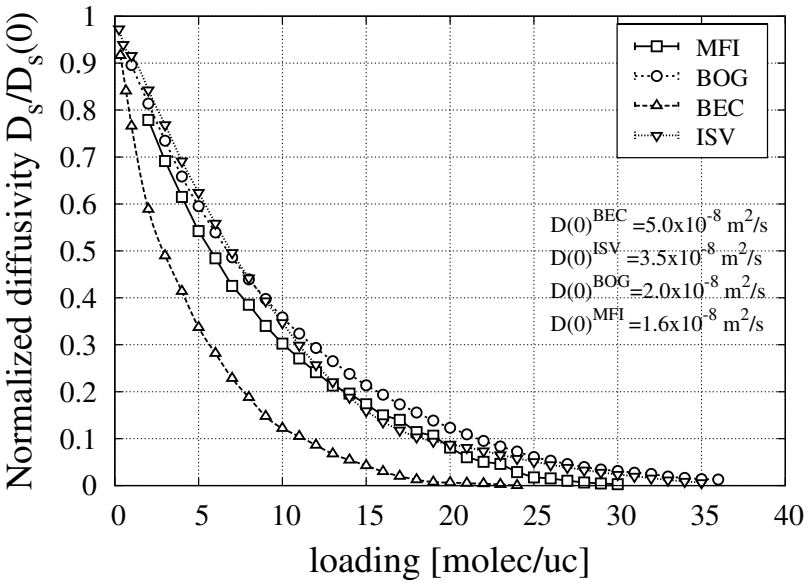

Figure 5.15: *Normalised self-diffusion of methane in intersecting channel-type zeolites MFI, BOG, BEC, and ISV, as a function of loading, at 300 K*

behaviour.

5.5.2.1 Cage-Type Zeolites

Figure 5.17 shows the collective diffusion of methane in LTA, CHA, ERI and FAU, normalised with respect to the diffusion in the infinite dilution limit. For LTA, CHA and ERI-type zeolites, the qualitative diffusion behaviour is similar to the self-diffusion: a maximum as a function of loading at about 2/3 of the maximum loading. As expected, the collective diffusion is higher than the self-diffusion, because of interparticle and back-correlations. Since at zero loading the self-diffusion is equal to the collective diffusion, $D_0^{FAU} > D_0^{LTA} > D_0^{ERI} > D_0^{CHA}$ also holds for the collective diffusion.

The *increase* in the collective diffusion compared to the infinite dilution limit is even higher than that in the self-diffusion. In ERI and CHA-type zeolites, the increase in the diffusion is almost two orders in magnitude.

Again, the diffusion in FAU-type zeolite is completely different from the diffusion in the other cage-type zeolites. It is an almost linearly decreasing function of loading, as expected of collective diffusion in a system where the

barriers do not change as a function of the loading. The collective diffusion of FAU-type zeolite will be treated in more detail in section 5.5.3.

5.5.2.2 Channel-Type Zeolites

As in the case of self-diffusion, the diffusion behaviour as a function of loading is highly dependent on the amount of 'cagelikeness', for which R_{wtc} is a good indicator. For our four channel-type zeolites $R_{wtc}^{SAS} > R_{wtc}^{LTL} > R_{wtc}^{MTW} > R_{wtc}^{AFI}$, and this is clearly reflected in the diffusion curves in figure 5.18. The diffusion of methane in AFI and MTW-type zeolites is a continuously decreasing function of loading. The curve is more convex for MTW, because of the higher R_{wtc}. As in the case of self-diffusion, a small maximum is found at about 10 and 13 molecules per unit cell, in MTW and AFI, respectively, because of a reordering of adsorbed molecules inside the zeolite.

In LTL the difference in width between the windows and the cage regions is quite large, and therefore, at low loadings we still observe some cagelike behaviour in the collective diffusion. There is a small peak in the diffusion at a loading of about 3 molecules per unit cell. When the loading is further increased, the diffusion slows down, as is expected in a tubelike structure. As in the case of self-diffusion, SAS-type zeolite clearly exhibits cage-type behaviour.

The collective diffusion of methane in channel-type zeolites SAS, LTL, MTW, and AFI is shown in figure 5.18.

5.5.2.3 Intersecting Channel-Type Zeolites

As an example of how free-energy profiles can contain a lot of detail about diffusion behaviour, we treat the diffusion in MFI-type zeolite in detail. The structure of MFI consists of two straight channels per unit cell, intersected by two zigzag channels. At low loadings, there are four favourable positions per straight channel and four favourable positions per zigzag channel, making the total number of preferential adsorption sites per unit cell 16.

Pascual et al. found that at low loadings, methane in MFI-type zeolite does not have any preference for either of these positions and is located everywhere inside the zeolite [92]. When the loading exceeds 16 molecules per unit cell, all these positions are filled, and new adsorption sites have to be formed in order to accommodate more molecules.

Again, our explanation of the diffusion behaviour comes from free-energy profiles, shown in figure 5.21. The x, y and z directions in MFI-type zeolite are not equivalent, therefore we have to consider them separately.

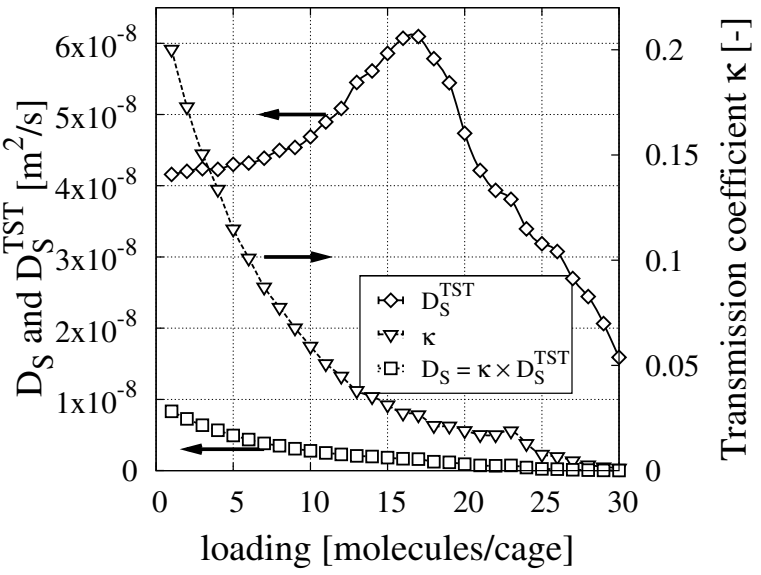

Figure 5.16: *$D_{S,y}$ of methane in MFI-type zeolite at 300 K as a function of loading (left axis), and the two contributions to this diffusion in the y direction: the free-energy part, given by the Transition-State self-diffusion coefficient D_y^{TST} (left axis), and the collision part, given by the transmission coefficient κ_y (right axis).*

The fastest diffusion occurs along the y direction, in the straight channels. At low loadings (up to about 13 molecules per unit cell), the particles are so far apart that they hardly influence each other's diffusion. $D_{C,y}$ is approximately constant and the free-energy profiles remain the same. The highest free-energy barrier is located at **B**. The minima in the free-energy profiles (at about 5 and 15 Å) correspond to the positions of the intersections and zigzag channels (all mapped onto the same y coordinate), the regions 5-15 Å and 15-20 plus 0-5 Å correspond to the interior of the straight channels. Apart from the intersections, there are four minima in the free-energy profiles along the direction of the straight channels, which correspond with four favourable adsorption positions.

When the loading exceeds 13 molecules per unit cell, the free-energy profile changes slightly (see figure 5.22 (top)): the barrier at **B** is lowered, and the smaller barrier at **D** is raised a bit. This indicates that, while the 'most common' configuration is still four adsorption sites per straight channel, the av-

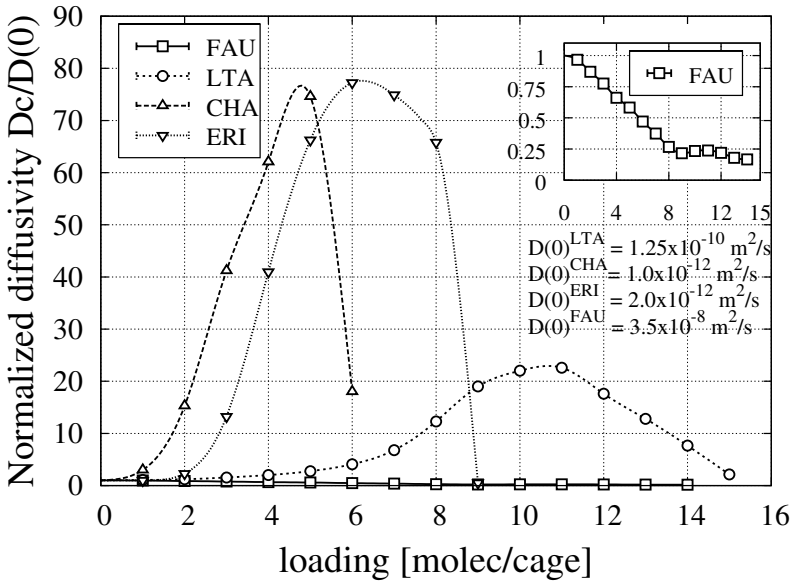

Figure 5.17: *Normalised collective diffusion of methane in cage-type zeolites LTA, CHA, ERI and FAU, as a function of loading, at 300 K*

erage loading of the straight channels increases and some molecules are located at nonstandard positions inside the straight channel. The observed free-energy profile is an average over all these configurations and as the net barrier decreases, we see a slight increase in the diffusion in the y direction, between 13 and 17 molecules per unit cell. At a loading of 17 molecules per unit cell and higher, the dominant change in the free-energy profiles is the sharp increase of the peak at **D**, causing a fast decrease of the $D_{C,y}$ as a function of loading (see figure 5.22 (middle)), until it reaches zero at the maximum loading, which is about 30 molecules per unit cell. The decrease is only interrupted by a small peak in $D_{C,y}$ at 23 molecules per unit cell. At a loading between 22 and 25 molecules per unit cell, the free-energy profiles change significantly (see figure 5.22 (bottom)): the peaks at **A** and **E** increase, the peak at **D** vanishes, and a new peak appears at **C**. This change signifies a transition from four to eight adsorption sites per straight channel. The appearance and disappearance of peaks does not occur simultaneously. At first, the dominating effect is the increase in the peak at **A** and the diffusion continues to decrease. The sudden disappearance of the peak at **D** causes a maximum in the diffusion at 23 molecules per unit cell, which immediately vanishes at higher loadings, when

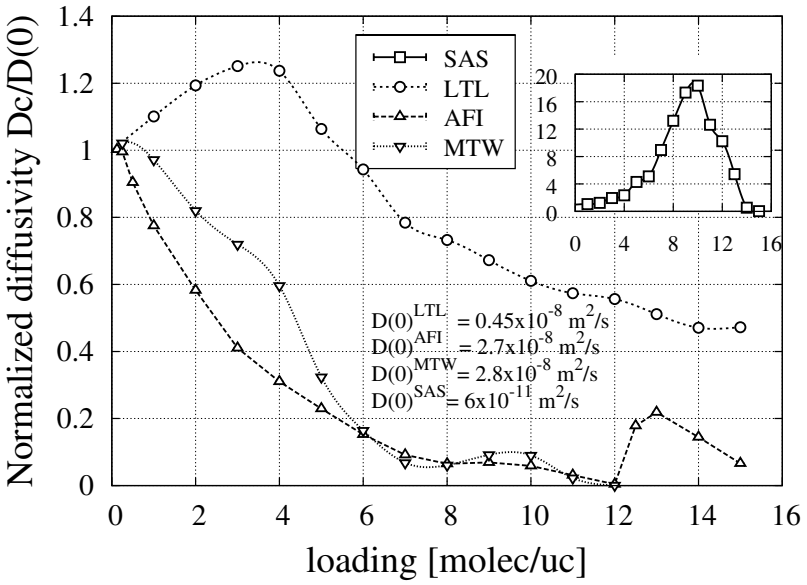

Figure 5.18: *Normalised collective diffusion of methane in channel-type zeolites AFI, MTW, LTL, and SAS (inset), as a function of loading, at 300 K*

the peak at **C** appears.

In a similar way, the diffusion in the x direction, $D_{C,x}$, can be explained. Up to a loading of about 16 molecules per unit cell, the free-energy profiles do not change much. Only the peak at **C** slightly increases, causing a very slow decrease in the diffusion. At a loading of 16 molecules per unit cell, which corresponds to four molecules per straight channel and four molecules per zigzag channel, a reordering of the adsorbates inside the zeolite takes place. As with the change in the straight channels, a transition takes place from four to eight molecules per zigzag channel. This transition gives rise to a new free-energy profile: first the free energy at **B** decreases, giving rise to a small increase in the diffusion at 18-19 molecules per unit cell, followed soon after by an increase of the free energy at **A** and **C**. This increase is so significant that the diffusion rapidly slows down until it reaches zero at the maximum loading. As is shown in figure 5.21, at very high loadings, from 29 molecules per unit cell, another transition takes place. The peak at **A** broadens to encompass **B** and, simultaneously, a new peak appears at **D**. This indicates that at higher loadings particles inside the straight channels are inclined to arrange in two

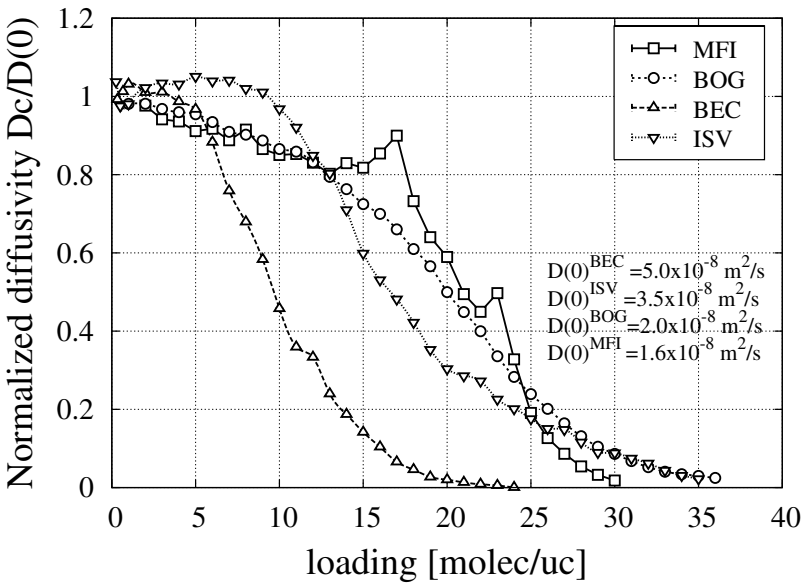

Figure 5.19: *Normalised collective diffusion of methane in intersecting channel-type zeolites MFI, BOG, BEC, and ISV, as a function of loading, at 300 K*

rows (left and right of peak **D**).

The diffusion in the z direction ($D_{C,z}$) finally, proceeds in a similar way as that in the x direction. At low loadings, the diffusion decreases as a function of loading. At a loading of 17 molecules per unit cell the free-energy profiles reflect the transition from four to eight molecules per zigzag channel. This transition causes a slight acceleration of the diffusion at 18-19 molecules per unit cell after which the diffusion slows down to zero. As in the x direction profiles, at very high loadings, we see another transition: the peak at **B** vanishes, and new peaks appear at **A** and **C**.

The total collective diffusion of methane in MFI-type zeolite is dominated by the diffusion in y direction. It is a slowly decreasing function of loading up to about 15 molecules per unit cell. There is a maximum in the diffusion at a loading of 16-17 molecules per unit cell, after which the diffusion rapidly decreases to reach zero at the maximum loading of 32 molecules per unit cell, interrupted by a small rise in the diffusion at 23 molecules per unit cell. This is in agreement with Skoulidas and Sholl, who simulated the collective diffusion of methane in MFI-type zeolite up to a loading of 18.5 molecules per unit cell [1]

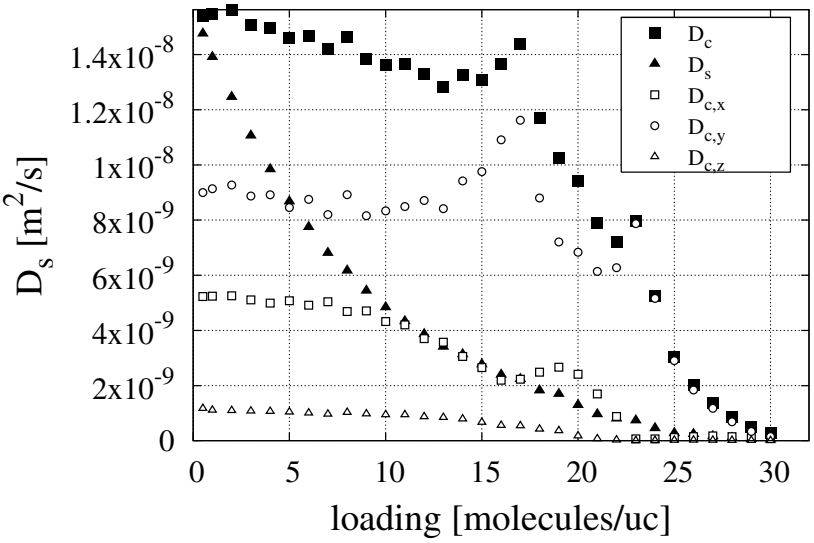

Figure 5.20: *D_S and D_C of methane in MFI-type zeolite, as a function of loading, D_C in x, y and z directions*

In other intersecting channel-type zeolites, such as BEC, ISV and BOG type zeolites we observe very similar behaviour, shown in figure 5.23.

This figure shows the diffusion relative to that in the infinite dilution limit. The diffusion behaviour of methane in BOG-type is almost identical to that in MFI. The maximum loading of the two zeolites is similar and the free-energy profiles (and thus the particle distributions) show a similar loading dependence. However, the diffusion in BOG-type zeolite does not have maxima at 17 and 23 molecules per unit cell. The diffusion in BEC-type zeolite is also very similar to the other intersecting channel-type zeolites, although the maximum loading is about half that of MFI and BOG, in agreement with the relative size of the unit cell, and therefore the diffusion behaviour is shifted to lower loadings. The loading dependence in ISV-type zeolite is, for most parts, in agreement with that in the other intersecting channel-type zeolites. However, the low-loading behaviour, where the diffusion slightly increases as a function of loading, is slightly different and could even be considered slightly cagelike.

In summary, the trends in the behaviour of the collective diffusion as a function of loading are very similar for all studied types of intersecting channel-type zeolites: at low loading it is a slowly diminishing function of loading, at

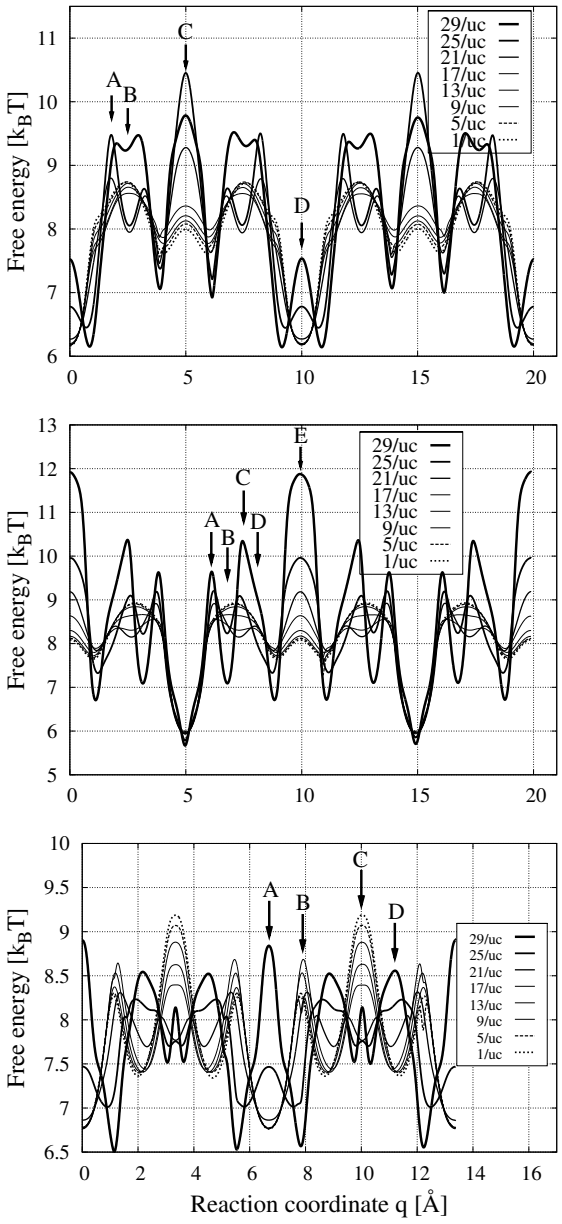

Figure 5.21: *Free-energy profiles, at 300 K, at different loadings for methane in MFI-type zeolite along the x direction, y direction and z direction, respectively. The straight channels run in the y direction, the zigzag channels run in x and z directions*

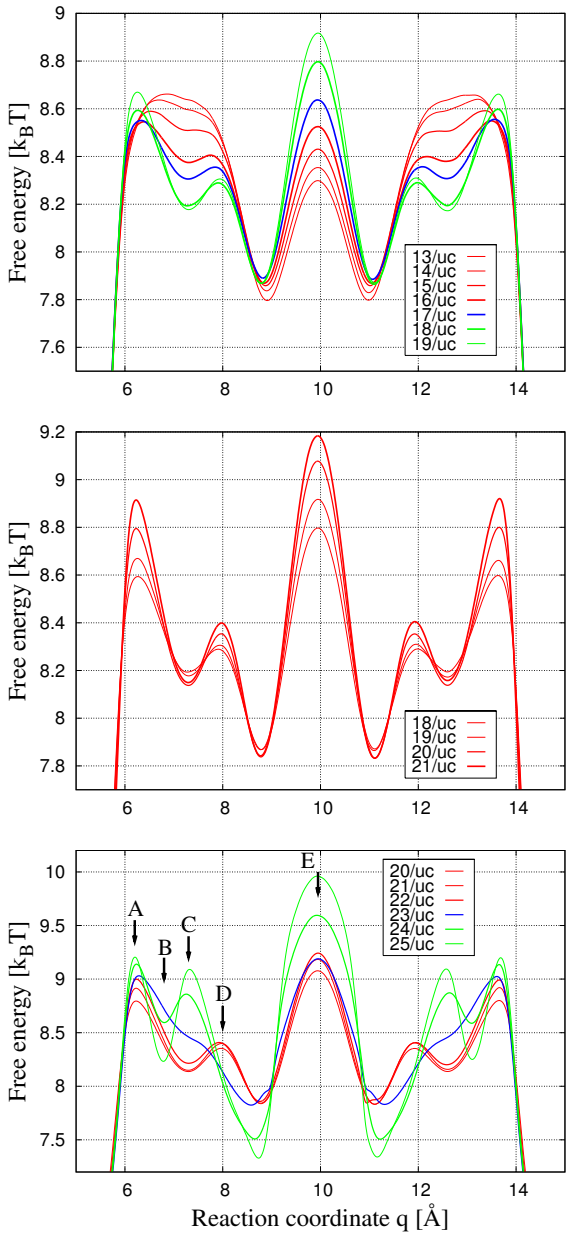

Figure 5.22: *Selected parts from free-energy profiles, at 300 K, of methane in MFI-type zeolite mapped along the y direction, at loadings of 13 to 19 (top), 18 to 21 (middle) and 20 to 25 (bottom) molecules per unit cell. Loadings that correspond to a peak in the diffusion are displayed in blue, lower loadings in red, higher loadings in green.*

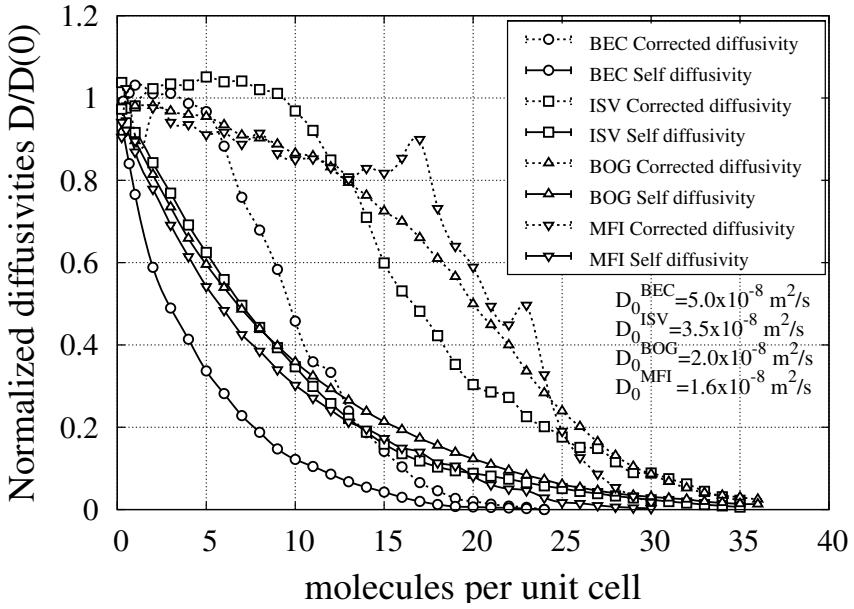

Figure 5.23: *Relative self and corrected diffusivity of methane in intersecting channel-type zeolites BEC, ISV, BOG and MFI, as a function of loading, at 300 K.*

intermediate loadings it decreases faster, until the diffusion comes to a halt at the maximum loading of the structure. There are small deviations from this behaviour, small peaks and valleys, and these can be accurately explained in the same manner as shown for MFI.

5.5.3 Diffusion in FAU-Type Zeolite

In discussing the diffusion of methane in cage-type zeolites, FAU-type zeolite clearly differed from other cage-type zeolites such as ERI, CHA and LTA, in the behaviour of both the self-diffusion and the collective diffusion. Whereas the diffusion of the other cage-type zeolites exhibits a maximum, for FAU both D_S and D_C are a decreasing function of loading (see figures 5.10 and 5.17). The self-diffusion seems to behave in a way similar to that in channel-type and intersecting channel-type systems, while the collective diffusion is almost linear, up to a loading of about 9 molecules per cage. In figure 5.24 we split the self-diffusion in the two contributions, D^{TST} and κ. The free-energy profiles from which the values of D^{TST} were calculated are shown in figure 5.25. These

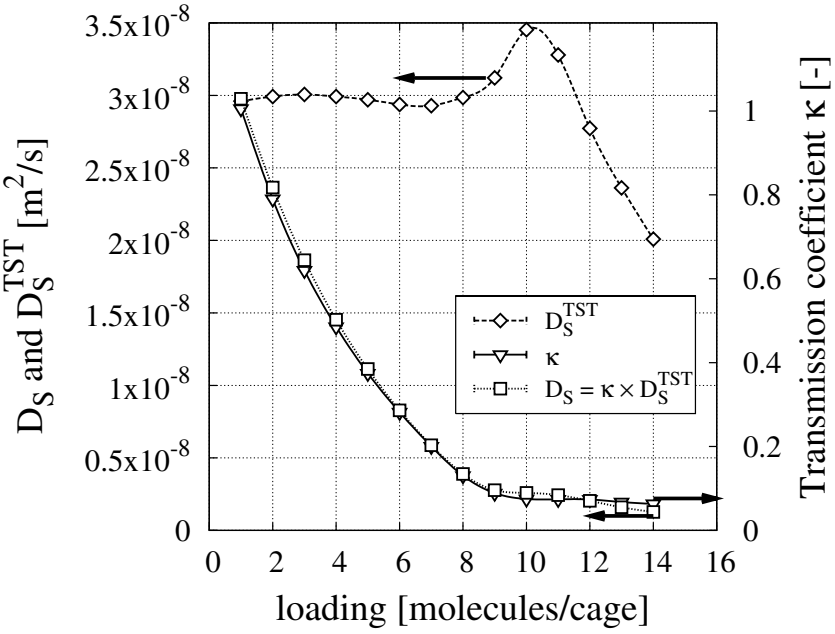

Figure 5.24: *Diffusion of methane in FAU-type zeolite as a function of loading, and the two contributions to this diffusion: the free-energy part, given by the Transition-State self-diffusion coefficient, and the collision part, given by the transmission coefficient*

profiles were obtained by choosing one of the body diagonals of the cubic unit cell as the reaction coordinate: the body diagonal from coordinate $(0, 0, 0)$ to $(1, 1, 1)$. In this way, the reaction coordinate passes through two FAU cages, and crosses the window dividing the two, perpendicularly. Figure 5.24 proves that this is a 'perfect' reaction coordinate, because the value of κ at zero loading is 1.

Surprisingly, while the free energy of the system does change when the loading is increased, the value of D^{TST} remains approximately constant, up to a loading of eight molecules per cage (see figure 5.25). It appears that, while the value of the free energy increases with loading, this change is more or less uniform over the entire reaction coordinate, resulting in a constant value of D^{TST}. Therefore, the behaviour of the self-diffusion is completely determined

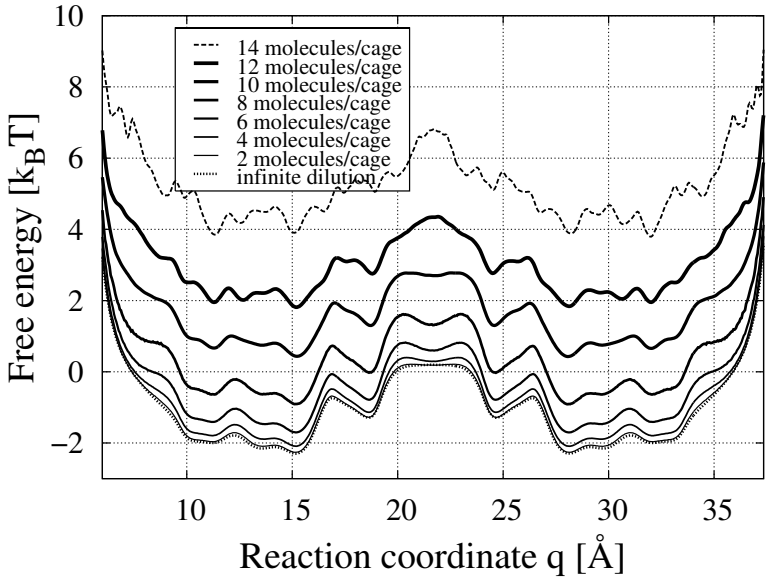

Figure 5.25: *Free-energy profiles for methane in FAU, at 300 K, mapped on the body diagonal (1,1,1)*

by κ. This can be explained by the fact that FAU-type zeolite not only consists of very large cages, its windows are also very large ($R_{wtc} = 1.22$), and up to intermediate loadings, the zeolite does not form a very strong confinement. Only at loadings higher than eight molecules per unit cell, we see a maximum in the diffusion. By now, the zeolite has filled up enough for the particles to experience the confinement as a cage/window type system and exhibit the associated diffusion behaviour. However, at these loadings the diffusion is very low in comparison to that at the infinite dilution limit and the cage-type behaviour is hardly distinguishable.

The collective diffusion at low loadings is equally unaffected by free-energy differences and follows approximately $(1 - \theta)$ behaviour: a linear decrease of the collective diffusion coefficient as a function of loading, as we would expect for particles performing a random walk on a lattice. Again, at loadings higher than eight molecules per cage, the collective diffusion coefficient increases, in accordance with D^{TST}, and goes through a maximum at about 11 molecules per cage. We can conclude that FAU-type zeolite forms a very weak confinement up to a loading of eight molecules per cage. At higher loadings it can be regarded as a cage-type zeolite.

5.6 Discussion

In the previous sections, we have divided the zeolites in four groups, that each have their own specific diffusion behaviour. In this section, we will compare the results with those predicted by the Reed-Ehrlich model. We calculated adsorption isotherms at 300 K for each of the zeolite types and obtained $1/\gamma$ by computing the derivative of the isotherm with respect to the fugacity, as a function of the loading:

$$\left(\frac{1}{\gamma}\right)(q) = \left(\frac{\partial \ln q}{\partial \ln f}\right)(q) \tag{5.21}$$

If adsorbed molecules do not change the energy of neighbouring sites, we expect that the free-energy profiles will not change as a function of loading, and the collective diffusion will behave as $1/\gamma$, as follows from eq. 5.8. However, if adsorbed molecules do have an effect on the energy inside the zeolite, we expect the behaviour of D_C to deviate from $1/\gamma$ behaviour. The Reed-Ehrlich model does not predict the value of the self-diffusion coefficient as a function of loading.

Figure 5.26 once more shows D_S and D_C as a function of loading for one representative of each zeolite class, LTA, AFI, MFI, and FAU. To compare the diffusion behaviour at finite loading at the infinite dilution limit, the plotted diffusion coefficients have been normalised with respect to the diffusion at zero loading, except for LTA. Also plotted are the two components of the self-diffusion, D^{TST} (also normalised with respect to D_0^{TST}) and κ and the Reed-Ehrlich prediction for the diffusion $1/\gamma$. The diffusion coefficients shown for MFI-type zeolite are for the y direction.

In LTA-type zeolite, the diffusion is clearly governed by the behaviour of D^{TST}; κ only has a quantitative influence. Both the self-diffusion and the collective diffusion exhibit a maximum as a function of loading. Especially in the case of the collective diffusion, the difference in the diffusion at the maximum with respect to the infinite dilution limit is almost two orders of magnitude. This sheds a new light on the orders of magnitude differences found experimentally in different diffusion measurements [7]. Macroscopic methods typically measure collective diffusivities (corrected and transport diffusion coefficients), while microscopic methods measure self-diffusion coefficients. Taking into consideration the loading dependence of both types of diffusion, it is not surprising that large deviations occur between different measurements.

It is clear that for cage-type zeolites such as LTA, the Reed-Ehrlich method requires modification. The adsorbed molecules have a strong influence on the

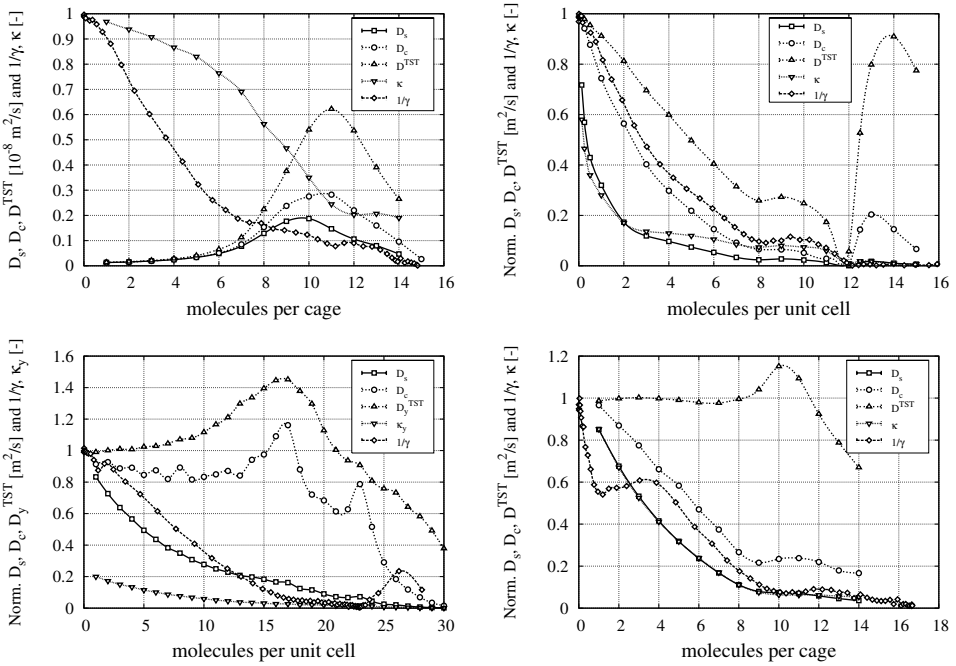

Figure 5.26: *Compiled data for one representative zeolite from each of the four zeolite classes, all at 300 K: cage-type zeolite LTA (top, left), channel-type zeolite AFI (top, right), intersecting channel-type MFI (bottom, left) and weak-confinement type FAU (bottom, right): diffusion coefficients D_S, D_C, and D^{TST} (normalised for AFI, MFI, and FAU type zeolites, not for LTA), κ and $1/\gamma$. The values of D_S, D_C, D^{TST} and κ for MFI are for the y direction only.*

energy of neighbouring adsorption sites, the free-energy barriers change significantly when the loading is increased, thereby raising the values of D^{TST}. The correlations in a high-barrier system such as LTA, contained in κ are relatively low, and furthermore, their decrease is slower than the rapid increase in D^{TST}. The result is that both D_S and D_C show a qualitative behaviour similar to D^{TST} and very much unlike the behaviour expected from the Reed-Ehrlich model.

In AFI-type zeolite, the behaviour is completely different. D_S, D_C and D^{TST} all are decreasing functions of loading. Up to a loading of eight molecules per unit cell, D^{TST} decreases approximately linearly and κ is rapidly decreasing function of loading. Although the adsorbed molecules do change the energy of their environment, and thus D^{TST}, the behaviour of D_S is governed by κ:

the higher the loading, the more interparticle collisions occur, and these are the limiting factor for the diffusion in smooth channel-type zeolites. When we compare the collective diffusion as a function of loading with $1/\gamma$, the form of the two functions is quite similar. The overlap with the Reed-Ehrlich prediction is not perfect, but it shows that the loading-dependent diffusion behaviour in AFI-type zeolite is determined for a large part by the presence of other particles, by way of vacancy correlations. The adsorption isotherm for AFI has a near-Langmuir form up to a loading of about eight molecules per unit cell. At this loading there is a clear inflection. A second inflection is visible at 12 molecules per unit cell. Both inflections are reflected in the value of $1/\gamma$, and even in D^{TST}: a reordering of the molecules gives rise to a new form of the free-energy profile. $1/\gamma$ gives a reasonable estimate of D_C. However, using the Reed-Ehrlich model to compute the exact value of D_C would require $1/\gamma$ and additional terms describing the energetic influence of adsorbed particles.

Figure 5.26 shows the diffusion data for MFI in y direction only. Based on this figure, we can state that, because the value of D^{TST} increases only slowly at low loadings, the self-diffusion is for a large part determined by the behaviour of κ.

In the collective-diffusion behaviour we can recognise the effect of the free-energy changes. While D_C does not exactly follow D^{TST}, the trends are similar. However, to understand the full behaviour of D_C, one needs to look at the separate free-energy profiles and analyse them carefully. Bot D^{TST} and D_C suggest that something is happening at 16 molecules per unit cell, which corresponds to the loading where all sixteen favourable adsorption site (four per straight channel and four per zigzag channel) have been occupied. To increase the loading any further, new, less favourable positions have to be occupied, or the molecules have to reorganise. The latter is happening, as is visible in the free-energy profiles. Interestingly, while $1/\gamma$ does not give a reasonable estimate of the collective diffusion behaviour, it does have a subtle bend at 16 molecules per unit cell.

We stress that MFI-type zeolite is a complex system. While the diffusion is highest in the y direction, the other two directions do have their influence on the total diffusion coefficient, and in order to understand the diffusion behaviour, all channel directions need to be taken into consideration.

For FAU, up to a loading of about eight molecules per unit cage, the loading-dependent diffusion behaviour is completely determined by interparticle collisions. Since the free-energy profiles barely change when the loading is increased, D_S has exactly the same form as κ, and D_C exhibits the typical behaviour of a particle jumping randomly on a lattice. One would expect that

the D_C in such a case would follow $1/\gamma$ exactly, but figure 5.26 makes clear that this is not the case. From four molecules per cage onward, the behaviour of D_C and $1/\gamma$ are alike, but $1/\gamma$ goes through a large minimum at one molecule per cage, which is not reflected in D_C. Why $1/\gamma$ shows this behaviour is unclear and would require additional research.

In summary, the diffusion of neither of the zeolites studied here can be explained by a Reed-Ehrlich model only. In each of the cage-type, channel-type and intersecting channel-type zeolites adsorbed particles influence the energy of their surroundings, thus rendering the Reed-Ehrlich theory, which – in its basic form – assumes constant-energy adsorption sites, invalid. Even in the case of FAU, where the loading-dependence of the net free-energy barriers can be considered negligible, the Reed-Ehrlich model cannot be used to describe the collective diffusion over the entire loading range.

The Reed-Ehrlich model can be adjusted to contain a term that changes as a function of the loading in the system [37], but this requires prior knowledge about the system. This term could be determined by calculating free-energy profiles, but when one has obtained these free-energy profiles, it is relatively easy and quick to compute a diffusion coefficient from them, using dcTST instead of the Reed-Ehrlich model. However, the Reed-Ehrlich model could perhaps be used to estimate the height of free-energy barriers, by using it in combination with MD.

Another remarkable observation can be made from the comparison of the four zeolite groups. Whereas the specific loading-dependence of the diffusion is different in each group, we observe that neither the self-diffusion, nor the collective diffusion is ever constant over the entire loading range. In every zeolite topology we can assign regimes where the diffusion increases or decreases. At high loadings it is imperative that both D_S and D_C approach zero, due to packing effects that halt the diffusion, irrespective of the type of zeolite. The loading at which the final decrease sets in is determined by the zeolite type, topology and size. Even in MFI-type zeolite, where D_C was hitherto believed to be constant [1], the diffusion eventually goes down to zero. This implies that the Darken approximation, that states that the collective diffusion can be assumed constant over loading, generally is not valid outside a small range near the infinite dilution limit, where D_S and D_C are equal.

5.7 Comparison with Experimental Data

To validate our method, we compare our simulation results with experimental results for the two most commonly used zeolites: MFI and FAU.

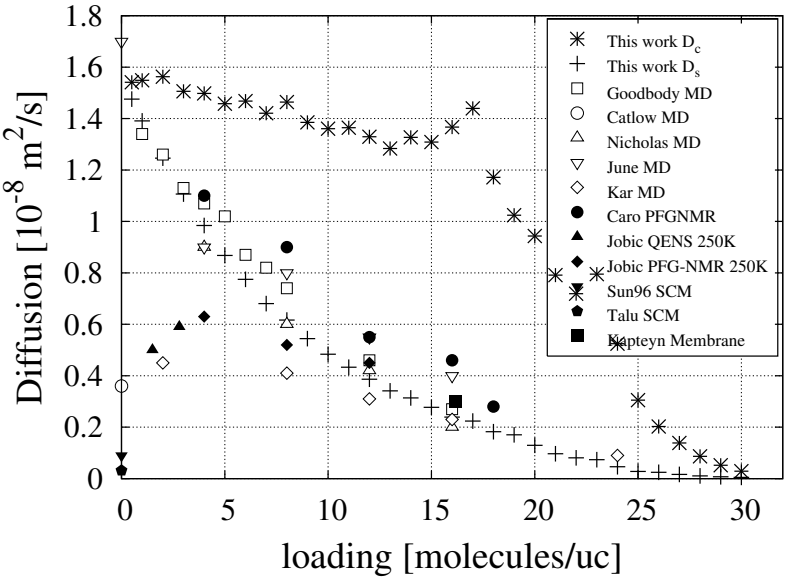

Figure 5.27: *Simulation results for the diffusion of methane in MFI-type silica as a function of the adsorbate loading, together with results obtained by several other groups, through simulation [13–17] and experiment [29–31, 93, 94]. Data were obtained at 300 K, except for the results of Jobic et al., which were obtained at 250 K.*

Figure 5.27 shows our simulation results for the diffusion of methane in MFI-type silica as a function of the adsorbate loading [33], together with results obtained by several other groups, through simulation [13–17] and experiment [29–31, 93, 94]. The experimental data (black symbols) are self-diffusion coefficients, except those obtained by single-crystal membrane (SCM) measurements, which should be corrected or transport diffusivities. The results have been plotted against the loading as reported in the original papers, wherever possible. Unspecified loadings have been estimated from the reported pressures with the aid of a calculated adsorption isotherm.

Although some results show a marked deviation – both single-crystal membrane studies [93, 94], carried out at the zero-loading limit, yielded a diffusion that is much slower than that found by other methods – the overall correlation between different experimental and simulation results is good. We can conclude that the methane force field of ref. [50] predicts the diffusion coefficient accurately.

The deviation observed between the single-crystal studies and most other studies is probably due to the existence of both internal and external diffusional barriers. The more macroscopic a measurement method is, the larger the influence of the internal barriers. QENS is the experimental technique which is least affected by the existence of internal barriers. [95, 96] As the internal barriers are relatively small for methane in MFI, it is expected that the diffusivities obtained by macroscopic and microscopic methods will be further apart for longer alkanes.

Since faujasite (FAU) is an important zeolite in practical applications, many experimental and simulation studies have been published about this structure. Most of these studies focus on the diffusion of aromatics [97–101] but some groups have also considered hydrocarbons [102–108].

It is interesting to compare our results with the simulations of Chempath et al [103]. The molecular-dynamics simulations of Chempath et al were interpreted assuming a linear decrease of the MS diffusion coefficient as a function of loading [37]. At a fractional loading of 0.8, a single simulation point was reported that deviated from this line. Comparison with our results show that this deviation is significant.

For benzene in FAU Auerbach and co-workers [101] and Snyder et al. [109] found in their kinetic Monte Carlo simulations an increase of the collective diffusion coefficient at high loading, which was attributed to the repulsive adsorbate-adsorbate interactions. We can now add that, as benzene is a much larger molecule than methane, the adsorbate experiences the cages of Y much more like cages, and hence this system behaves much more like a cage-type zeolite than methane in FAU. For hexane and 2-methyl pentane, Van Baten and Krishna [110] observed a behaviour similar to that of methane. It would be interesting to investigate the behaviour for longer chains, as one could argue that for the longer alkanes, the window of FAU might be an entropic barrier and this would show-cage like behaviour again.

5.8 Conclusion

We have compared the loading-dependent behaviour of the self-diffusion and collective diffusion for methane in twelve different zeolite topologies. Based on their characteristics, we can divide these twelve topologies into four zeolite groups. Each of the four zeolite groups shows very distinct diffusion behaviour as a function of loading.

In cage-type zeolites we observe a maximum in both the self and the collective diffusion, caused by decreased free energy barriers, after which both slow

down to zero. Diffusion behaviour in channel-type zeolites is highly dependent on the ratio between the narrowest and widest part of the channels R_{ctw}. In the smoothest channels, both D_S and D_C are a steeply decreasing function of loading. In the most cagelike channels, those with the highest value of R_{ctw}, D_S and D_C behave as true cage-type systems. The zeolites with an intermediate value of R_{ctw} have behave in an intermediate way. Generally D_S is still monotonously decreasing, though the curve is less steep than in the smoothest channels. Depending on the exact value of R_{ctw}, D_S can have slight cagelike behaviour, resulting in a small maximum at low loadings. In intersecting channel-type zeolites, D_S generally behaves similar to that in channel-type zeolites of intermediate smoothness. D_C has two consecutive diffusion regimes [111]: first a slow linear decrease, until at least one of the channels has reached its maximal loading, then a sharper plunge to reach zero at the saturation loading of the zeolite.

In any zeolite type, at high loadings both D_S and D_C drop to zero. This observation implies that the Darken approximation cannot be used outside a small region near zero loading. We note that in simulations one can apply pressures that are higher than those used in experiments, where full saturation is often defined as the loading at which there is an equilibrium with a surrounding liquid phase. The maximum loading in simulations is often higher than this full-saturation capacity. Experimentally is has been shown that the self-diffusion can slow down more than two orders of magnitude at these higher loadings (See for example Kärger et al. [112] for n-alkanes in NaX), but this diffusion was still nonzero.

We stress that the ordering of molecular sieve structures in classes depends strictly on the combination of adsorbate and adsorbent. For example, a cage that appears very large for methane molecules, can in fact be a very tight confinement for benzene. When applying this classification to larger molecules, sieve structures can therefore 'switch class', but the general behaviour will be the same: when the cages are large (with respect to the adsorbed molecule) and the windows are narrow, the diffusion as a function of loading will go through a maximum; when the confinement is experienced as a smooth channel, the diffusion is a decreasing function of loading (this has also been observed for small alkanes in carbon-nanotubes [113]); when the confinement consists of intersecting channels, D_S will be monotonously decreasing as a function of loading, and D_C will show a kink. The method employed in this study can be used to make a classification of pore structures for any given adsorbate molecule.

Bibliography

[1] Skoulidas, A.I.; Sholl, D. S. *J. Phys. Chem. A.* **2003**, *107*, 10132-10141.

[2] Fritzsche, S.; Gaub, M.; Haberlandt, R.; Hofmann, G. *J. Mol. Model* **1996**, *2*, 286-292.

[3] Snurr, R. Q.; Bell, A. T.; Theodorou, D. N. *J. Phys. Chem.* **1994**, *98*, 11948-11961.

[4] Auerbach, S. M. *International reviews in physical chemistry* **2000**, *19*, 155-198.

[5] Ramanan, H.; Auerbach, S. M., in *NATO-ASI Series C: Fluid Transport in Nanopores*, edited by Fraissard, J.; Conner, W.C. Kluwer Academic Publishers; Dordrecht, The Netherlands, 2004.

[6] Jobic, H.; Karger, J.; Bee, M. *Phys. Rev. Lett.* **1999**, *82*, 4260-4263.

[7] Kaerger, J.; Ruthven, D. M., *Diffusion in Zeolites and other microporous solids* John Wiley & Sons, Inc.; New York, 1992.

[8] Maginn, E. J.; Bell, A. T.; Theodorou, D. N. *J. Phys. Chem.* **1996**, *100*, 7155-7173.

[9] Krishna, R.; Baten, J. M.van ; Dubbeldam, D. *J. Phys. Chem. B.* **2004**, *108*, 14820.

[10] Xiao, J.; Wei, J. *Chem. Eng. Sci.* **1992**, *47*, 1123.

[11] Fritzche, S.; Wolfsberg, M.; Haberlandt, R.; Demontis, P.; Suffritti, G. B.; Tilocca, A. *Chem. Phys. Lett.* **1998**, *296*, 253.

[12] Saravanan, C.; Jousse, F.; Auerbach, S. M. *Phys. Rev. Lett.* **1998**, *80*, 5754-5757.

[13] Goodbody, S. J.; Watanabe, J. K.; Gowan, D. M.; Walton, J. P. R. B.; Quirke, N. *J. Chem. Soc. Farad. Trans.* **1991**, *87*, 1951.

[14] Catlow, C. R. A.; Freeman, C. M.; Vessal, B.; Tomlinson, S. M.; Leslie, M. *J. Chem. Soc. Farad. Trans.* **1991**, *87*, 1947.

[15] Nicholas, J. B.; Trouw, F. R.; Mertz, J. E.; Iton, L. E.; Hopfinger, A. J. *J. Phys. Chem.* **1993**, *97*, 4149.

[16] Kar, S.; Chakravarty, C. *JPCA* **2001**, *105*, 5785-5793.

[17] June, R. L.; Bell, A. T.; Theodorou, D. N. *J. Phys. Chem* **1990**, *94*, 8232-8240.

[18] Tepper, H. L.; Briels, W. J. *J. Chem. Phys* **2002**, *116*, 9464-9474.

[19] Schüring, A.; Auerbach, S. M.; Fritzsche, S.; Haberlandt, R. *J. Chem. Phys* **2002**, *116*, 10890-10894.

[20] Jousse, F.; Auerbach, S. M. *J. Chem. Phys.* **1997**, *107*, 9629-9639.

[21] Tunca, C.; Ford, D. M. *J. Chem. Phys.* **1999**, *111*, 2751-2760.

[22] Tunca, C.; Ford, D. M. *J. Phys. Chem. B* **2002**, *106*, 10982-10990.

[23] Tunca, C.; Ford, D. M. *Chem. Eng. Sci.* **2003**, *58*, 3373-3383.

[24] Ghorai, P. Kr.; Yashonath, S. *J. Chem. Phys* **2004**, *120*, 5315-5321.

[25] Heink, W.; Kärger, J.; Pfeifer, H.; Salverda, P.; Datema, K. P.; Nowak, A. *J. Chem. Soc. Faraday Trans.* **1992**, *88*, 515-519.

[26] June, R. L.; Bell, A. T.; Theodorou, D. N. *J. Phys. Chem.* **1991**, *95*, 8866-8878.

[27] Dubbeldam, D.; Calero, S.; Maesen, T. L. M.; Smit, B. *Phys. Rev. Lett.* **2003**, *90*, 245901.

[28] Dubbeldam, D.; Calero, S.; Maesen, T. L. M.; Smit, B. *Angew. Chem. Int. Ed.* **2003**, *42*, 3624-3626.

[29] Caro, J.; Bulow, M.; Schirmer, W.; Karger, J.; Heink, W.; Pfeifer, H. *J. Chem. Soc. Farad. Trans.* **1985**, *81*, 2541.

[30] Jobic, H.; Bee, M.; Caro, J.; Bulow, M.; Karger, J. *J. Chem. Soc. Farad. Trans.* **1989**, *85*, 4201.

[31] Kapteyn, F.; Bakker, W. J. W.; Zheng, G.; Moulijn, J. A. *Chem. Eng. J.* **1995**, *57*, 145-153.

[32] Beerdsen, E.; Smit, B.; Dubbeldam, D. *Phys. Rev. Lett.* **2004**, *93*, 248301.

[33] Beerdsen, E.; Dubbeldam, D.; Smit, B. *Phys. Rev. Lett.* **2005**, *95*, 164505.

[34] Beerdsen, E.; Dubbeldam, D.; Smit, B. *Phys. Rev. Lett.* **2006**, *96*, 044501.

[35] Dubbeldam, D.; Beerdsen, E.; Vlugt, T. J. H.; Smit, B. *J. Chem. Phys* **2005**, *122*, 224712.

[36] Reed, D. A.; Ehrlich, G. *Surf. Science* **1981**, *102*, 588-609.

[37] Krishna, R.; Paschek, D.; Baur, R. *Micropous and Mesoporous Materials* **2004**, *76*, 233-246.

[38] Papadopoulos, G. K.; Jobic, H.; Papadopoulos, D. N. *J. Phys. Chem. B.* **2004**, *108*, 12748-12756.

[39] Krishna, R.; Baten, J. M.van *Chem. Phys. Lett.* **2006**, *420*, 545-549.

[40] Krishna, R.; Baten, J. M.van *Ind. Eng. Chem. Res.* **2006**, *45*, 2084-2093.

[41] Krishna, R.; Paschek, D. *Chem. Phys. Lett.* **2001**, *33*, 278-284.

[42] Krishna, R.; Smit, B.; Calero, S. *Chem. Soc. Rev.* **2002**, *31*, 185-194.

[43] Vlugt, T. J. H.; Krishna, R.; Smit, B. *J. Phys. Chem. B.* **1999**, *103*, 1102-1118.

[44] Gorring, R. L. *J. Catal.* **1973**, *31*, 13-26.

[45] Nitsche, J. M.; Wei, J. *J. AlChe.* **1991**, *37*, 661-670.

[46] Runnebaum, R. C.; Maginn, E. J. *J. Phys. Chem. B.* **1997**, *101*, 6394-6408.

[47] Talu, O.; Sun, M. S.; Shah, D. B. *J. AlChe.* **1998**, *44*, 681-694.

[48] Bezus, A. G.; Kiselev, A. V.; Lopatkin, A. A.; Du, P. Q. J. *J. Chem. Soc., Faraday Trans. II* **1978**, *74*, 367-379.

[49] Ryckaert, J. P.; Bellemans, A. *Faraday Dicuss. Chem. Soc.* **1978**, *66*, 95-106.

[50] Dubbeldam, D.; Calero, S.; Vlugt, T. J. H.; Krishna, R.; Maesen, T. L. M.; Beerdsen, E.; Smit, B. *Phys. Rev. Lett.* **2004**, *93*, 088302-1.

[51] Dubbeldam, D.; Calero, S.; Vlugt, T. J. H.; Krishna, R.; Maesen, T. L. M.; Smit, B. *J. Phys. Chem. B.* **2004**, *108*, 12301-12313.

[52] Bennett, C. H., in *Diffusion in Solids: Recent Developments*, edited by Nowick, A.S.; Burton, J.J. Academic Press; New York, 1975, pp. 73–113.

[53] Chandler, D. *J. Chem. Phys* **1978**, *68*, 2959.

[54] Frenkel, D.; Smit, B., *Understanding molecular simulation 2nd edition* Academic Press; London, UK, 2002.

[55] Auerbach, S. M., in *NATO-ASI Series C: Fluid Transport in Nanopores*, edited by Fraissard, J.; Conner, W.C. Kluwer Academic Publishers; Dordrecht, The Netherlands (2004).

[56] Maesen, T. L. M.; Schenk, M.; Vlugt, T. J. H.; Jonge, J. P.de ; Smit, B. *J. Catal.* **1999**, *188*, 403-412.

[57] http://www.iza-structure.org/databases/.

[58] Pluth, J. J.; Smith, J. V. *J. Am. Chem. Soc.* **1980**, *102*, 4704-4708.

[59] Gard, J. A.; Tait, J. M., in *Proceedings of the third International Conference on Molecular Sieves, Recent Progress Reports*, edited by Uytterhoven, J. B. Leuven University Press; Zurich, 1973, pp. 94–99.

[60] Calligaris, M.; Nardin, G.; Randaccio, L. *Zeolites* **1986**, *3*, 205-208.

[61] Hriljac, J. J.; Eddy, M. M.; Cheetham, A. K.; Donohue, J. A. *J. Solid State Chem.* **1993**, *106*, 66-72.

[62] S.Qiu, ; Pang, W.; Kessler, H.; Guth, J. L. *Zeolites* **1989**, *9*, 440-444.

[63] Fyfe, C. A.; Gies, H.; Kokotailo, G. T.; Marler, B.; Cox, D. E. *J. Phys. Chem.* **1990**, *94*, 3718-3721.

[64] Barrer, R. M.; Villiger, H. *Z. Kristallogr.* **1969**, *128*, 352-270.

[65] Patinec, V.; Wright, P. A.; Lightfoot, P.; Aitken, R. A.; Cox, P. A. *J. Chem. Soc., Dalton Trans.* **1999**, 3909-3911.

[66] Koningsveld, H.van ; Bekkum, H.van ; Jansen, J. C. *Acta Cryst* **1987**, *B43*, 127-132.

[67] Pluth, J. J.; Smith, J. V. *American Mineralogist* **1990**, *75*, 501-507.

[68] Liu, Z.; Ohsuna, T.; Terasaki, O.; Camblor, M. A.; Diaz-Cabanas, M.; Hiraga, K. *J. Am. Chem. Soc.* **2001**, *123*, 5370-5371.

[69] Villaescusa, L. A.; Barrett, P. A.; Camblor, M. A. *Angew. Chem. Int. Ed.* **1999**, *38*, 1997-2000.

[70] Maesen, T. L. M.; Beerdsen, E.; Calero, S.; Dubbeldam, D.; Smit, B. *J. Catal.* **2006**, *237*, 278-290.

[71] Ribeiro, F. Ramoa; Rodriguez, A.; Rollmann, D.; Naccache, C., in *Zeolites: Science and Technology*, edited by Ribeiro, F. Ramoa Martinus Nijhoff Publishers; The Hague, 1984.

[72] Calero, S.; Schenk, M.; Dubbeldam, D.; Maesen, T. L. M.; Smit, B. *J. Catal.* **2004**, *228*, 121-129.

[73] Bhatia, S., *Zeolite Catalysis: Principles and Applications* CRC Press Inc.; Boca Raton - Florida, 1990.

[74] Gupta, V.; Nivarthi, S. S.; Keffer, D.; McCormick, A. V.; Davis, H. T. *Science* **1996**, *274*, 164-164.

[75] Gupta, V.; Nivarthi, S. S.; McCormick, A. V.; Davis, H. T. *Chem. Phys. Lett.* **1995**, *247*, 596-600.

[76] Hahn, K.; Kärger, J. *J. Phys. Chem. B* **1998**, *102*, 5766–5771.

[77] Jobic, H.; Hahn, K.; Karger, J.; Bee, M.; Tuel, A.; Noack, M.; Girnus, I.; Kearley, G. J. *J. Phys. Chem. B* **1997**, *101*, 5834-5841.

[78] Demontis, P.; Gonzalez, J. G.; Suffritti, G. B.; Tilocca, A. *J. Am. Chem. Soc.* **2001**, *123*, 5069-5074.

[79] Tepper, H. L.; Hoogenboom, J. P.; Vegt, N. F. A.van der ; Briels, W. J. *J. Chem. Phys.* **1999**, *110*, 11511-11516.

[80] MacElroy, J. M. D.; Suh, S. H. *J. Chem. Phys.* **1997**, *106*, 8595-8597.

[81] Nelson, P. H.; Auerbach, S. M. *Chem. Eng. J.* **1999**, *74*, 43-56.

[82] Nelson, P. H.; Auerbach, S. M. *J. Chem. Phys.* **1999**, *110*, 9235-9243.

[83] Sholl, D. S.; Fichthorn, K. A. *J. Chem. Phys.* **1997**, *107*, 4384-4389.

[84] Dume, C.; Holderick, W. F. *Appl. Catal. A* **1999**, *167*, 183-193.

[85] Schenk, M.; Calero, S.; Maesen, T. L. M.; Benthem, L. van; Verbeek, M. G.; Smit, B. *Angew. Chem. Int. Ed.* **2002**, *41*, 2500-2502.

[86] Davis, M. E. *Nature* **2002**, *417*, 813-821.

[87] Zhang, W.; Smirniotis, P. G. *Catal. Lett.* **1999**, *60*, 223-228.

[88] Triantafillou, N. D.; Miller, J. T.; Gates, B. C. *J. Catal.* **1995**, *155*, 131-140.

[89] Demontis, P.; Suffritti, G. B. *J. Phys. Chem. B.* **1997**, *101*, 5789-5793.

[90] Schüring, A.; Auerbach, S. M.; Fritzsche, S.; Haberlandt, R. *J. Chem. Phys* **2002**, *116*, 10890-10894.

[91] Maris, T.; Vlugt, T. J. H.; Smit, B. *J. Phys. Chem. B.* **1998**, *102*, 7183-7189.

[92] Pascual, P.; Ungerer, P.; Tavitian, B.; Pernot, P.; Boutin, A. *Phys. Chem. Chem. Phys.* **2003**, *5*, 3684-3693.

[93] Sun, M. S.; Talu, O.; Shah, D. B. *J. AlChe.* **1996**, *42*, 3001.

[94] Talu, O.; Sun, M. S.; Shah, D. B. *J. AlChe.* **1998**, *44*, 681-694.

[95] Vasenkov, S.; Kärger, J. *Microporous and Mesoporous Materials* **2002**, *55*, 139-145.

[96] Vasenkov, S.; Böhlmann, W.; Galvosas, P.; Geier, O.; Liu, H.; Kärger, J. *J. Phys. Chem. B.* **2001**, *105*, 5922-5927.

[97] Mosell, T.; Schrimpf, G.; Brickmann, J. *J. Phys. Chem. B.* **1997**, *101*, 9476-9484.

[98] Mosell, T.; Schrimpf, G.; Brickmann, J. *J. Phys. Chem. B* **1997**, *101*, 9485–9494.

[99] Saravanan, C.; Auerbach, S. M. *J. Chem. Phys.* **1997**, *107*, 8120-8131.

[100] Saravanan, C.; Auerbach, S. M. *J. Chem. Phys.* **1997**, *107*, 8132-8137.

[101] Saravanan, C.; Jousse, F.; Auerbach, S. M. *J. Chem. Phys.* **1998**, *108*, 2162-2169.

[102] Bandyopadhyay, S.; Yashonath, S. *Chem. Phys. Lett.* **1994**, *223*, 363–368.

[103] Chempath, S.; Krishna, R.; Snurr, R. Q. *J. Phys. Chem. B* **2004**, *108*, 13481-13491.

[104] Clark, L. A.; Ye, G. T.; Gupta, A.; Hall, L. L.; Snurr, R. Q. *J. Chem. Phys.* **1999**, *111*, 1209-1222.

[105] Sanborn, M. J.; Snurr, R. Q. *Sep. Purif. Technol.* **2000**, *20*, 1-13.

[106] Sanborn, M. J.; Snurr, R. Q. *Aiche J.* **2001**, *47*, 2032-2041.

[107] Yashonath, S.; Demontis, P.; Klein, M.L. *Chem. Phys. Lett.* **1988**, *153*, 551–555.

[108] Yashonath, S.; Thomas, J.M.; Nowak, A.K.; Cheetham, A.K. *Nature* **1988**, *331*, 601–604.

[109] Snyder, M. A.; Vlachos, D. G. *J. Chem. Phys.* **2005**, *123*, 184708.

[110] Baten, J. M.van ; Krishna, R. *Microporous Mesoporous Mat.* **2005**, *84*, 179-191.

[111] Krishna, R.; Vlugt, T. J. H.; Smit, B. *Chem. Eng. Sci.* **1999**, *54*, 1751-1757.

[112] Karger, J.; Pfeifer, H.; Rauscher, M.; Walter, A. *J.C.S. Faraday* **1980**, *76*, 717-737.

[113] Skoulidas, A. I.; Ackerman, D. M.; Johnson, J. K.; Sholl, D. S. *Phys. Rev. Lett.* **2002**, *89*, 185901.

We report molecular simulations of diffusion in confinement showing a phenomenon which we denote as Molecular Path Control (MPC); depending on loading, molecules follow a preferred pathway. MPC raises the important question to which extent the loading may affect the molecular trajectories in nanoporous materials. Through MPC one is able to manually adjust the ratio of the diffusivities through different types of pores, and as an application one can direct the flow of diffusing particles in membranes forward or sideward by simply adjusting the pressure, without the need for mechanical parts such as valves. We show that the key ingredient of MPC is the anisotropic nature of the nanoporous material which results in a complex interplay between different diffusion paths as a function of loading. These paths may be controlled by changing the loading, either through a change in pressure or temperature.

D. Dubbeldam, E. Beerdsen, S. Calero, and B. Smit

6 Molecular Path Control in Zeolite Membranes

6.1 Introduction

Among other emerging membrane technologies like polymer-inorganic composites, carbon films, and micro- and mesoporous silica films, zeolite membranes offer outstanding potential for molecular recognition at the sub-nanometer level and the ability to operate at high temperatures [1, 2]. Zeolites are crystalline structures made up of "T-atoms", where T is an aluminium or silicon atom, which are tetrahedrally bonded to one another with oxygen bridges. Because of the regularity of the crystalline structure and the pores with Ångstrom-size dimensions, these crystals, when grown together to form a membrane, can operate as separation devices for gas and liquid mixtures. From a scientific point of view zeolites are ideal systems to study the effect of confinement on the properties of the adsorbed molecules.

Transport of adsorbates in nanoporous adsorbents such as zeolites is de-

termined by a complex interplay between adsorbent-adsorbate and adsorbate-adsorbate interactions. Molecules diffuse through the pores via various diffusion mechanisms [3]. Although interesting effects like single-file diffusion [4], incommensurate diffusion [5, 6] and levitation effects [7] are well known, most of the effects of confinement on diffusion remain poorly understood. This is particularly true for loading effects in materials with different channels and/or cages in the x, y, and z direction. Anisotropic single-component diffusion in silicalite has been known for a long time [8–12]. In general, the diffusion coefficients in the different directions can have different dependencies on temperature and loading. A limited number of studies deal with nonzero loading. Bussai et al. [13] found little change in anisotropy for water in silicalite as a function of loading. In this work, we report a reversal of anisotropy, i.e. at low loading the diffusivity in the z direction is twice as *fast* as that in the xy direction for both the self- and the collective diffusivity, while for higher loadings this changes into a z diffusivity that is more than twice as *slow*. This behaviour is due to a complete change in the diffusion mechanism. Our results raise the unanswered question to which extent the loading may affect the molecular trajectories in nanoporous materials. Here, we focus on what we have named Molecular Path Control (MPC) where one and the same molecular species follows different pathways, depending on the loading. As a specific MPC example, we study the mechanism behind the *tunable* anisotropy of ethane in ERI-type zeolite membranes, but the concepts are by no means limited to zeolite materials.

6.2 Model and Computational Details

In our simulations, we neglect cations and study rigid, all-silica versions of the ERI- and CHA-type zeolites. Zeolites are designated by three capital letter codes derived from the names of the type materials, e.g. ERI (erionite), and CHA (chabazite). The positions of the atoms are taken from Ref. [14] and Ref. [15], respectively. Following the work of Bezus et al. [16], the zeolites are modelled as a rigid network of oxygen atoms. This is a very common approximation because the large oxygen atoms essentially shield the much smaller silicon atoms, and lattice flexibility is not important for small alkanes in all-silica zeolites [19]. The rectangular simulation box sizes we used are $4.5906 \times 3.9756 \times 4.443$ nm^3 for ERI-type zeolite, and $3.015 \times 4.7814 \times 2.7606$ nm^3 for CHA-type zeolite. Tests on larger systems did not show any significant finite-size effects. Periodic boundary conditions were employed. Adsorption in cation-free structures takes place at sites with little or no electric field. For these reasons the united atom model [17] is a straightforward choice. We con-

sider the CH_3 groups as single, chargeless interaction centers with their own effective potentials. The beads of ethane are connected by an harmonic bonding potential $U^{\text{bond}} = \frac{1}{2}k_1(r - r_0)^2$, with $k_1/k_B = 96500$ K/Å^2 and $r_0 = 1.54$ Å. The nonintramolecular energy is described with a Lennar-Jones potential using parameters $\sigma_{O-\text{CH}_3} = 3.17$ Å, $\epsilon_{O-\text{CH}_3}/k_B = 142$ K, $\sigma_{Si-\text{CH}_3} = 2.12$ Å, $\epsilon_{Si-\text{CH}_3}/k_B = 82$ K, and $\sigma_{\text{CH}_3-\text{CH}_3} = 3.78$ Å, $\epsilon_{\text{CH}_3-\text{CH}_3}/k_B = 104$ K, which were taken from Ref. [18]. The accuracy of the simulation techniques has been verified in several publications [6, 20–23] in which comparisons were made with experimental data, and can be considered state-of-the-art for computing adsorption and diffusivities in nanoporous materials.

The simulations were performed using two different methods: conventional Molecular Dynamics (MD) and the recently proposed dynamically corrected Transition-State Theory (dcTST) [24, 25]. In MD simulations [26–28], successive configurations of the system are generated by integrating Newton's laws of motion, which then yields a trajectory that describes the positions, velocities and accelerations of the particles as they vary with time. We used the velocity Verlet integration scheme with a time-step of 0.5 fs. The relative energy drift was smaller than 10^{-4}. For temperature control we employed the Nosé-Hoover chain (NHC) method as formulated by Martyna et al. [29]. Molecules were inserted into the framework at random positions as long as no overlaps occurred with the framework or other particles. During the initialisation period we performed an NVT Monte Carlo simulation to rapidly achieve an equilibrium molecular arrangement. After the initialisation period, we assigned velocities from the Maxwell-Boltzmann distribution at the desired average temperature to all the atoms. The total momentum of the system was set to zero. Next, we equilibrated the system further by performing an NVT MD simulation using the NHC thermostat. After the equilibration was completed, during the production run of more than 20 ns, we collected statistics using the NVT ensemble. Simulations using the NVE ensemble gave equivalent results. More details can be found in Ref. [25].

Although MD and dcTST give equivalent diffusivity results for these systems, dcTST is also applicable in the regime of very slow diffusion, where MD cannot be used, and the behaviour is better understood by analysing the free-energy profiles and lattice information provided by the dcTST method. In the dcTST formalism, the diffusion mechanism is divided in two parts. The first is a static term, corresponding to locations of preferable adsorption sites and the free-energy barriers in between, the second term generally decreases with loading and corresponds to the inverse of the collision frequency. As such, the dcTST method is able to explain different diffusion regimes over loading,

and provides insight into the mechanisms behind an increase or decrease in diffusivity with loading [24].

Using the dcTST method of refs. [24] and [25], the self-diffusivity is calculated directly by computing the hopping rate of a molecule over a typical length scale λ given by the smallest repeating zeolite-structure. The transmission rates are easily converted to diffusion coefficients, once the lattice distances and connectivities are known. In ERI-type lattices, shown in figure 6.3, diffusion in the xy plane occurs isotropically on a hexagonal lattice

$$D_{xy} = \frac{1}{4} k_{xy} \lambda_{xy}^2 \tag{6.1}$$

with λ_{xy} the lattice displacement distance, and k_{xy} the corresponding hopping rate. In ERI-type zeolite, each hop in the z direction is preceded by a hop in xy direction, and diffusion is anisotropic:

$$D_z = \frac{1}{2} \frac{k_{xy}\, k_z}{k_{xy} + k_z} \lambda_z^2 \tag{6.2}$$

Using MD, the self-diffusion coefficients D_S^α in the direction $\alpha = x, y, z$ are computed by taking the slope of the mean squared displacement (MSD) at long times

$$D_S^\alpha = \frac{1}{2N} \lim_{t\to\infty} \frac{d}{d\,t} \left\langle \sum_{i=1}^{N} \left(r_{i\alpha}\left(t\right) - r_{i\alpha}\left(0\right) \right)^2 \right\rangle \tag{6.3}$$

where N is the number of molecules, t the time, and $r_{i\alpha}$ the α component of the center of mass of molecule i. The collective diffusion coefficients D_C^α are calculated from

$$D_C^\alpha = \frac{1}{2N} \lim_{t\to\infty} \frac{d}{d\,t} \left\langle \left(\sum_{i=1}^{N} \left(r_{i\alpha}\left(t\right) - r_{i\alpha}\left(0\right) \right) \right)^2 \right\rangle \tag{6.4}$$

Collective diffusivity measures the transport of mass and the decay of density fluctuations in the system, whereas the self-diffusion measures the diffusive motion of a single particle [30]. The collective diffusivity D_C is related to the transport diffusivity D_T, defined as the proportionality constant between the macroscopic flux and concentration gradient, and is the quantity of experimental interest. In zeolite literature, sometimes the "corrected" diffusivity is used. This type of diffusivity is obtained from the transport diffusion by removal of the so-called thermodynamic factor $1/\xi$. The "corrected" diffusivity can be related directly to the mean squared displacement of the collective coordinate $\mathbf{R} = \sum_{i=1}^{N} \mathbf{r}_i$ (which is N times the coordinate of the center of mass), in analogy to the self-diffusivity. We note that the thermodynamic factor has no influence on the ratio of diffusivities.

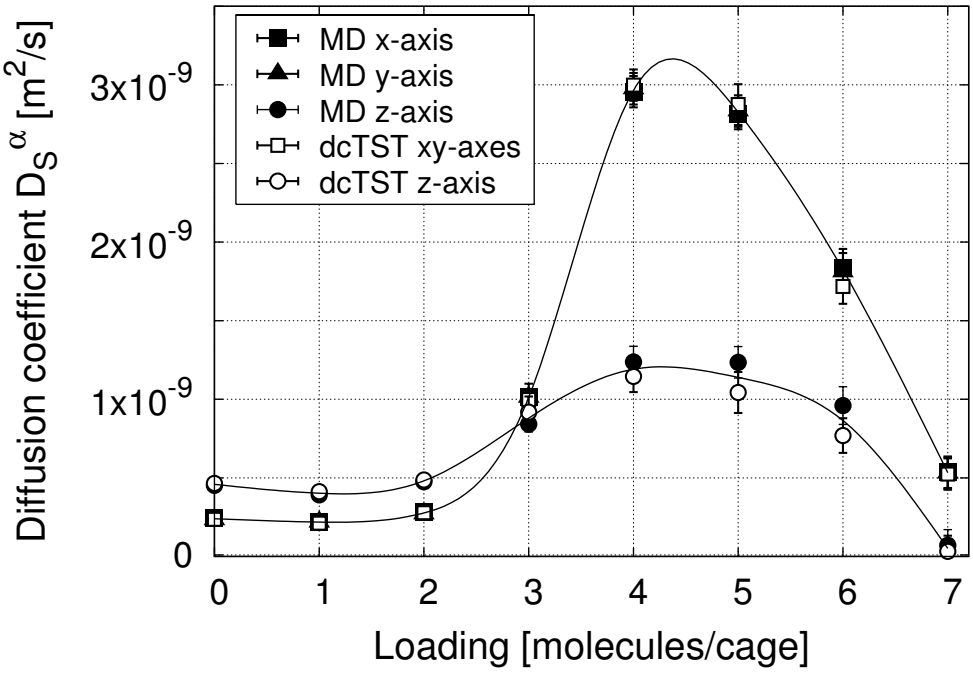

Figure 6.1: *Anisotropic self-diffusivity D_S^α of ethane in ERI-type zeolite computed by dcTST and conventional MD at 600 K.*

6.3 Results

In figure 6.1 we have plotted the self-diffusivity of ethane in ERI-type zeolite at 600 K as a function of loading. The ratios D_z/D_{xy} of the self and collective diffusivities are shown in figure 6.2. Very surprisingly, at low loading the diffusivity in the z direction is twice as *fast* as that in the xy direction for both the self- and collective diffusivity, while for higher loadings this changes into a z diffusivity that is more than twice as *slow*. This behaviour shows directly that the molecules follow different pathways when the loading is changed.

The dcTST gives results that are equivalent to conventional MD. Importantly, the method allows for a more detailed analysis in terms of free-energy profiles and transmission coefficients. Eq. 6.2 shows that diffusion in the z direction is dependent on both the hopping rate in the z direction *and* in the xy direction. An investigation of these hopping rates is made by analysing the free-energy barriers for diffusion in the xy plane. For the diffusion in the xy plane we find "normal" behaviour, typical for cage/window-type zeolites [24]:

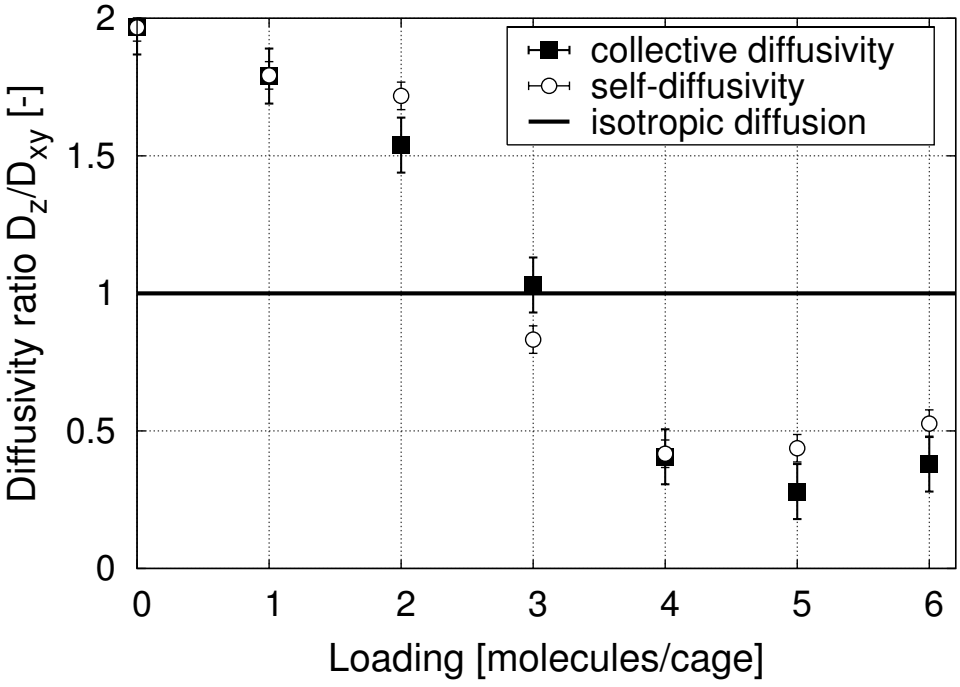

Figure 6.2: *Anisotropic diffusivity ratio D_z/D_{xy} of ethane in ERI-type zeolite computed by MD at 600 K for self and collective diffusion.*

the diffusivity increases with loading, because the free-energy barrier for diffusion decreases. This is due to the finite volume of a cage, where adding particles to the cage results in more repulsive interactions. In the z direction, we find different behaviour. Initially, at low loadings, there are no intracage barriers, and therefore the barriers to diffusion are formed by the xy barriers, i.e. the eight-ring windows between the adjacent cages. At higher loadings, the xy barriers decrease and new barriers are formed at the centers of the cages. Eventually the barriers at the centers of the cages dominate the diffusion mechanism, thereby reversing the anisotropy of the diffusion.

It is interesting to note that when the elongation of the erionite cages is removed, i.e. in CHA-type zeolites (figure 6.4), no significant anisotropy is observed in our simulations (figure 6.5). We note that the lattice is only slightly distorted from a cubic lattice and for symmetry reasons the free-energy profiles are all equivalent, i.e. there is only one hopping rate k from a cage to *any* of the neighbouring cages in CHA-type zeolites. The orientationally averaged diffusion coefficient is *not* affected in CHA-type lattices by the distortion effect,

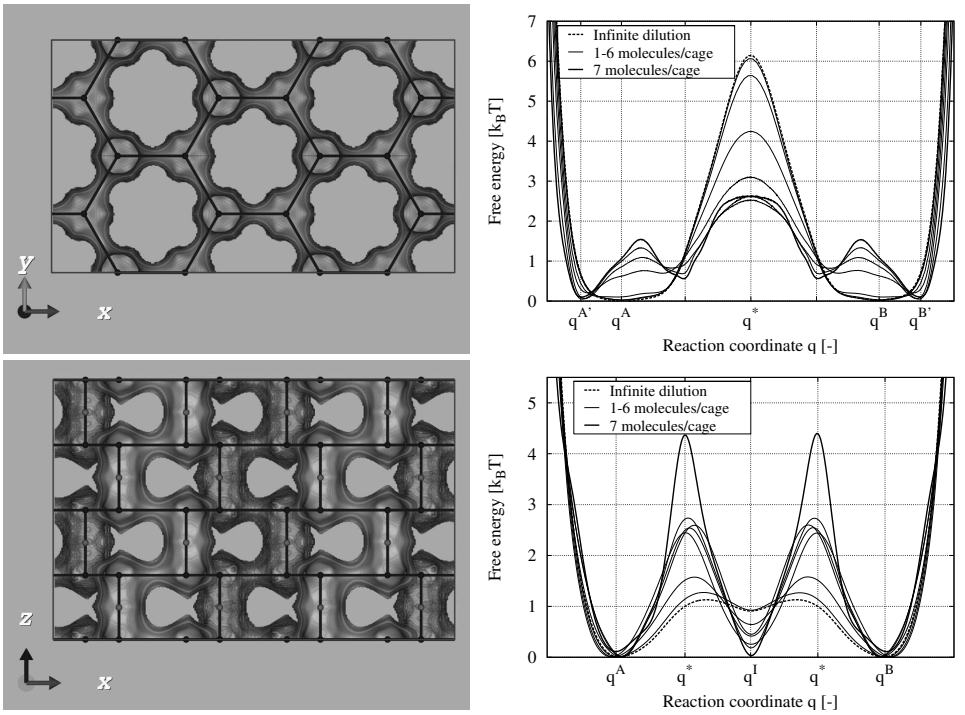

Figure 6.3: *The ERI-type silica structure crystallises in the hexagonal bipyramidal space group $P6_3/mmc$ with $a = b = 1.327$ nm, $c = 1.505$ nm, and $\alpha = \beta = 90°$, $\gamma = 120°$. We show the topology of the ERI-type lattice (Upper left) In the xy direction the hopping takes place on a hexagonal lattice. (Lower left) in the z direction a displacement* has *to be preceded first by an xy hop. The lattice is drawn as dots connected by dark lines of lattice distance $\lambda \approx 0.75$ nm for x, y, and z directions. (Upper right) Free-energy profiles $\beta F(q)$ at 600 K of ethane in ERI at various loadings (infinite dilution, 1, 2, 3, 4, 5, 6, and 7 molecules per ERI-type cage) in the hexagonal xy plane with q^A the center of a cage, and q^B the center of a neighbouring cage. (Lower right) in the z direction across a cage with q^A the top of the cage, q^I the middle of the cage, and q^B the bottom of the cage.*

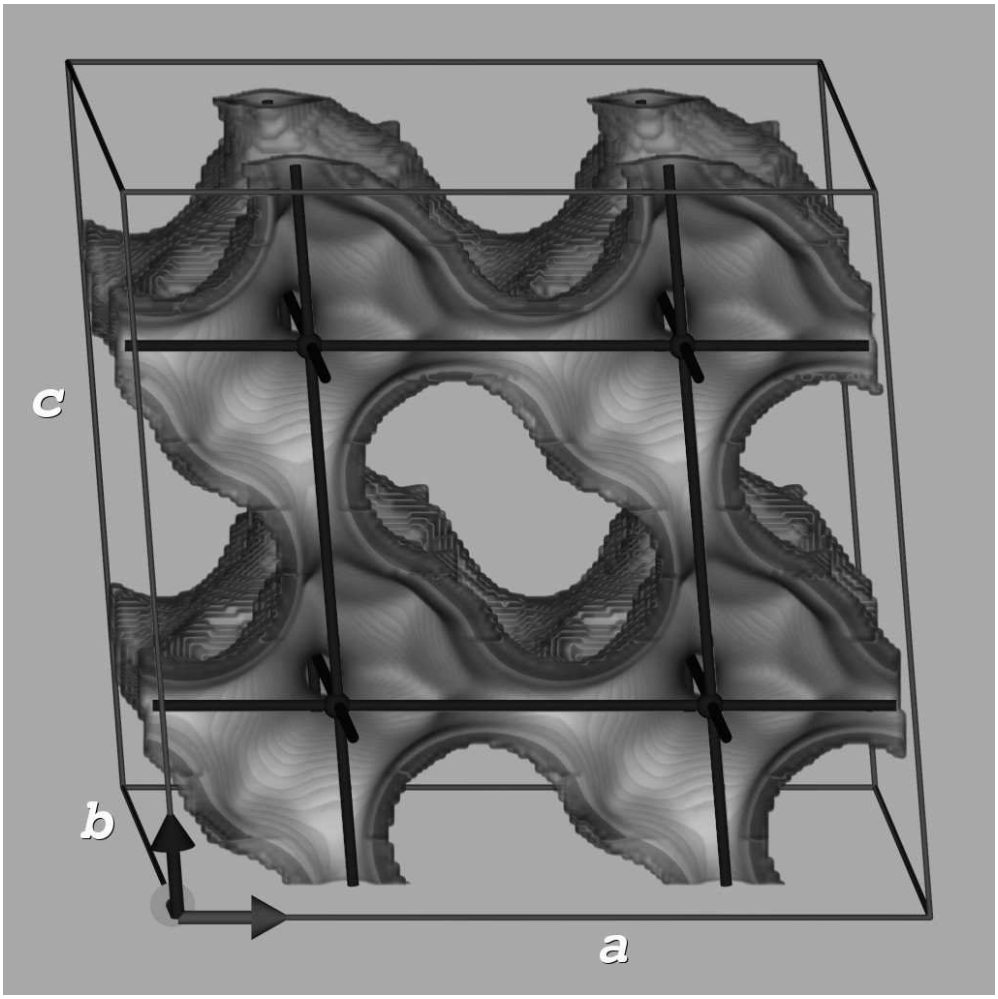

Figure 6.4: *The CHA-type structure [15] has the space group $R\bar{3}m$ (a squashed cube) with $a = b = c = 0.9459$ nm, and $\alpha = \beta = \gamma = 94.07°$. The topology of the CHA-type lattice is shown, where the lattice is drawn as dark spheres connected by dark lines.*

but the individual components are, although the effect for 94.07° compared to 90° is negligibly small (less than 2%). Therefore, diffusion in CHA-type zeolite can be considered isotropic in practice. Also experimentally, tracer diffusion measurements in natural chabazite by Raman spectroscopy did not indicate any substantial deviation from isotropic diffusion [31]. However, using the pulsed field gradient NMR technique, Bär et al. [32] reported an orientation-dependent

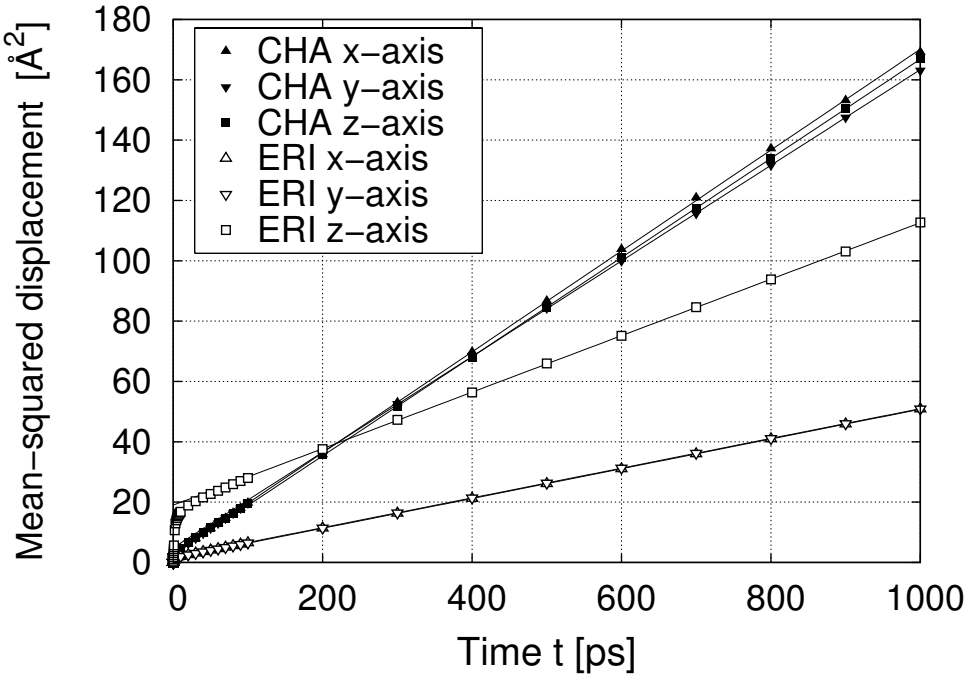

Figure 6.5: *Mean squared displacements of self-diffusivity of ethane in CHA-type and ERI-type zeolite at 600 K. The diffusion coefficients in the direction $\alpha = x, y, z$ are computed by taking the slope of the mean squared displacements at long times.*

diffusivity with a ratio between the maximum and minimum diffusivity of a factor of two, also for water in natural chabazite.

6.4 Discussion

We stress that the concept of Molecular Traffic Control [33] is different from our Molecular Path Control. It is thought that the origin of MTC lies in the mutual correlation in the movement of a multicomponent fluid through two types of pores [34]. MTC has never been convincingly established and has remained a controversial subject for over two decades now, although recently some theoretical progress has been achieved [35–37]. The current work demonstrates only how the diffusivity of *one* component may vary between pore systems in the same zeolite. The concept of MTC requires various molecules (reactants and products) to exhibit preferences for different pore systems. However, our

results show that these preferences might not only be due to shape-selectivity, but also due to (local) differences in loading. Moreover, the fact that a *single* component can be tuned to show a preference of one type of pore over another and that this preference can be manually adjusted might be considered even more surprising. This controllability implies the ability of directing adsorbates at the molecular level.

MPC originates from the anisotropic nature of the nanoporous material, e.g. the presence of different channel types or elongated cages. Our results suggest that it is possible to actively design and screen for zeolites with molecular path control properties. As an example, we reported the diffusion of ethane in an erionite-type structure with different diffusion paths, which may be controlled by changing the loading or pressure and temperature. However, the phenomenon is general and by no means limited to zeolites. We have shown that the crucial ingredient is the asymmetric nature of a structure which can be exploited, even for a single component fluid, by using appropriate operating conditions.

Bibliography

[1] Davis, M. E. (2003) *Science* **300**, 438–439.

[2] Lai, Z, Bonilla, G, Diaz, I, Nery, J. G, Sujaoti, K, Amat, M. A, Kokkoli, E, Terasaki, O, Thompson, R. W, Tsapatsis, M, & Vlachos, D. G. (2003) *Science* **300**, 456–460.

[3] Kärger, J & Ruthven, D. M. (1992) *Diffusion in Zeolites and other microporous solids.* (John Wiley & Sons, Inc., New York).

[4] Hahn, K, Kärger, J, & Kukla, V. (1996) *Phys. Rev. Lett.* **76**, 2762–2765.

[5] Gorring, R. L. (1993) *J. Catal.* **31**, 13–26.

[6] Dubbeldam, D, Calero, S, Maesen, T. L. M, & Smit, B. (2003) *Phys. Rev. Lett.* **90**, 245901.

[7] Ghorai, P. K, Yashonath, S, Demontis, P, & Suffritti, G. B. (2003) *J. Am. Chem. Soc.* **125**, 7116–7123.

[8] June, R. L, Bell, A. T, & Theodorou, D. N. (1990) *J. Phys. Chem.* **94**, 8232–8240.

[9] Kärger, J. (1991) *J. Phys. Chem.* **95**, 5558–5560.

[10] Hong, U, Kärger, J, Kramer, R, Pfeifer, H, Seiffert, G, Muller, U, Unger, K. K, Luck, H. B, & Ito, T. (1991) *Zeolites* **11**, 816–821.

[11] June, R. L, Bell, A. T, & Theodorou, D. N. (1992) *J. Phys. Chem.* **96**, 1051–1060.

[12] Maginn, E. J, Bell, A. T, & Theodorou, D. N. (1996) *J. Phys. Chem.* **100**, 7155–7173.

[13] Bussai, C, Fritzsche, S, Haberlandt, R, & Hannongbua, S. (2003) *J. Phys. Chem. B.* **107**, 12444–12450.

[14] Gard, J. A & Tait, J. M. (1973) ed. Uytterhoeven, J. B. (Proceedings of the Third International Conference on Molecular Sieves; Recent Progress Reports, Leuven University Press, Zurich), pp. 94–99.

[15] Calligaris, M, Nardin, G, & Randaccio, L. (1983) *Zeolites* **3**, 205–208.

[16] Bezus, A. G, Kiselev, A. V, Lopatkin, A. A, & Du, P. Q. J. (1978) *J. Chem. Soc., Faraday Trans. II* **74**, 367–379.

[17] Ryckaert, J. P & Bellemans, A. (1978) *Faraday Dicuss. Chem. Soc.* **66**, 95–106.

[18] Schüring, A, Auerbach, S. M, Fritzsche, S, & Haberlandt, R. (2002) *J. Chem. Phys* **116**, 10890–10894.

[19] Vlugt, T. J. H & Schenk, M. (2002) *J. Phys. Chem. B.* **106**, 12757–12763.

[20] Calero, S, Dubbeldam, D, Krishna, R, Smit, B, Vlugt, T. J. H, Denayer, J. F. M, Martens, J. A, & Maesen, T. L. M. (2004) *J. Am. Chem. Soc.* **126**, 11377–11386.

[21] Dubbeldam, D, Calero, S, Vlugt, T. J. H, Krishna, R, Maesen, T. L. M, Beerdsen, E, & Smit, B. (2004) *Phys. Rev. Lett.* **93**, 088302–1.

[22] Dubbeldam, D, Calero, S, Vlugt, T. J. H, Krishna, R, Maesen, T. L. M, & Smit, B. (2004) *J. Phys. Chem. B.* **108**, 12301–12313.

[23] Vlugt, T. J. H, Krishna, R, & Smit, B. (1999) *J. Phys. Chem. B.* **103**, 1102–1118.

[24] Beerdsen, E, Smit, B, & Dubbeldam, D. (2004) *Phys. Rev. Lett.* **93**, 248301.

[25] Dubbeldam, D, Beerdsen, E, Vlugt, T. J. H, & Smit, B. (2005) *J. Chem. Phys* **122**, 224712.

[26] Allen, M. P & Tildesley, D. J. (1987) *Computer simulation of liquids.* (Clarendon Press, Oxford).

[27] Rapaport, D. C. (2004) *The art of molecular dynamics simulation 2nd edition.* (Cambridge University Press, Cambridge).

[28] Frenkel, D & Smit, B. (2002) *Understanding molecular simulation 2nd edition.* (Academic Press, London, UK).

[29] Martyna, G. J, Tuckerman, M, Tobias, D. J, & Klein, M. L. (1996) *Mol. Phys.* **87**, 1117–1157.

[30] Ala-Nissila, T, Ferrando, R, & Ying, S. C. (2002) *Advances in Physics* **51**, 949–1078.

[31] Goryainov, S. V & Belitsky, I. A. (1995) *Phys. Chem. Miner.* **22**, 433–452.

[32] Bär, N.-K, Kärger, J, Pfeifer, H, Schäfer, H, & Schmitz, W. (1998) *Microp. Mesop. Materials* **22**, 289–295.

[33] Derouane, E. G & Gabelica, Z. (1980) *J. Catal.* **65**, 486–489.

[34] Clark, L. A, Ye, G. T, & Snurr, R. Q. (2000) *Phys. Rev. Lett.* **84**, 2893–2896.

[35] Bräuer, P, Brzank, A, & Kärger, J. (2003) *J. Phys. Chem. B.* **107**, 1821–1831.

[36] Neugebauer, N, Bräuer, P, & Kärger, J. (2000) *J. of Catal.* **194**, 1–3.

[37] Bräuer, P, Neugebauer, N, & Kärger, J. (2001) *Coll. and Surf.* **187-188**, 459–467.

We apply the dynamically corrected Transition-State Theory to confinements with complex structures. This method is able to compute self-diffusion coefficients for adsorbate-adsorbent system far beyond the time scale accessible to Molecular Dynamics. Two exemplary cage/window-type confinements are examined: ERI-type and CHA-type zeolites. In ERI-type zeolite, each hop in the z direction is preceded by an hop in xy direction, and diffusion is anisotropic. The lattice for CHA-type zeolite is a rhombohedral Bravais lattice, and diffusion can be considered in practice The anisotropic behaviour of ERI-type cages reverses with loading, i.e. at low loading the diffusion in the z direction is two times as fast as in the xy direction, while for higher loadings this changes to a z diffusivity that is more than two times as slow. At low loading the diffusion is impeded by the eight-ring windows, i.e. the exits out of the cage to the next, but at higher loadings the barrier is formed by the center of the cages.

D. Dubbeldam, E. Beerdsen, S. Calero, and B. Smit

7

Applying Dynamically Corrected Transition-State Theory in Complex Lattices

7.1 Introduction

Transport of adsorbates in nanoporous adsorbents such as zeolites is determined by a complex interplay between adsorbent-adsorbate and adsorbate-adsorbate interactions. From a scientific point of view zeolites are ideal systems to study the effect of confinement on the properties of the adsorbed molecules because of their regularity and periodicity. Although interesting effects like single-file diffusion [1–3], incommensurate diffusion [4–7], and levitation effects [8] are well known, most of the effects of confinement on diffusion remain poorly understood. This is particularly true for loading effects in materials with different channels and/or cages in the x, y, and z direction.

Anisotropic single-component diffusion in nanoporous materials has been known for a long time. A well-known example is diffusion in silicalite [9–13]. In

general, the diffusion coefficients in the different directions can have different dependencies on temperature and loading. A limited number of studies deal with nonzero loading. Bussai *et al.* [14] found little change in anisotropy for water in silicalite as a function of loading, while Skoulidas and Sholl found a more irregular loading dependence of the anisotropy [15]. Anisotropic behaviour is very common in nanoporous materials. The papers of Skoulidas and Sholl [16] (molecular-dynamics simulations), Trinh *et al.* [17] (Monte Carlo simulations), Su *et al.* [18] (molecular-dynamics simulations in clay), Powles *et al.* [19] (a model for permeable micropores with variable anisotropic diffusion), Yokoyamaa and Nakashimav [20] (diffusion experiments on a rhyolite rock having an anisotropic pore structure), Wingen *et al.* [21] (anisotropic motion of water in zeolites EMT, L, and ZSM-5 as studied by D and H NMR line splitting), Nelson *et al.* [22, 23] (modelling permeation through anisotropic zeolite membranes), Furo and Dvinskikh [24] (methodology of NMR experiments intended to measure anisotropic diffusion), and Manzel *et al.* [25] (NMR characterisation of the pore structure and anisotropic self-diffusion in saltwater ice) are just a few examples.

Although Molecular Dynamics (MD) is a very powerful technique to study these effects, MD is typically limited to diffusion rates in the order of 10^{-12} m^2/s. To overcome this, some studies have used dynamically corrected Transition-State Theory (dcTST) methods (see Ref. [26] and references therein). Hitherto, studies were limited to the infinite dilution limit, whereas many of the processes of practical importance occur at nonzero loading. In ref. [29] this problem was resolved extending the dcTST Bennett-Chandler approach to include diffusion of molecules at nonzero loading using only assumptions already present in TST.

In this work, we report molecular simulations of diffusion in confinement showing a phenomenon previously denoted as molecular path control (MPC)l depending on loading, molecules follow a preferred pathway [32]. We note that MPC is different from molecular traffic control [33], which is caused by mutual correlations in the movement of a multicomponent fluid through two types of pores. As a specific MPC example, we study the mechanism behind the *tunable* anisotropy of ethane in ERI-type zeolite membranes. In ERI-type zeolite, the diffusion is characterised by complex diffusion paths. Each hop in the z direction is preceded by a hop in the xy direction. At low loadings, the diffusivity in the z direction is two times as *fast* as that in the xy direction for both the self- and the collective diffusivity, while for higher loadings this changes into a z diffusivity that is more than two times as *slow*. Additionally, we study a closely related zeolite known as Chabazite (CHA). The cages of CHA-type zeolites are somewhat smaller than ERI-type cages, and more spherical. In

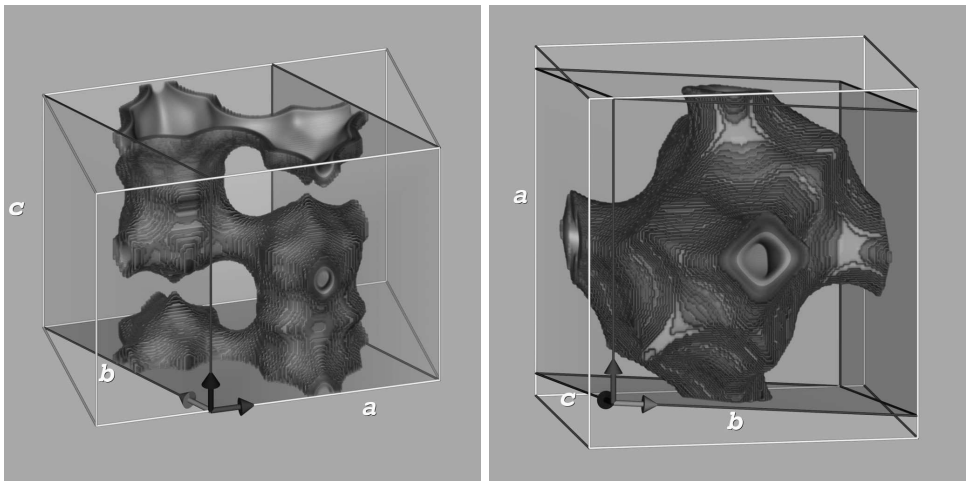

(a) (b)

Figure 7.1: *Unit cell of (a) ERI-type zeolite, and (b) CHA-type zeolite. The ERI-type silica structure [30] crystallises in the hexagonal bipyramidal space group $P6_3/mmc$ with $a = b = 1.327$ nm, $c = 1.505$ nm, and $\alpha = \beta = 90°$, $\gamma = 120°$. The CHA-type structure [31] has the space group $R\bar{3}m$ (a squashed cube) with $a = b = c = 0.9459$ nm, and $\alpha = \beta = \gamma = 94.07°$. A unit cell of erionite contains two cages, while a unit cell of chabazite contains a single cage.*

literature, a rectangular hopping lattice has been used for CHA to compute diffusion in simulations [34, 35]. For this lattice the diffusion 'appears' to be anisotropic. However, for a different lattice, properly aligned with the crystal axes, we show that in fact diffusion in CHA-type zeolites is nearly isotropic. We note that the problem in zeolites is the reverse of that in lattice theory, where the hopping rates and lattice type are given. Here, we need to resolve both, and for this we apply the dcTST method. We use dcTST and MD to study changes in diffusion behaviour in ERI-type and CHA-type zeolites over loading.

The remainder of this chapter is organised as follows. In section 7.2 we start with a detailed description of the ERI-type and CHA-type zeolites. Next, we describe the dcTST method to compute the effective hopping rate for these lattices. In the results section 7.3 we derive the correct conversions from hopping rates to diffusivities, and show results for ethane at 600 K in ERI-type

and CHA-type zeolites using dcTST and MD. The free-energy profiles, the transmission coefficients, the hopping rate, and self-diffusion coefficients for both zeolites are evaluated. Here, we explain our choice of the hopping lattice, being closely related to the computed free-energy profiles. We end with some conclusions on anisotropic behaviour in zeolites as a function of loading, and why the dcTST method is a suitable method to provide detailed insight into mechanisms behind it.

7.2 Methods

7.2.1 Zeolite Descriptions

The ERI-type silica structure [30] crystallises in the hexagonal bipyramidal space group $P6_3/\mathrm{mmc}$ with $a = b = 1.327$ nm, $c = 1.505$ nm, and $\alpha = \beta = 90°$, $\gamma = 120°$. The elongated erionite cages approximate the shape of 1.3×0.63 nm cylinders connected by 0.36×0.51 nm windows. Only linear molecules are able to penetrate the eight-membered-ring windows. There are three windows at the top of the cage rotated 120° with respect to one another. At the bottom of the cage, there are also three windows rotated 120° with respect to one another. The top three windows are aligned with the windows at the bottom. Each ERI-type unit cell contains two erionite cages as shown in figure 1(a).

The CHA-type structure [31] has the space group $R\bar{3}m$ (a squashed cube) with $a = b = c = 0.9459$ nm, and $\alpha = \beta = \gamma = 94.07°$. The framework contains double six-membered rings joined together through four-membered rings. The resulting three-dimensional structure has large ellipsoidal chabazite (CHA) cages. Small guest molecules can enter the cages through eight-membered 0.38 nm wide ring windows. Only linear alkanes are able to penetrate the windows. Each CHA-type unit cell contains a single chabazite cage as shown in figure 1(b).

7.2.2 The dcTST Method

Slow diffusion of molecules in zeolites can be considered an activated process, in which the particle hops from one free-energy minimum to the next, and the actual crossing time is negligible compared to the time a particle spends inside the cage. One can exploit the large separation in time scales using rare-event simulation techniques [36,37]. We consider a system which can be in two stable states, A and B with a dividing free-energy barrier between them. The reaction coordinate q, indicates the progress of the diffusion event from cage A to cage B. The location of the dividing barrier is denoted by q^*. We introduce

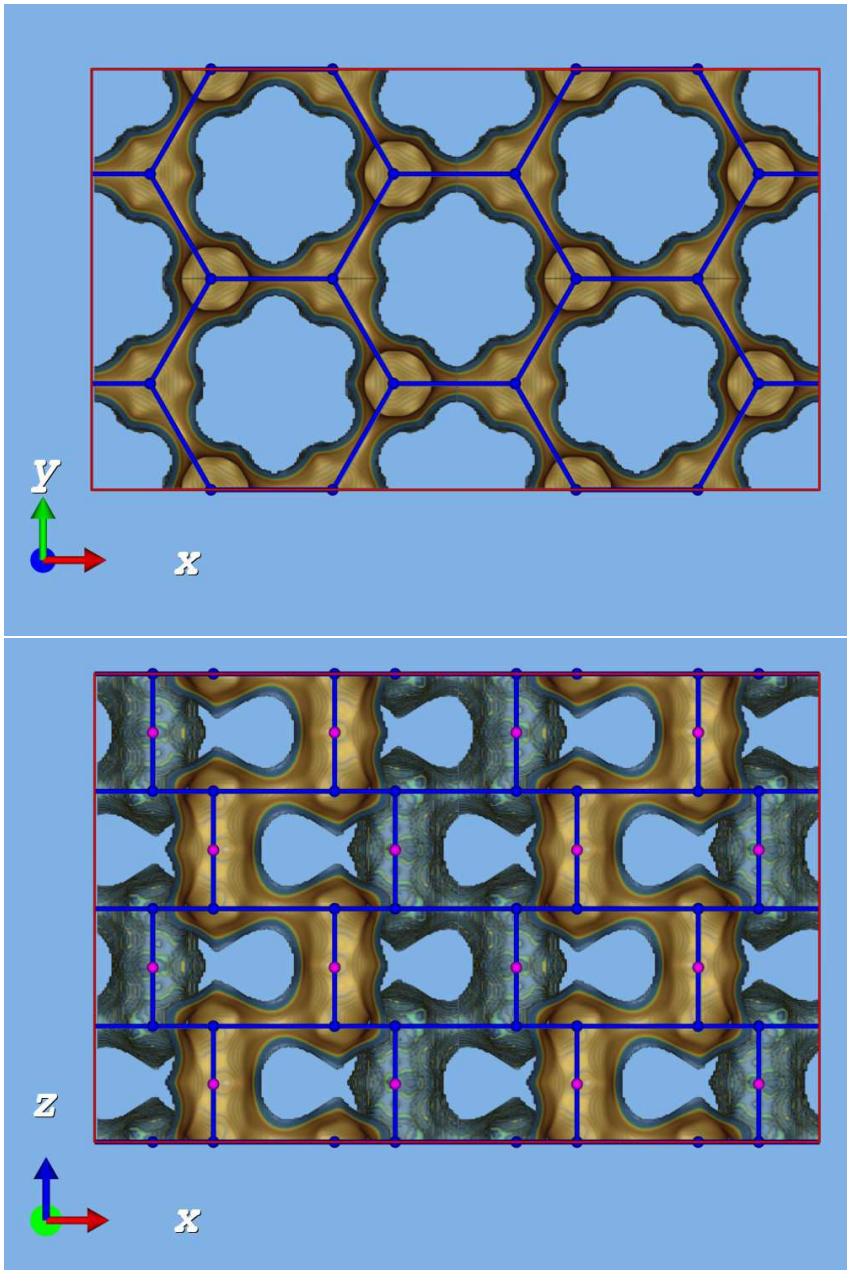

Figure 7.2: *The topology of the ERI-type lattice in (a) xy direction the hopping takes place on a hexagonal lattice, in (b) the z direction a displacement* has *to be preceded by a xy hop. The lattice is drawn in blue dots connected by blue lines of lattice distance* $\lambda \approx 0.75$ *nm for x, y, and z directions.*

two characteristic functions n_A and n_B that measure whether the system is in state A or B. A possible and often used definition is

$$n_A = \theta\left(q^* - q\right), \tag{7.1}$$

$$n_B = \theta\left(q - q^*\right), \tag{7.2}$$

where θ is the Heaviside function $\theta(x)$, which has value 0 for $x < 0$ and value 1 for $x \geq 0$.

In the Bennett-Chandler approach [26, 36, 37] one computes the hopping rate over the barrier in two steps

$$k_{A\to B} = \underbrace{\frac{\langle \delta\left(q^* - q\right)\rangle}{\langle \theta\left(q^* - q\right)\rangle}}_{P(q^*)} \times \underbrace{\frac{\langle \dot{q}(0)\delta\left(q^* - q(0)\right)\theta\left(q\left(t\right) - q^*\right)\rangle}{\langle \delta\left(q^* - q(0)\right)\rangle}}_{R(t)} \tag{7.3}$$

$$= \frac{e^{-\beta F(q^*)}}{\int_{\text{cage A}} e^{-\beta F(q)}\,\mathrm{d}dq} \tag{7.4}$$

where δ is the Dirac delta function. $q(t)$ the reaction coordinate at time t, m is the mass of the segments of the particle involved in the reaction coordinate, κ the transmission coefficient, k_B the Boltzmann constant, T the temperature, $\beta = 1/k_BT$ the inverse temperature, and F the free energy of position related to the probability $P(q)$ by $\beta F = -ln\langle P(q)\rangle$.

O. Braun and C. Sholl [38] developed a technique to calculate the diffusion tensor for the lattice-gas model at infinite dilution for any complex elementary cell. Although sometimes lengthy calculations are involved, in many cases analytical expressions for the diffusion tensor may be obtained. It is important to note that the extension to higher loading requires an estimate of the correlations between the particles, which tends to reduce the diffusion. Transition-State Theory methods such as the methods of Tunca and Ford [39–41] neglect the correlations while computing the hopping rate, but hope to regain these correlations during a coarse-grained kinetic Monte Carlo simulation. In addition, various approximations are made to make the computation tractable, using multidimensional TST. Their method underpredicted the diffusivity at low loading, while significantly overpredicting the diffusivities at higher loadings, in comparison to conventional MD (see figure 6 of ref. [41]) for methane in LTA-type silica.

The newly developed method of ref. [29] computes an *effective* hopping rate, i.e. a hopping rate including correlations. The conversion of the hopping rate at nonzero loading is therefore the same as for the infinite dilution case. Importantly, the study of diffusion over long time and space regions can then

be restrcitred to the analysis of the free-energy profiles of a *single* unit cell (the surrounding cages influence this profile and have to be properly modelled [29]). For the same system, methane in LTA-type silica, the dcTST method of ref. [29] gives exact overlap with MD results (see figure 3 of ref. [29]).

For systems with erratic free-energy landscapes, e.g. multiple barriers of different heights, the dcTST method can be generalised using

$$k_{A\to B} = \frac{1}{\langle n_A \rangle} \frac{\left\langle \int_0^\infty \dot{q}\left(t\right) \dot{q}\left(0\right) \frac{w(q(t))}{w(q(0))} \frac{e^{-\beta F(q(t))}}{e^{-\beta F(q(0))}} \, dt \right\rangle_\pi}{\int_{q_A}^{q_B} e^{\beta F(q)} \, dq \int_{-\infty}^{\infty} e^{-\beta F(q)} \, dq} \tag{7.5}$$

with a biasing function $w(q)$ operating on the regions A and B:

$$\begin{aligned} w(q) &= e^{a\beta F(q)} \\ \pi\left(q\right) &\propto e^{(a-1)\beta F(q)} \end{aligned} \tag{7.6}$$

where $a > 0$ is an integer to be chosen freely. A value of $a = 1$ would flatten the free-energy landscape, a value of $a = 2$ would reproduce the Ruiz-Montero method (if the approximate free energy is taken to be the true free energy) [42]. Starting configurations at the desired loading are sampled using NVT MC (with the biased, tagged particle in the π ensemble), and subsequently a weighted velocity autocorrelation of the tagged particle is computed using conventional NVE MD. For more details on the dcTST methods see refs. [26] and [29], and see ref. [43] for another application on MFI-type zeolite.

7.2.3 Nonrectangular Unit Cells and Reaction Coordinates

ERI-and CHA-type zeolite can be described both in terms of rectangular unit cells, and in their crystallographic nonrectangular unit-cell definitions. In crystallography, the crystal structure is defined by the unit cell, and by the fractional coordinates of the atoms within the unit cell. These coordinates form an orthonormal dimensionless $\mathcal{S}$ space. $\mathcal{S}$ space is often more convenient for the computation of the free-energy profiles. The transformation from $\mathcal{S}$ space to real $\mathcal{R}$ space can be carried out by the matrix $\mathcal{H}$:

$$\mathcal{H} = \begin{pmatrix} a & b\cos\left(\gamma\right) & c\cos\left(\beta\right) \\ 0 & b\sin\left(\gamma\right) & c\zeta \\ 0 & 0 & c\sqrt{1-\cos^2\beta-\zeta^2} \end{pmatrix} \tag{7.7}$$

with

$$\zeta = \frac{\cos\alpha - \cos\gamma\cos\beta}{\sin\gamma} \tag{7.8}$$

Conversely, $\mathcal{H}^{-1}$ transforms real coordinates into fractional coordinates. With the chosen $\mathcal{H}$ the scaled box has a length of 1. Our potential forcefield is defined in real space, therefore it is convenient to store position in $\mathcal{R}$ space, transform them to $\mathcal{S}$ space, apply periodic boundary conditions in $\mathcal{S}$ space, and transform back to $\mathcal{R}$ space to compute distances within the simulation box

$$\begin{aligned} \mathbf{s} &= \mathcal{H}^{-1}\mathbf{r} \\ \mathbf{s}' &= \mathbf{s} - \mathrm{rint}\,(\mathbf{s}) \\ \mathbf{r}' &= \mathcal{H}\mathbf{s}' \end{aligned} \tag{7.9}$$

where the "rint" function returns the rounded-integer value of its argument. The smallest perpendicular width of the unit cell has to be larger than twice the spherical cutoff in $\mathcal{R}$ space.

For computational reasons a rectangular unit cell is preferred. Not only is the matrix conversion more expensive, if the unit cell is severely distorted from cubic, many redundant distance calculations will be performed for particles lying outside of the cutoff in $\mathcal{R}$ space, further reducing the efficiency. However, for computation of free-energy profiles in complex zeolite structures, the fractional space is often very convenient.

We can choose q as the position of one of the two beads of ethane [6,7]. This choice of order parameter underestimates the free energy of the true transition state, but the dynamical correction κ is the *exact* correction compensating our choice of reaction coordinate [37].

The monoclinic unit cell definition for an ERI-type cage is shown in Figure 1(a). Because two cages are present in the unit-cell definition it is convenient to be able to select a single cage by using

$$q = \begin{cases} s_x + (1 - s_y) < 1 & \text{for cage } A \\ s_x + (1 - s_y) > 1 & \text{for cage } B \end{cases} \tag{7.10}$$

where s are the fractional coordinates of a single ERI-type unit cell in $\mathcal{S}$ space. For xy computations the barrier is located at $s_{xy} = \{\frac{1}{2}, \frac{1}{2}\}$, and by symmetry all positions in the unit cell can be mapped on the reaction coordinate. For the z computation we select only cage A and use

$$q = s_z \tag{7.11}$$

The barrier at the center of the cage is located at $s = \{\frac{1}{3}, \frac{2}{3}, \frac{3}{4}\}$, while the free-energy minima q^A and q^B are located at $s = \{\frac{1}{3}, \frac{2}{3}, \frac{1}{2}\}$ and $s = \{\frac{1}{3}, \frac{2}{3}, 1\}$,

respectively. Using the projection of eq. 7.11 and the positions of cage A only, q^A is located at $s_z = \frac{1}{2}$, the barrier q^* at $s_z = \frac{3}{4}$, and q^B at $s_z = 1$.

The unit-cell definition for a CHA-type cage is shown in figure 1(b) (the rhombohedral lattice can be thought of as a cube slightly pulled along its space diagonal). The reaction coordinate can now be chosen from the center of the cage ($\mathbf{s}_0 = \{0.5, 0.5, 0.5\}$) to any of the six exits through the center of the windows ($\mathbf{s}_1 = \{1, 0.5, 0.5\}$, $\mathbf{s}_2 = \{0.5, 1, 0.5\}$, $\mathbf{s}_3 = \{0.5, 0.5, 1\}, \mathbf{s}_4 = \{0, 0.5, 0.5\}$, $\mathbf{s}_5 = \{0.5, 0, 0.5\}$, $\mathbf{s}_6 = \{0.5, 0.5, 0\}$), i.e. the space is simply mapped onto the three orthonormal axes in scaled space. The other half of the profile, i.e., from q^* to q^B follows by symmetry. For symmetry reasons, the free-energy profiles are all equivalent, and there is only one hopping rate k from a cage to any of the neighbouring cages in CHA-type zeolites.

7.2.4 Force Field Potentials and Simulation Details

We neglect cations and study rigid, all-silica versions of the ERI-type and CHA-type zeolites. The positions of the atoms are taken from Ref. [30] and [31], respectively. Following the work of Bezus et al. [44], the zeolites are modelled as a rigid network of oxygen atoms. This is a very common approximation because the large oxygen atoms essentially shield the much smaller silicon atoms and lattice flexibility is not important for small alkanes in all-silica zeolites [45]. The simulation box sizes we used are $3 \times 3 \times 3$ unit cells (perpendicular widths are $3.447647 \times 3.447647 \times 4.515$ nm) for ERI-type zeolite, and $3 \times 3 \times 3$ unit cells (perpendicular widths are $2.809895 \times 2.809895 \times 2.809895$ nm) for CHA-type zeolite. Tests on larger systems did not show any significant finite-size effects. Periodic boundary conditions were employed. Adsorption in cation-free structures takes place at sites with little or no electric field. For these reasons the united atom model [47] seems the most straightforward choice. We consider the CH_3 groups as single, chargeless interaction centers with their own effective potentials. The beads of ethane are connected by an harmonic bonding potential

$$U^{\text{bond}} = \frac{1}{2} k_1 (r - r_0)^2 \tag{7.12}$$

with $k_1/k_B = 96500$ K/Å^2 and $r_0 = 1.54$ Å. The extramolecular energy consists of a guest-guest intermolecular energy U^{gg}, a host-guest interaction U^{hg}, modelled with a Lennard-Jones potential with a cutoff radius of 12 Å. The parameters $\sigma_{O-\text{CH}_3} = 3.17$ Å, $\epsilon_{O-\text{CH}_3}/k_B = 142$ K, $\sigma_{Si-\text{CH}_3} = 2.12$ Å, $\epsilon_{Si-\text{CH}_3}/k_B = 82$ K, and $\sigma_{\text{CH}_3-\text{CH}_3} = 3.78$ Å, $\epsilon_{\text{CH}_3-\text{CH}_3}/k_B = 104$ K were taken from Ref. [48]. Although the size parameters are rather small, for this

study we prefer to use these parameters because then diffusion of ethane in ERI-type and CHA-type zeolite is still feasible using conventional MD.

The simulations were performed using two different methods: conventional Molecular Dynamics (MD) and the recently proposed dynamically corrected Transition-State Theory (dcTST) [26,29]. We used the velocity Verlet integration scheme with a time step of 0.5 fs. The relative energy drift was smaller than 10^{-4}. For temperature control we employed the Nosé-Hoover chain (NHC) method as formulated by Martyna et al. [49]. Molecules were inserted into the framework at random positions as long as no overlaps occurred with the framework or other particles. During the initialisation period we performed an NVT Monte Carlo (MC) simulation to achieve rapidly an equilibrium molecular arrangement. After the initialisation period, we assigned velocities from the Maxwell-Boltzmann distribution at the desired average temperature to all the atoms. The total momentum of the system was set to zero. Next, we equilibrated the system further by performing an NVT MD simulation using the NHC thermostat. After the equilibration was completed, during the production run of more than 20 ns, we collected statistics using the NVT ensemble. Simulations using the NVE ensemble gave equivalent results. More details can be found in Ref. [26].

Transmission coefficients are computed from at least 50000 independent configurations. These configurations are obtained from Monte Carlo simulations, a configuration is stored every 500 cycles. A cycle is defined as N steps, where N is the number of molecules, and a step is one Monte Carlo move (translation, rotation, full regrow). On average, there is one Monte Carlo move per particle in a single cycle. The free-energy profiles are obtained using MD and MC; both give equivalent results.

7.3 Results

7.3.1 Ethane in ERI-Type Zeolite (Anisotropic Diffusion)

In an ERI-type lattice, diffusion in the xy plane occurs isotropically on a hexagonal lattice:

$$D_{xy} = \frac{1}{4} k_{xy} \lambda_{xy}^2 \tag{7.13}$$

with λ_{xy} the lattice displacement distance and k_{xy} the corresponding hopping rate. The z diffusion is dependent on the hopping in the xy plane. In general, the method of Braun and Sholl [38] can be used to compute diffusivity tensors. However, for such sequential hops, we can derive a simple formula for the combined hopping rate, based on the mean first-passage time. Consider a hop

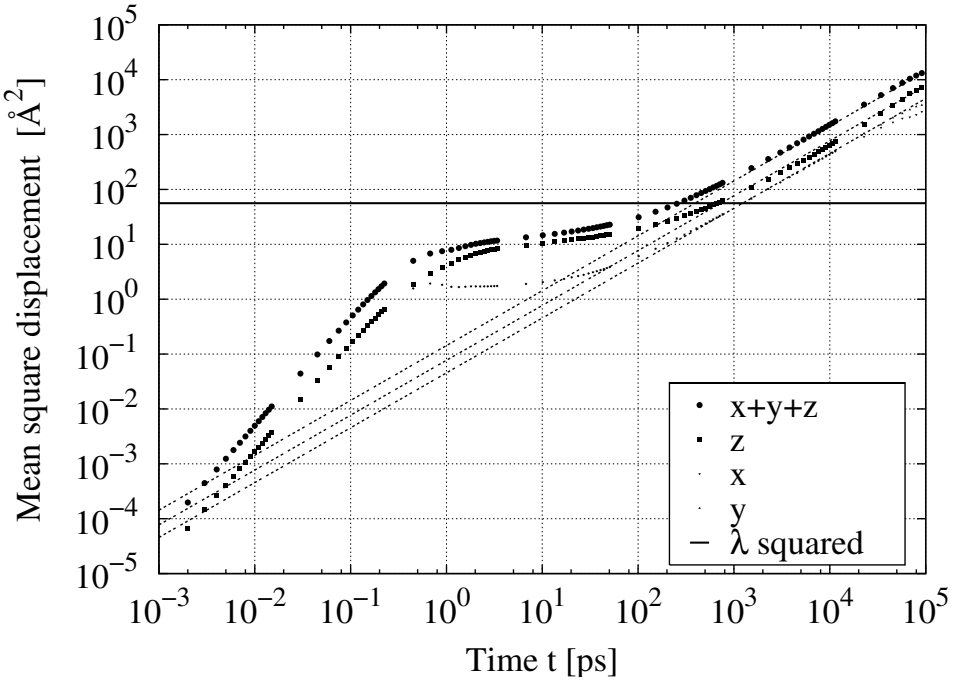

Figure 7.3: *Mean squared displacement of ethane in ERI-type zeolite at 600 K and a loading of one molecule per cage. The MSD is equal for x and y directions, and different in the z direction. The horizontal line is the cage-to-cage hopping distance λ (approximately 7.5 Å for both xy and z direction). The different regimes of diffusion are clearly visible, and only after a single cage crossing the MSD has become linear (a straight line of slope one in log-log scale). The slope over the linear regime corresponds to the limit of long times and can then be reliable measured. The diffusion coefficient is the slope at long times divided by two times the number of spatial dimensions.*

from A to C with an intermediate state B. We have

$$\frac{P_{B\to A}}{P_{B\to C}} = \frac{k_{B\to A}}{k_{B\to C}} \tag{7.14}$$

$$P_{B\to A} + P_{B\to C} = 1 \tag{7.15}$$

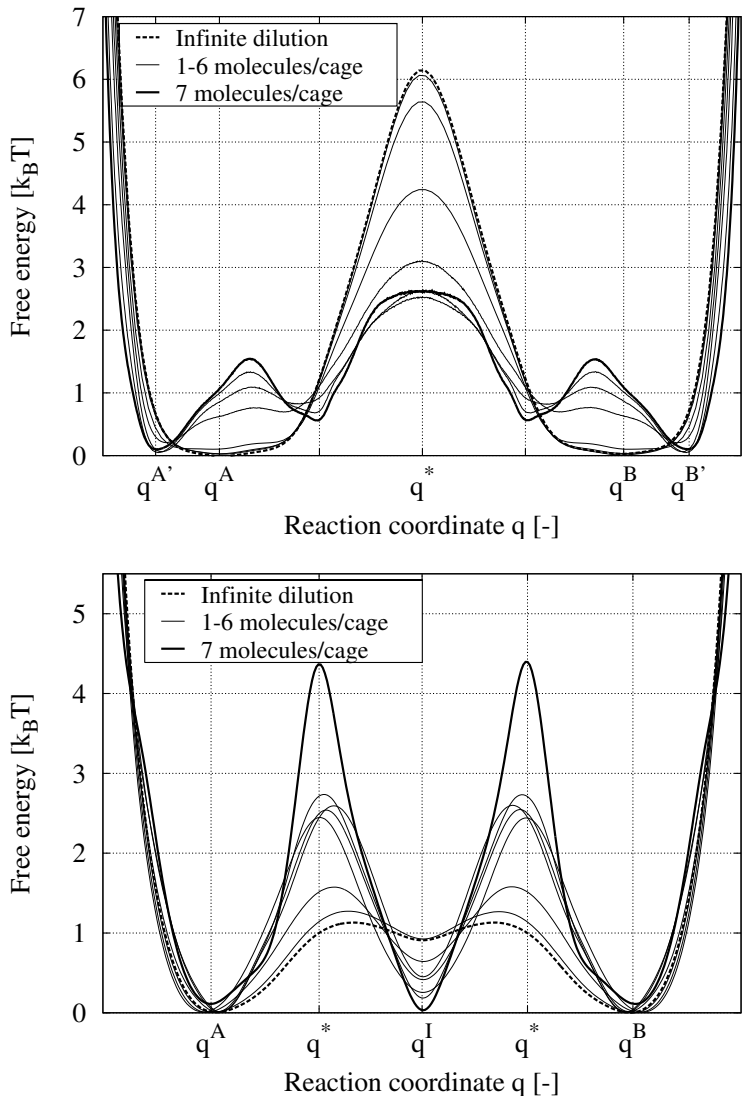

Figure 7.4: *Free-energy profiles $F(q)$ at 600 K of ethane in ERI at various loadings (infinite dilution, 1, 2, 3, 4, 5, 6, and 7 molecules per erionite cage) (top) in the hexagonal xy plane with q^A the center of a cage and q^B the center of a neighbouring cage, (bottom) in the z direction across a cage with q^A the top of the cage, q^I the middle of the cage, and q^B the bottom of the cage.*

and therefore

$$P_{B\to C} = P_{B\to A}\frac{k_{B\to C}}{k_{B\to A}} \tag{7.16}$$

$$= (1 - P_{B\to C})\frac{k_{B\to C}}{k_{B\to A}} \tag{7.17}$$

from which $P_{B\to C}$ can be solved:

$$P_{B\to C} = \frac{k_{B\to C}}{k_{B\to A} + k_{B\to C}} \tag{7.18}$$

The hopping rate from A to C is the hopping rate from A to B times the probability $P_{B\to C}$ to go from B to C

$$k_{A\to C} = k_{A\to B}P_{B\to C} \tag{7.19}$$

In general, a serial combination of hops is then described by

$$k_{A\to C} = \frac{k_{A\to B}k_{B\to C}}{k_{B\to A} + k_{B\to C}} \tag{7.20}$$

Equation 7.20 proves convenient for finding the relation between hopping rates on non-Bravais lattices. The relation between $k_{A\to B}$ and $k_{B\to A}$ is given by

$$\frac{k_{A\to B}}{k_{B\to A}} = \frac{\langle n_B\rangle}{\langle n_A\rangle} \tag{7.21}$$

where $\langle n_A\rangle = 1 - \langle n_B\rangle$ is the equilibrium mole fraction of particles in state A. For a symmetric barrier $\langle n_A\rangle = \langle n_B\rangle$ and $k_{A\to B} = k_{B\to A}$, so

$$k_{A\to C} = \frac{k_{A\to B}k_{B\to C}}{k_{A\to B} + k_{B\to C}} \tag{7.22}$$

The lattice displacement vector λ_z is orthogonal to λ_{xy} and, using eq. 7.22 with the symmetry of the lattice, we derive immediately

$$D_z = \frac{1}{2}\frac{k_{xy}k_z}{k_{xy} + k_z}\lambda_z^2 \tag{7.23}$$

Diffusion in ERI-type lattices is strongly anisotropic. In figure 7.3 we show the measured mean squared displacements for ethane obtained using MD at 600 K and a loading of one molecule per cage. Mean squared displacements (MSDs) are equal for the x and y directions, and different in the z direction. The units are convenient for simulation purposes, because distances are often

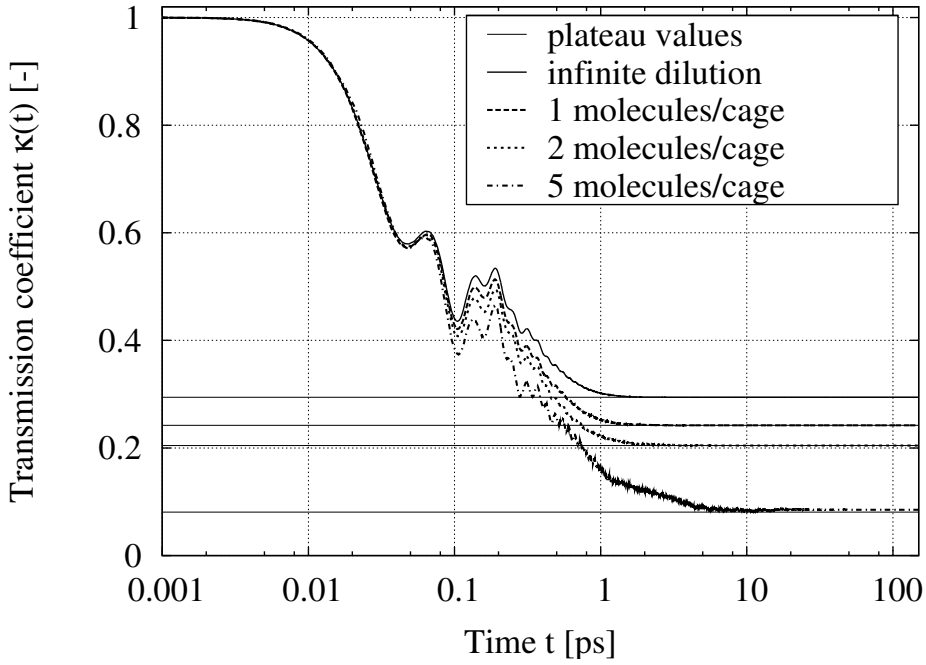

Figure 7.5: *Transmission coefficient $\kappa(t)$ for ethane at 600 K in ERI-type zeolite as a function of time for various loadings.*

defined in Ångstroms, and the relevant time scale is in the picosecond range. Slopes of MSDs are therefore in units of 1×10^{-8} m^2/s. The different regimes of diffusion are clearly visible, and only after a single cage crossing the MSD has become linear (a straight line of slope one in log-log scale). For interacting particles, particle-particle and particle-zeolite collisions occur on a different time scale.. The mean squared displacement thus bends over to attain a different slope. We are interested in the long-time diffusion coefficient. The self-diffusion coefficients D_α in the direction $\alpha = x, y, z$ are computed by taking the slope at long times

$$D_\alpha = \frac{1}{2N} \lim_{t\to\infty} \frac{1}{t} \left\langle \sum_{i=1}^{N} \left(r_{i\alpha}(t) - r_{i\alpha}(0) \right)^2 \right\rangle \tag{7.24}$$

where N is the number of molecules, t the time, and $r_{i\alpha}$ the α component of the center of mass of molecule i. The diffusion coefficients at one molecule per cage at 600 K are $D_{xy} = 2.1 \times 10^{-9}$ m^2/s and $D_z = 4.2 \times 10^{-9}$ m^2/s. This indicates that diffusion is a rare event and the windows form obstructions to

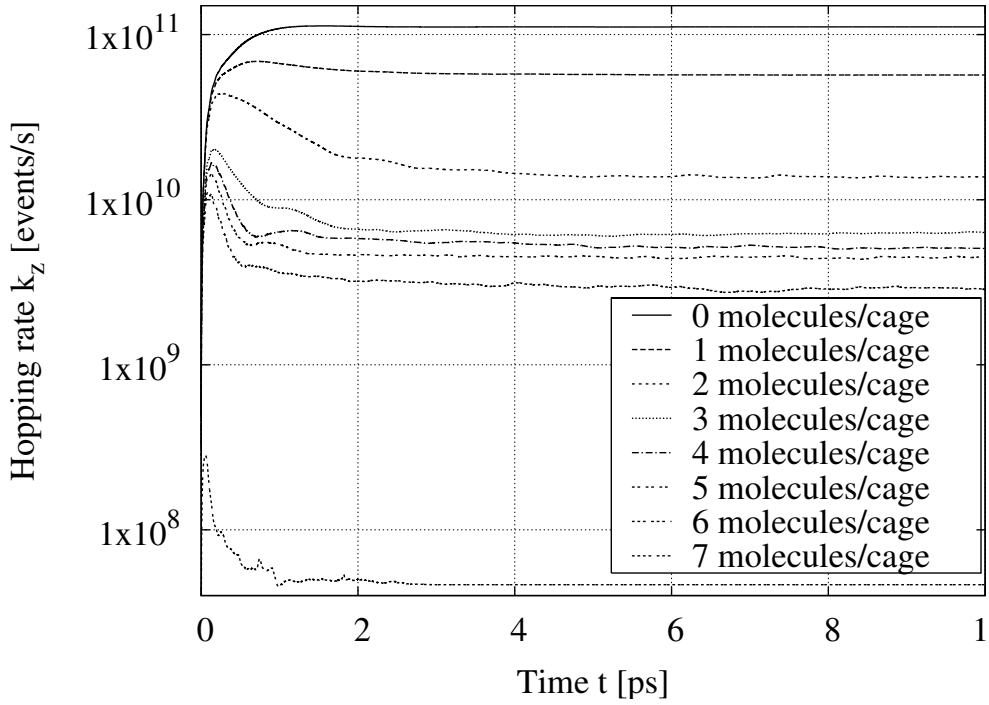

Figure 7.6: *Intracage hopping rate in the z direction obtained using biased MD for ethane in elongated ERI-type cages at 600 K.*

diffusion. Because $D_z \approx 2D_{xy}$, there are apparently no significant free-energy barriers inside an erionite cage at low loading.

The hopping lattice for most cage/window-type zeolites are formed by the lattice spanned by their cage centers. However, for elongated cages as those in erionite, intracage barriers are formed at higher loadings. For an analysis we measure the free-energy profiles along the cage length (the z direction), and along the center-to-center line in the hexagonal xy plane. The profiles of ethane plotted in figure 7.4 over various loadings indicate that indeed there are internal cage barriers, and for the xy plane the barrier is formed by the dividing eight-ring window. The diffusion coefficient in the z direction depends on both the hopping rate in z direction and the xy direction (eq. 7.23), because each hop in the z direction has to be preceded by a hop in the xy plane.

The free-energy barrier in the xy plane is a sharply peaked, and therefore the transmission coefficient is straightforward to evaluate using the Bennett-Chandler approach. The transmission coefficients $\kappa(t)$ are shown in figure 7.5. The starting configurations, with a particle constrained to the top of the

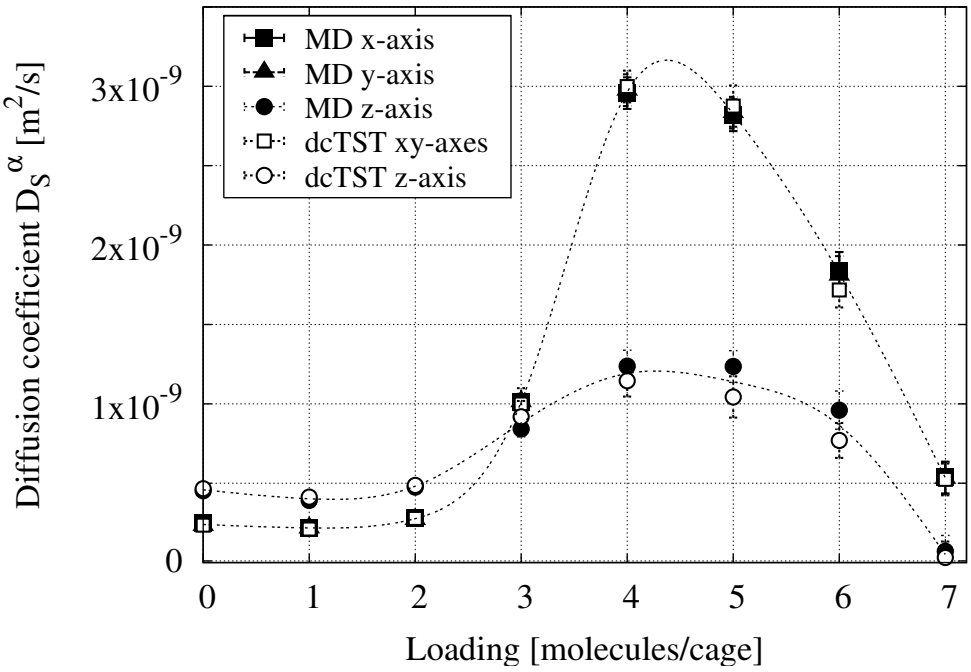

Figure 7.7: *Anisotropic diffusion of ethane in ERI-type zeolite computed by dcTST and conventional MD at 600 K.*

barrier q^*, were sampled using a Monte Carlo scheme. After approximately 10 picoseconds, the time-dependent transmission coefficient $\kappa(t)$ reached its plateau value κ. Using eq. 7.4 and eq. 7.13 the hopping rate and diffusion coefficient in the xy plane can be computed.

The free energy in the z direction across an erionite cage is initially rather flat, and with increasing loading a clear free-energy minimum is formed in the center of the cage. There are two solutions to this problem. The first would be to use a different hopping lattice and include the pink points in figure 7.2 in the hopping lattice. An hop in z direction is now a sequential process of two hops and the total hopping rate can be obtained using eq. 7.22. However, when there are several hopping rates very different in magnitude, it is more complicated to define a hopping rate for the fast-jumping particles, because kinetic correlations are abundant. A second method, and the method of our choice here, is to use biased MD to compute the total hopping rate from the top of the cage to the bottom of the cage *directly*. The reasons are two-fold, first the method is applicable to low free-energy barriers, and second, the method

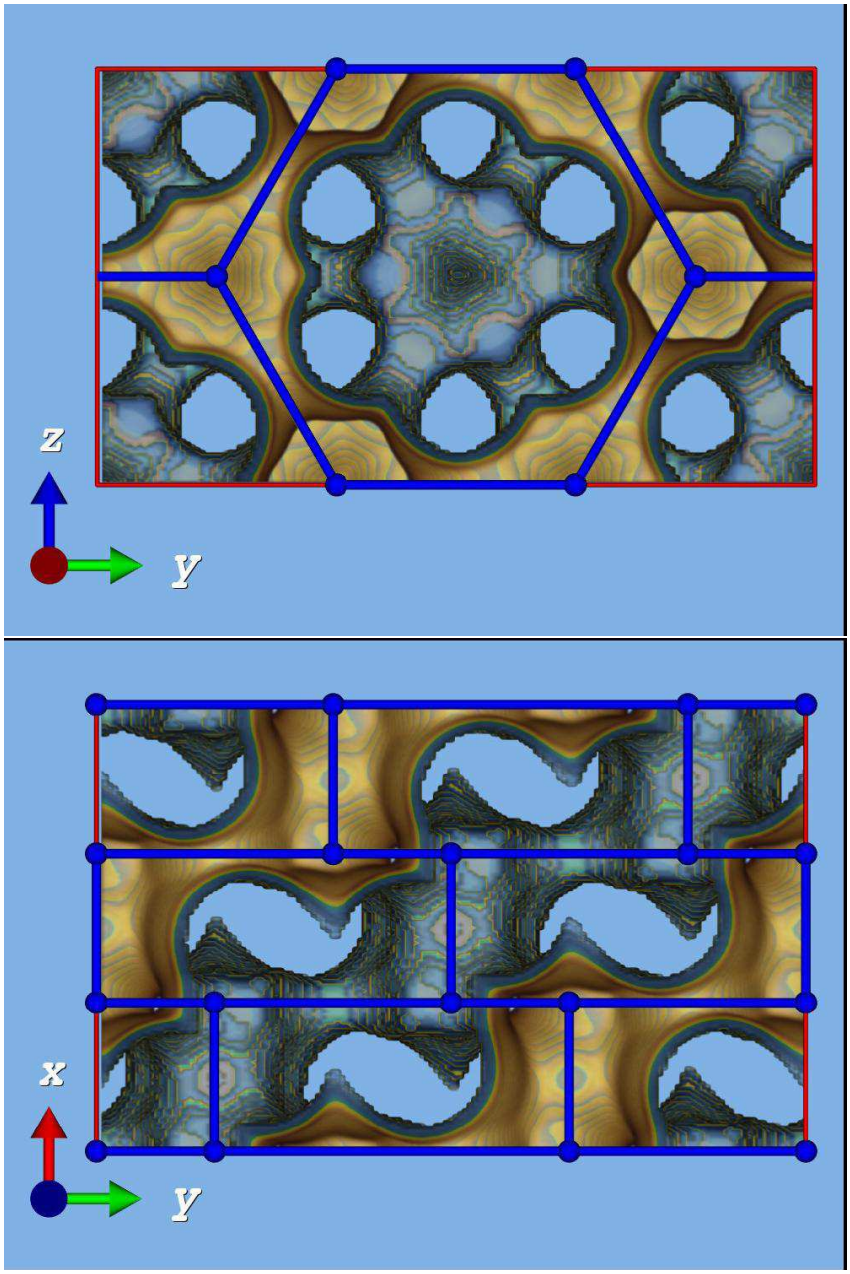

Figure 7.8: *A possible rectangular topology of the CHA-type lattice used in literature [34, 35]. In the zy direction (top), the hopping takes place on a hexagonal lattice; in the x direction (bottom), a displacement has to be preceded by a zy hop. The lattice is drawn in blue dots connected by blue lines.*

is able to compute hopping rates over complicated free-energy landscapes such as, in this case, two barriers. The reaction coordinate is the projection on the z axis (eq. 7.11), where q_A denotes the top of the cage, q_B the bottom of the cage, and q_I the intermediate free-energy minimum. There are two barriers, one separating q_A and q_I, and another one between q_I and q_B. The biased MD method computes the total hopping rate from q_A to q_B by computing an effective diffusion coefficient over the entire q domain (q^A to q_B), i.e., there is no separate computation of the transmission coefficient. The results are shown in figure 7.6. The plateau value at long times is the hopping rate of interest.

The self-diffusion coefficients of ethane in ERI-type zeolite at 600 K using dcTST and conventional MD are shown in figure 7.7. Surprisingly, the anisotropic behaviour of ERI-type cages reverse with loading, i.e. at low loading the diffusion in the z direction is two times as *fast* as that in the xy direction, while for higher loadings this changes to a diffusion that is more than two times as *slow*. Although MD and dcTST give equivalent diffusivity results, the behaviour is better understood by analysing the free-energy profiles (and transmission coefficients). At low loading the diffusion is impeded by the eight-ring windows, i.e. the exits out of the cage to the next, but at higher loadings the barrier is formed by the center of the cages.

7.3.2 Ethane in CHA-Type Zeolite

We note that the same formulas have been derived before, but for CHA-type zeolites by Schüring *et al.* [35]. Examining figure 7.8, it appears that CHA-type and ERI-type zeolites are very similar, the difference being the more elongated shape of ERI-type cages. In such a lattice, one expects the diffusion to be anisotropic, and this is indeed the case, as evidenced by the mean squared displacements in figure 7.10. To convert the hopping rate in CHA-type zeolites to a diffusion coefficient, we note that the lattice is actually only slightly distorted from a cubic lattice (figure 7.9). The orientationally averaged diffusion coefficien is *not* affected by the distortion in CHA-type lattices, but the individual components are. However, the distortion effect for the CHA-type lattice is negligibly small (smaller than 2%). Therefore, diffusion in CHA-type zeolite can be considered isotropic in practice using this lattice (see figure 7.10). CHA-type zeolites only appear to be anisotropic when the lattice is not properly aligned with the crystal axes. We note that, unlike in lattice theory, in our systems both the lattice and the hopping rates need to be found.

A similar free-energy analysis as for ERI-type zeolites can be performed for CHA-type zeolites. However, for the 'squashed cube' the free-energy profiles and transmission rates are equal for the a, b, and c directions. Hence, there is

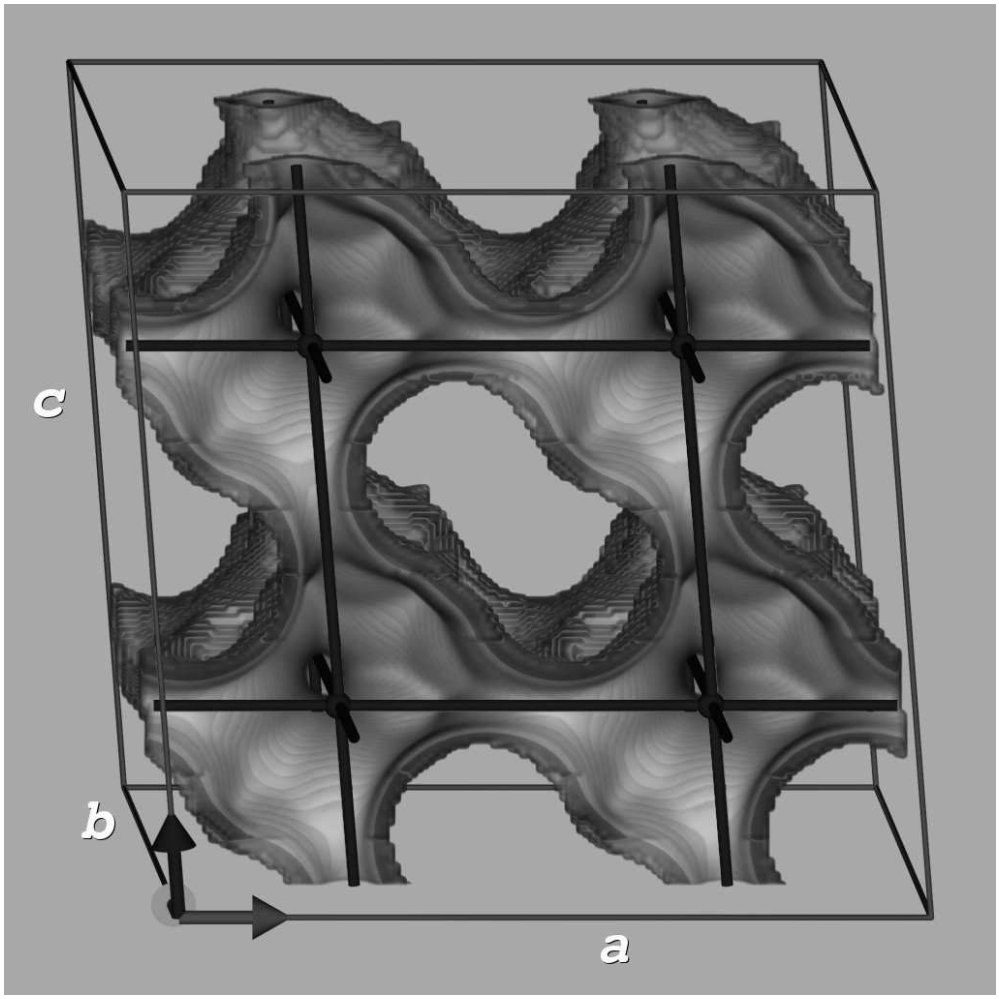

Figure 7.9: *'Squashed cube' topology of the CHA-type lattice. The lattice is drawn as dark spheres connected by dark lines of lattice distance* $\lambda \approx 0.9459$ *nm for a, b, and c directions.*

only one hopping rate, and any anisotropy is entirely due to the small distortion from a perfect cube. In figure 7.11 we show the free-energy profiles for CHA-type zeolites. The barrier is formed by the eight-membered ring for all loadings, and at higher loadings some intracage reorganisation is observed as more and more molecules have to be accommodated inside the chabazite cage.

Our simulations indicate no significant anisotropy (less than 2%) and therefore we plot the orientational averaged self-diffusivity only, for both MD and

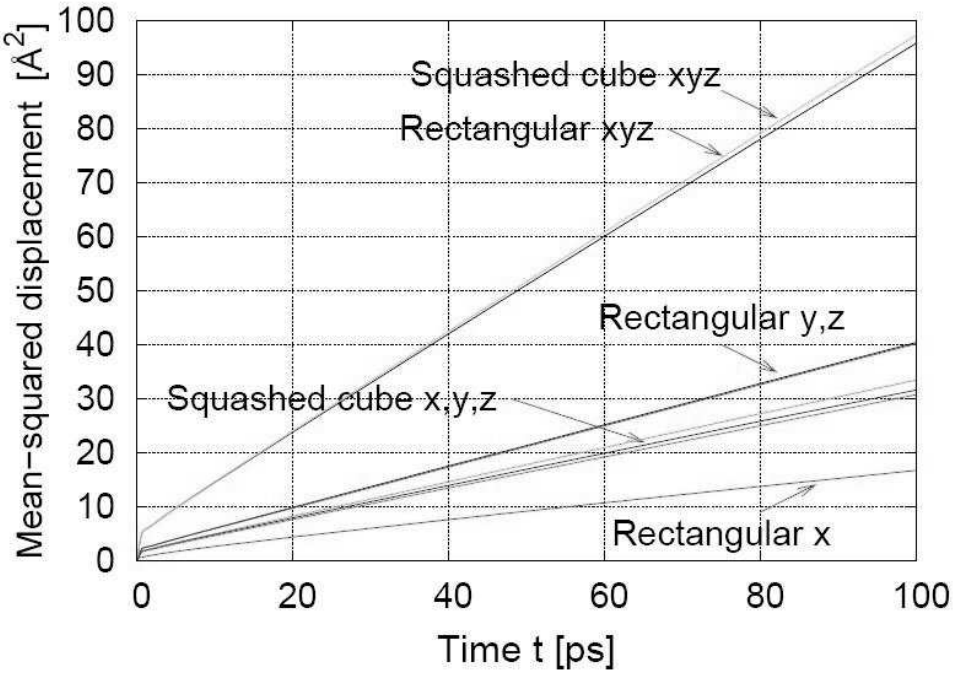

Figure 7.10: *Mean squared displacements of ethane at 600 K and a loading of one molecule per cage for the rectangular and 'squashed cube' version of CHA-type zeolites.*

dcTST in figure 7.12. A similar diffusivity behaviour to ERI-type zeolites is observed for CHA-type cages. Indeed, the increase in diffusivity is a general feature present due to cage confinement. The maximum in the diffusivity is shifted to lower loading, consistent with the smaller cage size of chabazite in comparison to erionite.

As mentioned previously, the diffusion in CHA-type zeolite can be considered isotropic in practice. Indeed, tracer-diffusion measurements of water in natural chabazite by Raman spectroscopy did not indicate any substantial deviation from diffusion isotropy [50]. However, using the pulsed field gradient NMR technique Bär et al. [34] reported an orientation-dependent diffusivity with a ratio between the maximum and minimum diffusivity of a factor of two, also for water in natural chabazite. Such a significant anisotropy can potentially originate from a significant symmetry breaking in the zeolite sample, caused by for instance a nonrandom arrangement of cations and/or imperfections inside the crystal.

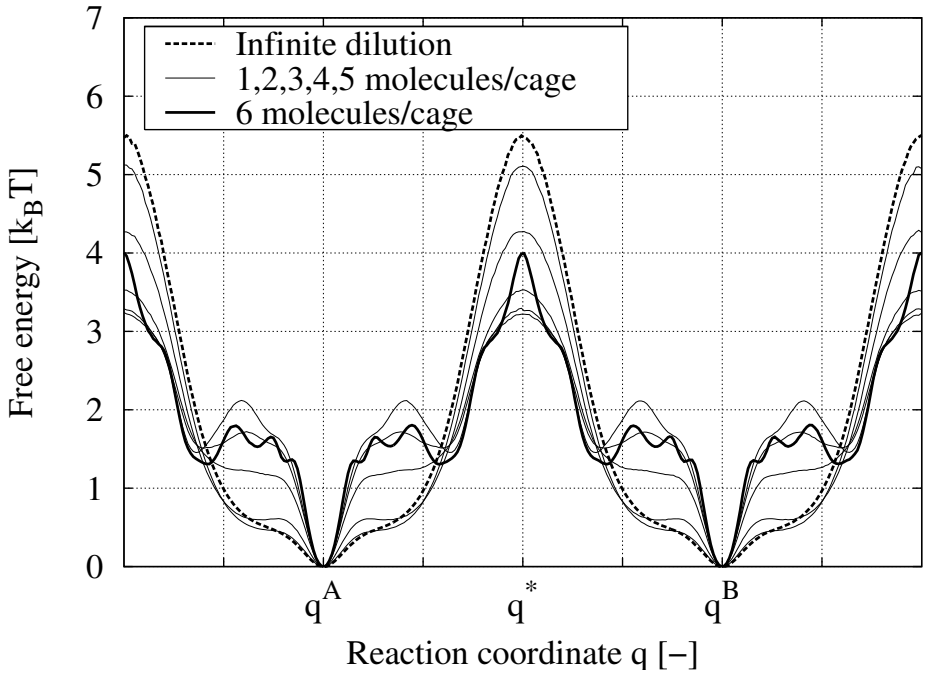

Figure 7.11: *Free-energy profiles $F(q)$ at 600 K of ethane in CHA at various loadings (infinite dilution, 1, 2, 3, 4, 5, and 6 molecules per chabazite cage). The reaction coordinate is the position of the first bead along the center line connecting the center points of two cages. (lines from top to bottom in order of the legend).*

7.4 Conclusions

The dcTST gives equivalent results to conventional MD, but is also applicable in the regime of very slow diffusion, where MD can not be used. Moreover, the method allows for a more detailed analysis in terms of free-energy profiles and transmission coefficients. The first is a static term, corresponding to locations of preferable adsorption sites and estimates of free-energy barriers in between, the latter (or actually the inverse of the transmission coefficient: the recrossing) corresponds to collision frequencies, which generally increase with loading. Here, we have shown how to apply the dcTST to nontrivial lattices: (a) ERI-type lattices are non-Bravais, (b) CHA-type lattices are rhombohedral. Both zeolites are cage/window-type zeolites, and in both zeolites the diffusion increase with loading and decrease only close to saturation loading.

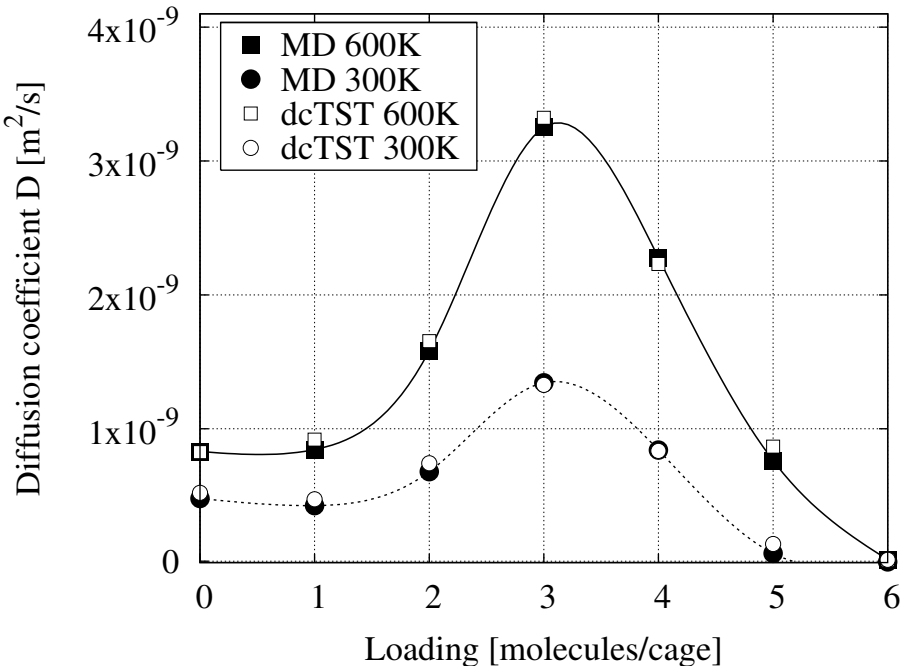

Figure 7.12: *Orientationally averaged diffusion of ethane in CHA-type zeolite computed by dcTST and conventional MD at 300 K and 600 K.*

The diffusion of CHA-type zeolites is nearly isotropic, the diffusion of ERI-type zeolites is strongly anisotropic. Surprisingly, the anisotropic behaviour of ERI-type cages reverses with loading, i.e. at low loading the diffusion in the z direction is two times as *fast* as that in the xy direction, while for higher loadings this changes to a diffusion that is more than two times as *slow*. The computation using TST for ERI-type zeolites required the combination of tw methods: dcTST for the xy plane, and biased MD to compute the much faster intracage hopping rates. Although MD and dcTST give equivalent diffusivity results, the behaviour is better understood by analysing the free-energy profiles (and transmission coefficients). At low loading the diffusion is impeded by the eight-ring windows, i.e. the exits out of the cage to the next, but at higher loadings the barrier is formed by the center of the cages.

Bibliography

[1] V. Gupta, S. S. Nivarthi, A. V. McCormick, and H. T. Davis, Chem. Phys. Lett. **247**, 596 (1995).

[2] V. Kukla, J. Kornatowski, D. Demuth, I. Girnus, H. Pfeifer, L. V. C. Rees, S. Schunk, K. K. Unger, and J. Kärger, Science **272**, 702 (1996).

[3] K. Hahn, J. Kärger, and V. Kukla, Phys. Rev. Lett. **76**, 2762 (1996).

[4] R. L. Gorring, J. Catal. **31**, 13 (1993).

[5] K. Yoo, R. Tsekov, and P. G. Smirniotus, J. Phys. Chem. B. **7**, 13593 (2003).

[6] D. Dubbeldam, S. Calero, T. L. M. Maesen, and B. Smit, Phys. Rev. Lett. **90**, 245901 (2003).

[7] D. Dubbeldam and B. Smit, J. Phys. Chem. B. **107**, 12138 (2003).

[8] P. K. Ghorai, S. Yashonath, P. Demontis, and G. B. Suffritti, J. Am. Chem. Soc. **125**, 7116 (2003).

[9] R. L. June, A. T. Bell, D. N. Theodorou, J. Phys. Chem. **94**, 8232 (1990).

[10] J. Kärger, J. Phys. Chem. **95**, 5558 (1991).

[11] U. Hong, J. Kärger, R. Kramer, H. Pfeifer, G. Seiffert, U. Muller, K. Unger, H. B. Luck, T. Ito, Zeolites **11**, 816 (1991).

[12] R. L. June, A. T. Bell, D. N. Theodorou, J. Phys. Chem **96**, 1051 (1992).

[13] Maginn, E. J.; Bell, A. T.; Theodorou, D. N. *J. Phys. Chem.* **1996**, *100*, 7155-7173.

[14] C. Bussai, S. Fritzsche, R. Haberlandt, S. Hannongbua, J. Phys. Chem. B **107**, 12444 (2003).

[15] A. I. Skoulidas, D. S. Sholl, J. Phys. Chem. B **106**, 5058 (2002).

[16] Skoulidas, A.I.; Sholl, D. S.,J. Phys. Chem. A. **2003**, **107**, 10132-10141.

[17] S. Trinh, B. R. Locke, P. Arce, Transp. Por. Med. **47**, 279 (2002).

[18] Z. Su, J. H. Cushman, J. E. Currya, J. Phys. Chem. B **118**, 1417 (2002).

[19] J. G. Powles, S. Murad, P. V. Ravi, Chem. Phys. Lett. **188**, 21 (1992).

[20] T. Yokoyamaa, S. Nakashimab, Eng. Geology **80**, 328 (2005).

[21] A, Wingen, W. Basler, H. Lechert, Stud. Surf. Sci. Catal. **105**, 495 (1997).

[22] P. H. Nelson, M. Tsapatsis, S. M. Auerbach, J. Membr. Sci. **184**, 245 (2001).

[23] P. H. Nelson, S. M. Auerbach, Chem. Eng. J. **74**, 43 (1999).

[24] I. Furo, S. V. Dvinskikh, Magn. Reson. Chem. **40**, S3 (2002).

[25] M. I. Menzel, S. Han, S. Stapf, B. Blümich, J. Chem. Phys. **143**, 376 (2000).

[26] D. Dubbeldam, E. Beerdsen, T. J. H. Vlugt, and B. Smit, J. Chem. Phys **122**, 224712 (2005).

[27] A. F. Voter, F. Montalenti, T.C. Germann, Annu. Rev. Mater. Res. **32**, 321 (2002).

[28] Auerbach, S. M. *International reviews in physical chemistry* **2000**, *19*, 155-198.

[29] E. Beerdsen, B. Smit, and D. Dubbeldam, Phys. Rev. Lett. **93**, 248301 (2004).

[30] J. A. Gard and J. M. Tait, Proceedings of the Third International Conference on Molecular Sieves; Recent Progress Reports, edited by J. B. Uytterhoeven (Leuven University Press, Zurich, 1973), pp. 94–99.

[31] M. Calligaris, G. Nardin, and L. Randaccio, Zeolites **3**, 205 (1983).

[32] D. Dubbeldam, E. Beerdsen, S. Calero, B. Smit, Proc. Natl, Acad. Sci. U.S.A. **102**, 12317 (2005).

[33] L. A. Clark, G. T. Ye, R. Q. Snurr, Phys. Rev. Lett **84**, 2893 (2000).

[34] N.-K. Bär, J. Kärger, H. Pfeifer, H. Schäfer, and W. Schmitz, Microp. Mesop. Materials **22**, 289 (1998).

[35] A. Schüring, S. M. Auerbach, S. Fritzsche, R. Haberlandt, In *Random Walk Treatment of Dumb-Bell Molecules in an LTA Zeolite and in Chabazite*; Proceedings of the 14th International Zeolite Conference; E. van Steen, L. Callanan, M. Claeys, Eds.; Elsevier: Cape Town pp 2110-2117 (2004).

[36] C. H. Bennett, in *Diffusion in Solids: Recent Developments*, edited by A. Nowick and J. Burton (Academic Press, New York, 1975), pp. 73–113.

[37] D. Chandler, J. Chem. Phys **68**, 2959 (1978).

[38] O. M. Braun, C. A. Sholl, Phys. Rev. B **22**, 289 (1998).

[39] Tunca, C.; Ford, D. M. *J. Chem. Phys.* **1999**, *111*, 2751-2760.

[40] Tunca, C.; Ford, D. M. *J. Phys. Chem. B* **2002**, *106*, 10982-10990.

[41] Tunca, C.; Ford, D. M. *Chem. Eng. Sci.* **2003**, *58*, 3373-3383.

[42] M. J. Ruiz-Montero, D. Frenkel, J. Brey, J. Mol. Phys. **90**, 925 (1996).

[43] Beerdsen, E.; Dubbeldam, D.; Smit, B. *Phys. Rev. Lett.* **2005**, *95*, 164505.

[44] A. G. Bezus, A. V. Kiselev, A. A. Lopatkin, and P. Q. J. Du, J. Chem. Soc., Faraday Trans. II **74**, 367 (1978).

[45] T. J. H. Vlugt and M. Schenk, J. Phys. Chem. B. **106**, 12757 (2002).

[46] F. Leroy, B. Rousseau, A. H. Fuchs, Phys. Chem. Chem. Phys. **6**, 775 (2004).

[47] J. P. Ryckaert and A. Bellemans, Faraday Dicuss. Chem. Soc. **66**, 95 (1978).

[48] A. Schüring, S. M. Auerbach, S. Fritzsche, and R. Haberlandt, J. Chem. Phys **116**, 10890 (2002).

[49] G. J. Martyna, M. Tuckerman, D. J. T. M. L., and Klein, Mol. Phys. **87**, 1117 (1996).

[50] S. V. Goryainov and I. A. Belitsky, Phys. Chem. Miner. **22**, 433 (1995).

We introduce a computational method to directly relate diffusivities to the microscopic behaviour of the adsorbed molecules. We apply this method to gases in MFI-type molecular sieve, the reference system in this field. Transitions in the number and nature of adsorption sites result in temporary local increases in the diffusion. This occurs at different loadings in each of the x, y, and z directions, giving rise to the complex loading behaviour found experimentally. Our method can be applied to any adsorbent-adsorbate system, and provides a fundamental understanding of diffusion in confinement on a molecular level.

E. Beerdsen, D. Dubbeldam, and B. Smit

8

A Molecular Understanding of Diffusion in Confinement

Of all nanoporous materials, zeolites are best known. Not only are they used in many industrial applications, they are also widely studied, owing to their regular crystalline shapes and wide variety of topologies [1]. Out of more than 150 zeolite topologies known to date [2], MFI (figure 8.1) is one of the most important structures [3–7]. It is used in many commercial petrochemical and separation processes. Moreover, as large nearly perfect crystals of this material can be synthesised, it has become one of the most extensively studied materials in this field. Considering the importance of MFI for both industry and science, it is surprising that its diffusion properties are poorly understood. In particular, the loading-dependence of the diffusion has remained elusive.

Many studies have addressed the diffusion of gases in zeolites, finding a wide variety in diffusion behaviour [8–11]. In many chemical-engineering applications it is assumed that the collective diffusion coefficient of particles in confinement is independent of loading [3,4,12–14]. In an elaborate study, comparing the diffusion of four gases in four zeolite topologies, Skoulidas and Sholl confirmed the validity of this assumption (the so-called Darken assumption) for *one* system only: CH_4 in MFI; in other systems it was refuted, but a general rationale for these phenomena was not discovered [5,11]. Despite the importance for many applications, conventional methods cannot explain when

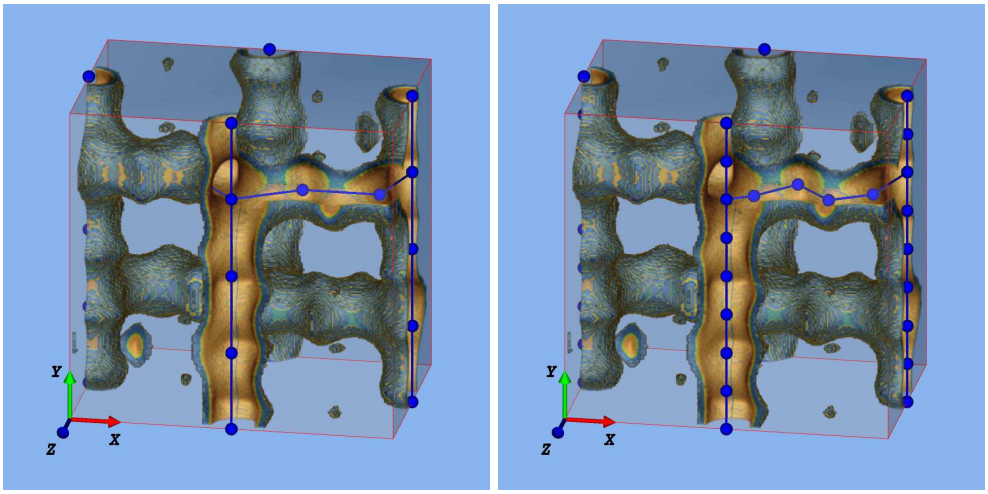

Figure 8.1: *One unit cell of MFI-type zeolite at low loading (top) and at high loading (bottom), with the lattice spanned by the preferred adsorption sites. At low loadings, there are four favourable positions per straight channel and four per zigzag channel, making the total number per unit cell 16. At higher loadings the number of preferential sites is 32. The dimensions of the cell are* 20.022 *x* 19.899 *x* 13.383 *Å.*

and why, for a given system, the diffusion will increase, decrease, or remain constant as a function of loading. A good discussion of the Darken assumption can be found in section 5.11 of ref. [15], and in ref. [13].

The fact that the loading-dependence for even simple molecules in MFI is not yet understood points at a fundamental difficulty in interpreting diffusion coefficients in nanoporous materials. This observation motivated us to develop an alternative approach that allows for a direct molecular interpretation. Recently, we have extended dynamically corrected Transition-State Theory to include loading effects [16]. In this chapter we will demonstrate that this method has an advantage over other methods, because it provides a direct molecular interpretation of the observed loading dependence.

In this chapter we illustrate this for two of the best-studied systems [5,9,10]: CH_4 and CF_4 in MFI-type zeolite, following the work of Skoulidas and Sholl [5]. Using molecular dynamics simulations, they showed that in MFI the Darken assumption would hold for methane, but not for CF_4. To find a molecular interpretation of the diffusion in these systems, we compute the diffusivity as a function of loading up to the maximum loading, which we, in contrast to previous studies, define as the loading where the diffusion (both self and

collective) comes to a complete halt. We show that the very irregular loading dependence that is observed in simulation is intrinsic to these types of systems and can be explained in detail, using the aforementioned method. To conclude, we discuss the consequences of our results for kinetic Monte Carlo simulations.

MFI-type zeolite is a so-called intersecting channel-type zeolite. It consists of straight 10-ring channels, running in the y direction, intersected by zigzag channels that run in the x and z directions and also consist of 10-membered ring windows (see figure 8.1). One unit cell of MFI contains two straight channels and two zigzag channels. At low loadings, there are four favourable positions per straight channel and four favourable positions per zigzag channel, making the total number of preferential adsorption sites per unit cell 16. The MFI structure was taken from ref. [17]. To model the CH_4 molecules, we used the united atom model of Dubbeldam et al. [18,19], for the CF_4 molecules the force field of Heuchel et al. was used [20].

We calculated self- and collective diffusion coefficients using conventional Molecular Dynamics (MD) calculations for the full loading range of CH_4 and CF_4 in MFI. In an MD calculation, Newton's equations are being solved to study particle positions as a function of time and thus obtain a mean squared displacement of a tagged particle as a function of time. This mean squared displacement can easily be converted into a self diffusion coefficient D_S. In a similar fashion, the collective diffusivity D_C is related to the mean squared displacement of the center of mass. We used the velocity-Verlet integration algorithm with a time step of 0.2 fs and a total simulation time of between 1.5 and 1000 ns, depending on the diffusion speed, such that the error bars were less than 5%.

While MD calculations are powerful and practical, the diffusion behaviour is better understood by using the dynamically corrected Transition-State Theory (dcTST) method of ref. [16]. In addition to diffusion coefficients, this method can yield an explanation of the diffusion behaviour in terms of free-energy differences. Transition-State Theory regards diffusion as a hopping process on a lattice, where the hopping from some state A to another state B is impeded by a free-energy barrier between the two states. Together with the dynamical correction factor, free-energy profiles can be used to compute a hopping rate between state A and B, which in turn can be converted to a self-diffusion coefficient. The free-energy profiles are computed during an NVT-ensemble MC or MD simulation, in which we compute the probability to find a particle at a particular value of the reaction coordinate q. We look at a single particle, regarding all other particles as a contribution to the external field, and implicitly averaging over all adsorption sites. The method relies on the direct inclusion

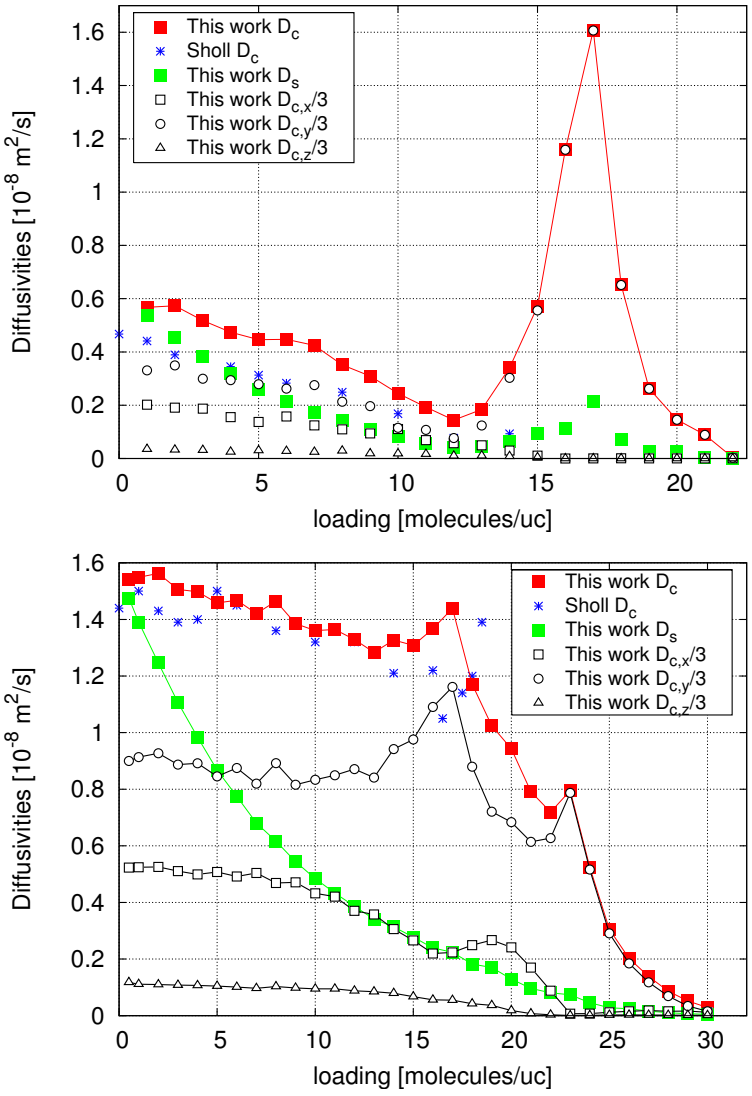

Figure 8.2: *Diffusion of CF_4 (top) and CH_4 (bottom) in MFI-type zeolite at 300 K, as a function of loading, from MD simulations, and D_C as calculated by Skoulidas and Sholl. The x, y, and z components of D_C are plotted as $D_{C,x}/3$, $D_{C,y}/3$, and $D_{C,z}/3$, so that their sum equals D_C. The fastest diffusion occurs in the y direction, the slowest in the z direction, since a particle diffusing in this direction has to pass both an x and a z channel, the x channel being longer.*

of all interparticle correlations in the *effective* hopping rate of a particle travelling from cage A to cage B. Further details about the method can be found in refs. [16, 21].

For CF_4 in siliceous MFI, up to a loading of 12 molecules per unit cell, both the self-diffusion coefficient D_S and the collective diffusion coefficient D_C are a decreasing function of loading (see figure 8.2). When the loading is further increased, a striking phenomenon is observed: the diffusion coefficient increases by one order of magnitude and decreases to zero at the maximum loading. As the x, y, and z directions in MFI-type zeolite are crystallographically different, we have to consider them separately. In 8.2 the x, y, and z components of D_C are plotted as $D_{C,x}/3$, $D_{C,y}/3$, and $D_{C,z}/3$, so that their sum equals D_C. The diffusion in the y direction (the direction of the straight channels) is highest, followed by that in x direction, $D_{C,x}$. Figure 8.2 shows that both $D_{C,x}$ and $D_{C,z}$ decrease (nearly) monotonically, and above a loading of 16 molecules per unit cell the diffusion coefficients in these directions are nearly zero. $D_{C,y}$ has a much more complex loading behaviour, with a maximum at a loading of 17 molecules per unit cell, from this loading onwards rapidly decreasing to reach zero at a loading of 22 molecules per unit cell.

To explain this behaviour, we analyse the free-energy profiles. The diffusion can be fully accounted for by the loading dependence of the free-energy profiles, i.e. the dynamical correction is a monotonously decreasing function of loading. As the interesting behaviour is observed in the xy direction, we focus on the profiles along these axes (figure 8.3). The diffusion coefficients calculated from these profiles are consistent with MD results. The minima in the profiles are entropic traps: at the intersections the particles can enter a channel perpendicular to the present reaction coordinate. At low loadings one can observe two local minima located inside the y channels, corresponding to the energetically most favourable adsorption sites. Because of the size of CF_4, only one of these sites can be occupied at any given time. In the x direction there is one adsorption site in each channel.

At low loadings, the particles in the zigzag channels increase the barrier at the entry of the straight channel. From 12 molecules per unit cell onward, the molecules in the zigzag channels start to pack more tightly. Since a packing of 2 molecules per zig or zag channel is commensurate with the structure of this channel, they form a tight ordering with very large barriers for diffusion. As a consequence, the diffusion in both the x and z directions halts. Because the zigzag channels are blocked, particles coming from the straight channel cannot enter. The result is a very flat free-energy profile and a remarkable increase in the diffusion coefficient. At a loading of 16 molecules per unit cell, all favourable

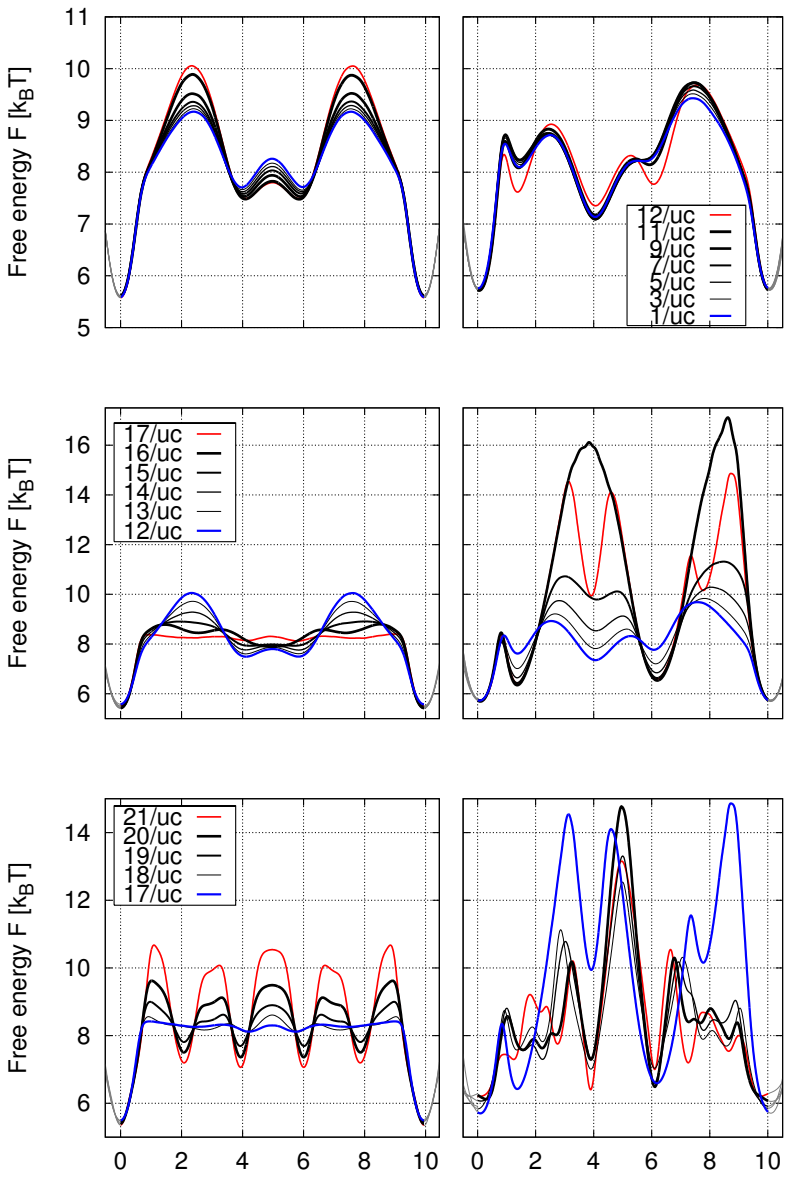

Figure 8.3: *Free-energy profiles for CF4 in MFI-type zeolite along the y (left) and x (right) directions, for 1-12 molecules per unit cell (top), 12-17 molecules per unit cell (middle) and 17-21 molecules per unit cell (bottom). The global minima at 0 Å and 10 Å correspond to the intersections of the straight channels with the zigzag channels (in the xz plane).*

positions inside the zeolite (4 per straight channel and 4 per zigzag channel) are occupied. In order to accommodate more molecules, new adsorption positions have to be created. A reordering takes place, changing the adsorption lattice from figure 8.1 (top) to figure 8.1 (bottom). From these loadings onwards, the diffusion becomes ever more slow, until it comes to a complete halt at the maximum loading, of about 24 molecules per unit cell. Not all 32 adsorption sites are being filled. Because CF_4 molecules are rather large, once adsorbed they have a large energetic influence on close-by neighbouring sites, preventing all 32 sites to be filled simultaneously. Note that the reordering at 12 molecules per unit cell, which causes a peak in the diffusion graph, is also reflected in the adsorption isotherm, as found earlier by Krishna et al. [6], confirming that events on a molecular scale affect both adsorption and diffusion.

A more complex diffusion behaviour is found for CH_4 in MFI. CH_4 is a slightly smaller molecule (see figure 8.2) than CF_4. Again, we observe an increase in the $D_{C,y}$, caused by the 'freezing' of particles in the zigzag channels that 'smoothens' the straight channels, and a transition to a different adsorption lattice beyond a loading of 16 molecules per unit cell. However, in the case of CH_4, the peak is smaller and is counterbalanced by the general decreasing trend in $D_{C,x}$ and $D_{C,z}$. We do not observe a maximum in D_C, but there is a distinct 'kink' at a loading of about 16 molecules per unit cell. As in the case of CF_4, the high-loading lattice has 32 adsorption sites, and since CH_4 molecules are smaller than CF_4, all of them can be filled simultaneously, making the maximum loading 32 molecules per unit cell.

The simulations have been run sufficiently long for the error bar to be smaller than twice the symbol size. Therefore, the irregular behaviour of the diffusion coefficient is not the result of poor statistics, but an intrinsic phenomenon in these systems. It has some very characteristic features that could easily be dismissed as 'noise', if the free-energy profiles are not examined. Detailed inspection of the components of the diffusion coefficients shows that these humps can be related to events in one of the components. It is possible to attribute each hump to a reordering of the adsorbed molecules, often being a transition in the number of adsorption sites. For example, the small maximum in $D_{C,x}$ is caused by a transition in the zigzag channel from 4 adsorption sites (2 per zig and 2 per zag channel) to 8 adsorption sites. As the transition takes place, the system is temporarily incommensurate with both 4 and 8 adsorption sites. This causes a lowering of the free-energy barrier and hence an increase in the diffusion coefficient. In addition, an increase in the number of adsorption sites raises the number of vacancies, which often results in an increase in the mobility. Based on free-energy profiles, we are able to explain diffusion

behaviour on a molecular level.

While our data are in good agreement with those of Skoulidas and Sholl, we do not support their conclusion that the Darken approximation holds for CH_4 in MFI-type zeolite. While it seems safe to use the Darken approximation to estimate the CH_4 diffusion at experimentally accessible pressures (10^6 kPa is required at 300 K for 16 molecules per unit cell of CF_4, 100 kPa for 18 molecules per unit cell of CH_4), the diffusion is not constant over the entire loading range.

Our results have considerable consequences for kinetic Monte Carlo simulations on these systems. In these simulations, diffusion is considered as a hopping process on a loading-independent lattice of adsorption sites. Previous studies have shown that in three-dimensional systems, such as MFI, geometric correlations are present that are difficult to capture in a lattice model [11,22,23]. Here we have shown that, on top of these problems, as the effective topology changes as a function of loading, these correlations change too, making lattice model simulations highly impractical.

We note that the presented method is by no means limited to simple molecules in zeolites, but can be extended to more complex molecules, including mixtures, in arbitrary geometries. We have focused on simple gases in MFI as this is considered to be the reference system in this field.

Bibliography

[1] M. E. Davis, Nature **417**, 813 (2002).

[2] http://www.iza-structure.org/databases, 2005.

[3] H. Jobic, J. Karger, and M. Bee, Phys. Rev. Lett. **82**, 4260 (1999).

[4] S. M. Auerbach, International reviews in physical chemistry **19**, 155 (2000).

[5] A. I. Skoulidas, D. S. Sholl, and R. Krishna, Langmuir **19**, 7977 (2003).

[6] R. Krishna, J. M. van Baten, and D. Dubbeldam, J. Phys. Chem. B. **108**, 14820 (2004).

[7] C. Tunca and D. M. Ford, Chem. Eng. Sci. **58**, 3373 (2003).

[8] A. I. Skoulidas and D. S. Sholl, J. Phys. Chem. B. **105**, 3151 (2001).

[9] E. J. Maginn, A. T. Bell, and D. N. Theodorou, J. Phys. Chem. **97**, 4173 (1993).

[10] H. Jobic, A. I. Skoulidas, and D. S. Sholl, J. Phys. Chem. B. **108**, 10613 (2004).

[11] A. I. Skoulidas and D. S. Sholl, J. Phys. Chem. A **107**, 10132 (2003).

[12] J. Kaerger and D. M. Ruthven, *Diffusion in Zeolites and other microporous solids* (John Wiley & Sons, Inc., New York, 1992).

[13] Ramanan, H.; Auerbach, S. M., in *NATO-ASI Series C: Fluid Transport in Nanopores*, edited by Fraissard, J.; Conner, W.C. Kluwer Academic Publishers; Dordrecht, The Netherlands, 2004.

[14] S. M. Auerbach, in *NATO-ASI Series C: Fluid Transport in Nanopores*, edited by J. Fraissard and W. Conner (Kluwer Academic Publishers, Dordrecht, The Netherlands, 2004.

[15] F. J. Keil, R. Krishna, and M. O. Coppens, Rev. Chem. Eng. **16**, 71 (2000).

[16] E. Beerdsen, B. Smit, and D. Dubbeldam, Phys. Rev. Lett. **93**, 248301 (2004).

[17] H. van Koningsveld, H. van Bekkum, and J. C. Jansen, Acta Cryst **B43**, 127 (1987).

[18] D. Dubbeldam, S. Calero, T. J. H. Vlugt, R. Krishna, T. L. M. Maesen, E. Beerdsen, and B. Smit, Phys. Rev. Lett. **93**, 088302 (2004).

[19] D. Dubbeldam, S. Calero, T. J. H. Vlugt, R. Krishna, T. L. M. Maesen, and B. Smit, J. Phys. Chem. B. **108**, 12301 (2004).

[20] M. Heuchel, R. Q. Snurr, and E. Buss, Langmuir **13**, 6795 (1997).

[21] D. Dubbeldam, E. Beerdsen, T. J. H. Vlugt, and B. Smit, J. Chem. Phys. **122**, 224712 (2005).

[22] J. Kaerger, J. Phys. Chem. **95**, 5558 (1991).

[23] F. Jousse, S. M. Auerbach, and D. P. Vercauteren, J. Chem. Phys **112**, 1531 (2000).

The diffusion of alkanes in nanoporous materials as measured by different experimental techniques is thought to be highly dependent on the measuring technique employed. However, when the data are corrected for the loading at which the measurement was performed, the different data series correspond with each other much better than expected.

E. Beerdsen and B. Smit

9

Diffusion in Confinement - Agreement Between Experiments Better than Expected

9.1 Introduction

Detailed knowledge of the diffusion behaviour of hydrocarbons in molecular sieves is of importance in many petrochemical processes. Zeolites are nanoporous materials, often used as model structures to study diffusion in confinement, owing to their regular, well-defined crystalline nature. Although there are over 130 different known zeolite topologies, most groups focus on the understanding of the diffusion in silicalite (MFI), as this material is very well characterised and the MFI structure is used in many industrial applications [1–12].

Talu et al. [1] made a comparison of the various techniques used to measure diffusion in confinement. Figure 9.1 is based on their results. This figure illustrates why until recently it was considered common knowledge in zeolite science that diffusion measurements obtained by different techniques rarely correspond to one another and that the differences between different experimental techniques and simulations can be as great as five orders of magnitude. However, a closer inspection of the experimental data shows that the compilation in figure 9.1 has been made with the assumption (the so-called Darken approximation) that the diffusion coefficient is independent of the loading [13]. For a long time this was considered a very reasonable assumption in MFI [14], and, in accordance with this view, no corrections have been made for loading effects in plotting the data. However, in recent years molecular simulations have shown that for MFI, as for other zeolites, there is a significant loading

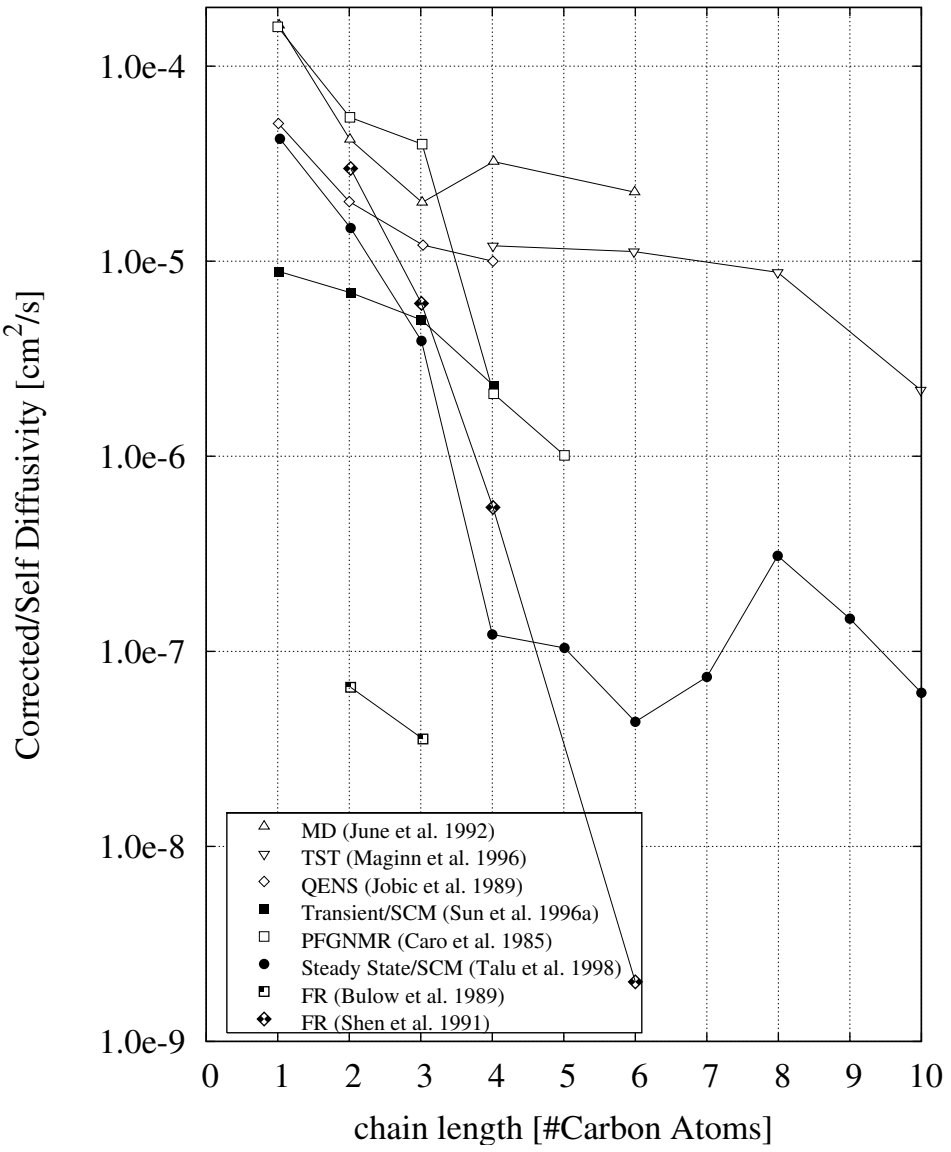

Figure 9.1: *Alkane diffusion in MFI as a function of chain length, based on a graph from Talu et al. [1], summarising data from several groups obtained by various methods, at 300 K.*

dependence [15]. This observation motivated us to re-analyse the experimental data.

A second motivation lies in the desirability of a comparison between different data sets. Most force fields have been optimised and validated using adsorption data. It is therefore very important to know whether or not these force fields also give an accurate description of the diffusion behaviour. Until now, this question could not be addressed, because the large differences between the various data made it impossible to draw any conclusions.

In this letter we strive to solve the riddle behind the graph: why is the measured diffusion so high in some methods, while it comes out so low in others? We pick out a simple test case: the diffusion of methane, which differs more than one order of magnitude between the lowest and the highest measurement.

9.2 Measuring Diffusion

Diffusion can be expressed in a diffusion coefficient in several ways. In practical experiments, such as measurements of the uptake and permeation rate, the diffusion measured is usually the transport diffusion coefficient D_T, defined by Fick's law [14, 16]. To obtain a quantity that is independent on concentration gradients, D_T can be converted to the corrected diffusivity D_C [17, 18], also known as the Maxwell-Stefan, Darken or collective diffusion coefficient. It is the collective diffusion behaviour of all adsorbate particles, and can be interpreted as the movement of the centre of mass of all particles together. Another common measure of diffusivity is the self-diffusion coefficient D_S. It is the diffusion of a single tagged particle moving around in a sea of other particles. This is the diffusion coefficient that can be obtained by microscopic methods, such as pulsed field gradient NMR (PFG-NMR). In general, the corrected diffusion is higher than the self-diffusion, because the corrected diffusion contains interparticle correlations, which have a positive contribution, or, viewed differently, the self-diffusion is lowered by single-particle back-correlations (the increased probability of a particle jumping back to its previous position because this position has a higher probability of being empty).

9.3 Results

Figure 9.2 shows our recent simulation results for the diffusion of methane in MFI-type silica as a function of the adsorbate loading [15], together with results obtained by several other groups, through simulation [2–6] and experiment [1,7–10]. Note that the potential parameters used in the simulations have been

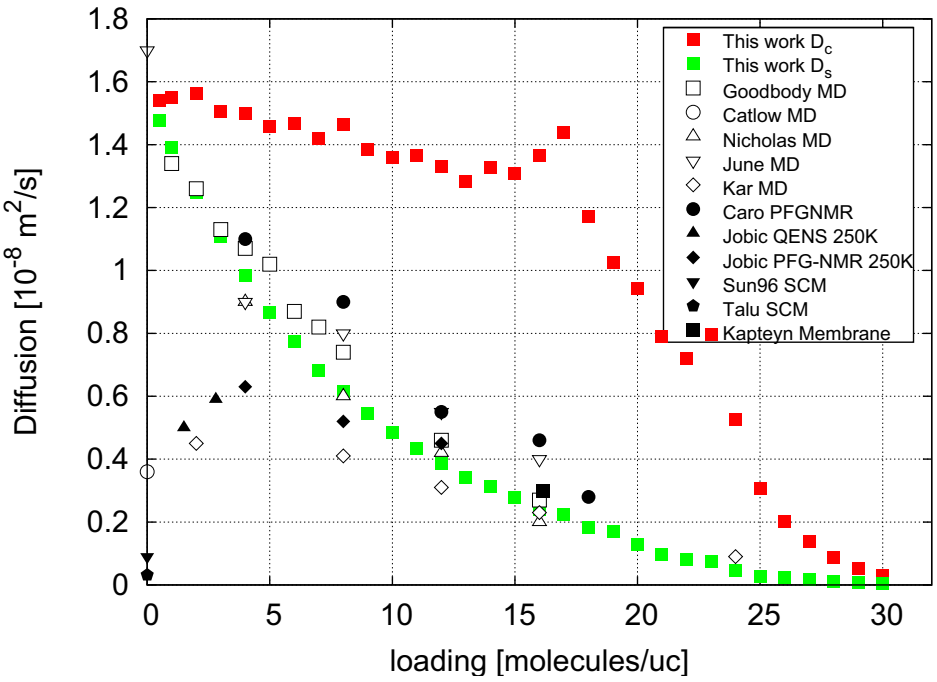

Figure 9.2: *Recent simulation results for the diffusion of methane in MFI-type silica as a function of the adsorbate loading [15], together with results obtained by several other groups, through simulation [2–6] and experiment [1, 7–10]. Data were obtained at 300 K, except for the results of Jobic et al., which were obtained at 250 K.*

fitted to adsorption data, not diffusion data [19]. The experimental data (black symbols) are self-diffusion coefficients, except those obtained by single-crystal membrane (SCM) measurements, which should be corrected diffusivities. The results have been plotted against the loading as reported in the original papers, wherever possible. Unspecified loadings have been estimated from the reported pressures with the aid of a calculated adsorption isotherm.

Although some results show a marked deviation – both single-crystal membrane studies [1,9], carried out at the zero-loading limit, yielded a diffusion that is much slower than that found by other methods – the overall correlation between different experimental and simulation results is remarkably good, much better than we expected from methods that are often said to be irreconcilable.

Furthermore, we conclude that the one-order difference in methane diffusion found in figure 9.1 can be ascribed to the differences in loading at which

the different experiments have been carried out. Larger differences are to be expected for longer alkanes.

9.4 Concluding Remarks

To compare diffusion measurements obtained by different methods, it is very important to know the loadings at which the measurements were performed. Loadings, if known, or pressures should be mentioned along with the reported diffusivity data. In addition, we can conclude that the methane force field of ref. [19] predicts the diffusion coefficient accurately.

The deviation observed between the single-crystal studies and most other studies is probably due to the existence of both internal and external diffusional barriers. The more macroscopic a measurement method, the larger the influence of the internal barriers [12]. As the internal barriers are relatively small for methane in MFI, it is expected that the diffusivities obtained by macroscopic and microscopic methods will be further apart for longer alkanes.

Bibliography

[1] O. Talu, M. S. Sun, and D. B. Shah, J. AIChE. **44**, 681 (1998).

[2] S. J. Goodbody, J. K. Watanabe, D. M. Gowan, J. P. R. B. Walton, and N. Quirke, J. Chem. Soc. Farad. Trans. **87**, 1951 (1991).

[3] C. R. A. Catlow, C. M. Freeman, B. Vessal, S. M. Tomlinson, and M. Leslie, J. Chem. Soc. Farad. Trans. **87**, 1947 (1991).

[4] J. B. Nicholas, F. R. Trouw, J. E. Mertz, L. E. Iton, and A. J. Hopfinger, J. Phys. Chem. **97**, 4149 (1993).

[5] S. Kar and C. Chakravarty, JPCA **105**, 5785 (2001).

[6] R. L. June, A. T. Bell, and D. N. Theodorou, J. Phys. Chem **94**, 8232 (1990).

[7] J. Caro, M. Bulow, W. Schirmer, J. Karger, W. Heink, and H. Pfeifer, J. Chem. Soc. Farad. Trans. **81**, 2541 (1985).

[8] H. Jobic, M. Bee, J. Caro, M. Bulow, and J. Karger, J. Chem. Soc. Farad. Trans. **85**, 4201 (1989).

[9] M. S. Sun, O. Talu, and D. B. Shah, J. AIChE. **42**, 3001 (1996).

[10] F. Kapteyn, W. J. W. Bakker, G. Zheng, and J. A. Moulijn, Chem. Eng. J. **57**, 145 (1995).

[11] S. Vasenkov, W. Böhlmann, P. Galvosas, O. Geier, H. Liu, and J. Kärger, J. Phys. Chem. B. **105**, 5922 (2001).

[12] S. Vasenkov and J. Kärger, Microporous and Mesoporous Materials **55**, 139 (2002).

[13] S. M. Auerbach, International reviews in physical chemistry **19**, 155 (2000).

[14] J. Kaerger and D. M. Ruthven, *Diffusion in Zeolites and other microporous solids* (John Wiley & Sons, Inc., New York, 1992).

[15] E. Beerdsen, D. Dubbeldam, and B. Smit, Phys. Rev. Lett. **95**, 164505 (2005).

[16] R. Krishna and D. Paschek, Chem. Phys. Lett. **33**, 278 (2001).

[17] Ramanan, H.; Auerbach, S. M., in *NATO-ASI Series C: Fluid Transport in Nanopores*, edited by Fraissard, J.; Conner, W.C. Kluwer Academic Publishers; Dordrecht, The Netherlands, 2004.

[18] R. Krishna, D. Paschek, and R. Baur, Micropous and Mesoporous Materials **76**, 233 (2004).

[19] D. Dubbeldam, S. Calero, T. J. H. Vlugt, R. Krishna, T. L. M. Maesen, E. Beerdsen, and B. Smit, Phys. Rev. Lett. **93**, 088302 (2004).

Summary

This thesis is about diffusion in zeolites. Zeolites are porous structures with pore sizes comparable to the size of small alkane molecules. Because of this similarity in size, some molecules can enter more easily than others, and, once inside, diffuse faster or slower.

Owing to their special structures, they are used for a variety of tasks. They are added to detergents to remove unwanted ions (calcium and magnesium) from tap water, they are used for catalysis, cracking, and separation in the petrochemical industry, and they can be found as desiccants in kitty litter and shoe boxes. A large number of zeolitic structures exist, which differ from one another in the shape of the pores and in chemical composition. Finding the right zeolite for the right process is a task of industrial importance. For catalysis, for example, it is imperative that the zeolite have the right catalytic properties, but also that the adsorption and diffusion properties of the structure be conducive to the process. Although zeolites are widely used, their workings are not entirely understood. Until recently, it was impossible to look at a zeolite structure and predict how the diffusivity would be influenced by a change in the concentration of the molecules inside (the sorbate loading).

Diffusion processes in microporous materials are very difficult to study experimentally, because the diffusion is often very slow, requiring very long equilibration and measuring times. In addition, since it is not possible to look inside a zeolite, extracting information about the positions and movements of molecules inside the pores is a challenge. Computer simulations, on the other hand, are very suitable to study such systems. They allow us to see the molecules, analyse their positions and trajectories, and thereby gain an understanding of their behaviour.

To study diffusion in zeolites, we developed a new simulation method to allow us to compute the diffusion as a function of the sorbate loading, even in systems where the diffusion is very slow, which was impossible with existing techniques. The new methods has the additional advantage that it allows us to analyse the movement of the molecules inside the structure in high detail, which was not possible before. We applied this method to a wide variety of zeolites to gain a better understanding of diffusion of small alkane molecules in confinement.

Method Development

Chapters 2 and 3 describe the development of the new method to calculate slow diffusion in porous materials. It is based on an existing method, dynamically corrected Transition-State Theory (dcTST), but contrary to this original technique it is applicable at any desired loading, for any system that contains high barriers for the diffusion. The method gives results that are in agreement with the method that is traditionally used to study such systems, Molecular Dynamics (MD). In addition, however, it is also applicable in the regime of very slow diffusion, where MD cannot be used. This extends the range of accessible time scales significantly beyond previously available methods. Moreover, the method allows a detailed analysis of the diffusion aided by free-energy profiles. It can be used in any zeolite and for any type of adsorbing molecule.

Applying the Method to a Representative Set of Zeolites

In chapters 4 and 5, we applied this new simulation method to study the diffusion of methane in twelve different zeolite topologies, to gain an understanding of diffusion behaviour as a function of loading. We calculated the self-diffusion (D_S, the diffusion of a single particle in a sea of other particles), and the collective diffusion (D_C, the diffusion of all the particles in the system together). Based on their characteristics, we were able to divide these twelve topologies into four groups, each with their own distinct diffusion behaviour: cage-type zeolites (where large cagelike pores are separated by narrow windows), channel-type zeolites (where the pores are linear and do not intersect), intersecting channel-type zeolites (where the linear pores intersect one another), and weak-confinement-type zeolites (where the pores are so large compared to the molecules diffusing through them, that they hardly affect the molecules).

In cage-type zeolites we observed a maximum in both the self and the collective diffusion. In channel-type zeolites the diffusion behaviour is highly dependent on the smoothness of the channel: the difference in width between the widest and the narrowest parts. In the smoothest channels the diffusion is a very rapidly decreasing function of loading; in the less smooth channels, the diffusion is more similar to that in cage-type systems. In intersecting channel-type zeolites, D_S generally behaves similar to that in channel-type zeolites of intermediate smoothness. D_C has two consecutive diffusion regimes: a slow linear decrease, until at least one of the channels has reached its maximum loading, followed by a sharper plunge that reaches zero at the saturation loading of the zeolite. The exact shape of the graph depends on the details of the

zeolite structure. Weak-confinement-type zeolites differ from all other zeolites in the behaviour of both the self-diffusion and the collective diffusion. The self-diffusion behaves in a way similar to that in channel and intersecting channel-type systems, while the collective diffusion is almost linear, up to fairly high loadings.

Molecular Path Control

While studying the diffusion in various zeolites, we discovered a remarkable effect that occurs for ethane molecules in zeolite erionite: the preferential direction of the diffusion reverses when the loading is increased. At low loadings, the diffusion in the z direction is twice as fast as that in the xy direction; at high loadings it is more than twice as *slow*. Our newly developed dcTST method enabled us to analyse this effect in detail, by studying the free-energy profiles, as described in chapters 6 and 7.

Explaining Diffusion Phenomena with Free-Energy Profiles

Chapter 8 shows for another oft-studied example, methane in MFI, how a wealth of information can be obtained by studying free-energy profiles. The graph of the diffusion as a function of loading looks very 'noisy', with many small valleys and peaks, but with the aid of these profiles it is possible to attribute each feature of the graph to a transition in the ordering of the adsorbed molecules. For example, molecules can temporarily 'freeze' in one of the channels, and thereby speed up the movement of molecules in the perpendicular channels. Transitions in the effective number of adsorption sites can change the number of available vacancies, resulting in an increase or decrease of the mobility.

Comparison with Experimental Results

In chapter 9 diffusion results from simulation are compared to experimental data. The order or magnitude difference in methane diffusion between different experimental techniques can be ascribed to the differences in experimental loadings. When loading effects are taken into account, the overall correlation between different experimental and simulation results is remarkably good, much better than we expected from methods that are often said to be irreconcilable.

Samenvatting (Summary in Dutch)

Dit proefschrift gaat over diffusie in zeolieten. Zeolieten zijn poreuze structuren met poriegrootten die vergelijkbaar zijn met de grootte van kleine alkaanmoleculen. Doordat de afmetingen zo dicht bij elkaar liggen, kunnen sommige moleculen makkelijker het zeoliet binnendringen dan andere, en, als ze eenmaal binnen zijn, sneller of langzamer diffunderen.

Vanwege hun bijzondere structuren, worden zeolieten gebruikt in vele toepassingen. Ze worden toegevoegd aan wasmiddel om ongewenste ionen (calcium en magnesium) uit kraanwater te verwijderen, in de olie-industrie worden ze gebruikt voor katalyse, en het kraken en scheiden van lange moleculen en ze komen voor als vochtopnemers in kattenbakkorrels en schoenendozen. Er bestaan heel veel verschillende zeolietstructuren, die onderling van elkaar verschillen in de vorm van de poriën en in de chemische samenstelling. Het vinden van het juiste zeoliet voor het juiste proces is een taak van industrieel belang. Voor katalyse bijvoorbeeld is het essentieel dat het gebruikte zeoliet de juiste katalytische eigenschappen heeft, maar ook dat de adsorptie- en diffusie-eigenschappen bijdragen aan het proces, of het proces in elk geval niet tegenwerken.

Hoewel zeolieten alom gebruikt worden, wordt hun werking niet helemaal begrepen. Tot kort geleden was het onmogelijk om naar een zeoliet te kijken en op basis van de structuur te voorspellen hoe de diffusie zou worden beïnvloed door een verandering in de concentratie van de moleculen binnenin (de belading).

Diffusieprocessen in microporeuze materialen zijn moeilijk te bestuderen met experimentele technieken, omdat de diffusie vaak erg traag is, waardoor erg lange equilibratie- en meettijden nodig zijn. Bovendien is het lastig om informatie over de posities en bewegingen van de moleculen in de poriën uit experimenten te halen, omdat het niet mogelijk is om de binnenkant van het zeoliet te bekijken. Computersimulaties zijn daarentegen zeer geschikt voor de bestudering van zulke systemen. Ze maken het mogelijk om de moleculen te zien, hun posities en trajecten te analyseren, en daardoor inzicht te krijgen in hun gedrag.

Om diffusie in zeolieten te bestuderen, hebben we een nieuwe simulatietechniek ontwikkeld, die het ons mogelijk maakt de diffusie te berekenen als functie van de belading, zelfs in systemen waar de diffusie erg langzaam is, wat met de bestaande technieken niet mogelijk was. De nieuwe methode heeft

als bijkomend voordeel dat zij ons de mogelijkheid geeft de bewegingen van de moleculen in de poriën van het zeoliet in detail te analyseren, wat voorheen niet mogelijk was. We hebben de methode toegepast op een grote serie zeolieten, om zo een beter begrip te krijgen van de diffusie van kleine alkanen in begrensde ruimten.

Methodeontwikkeling

Hoofdstukken 2 en 3 beschrijven de ontwikkeling van een nieuwe methode voor de berekening van langzame diffusie in poreuze materialen. Het uitgangspunt is een bestaande methode, *dynamically corrected Transition-State Theory* (dcTST), maar, in tegenstelling tot deze oorspronkelijke techniek, is zij toepasbaar bij elke gewenste belading, en voor elk systeem met hoge diffusiebarrières. De methode levert resultaten op die in overeenstemming zijn met de gebruikelijke methode voor de bestudering van dit soort systemen, *Molecular Dynamics* (MD), maar kan bovendien gebruikt worden in het regime van heel langzame diffusie, waar MD niet toepasbaar is. Dit maakt tijdschalen toegankelijk die met eerdere technieken niet te bestuderen waren. Daarenboven maakt deze methode het mogelijk om diffusie in detail te analyseren met behulp van vrije-energieprofielen. In principe kan dcTST gebruikt worden voor elk zeoliet en elk geadsorbeerd molecuul.

De methode toegepast op een representatieve set van zeolieten

Om een beter begrip te krijgen van het diffusiegedrag als functie van de belading, hebben we in hoofdstukken 4 en 5 de nieuwe simulatietechniek toegepast op de diffusie van methaan in twaalf verschillende zeoliettopologieën. We berekenden de zelfdiffusie (D_S, de diffusie van een enkel deeltje in een zee van andere deeltjes) en de collectieve diffusie (D_C, de diffusie van alle deeltjes in het systeem samen). Op basis van hun karakteristieke eigenschappen konden we de twaalf topologieën indelen in vier groepen, elk met zijn eigen diffusiegedrag: kooistructuren (waar grote kooi-achtige poriën worden gescheiden door nauwe doorgangen), kanaalstructuren (waar de poriën lineair zijn en elkaar niet kruisen), kruisende kanaalstructuren (waar de kanalen elkaar wel kruisen), en 'structuren van zwakke begrenzing' (waar de poriën en doorgangen zo groot zijn in verhouding met de moleculen die erdoorheen diffunderen dat zij de moleculen nauwelijks beïnvloeden).

In kooistructuren namen we een maximum waar in zowel de zelf- als de collectieve diffusie als functie van de belading. In kanaalstructuren is het dif-

fusiegedrag sterk afhankelijk van de 'gladheid' van het kanaal: het verschil in breedte tussen de breedste en de smalste delen. In de gladste kanalen is de diffusie een zeer snel dalende functie van de belading; in de minder gladde kanalen is de diffusie meer vergelijkbaar met die in kooistructuren. In kruisende kanaalstructuren gedragen D_S en D_C zich verschillend: D_S gedraagt zich in het algemeen als D_S in kanaalstructuren van gemiddelde gladheid. D_C heeft twee opeenvolgende diffusieregimes: een langzame lineaire afname van de diffusie tot ten minste één kanaal zijn maximale belading heeft bereikt, gevolgd door een scherpere afname, die het nulpunt bereikt bij de volledige belading van het zeoliet. De precieze vorm van de grafiek hangt af van de details van de zeolietstructuur. 'Structuren van zwakke begrenzing' verschillen van alle andere zeolieten in het gedrag van zowel de zelf- als de collectieve diffusie. De zelfdiffusie heeft een vorm die vergelijkbaar is met die in kanaal- en kruisende kanaalstructuren, maar de collectieve diffusie is bijna lineair tot vrij hoge beladingen.

Moleculaire routecontrole

Tijdens het bestuderen van de diffusie in verschillende zeolieten, vonden we een opmerkelijk effect dat optreedt voor ethaanmoleculen in het zeoliet erioniet: de voorkeursrichting van de diffusie draait om wanneer de belading wordt verhoogd. Bij lage beladingen is de diffusie in de z-richting twee keer zo hoog als die in de xy-richting; bij hoge beladingen is deze meer dan twee keer zo *laag*. Onze nieuwe dcTST-methode maakte het ons mogelijk om dit effect in detail te analyseren, door naar de vrije-energieprofielen te kijken, zoals beschreven in hoofdstukken 6 en 7.

Verklaring van diffusiefenomenen met vrije-energieprofielen

Hoofdstuk 8 toont voor een ander vaak bestudeerd voorbeeld, methaan in MFI (een kruisende kanaalstructuur), hoe een schat aan informatie kan worden verkregen door het bestuderen van vrije-energieprofielen. De grafiek van de diffusie als functie van de belading ziet er nogal 'ruizig' uit, met veel kleine pieken en dalen, maar met behulp van deze profielen is het mogelijk om elk van deze kronkels in de grafiek toe te schrijven aan een overgang in de ordening van de geadsorbeerde moleculen. Moleculen kunnen bijvoorbeeld tijdelijk 'bevriezen' in een van de kanalen, waardoor de beweging van de moleculen in de kanalen loodrecht op dat kanaal wordt versneld. Overgangen in het effectieve aantal adsorptieplaatsen kan het aantal beschikbare lege plekken veranderen,

wat kan resulteren in een verhoging of verlaging van de mobiliteit.

Vergelijking met experimentele resultaten

In hoofdstuk 9 vergelijken we diffusieresultaten uit simulaties met experimentele gegevens. De grootte-orde verschil in methaandiffusie tussen de verschillende experimentele technieken kan worden toegeschreven aan het verschil in experimentele beladingen. Wanneer rekening wordt gehouden met beladingseffecten, is de correlatie tussen de verschillende experimentele en simulatieresultaten opmerkelijk goed, veel beter dan we hadden verwacht van methoden die vaak onverenigbaar worden geacht.

Acknowledgements

To start the traditional acknowledgements, I would like to thank my advisor Berend Smit for the opportunity to do promotion research in his group. You have always let me choose topics I found interesting, while convincing me at the right moment that something was really worth pursuing, when I was ready to give up. I always felt that anything was possible, as long as it was reasonable. Thank you.

I owe a lot of gratitude to David Dubbeldam who has taught me all I needed to know and more about zeolites, computers, and the world of zeolite scientists. Without David this thesis would never have become what it is now.

Theo Maesen: it was a pleasure to work for and with you. You gave me the chance to see zeolite science as it is practised in industry. Thank you very much for having me as a temporary co-worker. And to both of you, Theo and Christa, many thanks for your great hospitality and support.

Many thanks also to "The Germans", Sven Jakobtorweihen and Nils Zimmermann, my collaborators on zeolites, nanotubes and all the other Supergeile Simulazionen.

Computers can have a mind of their own, as anyone who has spent four years working with one could testify. Gooitzen Zwanenburg deserves special mention for his endless patience in all matters computer related: solving problems, installing libraries, and being a general go-to person for things that don't work to have them magically solved. You are great! Abdon, Bastiaan, Evert, and Jasper are more of these computer-wiz saints who helped me out countless times. Other people who don't get thanked often enough are Renate Hippert and Maureen Sabandar: thanks for all your help.

I am indebted to Bastiaan Huisman, Elske Leenders and Jocelyne Vreede for a critical reading of parts of the manuscript, to Bastiaan also for advice on the cover.

I had a great time for four years in our MolSim group, and I have to thank all of my colleagues and former colleagues for that. My (former) room mates

Abdon, Bei, Jarek, Jocelyne, Marieke, and Merijn, my 'paranymphs' Bastiaan and Elske, and all the other people of the extended MolSim group: Arjen, Daniele, David, Dirk, Evert, Francesco, Jan-Willem, Jantien, Jasper, Jean-Pierre, Jochem, Live, Luca, Maddalena, Menno, Ranieri, Rini, Sofia, Thijs, Tim, Vincent. Thank you all for movie nights, coffee breaks, Chinese, Polish, and Italian lessons, silly arguments and 'slappe grappen', AIO-weekends, parties and dinners.

Patrick and Maddalena for a wonderful time teaching molecular simulations in India, and long evenings editing the course manual afterwards. My former house mates Marije, Rob, Saskia, Ivo, Najim and Rafik, for good times and pots of tea. Arjen v. L. for much more than that.

Above all I thank my parents who always support me no matter what I do, my sister Daphna, and my grandparents Saba and Sabta, who have jokingly called me "dr. Beerdsen"longer than I can remember. Neshikot we khibukim!

Published Work

Loading Dependence of the Diffusion Coefficient of Methane in Nanoporous Materials
E. Beerdsen, D. Dubbeldam, and B. Smit
Journal of Physical Chemistry B 110 (45) **2006**, 22754-22772

Diffusion in Confinement - Agreement Between Experiments Better than Expected
E. Beerdsen and B. Smit
Journal of Physical Chemistry B 110 (30) **2006**, 14529-14530

Dynamically Corrected Transition-State Theory Calculations of Self-Diffusion in Anisotropic Nanoporous Materials
D. Dubbeldam, **E. Beerdsen** and B. Smit
Journal of Physical Chemistry B 110 (7) **2006**, 3164-3172

Understanding Cage Effects in the n-Alkane Conversion on Zeolites
T. L. M. Maesen **E. Beerdsen**, D. Dubbeldam, and B. Smit
Journal of Catalysis 237 (2) **2006**, 278-290

Understanding Diffusion in Nanoporous Materials
E. Beerdsen, D. Dubbeldam, and B. Smit
Physical Review Letters 96 (4) **2006**, Art. No. 044501

A Molecular Understanding of Diffusion in Confinement
E. Beerdsen, D. Dubbeldam, and B. Smit
Physical Review Letters 95 (16) **2005**, Art. No. 164505

Molecular Path Control in Zeolite Membranes
D. Dubbeldam, **E. Beerdsen**, S. Calero, and B. Smit
Proc. Natl. Acad. Sci. U.S.A. 102 (35) **2005**, 12317-12320

Molecular Simulation of Loading-Dependent Diffusion in Nanoporous Materials using Extended Dynamically Corrected Transition State Theory
D. Dubbeldam, **E. Beerdsen**, T. J. H. Vlugt, and B. Smit
Journal of Chemical Physics 122 **2005**, Art. No. 224712

Molecular Simulation of Loading-Dependent Slow Diffusion in Confined Systems
E. Beerdsen, B. Smit, and D. Dubbeldam
Physical Review Letters 93 (24) **2004**, Art. No. 248301

Force Field Parameterization through Fitting on Inflection Points in Isotherms
D. Dubbeldam, S. Calero, T. J. H. Vlugt, R. Krishna, T. L. M. Maesen, **E. Beerdsen**, and B. Smit
Physical Review Letters 93 (8) **2004**, Art. No. 088302

Simulating the effect of nonframework cations on the adsorption of alkanes in MFI-type zeolites
E. Beerdsen, D. Dubbeldam, B. Smit, T. J. H. Vlugt, and S. Calero
Journal of Physical Chemistry B 107 (44) **2003**, 12088-12096

The Influence of Non-Framework Sodium Cations on the Adsorption of Alkanes in MFI- and MOR-type Zeolites
E. Beerdsen, B. Smit, and S. Calero
Journal of Physical Chemistry B 106 (41) **2002**, 10659-10667

Patent

Dewaxing process using zeolites MTT and GON. (Chevron U.S.A. Inc., USA)
T. L. M. Maesen, B. Smit, **E. Beerdsen**
US 2007029229, **2007**, 5pp.